UNIVERSITY OF BIRMINGHAM

NONLINEAR CHARACTERISATION OF RECONFIGURABLE ANTENNAS

BY

SHAHARIL MOHD SHAH

A thesis submitted to
the University of Birmingham
for the degree of
DOCTOR OF PHILOSOPHY

School of Electronic, Electrical and Systems Engineering
College of Engineering and Physical Sciences
University of Birmingham
March 2016

ABSTRACT

The lack of references on nonlinearity issue faced in reconfigurable antennas has motivated the work described in this thesis. The nonlinear behaviour is caused by active switches introduced on the radiating structure of the reconfigurable antennas. Depending on the type of active switches deployed on the antenna, the nonlinearity could be severe, which could have serious implications for antenna operation. Thus, the issue of nonlinearity in reconfigurable antennas should not be ignored and nonlinearity measurements should be performed to ensure the nonlinear performance is within an acceptable level. A set of nonlinearity measurements has been identified and performed on the proposed reconfigurable PIFAs. Prototypes are presented with PIN diode and E-PHEMT switches. For the purpose of comparison, measurements were also made with the active switch replaced with a copper bridge for linear interconnection. The nonlinearity performance can be evaluated from the measurement values of third-order intermodulation distortion (IMD3) products, ratio of IMD3 products to carrier, IMD3 products asymmetry, third-order input intercept point (IIP3) and 1-dB gain compression point ($P_{1\text{-dB}}$). The measurements are performed when the antenna is transmitting signals. All measurements are performed on the state-of-the-art, 4-port ZVA67 Rohde & Schwarz VNA. Based on the nonlinearity measurements, it can be concluded that the presence of active switches has compromised the nonlinearity of the reconfigurable antennas. This is evident from the appearance of strong IMD3 products at the frequency of interest. In addition, the power-series-based approximation of 10 dB difference between the measured $P_{1\text{-dB}}$ and IIP3 is shown to be reasonable. Moreover, this work has demonstrated that the ratio of the IMD3 products to carrier does not vary significantly with radiation angles.

ACKNOWLEDGMENTS

I would like to express my immense and sincerest gratitude to my supervisor; Professor Peter Gardner for without his continuous support and careful guidance, this thesis would not have been possible. His vast knowledge has enabled me to develop a thorough understanding on the subject matter. His kindness and motivation, on the other hand, have helped me to overcome multiple obstacles and low periods during the whole research process until completion.

I also wish to thank my laboratory technician; Mr. Alan Yates for sharing his technical skills and knowledge. It was hard initially, but as time goes by, I have managed to pick up the required skills necessary to fabricate my own devices. The whole experience has taught me to have patience and keep moving forward.

I am indebted to my many colleagues who have supported me through thick and thin over the years. Their presence has made the whole journey to be more exciting and memorable.

I owe my deepest appreciation to my parents and siblings for their continuous love and care. A special thank you reaches out to my mother for all the late night calls and her strong encouragement words.

I also acknowledge the provision of Modelithics™ models utilised under the University License Program from Modelithics, Inc., Tampa, FL, USA.

Last but not least, to my sponsor and employee; Ministry of Education (MOE) Malaysia and Universiti Tun Hussein Onn Malaysia (UTHM), I am truly grateful for the funding and financial assistance.

TABLE OF CONTENTS

LIST OF FIGURES

LIST OF TABLES

LIST OF ABBREVIATIONS

3GPP	Third Generation Partnership Project
AC	Alternate Current
CPW	Co-Planar Waveguide
CR	Cognitive Radio
dB	Decibel
DC	Direct Current
DVB-H	Digital Video Broadcasting - Handheld
EM	Electro Magnetic
FET	Field Effect Transistor
GaAs FET	Gallium Arsenide Field Effect Transistor
HB	Harmonic Balance
IIP3	Input Third-Order Intercept Point
IMD	Inter Modulation Distortion
IMD3	Third-Order Inter Modulation Distortion
ISM	Industrial, Scientific and Medical
MESFET	Metal Semiconductor Field Effect Transistor
MIMO	Multiple Input Multiple Output
m-WiMAX	Microwave Worldwide Interoperability for Microwave Access
OIP3	Output Third-Order Intercept Point
PHEMT	Pseudomorphic High Electron Mobility Transistor
PIFA	Planar Inverted F Antenna
PIN DIODE	Positive-Intrinsic-Negative Diode
RF	Radio Frequency
RF MEMS	Radio Frequency Micro Electro Mechanical Systems
RF NEMS	Radio Frequency Nano Electro Mechanical Systems
RLC	Resistance, Inductance and Capacitance
SDR	Software-Defined Architecture

SMA	SubMiniature version A
SMD	Surface Mount Device
UMTS	Universal Mobile Telecommunication System
UNII	Unlicensed National Information Infrastructure
USPCS	United States Personal Communication Services
UWB	Ultra-Wideband
VNA	Vector Network Analyzer
VSWR	Voltage Standing Wave Ratio
WCDMA	Wideband Code Division Multiple Access
WLAN	Wireless Local Area Network

PUBLICATIONS IN PREPARATION

1. S. M. Shah and P. Gardner, "Nonlinear Characteristics of Reconfigurable Antenna with Active Switch", *IEEE Transactions on Antennas and Propagation*, 2016

2. S. M. Shah and P. Gardner, "Radiation of Nonlinear Products from a Reconfigurable Antenna", *Electronic Letters*, 2016

3. S. M. Shah and P. Gardner, "A Reconfigurable PIFA with ATF 54143 E-PHEMT Switch", *Microwave and Optical Technology Letters*, 2016

CHAPTER 1

1. INTRODUCTION

1.1 Background

The recent and continuing growth of wireless communication these days has inspired the design and production of multifunctional antennas that are able to cover the increasing number of wireless bands [1]. Second Generation (2G) as the first digital cellular standard used quad-band solutions while the Third Generation (3G) standard has already supported up to 8 frequency bands. Fourth Generation (4G) which is dominated by the need for global roaming and wider frequency bandwidth has introduced over 40 bands allocated to Long Term Evolution (LTE) applications.

For this reason, attention has been diverted into reconfigurable multiband antennas. Reconfigurable antennas are realized by altering the current distributions on the radiating planes of the antennas or altering the current paths. This is being made possible by using radio frequency (RF) switches such as positive-intrinsic-negative (PIN) diodes or field-effect transistors (FETs) and other devices for instance, varactors, mechanically movable parts, phase shifters or attenuators [2].

Solid state RF switches is a mature technology and steadily advancing. However, they still exhibit some degree of nonlinear behaviour under certain operating conditions at high frequencies which may cause signal distortion in the antenna systems. Signal distortion will cause an undesired change in an input signal waveform as the signal passes through the communication

network. This in return will introduce frequency components that do not exist in the input waveform. The nonlinear behaviour of a reconfigurable antenna can be described in terms of intermodulation distortion (IMD) products and gain compression. In the industry, Third Generation Partnership Project (3GPP) has determined the degree of RF switch linearity which is required to avoid an interference with other devices in mobile communication systems. This is done by specifying the third-order input intercept point (IIP3) [3] .

Radio frequency microelectromechanical system (RF MEMS) switches, on the other hand, offer significant advantage in terms of linearity performance [4]. RF MEMS switches are well-known for their excellent linearity. This is due to the mechanical passive nature of the device.

In general, reconfiguration mechanisms or control devices of reconfigurable antennas can be divided into four technologies [5]. They are solid state devices, electromechanical mechanisms, ferroic materials and fluidic reconfiguration. From these four technologies, solid state device technology is fully developed technology but still progressively advancing, while fluidic reconfiguration, at the extreme end, has not yet attained the level of maturity required to be applied on commercial antennas.

1.2 Aim

The aim of this project is to investigate the nonlinearity issues faced in active reconfigurable antennas. From the reviewed literature, references discussing linearity performance and nonlinearity measurements on reconfigurable antennas are still lacking. In addition, the related works that study the nonlinear behaviour of active devices mostly are being performed on other RF devices such as power amplifiers, filters and phase shifters but very few on reconfigurable

antennas. Furthermore, even though there are references found on nonlinearity measurements of reconfigurable antennas, majority of them are using varactors instead of active switches as discussed in Chapter 2.

In order to successfully complete this research work, a careful study has been conducted to choose the most appropriate type of antenna and the suitable reconfiguration technology. The first step is to choose the type of switching involved whether an electronic, mechanical or optical switching. In terms of efficiency and reliability, electronic switching is frequently used as compared to others. The next step is to determine which antenna is widely used in wireless applications and have been the popular choice of reconfiguration capability.

For this research work, two types of active switches were selected and each of them was implemented on a reconfigurable antenna. Theoretically, PIN diodes and E-PHEMT switches suffer from nonlinear behaviour at high frequencies and were chosen for nonlinearity measurements. For comparison purpose, reference antennas with copper bridges to replace the active switches were fabricated. The copper bridge serves as a linear interconnection. A comprehensive study on the nonlinear behaviour of the reconfigurable antennas was then conducted and in-depth analysis was performed to investigate the nonlinear properties of the active switches.

1.3 Problem Statement

Active switches are commonly applied on antennas to allow pattern, polarization and frequency reconfigurations. The switch selection is determined from three major considerations; high isolation, low insertion loss and high linearity. Each new generation of cellular networks

required progressively higher linearity and was required to support the increasing number of frequency bands for wireless applications. Thus, RF front ends have become extremely complex from the stringent requirements to reduce intermodulation and cross modulation from one or more receiver and transmitter paths. In this environment, linearity performance of RF components with RF switches in particular, is becoming a crucial specification. Thus, there is a continuous research dedicated into improving the RF switch linearity in reconfigurable devices.

The research work in this thesis will be devoted to switchable reconfigurable antennas. Solid state RF switches will be introduced to reconfigure the frequency of the antennas. From a linearity point of view, these active switches will behave in a nonlinear manner at high frequencies which can be measured from several nonlinearity parameters. Third-order intermodulation distortion (IMD3) products are crucial in nonlinearity measurements. From the output spectrum of a nonlinear circuit with two-tone input signals at f_1 and f_2, it can be observed that the IMD3 products are located very close to the fundamental signals. The worst case will happen when the IMD3 products appear within the operating bandwidth of any particular antenna as this will cause distortion to the output signals of communication systems.

However, there seems to be a reasonable gap in the open literature when it comes to addressing the issue of nonlinearity in reconfigurable antennas. Most of the available research papers are focussing on the linear characteristics of the reconfigurable antennas while neglecting the nonlinear characteristics. Therefore, based on the knowledge gap found from the literature, this research project will highlight the nonlinearity issues faced in reconfigurable antennas with active switches. In order to investigate the nonlinearity of the antennas, three experimental setups have been proposed.

1.4 Objectives

The objectives of this research work are listed below:

i. To design and fabricate frequency reconfigurable antennas for wireless communication applications by incorporating PIN diode and E-PHEMT switches within the frequency range from 1 to 6 GHz.

ii. To design and fabricate a reference antenna using a copper bridge to replace the active switch for comparison purpose and to provide a highly linear reference design.

iii. To conduct nonlinearity measurements on the reconfigurable and reference antennas in transmit mode and to provide a comprehensive study on the nonlinear behaviour of the antennas.

1.5 Scope

The research work focussed on reconfigurable antennas with active switches for wireless communication applications. Two types of active switches were used and they are listed as below:

i. BAR50-02V PIN diode

ii. ATF 54143 E-PHEMT switch

At the same time, two PIFAs with copper bridges were fabricated to replace the switches. The copper bridge serves as a linear interconnection to provide a highly linear reference.

In order to achieve the objectives, a number of activities were planned and identified as outlined below:

i. Investigate the characteristics of frequency reconfigurable antennas and various methods to implement them.

ii. Select the type of frequency reconfigurable antenna for wireless applications.

iii. Select the type of active switches to reconfigure the antenna.

iv. Design and simulate the reconfigurable antennas with similar geometry and dimensions.

v. Design and simulate the reference antennas with copper bridges.

vi. Fabricate and measure the antennas to ensure small signal properties agree well.

vii. Perform nonlinearity measurements on the antennas which are listed below:

    a. Investigate the experimental setups to measure the IMD3 products when the antenna is transmitting signals.

    b. Measure the ratio of the IMD3 products to carrier.

    c. Measure the input third-order intercept point (IIP3).

    d. Measure the 1-dB gain compression point ($P_{1\text{-dB}}$).

1.6 Contribution to Knowledge

The most significant contributions of this research work to the existing knowledge are outlined as follows:

i. The nonlinearity measurements of reconfigurable PIFAs with active switches

Two types of RF switches are used to reconfigure the frequencies of the reconfigurable PIFAs namely the BAR50-02V PIN diode and ATF 54143 E-PHEMT switch. Each type of switch is implemented on a PIFA with similar geometry and dimensions. The nonlinearity measurements are performed on these antennas in transmit mode to investigate their nonlinear characteristics. For linear comparisons, two antennas with copper bridges are fabricated to provide a highly linear interconnection to replace the active switches. Moreover, the nonlinearity performance of the reconfigurable antennas with PIN diode and E-PHEMT switches is compared for further investigation.

ii. The 10 dB power-series-based approximation

In this work, it has been shown that the difference between 1-dB gain compression point and IIP3 is close to 10 dB as predicted by the power-series-based approximation.

iii. The proposed reconfigurable PIFA with ATF 54143 E-PHEMT switch

The use of E-PHEMT switch to reconfigure the frequencies of a PIFA in this work can be considered as the first work reported in the literature. Prior to the design and fabrication of reconfigurable PIFA with E-PHEMT switch, the Modelithic™ model of the transistor has been obtained from the manufacturer and was simulated in AWR Microwave Office (MWO) software

with a dedicated biasing circuit for the transistor to behave as a switch within the operating frequency from 1 to 6 GHz.

iv. The IMD radiation patterns measurement

There are no measurements of radiation patterns at IMD frequencies reported in the literature. The nonlinearity measurements performed in this work indicate that the ratio of IMD3 products to carrier does not vary significantly with radiation angles.

1.7 Thesis Outline

In Chapter 1, a brief introduction on active switches for antenna reconfiguration is presented. Depending on the technology used to manufacture the switch, these switches behave nonlinearly at high frequencies. Thus, a continuous research is required to improve linearity. The effort is in line with the evolution of cellular networks which require a huge number of frequency bands to support wireless applications. The underlying problems concerning the issue of nonlinearity in active reconfigurable antennas are also addressed.

Chapter 2 describes cognitive radio (CR) and software defined radio (SDR) architectures with further justifications on the need of a reconfigurable antenna to be a part of the system. However, the inclusion of active switches to reconfigure the antenna has generated an interesting topic on the study of nonlinearity. Thus, nonlinearity measurements to evaluate the nonlinearity of reconfigurable antennas are identified and discussed. Previous works are also reviewed and summarized to establish the knowledge gap on the nonlinearity issue faced in reconfigurable antennas.

The next two chapters discuss the reconfigurable PIFA with PIN diode and E-PHEMT switches. The design, simulation and fabrication of the antennas are examined. For each type of active switch, a dedicated biasing circuit is proposed but the geometry and dimensions of the reconfigurable PIFA are similar.

In Chapter 3, a preliminary study is conducted on the reconfigurable PIFA to study its switching capability. The work on reconfigurable PIFA with PIN diode is also presented. The first resonant frequency remains similar in both states of the PIN diode. Depending on the switching state of the PIN diode, the second resonant frequency can be switched to the upper and lower resonant frequency.

In Chapter 4, the work on reconfigurable PIFA with E-PHEMT switch is discussed. Before the transistor can be used as a switch, two simulations are carried out to observe the performance of S_{11} and S_{21} of the transistor with its biasing circuit. In this case, a low insertion loss in the ON state and a high isolation in the OFF state are required before the transistor can be used as a switch.

For comparison purposes, two reference antennas with copper bridges are fabricated. Copper bridge is selected to replace the active switch as it provides a highly linear interconnection. The discussion can be read in Chapter 5.

In Chapter 6, the methodology to perform the nonlinearity measurements on the reconfigurable PIFAs is discussed. The nonlinearity measurement results are also presented and analyzed. The comparisons are made between the reconfigurable PIFAs and reference antennas.

Finally, Chapter 7 concludes the findings of this work and suggestions for future works.

CHAPTER 2

2. BACKGROUND AND LITERATURE REVIEW

2.1 Introduction

Software defined radio (SDR) and cognitive radio (CR) are two new concepts in wireless platforms which have greatly influenced the future antenna designs with varying degrees of reconfiguration and band tuning [6]. To begin with, CR is a wireless transponder which has the ability to sense the spectrum and changing system parameters such as frequency, transmitted power or standard, if required. SDR, on the other hand, is a technology that is necessary for a full implementation of CR [7].

CR communication is predicted to be the new unconventional paradigm to enhance the performance of radio communication systems which is realized via efficient utilization of the radio spectrum. A cognitive communication system is an intelligent communication system which is capable of learning from its radio environment and adapting its operational parameters to sense the spectrum for reliable communication and efficient utilization of radio spectrum.

Severe difficulties are expected in the implementation of CR from a system or network point of view and in the technology required to operate it. These can be attributed to the fact that the initial systems will have to operate in an environment populated by two groups of systems; those that are regulated and those that are allowed to operate as cognitive radios. Reconfigurable

antennas provide degree of freedom in system adaptation that can potentially help towards overcoming these difficulties.

Future cognitive communication systems require reconfigurable antennas as the underlying hardware to have the capability to operate over a wide range of frequencies and over a multiple wireless standards [8]. The design of reconfigurable antennas should allow the operations in multiple and wideband frequency bands to cover multiple standards simultaneously. This requirement can be made possible by the implementation of switchable antennas which use active switches to sustain their operations.

2.2 Software Defined Radio (SDR) Architecture

Enormous possibilities offered by modern signal processing have enlightened the software radio concept. From hardware point of view, SDR can be described as a system in which the majority of the functionality is defined by software algorithms. In the system, wideband antennas are connected directly to analogue-to-digital converters (ADC) and the digitized radio signal will then be processed [9]. Thus, the processor should contain all the processing which is done previously by analogue radio frequency (RF) and baseband circuits. The processor has a significant advantage of reconfiguration to the standard that the radio is using. This kind of flexibility seems to be necessary as more and more radios are being integrated to allow maximum connectivity in a single wireless platform.

In another approach, an amplifier followed by ADC has been used at very low frequency (VLF) applications but this concept has not been realized at microwave frequencies due to a very large power required to drive the ADC. However, the enhancement has been made with an additional

low noise amplifier (LNA) and power amplifier (PA) which has resulted in a possible SDR architecture [10]. Figure 2.1 shows the possible architecture of SDR.

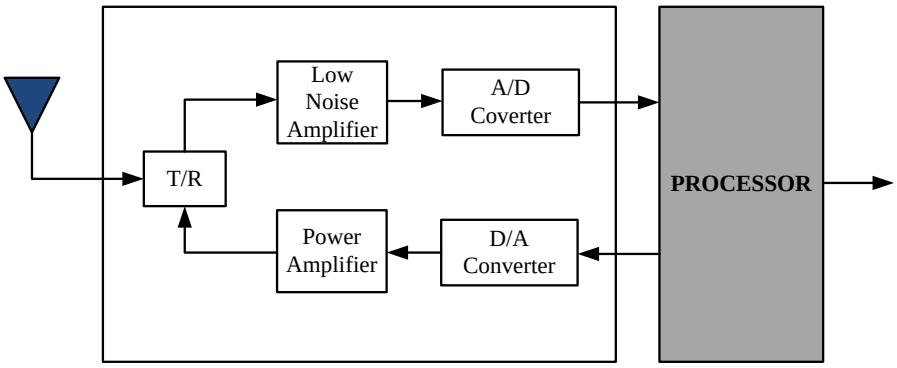

Figure 2.1: Possible software defined radio (SDR) architecture [10]

CR further enhances the concept of SDR using a model-based reasoning in handset to provide a local control which greatly increases capacity with the advantage of *spectrum pooling*. The increasing number of wireless communication applications with a particular emphasis placed on a frequency range from 0.8 to 3 GHz has caused a significant spectrum congestion [11]. CR, on the other hand, should be able to access the frequency band from 30 MHz to 5.9 GHz. A typical block diagram of a CR can be seen in Figure 2.2.

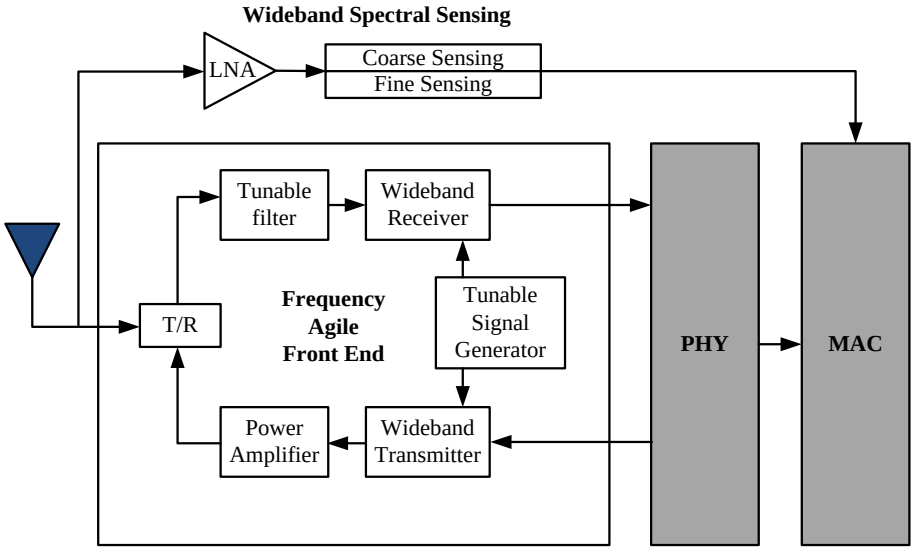

Figure 2.2: Cognitive radio architecture [10]

Wideband antennas in the transmitter and receiver have been implemented in the cognitive radio architecture in Figure 2.2. Wideband antennas can only produce coarse spectrum sensing while narrowband antennas can sense the spectrum accurately. Another disadvantage of wideband antennas is that they tend to be bigger than narrowband antennas which will be an issue in terms of portability in mobile handsets. This generates the need for substitution of wideband antennas with multiband or reconfigurable antennas which has greatly influenced the choice of antenna in this research work.

2.3 Fixed Multiband Antenna

Multiband antennas are those antennas which are able to operate at more than one band or service at the same time. It has been one of the most practical and affordable wireless module solutions. The term *fixed* can be referred to the operating frequency, radiation patterns and polarization that

are fixed depending on the applications and once the antenna has been fabricated and located in the system, the performance of the antenna remains unchangeable.

Fixed multiband antennas normally require complicated filters with flexible requirements to improve their out-of-band noise rejection. These filters are bulky and obviously will add complexity to the communication systems. This is the drawback of fixed multiband antennas as the next generation devices requires smaller built-in antennas to follow the downsizing trend of the terminal unit but at the same time, are able to support the growing number of wireless frequency bands [12].

These problems can be solved with deployments of reconfigurable antennas.

2.4 Reconfigurable Antenna

Fixed multiband antennas can be realized in various communication systems and devices. However, they are still lacking in terms of flexibility to accommodate new services. Those requirements have motivated the evolution of fixed multiband antennas to reconfigurable antennas. Reconfigurable antennas have the capability to change their radiation topology within the same physical dimension which is attributed to their selectivity of frequency, radiation or polarization, and compact size [5]. In other words, reconfigurable antennas can alter their resonant frequencies, radiation patterns, or polarization states depending on applications and their surrounding environment [13]. Antenna reconfiguration capabilities are usually achieved by incorporating switches or tunable devices such as PIN diodes, FET switches, RF MEMS switches, variable capacitors or varactor diodes in the design stage of the antenna [14]. These will

enable the frequency response, radiation patterns, gain or the combination of various antenna parameters to be controlled.

The main advantage of reconfigurable antennas is the ability to operate in multiple bands in which the total antenna volume can be reused [15]. This would greatly reduce the complexity but at the same time, increases the capability of the antenna system. As a result, a particular device that use a single compact antenna will allow reduction in its dimensions and this will provide more space to integrate other electronic components [16].

A number of papers on the design of switchable reconfigurable antennas have been reviewed and they are summarized and compared in Table 2.1.

Table 2.1: A review of switchable reconfigurable antennas

Reference	Antenna Type	Number of Bands	Number of Switch	Frequency Band
[17]	PIFA	5	1 RF MEMS	UTRA Bands of: Band I: 1901 – 2185 MHz Band II: 1849 – 2156 MHz Band III: 1840 – 2151 MHz Band V: 748 – 912 MHz Band VIII: 765 – 950 MHz
[18]	Slot-patch	3	3 PIN diodes	2.5 GHz (Bluetooth); 3.5 GHz (WiMAX); 5.8 GHz (WLAN)
[19]	Patch	1	2 PIN diodes	5.27 – 5.74 GHz
[20]	Slot-patch	4	2 PIN diodes	5.6 and 6.2 GHz (Dual-band) 5 and 5.7 GHz (Dual-band) 5 to 7 GHz (Wideband)
[21]	Slot-patch	1	2 PIN diodes	2.4 – 2.5 GHz (WLAN IEEE 802/11 b/g)
[22]	Printed dipole	1	2 PIN diodes	2.5 – 2.7 GHz (WiMAX)

From the table, there are two common traits of the reconfigurable antennas that may cause some problems and need to be addressed.

Firstly, the multiple numbers of switches will enhance the features of the antennas. However, this will add complexity to the communication systems as the biasing circuits will be more complicated and interference between the electronic components might disrupt the output signals. Thus, the number of switches should be reduced.

Secondly, the number of bands increases with the increase in the size of the antennas. However, the sizes of the devices are getting smaller these days while at the same time, must be able to support multiple wireless services. Thus, there is an urgency to reduce the size of the antennas. Table **2.2** further highlights the advantages of reconfigurable antennas [23].

Table 2.2: Comparison of antenna solutions for wireless mobile platforms

Characteristic	**Multiple Antennas**	**Multiband/Wideband Antennas**	**Reconfigurable Antennas**
Usage Model	Single-band antenna supports one frequency of wireless service	One antenna supports all frequency bands of wireless service/module	One antenna supports many wireless standards
Space Requirement	Multiple antennas require more spaces	Reduced space but wide bandwidth deters miniaturization efforts	Minimal space requirement
Front-end Complexity	Loose filter specification, simple front-end	Many stringent filters required, introduce high insertion loss and cost	Relaxed filter specifications but complex reconfigurable front end required
Individual Radio Performance	Excellent	Good; lower receiver sensitivity due to insertion loss at front end	Acceptable performance, additional loss introduced by switches

Radio Coexistence	Little spacing between antennas, strong coupling between radios	Poor out-of-band rejection, transmitted signal of other radio may cause noise jamming	Degraded through simultaneous operation as antenna supports one service at a time
Cost	Increased number of cables contributes most of the cost	High-cost stringent filters required at front end	Cost of low loss, low power consumption RF MEMS switch is high. However, other options of cheaper switching devices are also available.

2.5 Reconfigurable Performance Metrics

Reconfigurable performance metrics can be classified into three overarching categories which are listed as below:

i. Frequency reconfigurable

ii. Radiation pattern reconfigurable

iii. Polarization reconfigurable

2.5.1 Frequency Reconfigurable

Frequency reconfigurable antennas allow a single radio device to operate at multiple frequencies which is the advantage. Frequency reconfigurable antennas of this type are commonly applied to RF communication systems such as multiband mobile devices [24]. The frequency agility will include shifting or switching a resonant frequency, impedance bandwidth or facilitating multiband characteristics. The shape of the radiation patterns will remain unchanged as the

frequencies are tuned or switched from one frequency to another. For instance, a switching method can be used to switch into multiple bands for mobile applications as can be seen in [20]. The concept of frequency reconfiguration in that work can be further illustrated from the reflection coefficient graphs in Figure 2.3. From the figure, it can be seen that the reconfigurable antenna has the capability to shift from one frequency band to another depending on the states of the two PIN diodes.

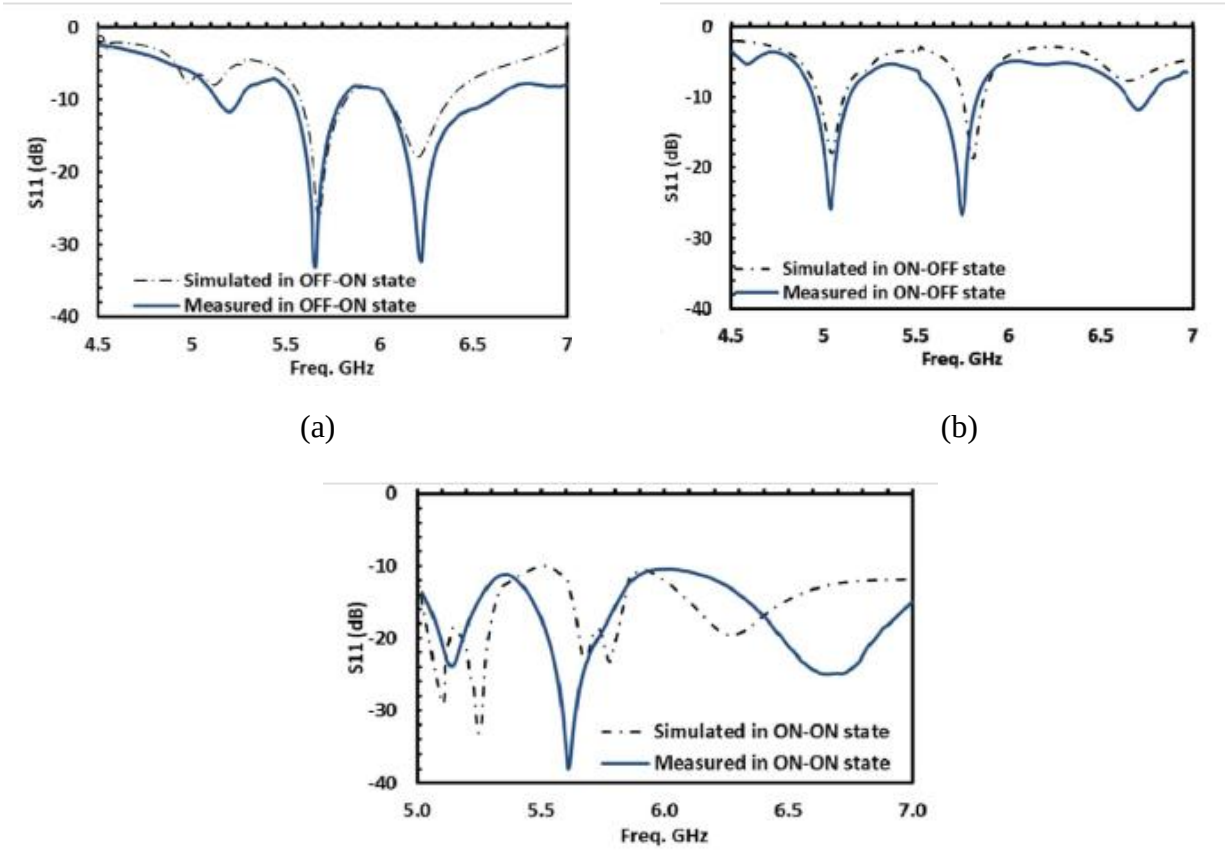

Figure 2.3: Multiple frequency bands achieved in frequency reconfigurable antenna in [20] when two PIN diodes are switched; (a) OFF - ON (b) ON - OFF (c) ON - ON

2.5.2 Radiation Pattern Reconfigurable

Radiation pattern reconfigurable antennas will enable changes in radiation pattern while maintaining the frequency bands based on the system requirements. As a result, the antennas can steer their radiation beams to different directions to enhance signal reception as can be seen in [25]. In this work, the radiation pattern will change depending on the current states of the two PIN diodes. This concept is explained further in Figure 2.4.

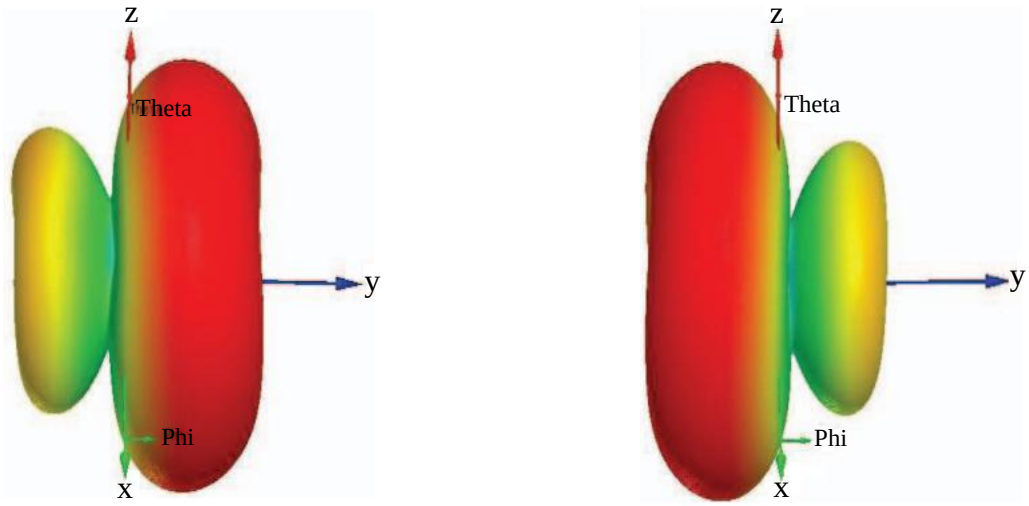

Figure 2.4: The radiation pattern in different states of PIN diodes in [25];
(a) Mode 1 (PIN diodes ON - OFF) (b) Mode 2 (PIN diodes OFF - ON)

2.5.3 Polarization Reconfigurable

Polarization reconfigurable antennas have significant advantages at improving signals reception performance in severe multipath fading environments in Wireless Local Area Networks (WLAN), as a modulation scheme in Radio Frequency Identification (RFID) systems and at

increasing security complexity in military wireless systems [26]. In general, microstrip antennas are designed to operate in a single polarization mode such as linear or circular polarization (CP). In wireless communications, CP is more favorable since the antennas of the transmitter and receiver do not have to be aligned to be parallel with each other. CP antennas exhibit both right-hand circular polarization (RHCP) and left-hand circular polarization (LHCP). In terms of implementation, a polarization reconfigurable antenna can be designed from a simple patch antenna. This can be performed by a proper design of the feed network and by adjusting the dimensions of the patch in such a way to excite two orthogonal modes with a phase difference of 90°. Figure 2.5 shows a CP reconfigurable antenna as proposed in [27]. The antenna employs two diagonal rectangular slots along two diagonals which are controlled by two pairs of PIN diodes. The antenna will radiate in RHCP mode when switches L are off and switches R are on. On the other hand, when switches L are on and switches R are off, the antenna will radiate in LHCP mode.

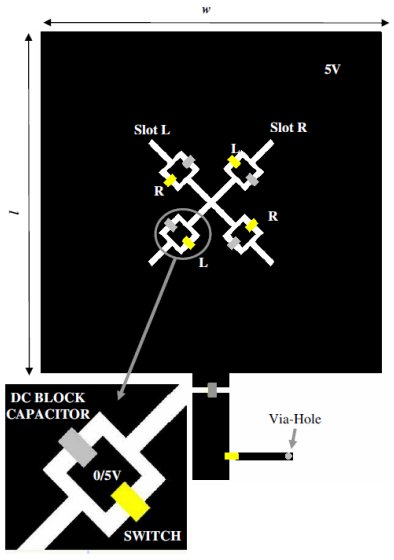

Figure 2.5: Polarization reconfigurable antenna [27]

2.6 Reconfiguration Mechanisms

There are three reconfiguration mechanisms which can be applied to reconfigurable antenna systems depending on their specific applications [28] which are:

i. Electronically controlled mechanism which is attached to the primary radiator. This includes any terminal-connected devices such as PIN diodes, RF MEMS, varactors and other terminal-connected components that require an applied electrical stimulus to facilitate reconfiguration.

ii. Pressure-driven or optically controlled mechanism which is connected to the parasitic radiator. This encompasses any terminal-free devices such as photodiodes, microfluidic mechanisms and other devices that do not require direct electrical stimulus or contact to facilitate reconfiguration.

iii. Dynamic material-based perturbation which includes similar technologies as in (i) and (ii) but it is embedded into the bulk or composite substrate and controlled both with and without a direct connection to the radiating and parasitic elements.

2.7 Reconfiguration Technologies

Reconfiguration mechanisms or control devices in the design of reconfigurable antenna systems can be further divided into four reconfiguration technologies. They are named as electromechanical, ferroic materials, solid state devices and fluidic reconfiguration [5].

2.7.1 Electromechanical Devices

Electromechanical devices can be very robust and can facilitate the operation of reconfigurable antennas. RF MEMS and RF NEMS have been used specifically in high frequency applications where loss mechanisms, electrical dimension, wave impedance and linearity are critical [29]. The small size of the electromechanical system is an attractive merit to incorporate switching and loading mechanisms in packaged configuration or as a mechanism that can be fabricated in situ or onto the antennas [30]. In addition, the small size will help to avoid unwanted transmission line effects or loading within the device and at the same time, can be used to create structurally reconfigurable electromechanical antenna systems where the moving parts act as the structural elements of the design [31].

MEMS, NEMS and other electromechanical mechanisms are often interfaced with through wire bonds and terminals for biasing and control [32] . These terminals must be sufficiently isolated by means of packaged and electromechanical design in order for the topology to be ideally suited for switching, routing and other tasks in the RF front-end chain [28]. The RF front-end chain requires electrically conductive bias and control lines to effectively navigate to and around the terminals in a multilayer environment. However, there is a design challenge when the electromechanical switches are to be integrated into reconfigurable antennas in terms of isolation. In this case, the isolation from bias and control structure must be sufficient to avoid interference with the intended operation of that particular antenna through spurious radiation or reactive loading.

There are a few fabrication methods to integrate RF MEMS and NEMS devices into the antenna structures which are discussed as follows:

2.7.1.1 Packaged RF MEMS and NEMS

Packaged RF MEMS and NEMS can be utilized in reconfigurable antenna designs as switching mechanisms or tunable discrete elements such as variable inductors and capacitors (varactors) [33]. RF MEMS and related micro or nano–scale components are sealed or packaged in these structures to protect the movable part from exposure to environmental parameters such as moisture and dust while at the same time, to provide physical protection from damage during handling or normal operation [34]. In addition, using a packaged unit makes it attractive for integration into platforms using rapid pick-and-place methods for mass fabrication. Two examples that demonstrate the implementation of packaged RF MEMS switches in reconfigurable antenna structures can be found in [35] and [36].

2.7.1.2 In Situ Fabricated RF MEMS and NEMS

This method is implemented by fabricating RF MEMS and NEMS onto or within the antenna structure which is a direct method for the integration of reconfiguration mechanisms into the antenna design. However, fabrication of these devices directly onto the antenna will give rise to undesired interaction with the packaging or hermetic sealing and loading from wire bonding. Thus, the challenge lies in providing bias signal and control to the antennas. The ability to provide biasing directly through these structures in a non-terminal configuration will create many opportunities. Previous works are exemplified in [37], [38] and [39].

2.7.1.3 Structurally Reconfigurable Electromechanical Systems

This method consists of a wide range of technologies which includes micro-machined Vee antenna [40]. However, material-based techniques using electroactive and shape-memory materials is the emerging technology which provides unique solutions and alternatives to electromechanical reconfiguration technology driven by electrostatic actuation of metallic elements. The material-based techniques will have the ability to transduce an electrical stimulus into a physical movement or displacement through their structure-property relations which serve as an advantage in providing continuous reconfigurability instead of a discrete set of reconfigurable states. Pattern reconfigurable antennas using electroactive polymer (EAP) actuators have been reported in [41, 42]. Two different types of EAP actuators have been applied in each of those works which are ionic and dielectric EAPs. Helical shape memory alloy (SMA) has been implemented in the design of an axial-mode pattern reconfigurable helix antenna [43].

2.7.2 Ferroic Materials

The *ferroic* term comes from the combination of ferroelectric and ferromagnetic. Ferroic materials have the special feature to alter the dielectric, magnetic and conductive material properties both locally and across an entire antenna structure or aperture. These materials have also shown the same capability to provide continuous tunability similar to the electroactive materials but do not make structural changes beyond changes to their crystallographic morphology when biased [44]. Barium Strontium Titanate (BST) is one example of ferroelectric material which has seen the application in tunable antennas due to high tunability, high dielectric constant, relatively low loss and fast switching speed as observed in [16, 45, 46].

2.7.3 Solid State Devices

The use of solid state devices in reconfigurable antenna designs is a very mature technology but steadily advancing. PIN diodes [47], GaAs FET switches [48] and varactors [49] which provide convenient reconfigurations are among the popular examples. These devices which are small in size are very well characterized to ease their implementation on reconfigurable antenna structures. However, difficulties are still observed in these terminally-connected devices in terms of biasing and operations.

GaAs FETs are used in switching mode with zero drain to source bias current, having low power consumption but with very poor linearity and high loss. PIN diodes, on the other hand, can achieve low loss at low cost but the drawback can be seen in the ON state with the existence of a forward bias DC current which will degrade the overall power efficiency. Varactor diodes have the advantage of providing continuous reactive tuning but suffer from poor linearity. In addition, high power level in the transmit configurations will introduce intermodulation distortion (IMD) products due to the nonlinear properties of the semiconductor materials used in these solid state devices.

Recently, there has been a focus on using photonic technologies for antenna reconfiguration due to the fact that it is possible to produce both radiation and frequency reconfiguration using photonically controlled devices (switches, reactive devices and photoconductive materials). Devices of this type do not require conducting lines to provide power, control or bias signals but use optical fibre cables or direct optical illumination to control the device or to manifest changes in the materials. Since the optical fibres are made of low permittivity dielectric materials, they do

not perturb the antenna fields significantly. In these photonic technologies, bias-free optical control of varactor diodes [50] and PIN diodes [51] has been observed.

An interesting example can be seen in [52] where the dipole antenna is being reconfigured with silicon switches. These silicon switches are controlled by using fiber optic cables and near infra-red laser diodes. The optically controlled reconfigurable coplanar strip (CPS) dipole antenna can be viewed in Figure 2.6.

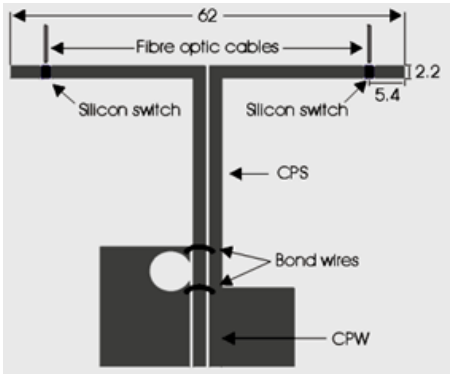

Figure 2.6: Optically reconfigurable CPS dipole antenna [52]

The optically activated silicon switches will increase or decrease the length of the dipole to achieve frequency shifting. Fibre optic cables do not have any metallic elements. Thus, they are electromagnetically transparent and do not interfere with the radiation patterns of the antenna. Two 980 nm lasers which operate at 100 mW are used to illuminate the switches. The silicon switches will start to conduct and increase the length of dipole arms when both switches are turned ON. Hence, the resonant frequency is decreased. During the OFF mode, silicon will behave like an insulator making the dipole arms shorter. Thus, it will resonate at higher

frequency. The antenna operates at either 2.26 or 3.15 GHz when both photoconducting switches are switched on or off.

2.7.4 Fluidic Reconfiguration

Fluidic-based control technology, which is the emerging counterpart to terminal-driven devices, have been considered in RF and other electromagnetic systems other than antennas [53] but their reaction time has not yet attained the level of maturity found in solid state, RF MEMS and ferroic devices. This can be attributed to the slower reconfiguration speed of the material-driven approach which has been applied in fluidic reconfiguration. The loss associated with ionic fluids and mixtures is another drawback of this technology when it comes to reconfigurable antenna applications. Nevertheless, microfluidics can remotely deliver pressure driven stimuli for reconfiguration which serves as a motivation for the sensitivity of the antennas to conductive bias and control lines.

2.8 Switching Speed

The speed at which active switches are operating is another crucial design parameter. More often, the switching speed is neglected as more attention is being diverted to understanding the antennas topology and identifying new designs. The speed, together with linearity, power handling capabilities and other operational parameters of the reconfiguration mechanism should be treated equally to enhance the antennas capability and stability [54].

Table 2.3 indicates the trade-offs in performance metrics for FET, PIN diodes and RF MEMS switches [28] . The values in the table will keep improving to cater for the need of an increasing

speed, better linearity and decreasing power consumption to fulfill the demand and growing needs of wireless applications. However, it still provides a general idea into the trade-offs that must be considered when a choice has to be made.

Table 2.3: Performance comparison of FET, PIN diode and RF MEMS switches

PARAMETER	FET	PIN DIODE	RF MEMS
Voltage (V)	±3 – 5	3 - 5	20 – 80
Current (mA)	0	3 – 20	0
Power Consumption (mW)	0.05 – 0.1	5 – 100	0.05 – 0.1
Switching Time	1 – 100 ns	1 – 100 ns	1 – 300 µs
Isolation (1 – 10 GHz)	Medium	High	Very High
Isolation (10 – 40 GHz)	Low	Medium	Very High
Isolation (60 – 100 GHz)	None	Medium	High
Loss (1 – 100 GHz) (dB)	0.4 – 2.5	0.3 – 1.2	0.05 – 0.2
Power Handling (W)	<10	<10	<1

2.9 Comparative Analysis of Switches based on PIN Diodes and FETs

This section will discuss the comparative analysis of PIN diode and FET when being used as switches for wireless applications. The analysis can be divided into five (5) different categories which are listed in the following sub-sections [55]:

2.9.1 System-on-Chip Integrability

The technologies used in manufacturing FETs are planar which allows the fabrication of passive elements on the surface of semiconductor plates such as resistors, inductors and capacitors. As the main fraction of the plate's thickness is occupied by semi-insulating material, this eliminates inter-element coupling within a chip. PIN diode manufacturing technology; on the other hand, is

vertical since the main fraction of the plate's thickness is occupied by cathodes of PIN diodes. This essentially complicates inter-diode isolation within a chip.

2.9.2 Control Current

A FET switch is controlled by the application of potential to the gate terminal. Gate leakage current (I_{gss}) is the only current that flows in the control circuit which usually does not exceed 1 μA. A PIN diode requires a significant injection of charge into I-layer during its operation in order to decrease the impedance to the desired level. A typical value of bias current for PIN diodes is between 10 to 20 mA.

2.9.3 Operating Frequency

A FET switch in an open state is represented by a resistor with a fixed value ranging from direct current to microwave frequency. A FET switch in a closed state is represented by a capacitor where the capacitance does not depend on the frequency. Meanwhile, a PIN diode in both ON and OFF states has limitations while operating in the low frequency range. Thus, it is most unlikely that PIN diodes would be used in devices that operate in a wide frequency range starting at direct current.

2.9.4 Switching Speed

A FET switch controls primary charge carriers by varying the depth of depletion layer in Gate-Channel region. The variation in depth of the depletion layer occurs very quickly as a response to changes in gate potential. PIN diode controls primary and secondary charge carriers by injecting carriers into the I-layer under forward bias. Under reverse bias, carriers need to be

removed from the I-layer to change the diode's impedance from low to high. The injection and removal of charge carriers in a PIN diode are taking more time than changing depth of the depletion layer. Thus, a PIN diode has much slower switching speed.

2.9.5 Nonlinear Distortions

In a FET switch, the control of the depth of depletion layer is accomplished via Gate-Source junction that represents a Schottky diode. Schottky diode is a nonlinear circuit element which will cause a high level of nonlinear distortions. The resistance of a PIN diode will be close to linear if current injected by constant bias voltage exceeds by a magnitude the current injected and removed by voltage of microwave signal. In the OFF state, a PIN diode is represented by a capacitor. At frequencies above 100 MHz, the value of this capacitance has no dependence on microwave voltage. Thus, PIN diode has the capability to operate with minimum nonlinear distortions.

2.10 Antennas for Multi-radio Wireless Platforms

There are three major antenna types which are commonly used for multi-radio wireless platforms namely patch antennas, wire antennas and PIFAs. Those antennas have been identified as suitable candidates to implement reconfiguration.

2.10.1 Patch Antennas

Patch antennas have provided an attractive solution for various types of wireless platforms such as mobile phones and mobile internet devices (MIDs). The main characteristics of patch antennas are the wide beam angle with an almost uniform radiation pattern at broadside and which have

inherent ground shields which serve as an advantage at improving the mobile phone compliance with specific absorption rate (SAR) constraints [56]. In addition, patch antennas have a high radiation efficiency [57]. Thus, a lot of efforts have been undertaken to extend their operation from a single frequency to cover multiple frequency bands by reconfiguring the antenna structure. One way is to introduce slots on the patch which are controlled by active switches [58, 59] . The function of active switches is to divert the current path along the slots. The movement of current along the slots will control the length of those slots which in return will control the operating frequencies of the antennas. Figure 2.7 shows a basic patch antenna with a switchable slot (PASS) [60].

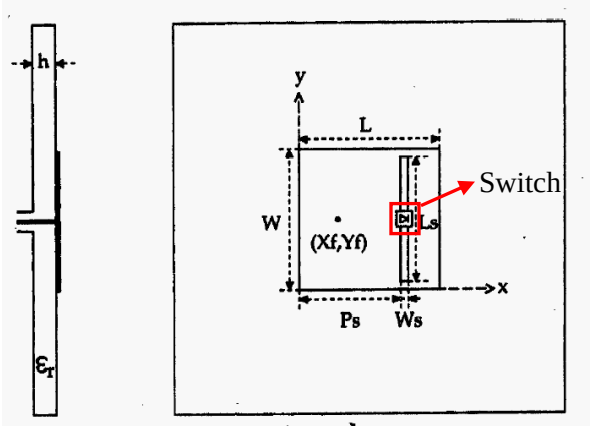

Figure 2.7: Geometry of a patch antenna with a switchable slot (PASS) [60]

A slot with a length of L_s and W_s is incorporated on the patch with a switch inserted at the centre of the slot to reconfigure the antenna. The switch can be a FET, PIN diode or RF MEMS switch depending on intended applications. However, in this example, the switch is modeled as a metal tape. The metal tape will be removed from the antenna in the OFF mode. The antenna resonates at 4.75 GHz when a slot is introduced with a metal tape. The resonant frequency is further shifted

to 4.40 GHz when the metal tape is removed. This phenomenon can be explained by investigating the electric currents on the patch antenna. This can be viewed in Figure 2.8.

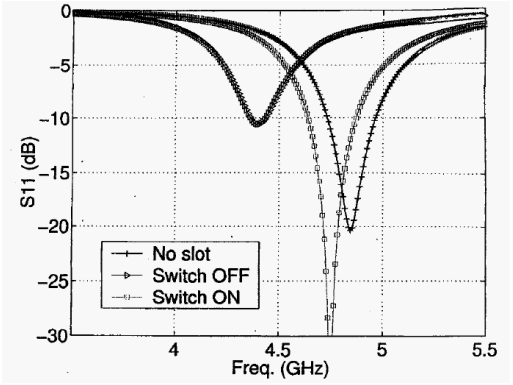

Figure 2.8: Simulated reflection coefficient for each mode of the switch in [60]

It is observed that when the switch is in the OFF mode, the electrical currents on the surface of the patch will have to flow around the slot which results in a relatively longer current path. Thus, the antenna will resonate at a lower frequency. On the contrary, in the ON mode, some of the electrical currents will go directly through the switch which leads to shorter current path. Hence, the antenna will resonate at a higher frequency. The variation of resonant frequencies with respect to the slot lengths can be seen in Figure 2.9.

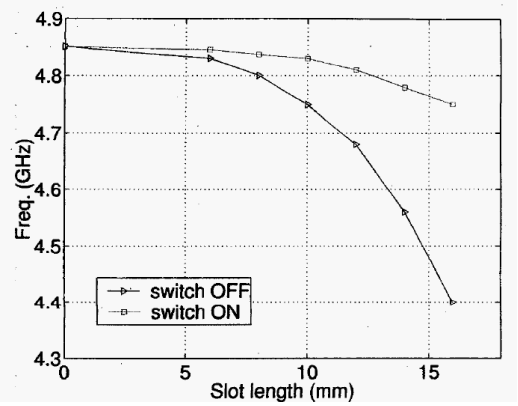

Figure 2.9: Variation of resonant frequencies with slot lengths [60]

2.10.2 Wire Antennas

Basic wire antenna structures include monopole, dipole and loop antennas. The resonant frequency of wire antennas is primarily defined by the length or perimeter of the wire which can be controlled to reconfigure [23]. For instance, the first resonance will be observed when the length of a monopole is about a quarter-wavelength. A loop antenna will resonate at a certain frequency when the perimeter is approximately one wavelength. It has been demonstrated from previous work in [61, 62] that a loop antenna is a potential candidate to achieve dual-band or multiband operation in a mobile phone. A switch can be incorporated to alter the length or perimeter of these wire antennas to operate over different frequency bands. This will lead to current distribution at a new resonant frequency which is very close to the original resonance. Hence, the same radiation characteristics and input impedance can be seen in the new structure as in the original wire antenna structure. A compact internal antenna comprised of a loop antenna and a monopole antenna is presented in [63] for wireless frequency applications. The proposed antenna can be printed on the system circuit board of the mobile phone and short-circuited to the system ground plane to form a loop-type structure.

2.10.3 Planar Inverted F Antennas (PIFAs)

Inverted F antenna (IFA) is the most common embedded antenna in use today for wireless communication devices with frequency range from 900 MHz to 6 GHz [64]. It can be formed in multiple ways, has an excellent multiband capability and is highly efficient. Originally designed in the early 1960s as a single-band conformal ultra high frequency (UHF) antenna for use on an

aircraft, IFA has evolved into a low profile, multiband antenna that can be integrated into today's small and compact product designs [65].

In its most basic form, IFA is a quarter-wavelength long conductor parallel to and within a few millimeters distance from an RF ground plane, grounded at one end and has a 50-Ω feed point close to the grounded end [64]. The quarter-wavelength conductor can be a thin wire, a trace on a PCB or a three-dimensional (3D) surface that can be straight or folded into complex shapes. The 3D version is commonly called a Planar IFA (PIFA). In other words, an IFA can be referred to as a two-dimensional (2D) antenna and a PIFA would be a 3D antenna.

PIFA is a very popular type of antenna for internal mobile communication handsets [10]. This is due to their low profile, ease of fabrication and relatively small footprint [66]. The structure of PIFA can be considered as a half-size slot where the feed and ground location determines the input impedance of the antenna. The mode of operation of PIFA can be reconfigured by changing the feed or ground location allowing the resonant frequency to be controlled. A PIFA usually consists of a radiating wire that is short-circuited to the ground plane with a shorting pin located at a certain distance from the feed point [23]. The input matching can be further improved by optimizing the location of the feed point with respect to the location of the shorting pin which generally happens when the length of the antenna is approximately a quarter-wavelength at the operating frequency [67].

Frequency reconfiguration can be achieved by implementing the techniques discussed in patch and wire antennas [68, 69]. For instance, a thermal MEMS switch which has been placed across the L-shaped slot has reconfigured the resonant frequencies by controlling the length of the

slot [70]. The open slot is inserted to decrease the resonant frequencies of higher order modes. Proper placement of the switch has enabled Global Systems for Mobile Communications (GSM) frequency band to be always supported while additional resonant frequencies ranging from 1 to 3 GHz are achieved with different switch locations. The antenna geometry can be seen in Figure 2.10.

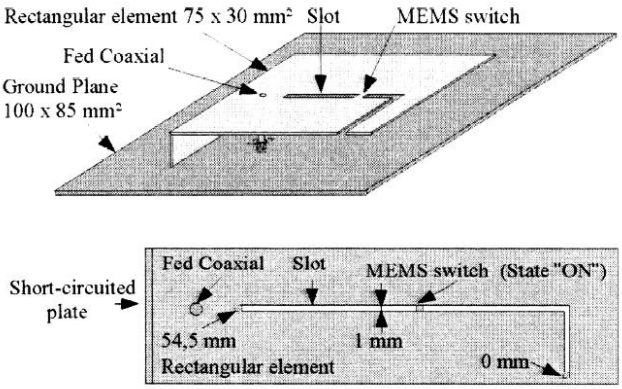

Figure 2.10: Antenna geometry of MEMS-based L-shaped slot PIFA in [70]

2.11 Antenna for Smartphones

In smartphones, the same antenna should be used for both searching or spectrum sensing and communication [71]. The number of antennas has been continuously increased together with the frequency bands allocated for cellular use. Even so, the volume reserved for the antennas has remained the same or even reduced.

The research work during the past decade has been focusing on the importance and the need to cover multiple and ever larger bandwidths used in smartphone systems. The multiband planar inverted-F antenna (PIFA) has greatly influenced the design of smartphone antennas which

implements volume sharing principles to enable different portions of the antenna to be excited in different frequency bands. Furthermore, they exhibit an inherently low specific absorption rate (SAR) and can be installed above other components [17].

The concept of multiband PIFA can be further extended to reconfigurable PIFA to comply with the objectives of this research work. The design of reconfigurable PIFA in this research work is inspired from the previous work in [72]. The reconfigurable PIFA is reconfigured with a PIN diode and a varactor to operate in USPCS (1.85 – 1.99 GHz), WCDMA (1.92 – 2.18 GHz), m-WiMAX (3.4 – 3.6 GHz) and WLAN (5.15 – 5.825 GHz) frequency bands.

It is reported that m-WiMAX band of 2.3 - 2.4 GHz is used in South Korea, Malaysia, Singapore and other East Asian countries. Another band of 2.5 – 2.7 GHz is implemented in Japan, Russia and Taiwan. The third band which is being used in China, Italy and Philippines, is from 3.4 – 3.6 GHz [73].

2.12 Third-Order Intermodulation Distortion (IMD) Products

Linearity has become a crucial device characteristic for wireless application systems which require high power RF signals as it dictates the independence of device impedance from RF input power [74]. The linearity of such systems is often limited by active switching and tuning devices [75]. Hence, there is a growing and continuous works that are dedicated to improving the linearity of active switches at high frequencies. The integration of nonlinear active switches in reconfigurable antennas will degrade the antenna performance as the switches will generate intermodulation distortion (IMD) products [76].

IMD products are multi-tone distortion products that result when two or more signals are present at the input of a nonlinear device [77]. All semiconductor-based switches or tuning devices inherently will still exhibit a degree of nonlinearity even though they have been biased for linear operation [78]. These IMD products may be radiated by the antenna or reflected back through the feed networks.

A case in particular is the third-order IMD products. For instance, if two signals are separated by 1 MHz, then the third-order IMD products will be at 1 MHz on either side of the two fundamental signals. Third-order IMD products appear at frequencies which are the closest to the fundamental frequencies. As a result, they are very likely to fall in-band and will add to the nonlinearity and distortion to the output signals [79]. In communication systems, the occurrence of this behaviour arising from signals in one channel will cause interference to adjacent channels.

A practical example can be observed in a cellular system. Whenever strong signals from more than one transmitter are present at the input to the receiver, IMD products will be generated. The level of these undesired products is a function of the power received and the linearity of the receiver or pre-amplifier [77]. In this case, the third-order IMD products are of particular concern for those reasons discussed previously.

Thus, a metric of third-order IMD products is very important for evaluating linearity performance of reconfigurable antennas [74]. As the spectrum becomes busier and the channels are tightly spaced, RF researchers and engineers should find ways to minimize IMD products.

2.12.1 Model of Intermodulation Distortion (IMD) Products

Radio channels that are used to transmit signals should occupy a frequency bandwidth, BW. In other word, the circuit components that are involved in the transmission of signals no longer have just a single frequency applied to them. A simple test signal that at least partially mimics the occupied bandwidth consists of two sinusoidal oscillations with the same amplitude, $\mathbf{A}_1 = \mathbf{A}_2$ and a frequency spacing of BW [80]. This is known as a two-tone signal. Typically, the normally encountered frequency spacing of $f_1 - f_2$ is from 10 kHz to 10 MHz. Consider a two-tone input voltage consisting of two closely spaced frequencies of f_1 and f_2:

$$v_{in}(t) = \mathbf{A_1}\, cos(2\pi f_1 t + \varphi_1) + \mathbf{A}_2 cos(2\pi f_2 t + \varphi_2) \qquad 2\text{-}1$$

In principle, in the absence of memory effects, the output signal can be approximated by Taylor series. In the most general sense, the output response of a nonlinear circuit can be modeled in terms of the input signal voltage [81]. Thus, by inserting the equation into the Taylor series in Equation **2-2** below with a maximum k value of 3, a set of results can be summarized in Table 2.4.

$$v_{out}(t) \approx a_o + a_1 \cdot v_{in} + a_2 \cdot v_{in}^2 + \cdots + a_k \cdot v_{in}^k \qquad 2\text{-}2$$

Where: the Taylor coefficients can be defined as:

$$a_o = v_{out}(0) \qquad \text{(DC output)} \qquad 2\text{-}3$$

$$a_1 = \left.\frac{dv_{out}}{dv_{in}}\right|_{v_{in}=0} \qquad \text{(Linear output)} \qquad 2\text{-}4$$

$$a_2 = \left.\frac{d^2 v_{out}}{dv_{in}^2}\right|_{v_{in}=0} \quad \text{(Squared output)} \qquad 2\text{-}5$$

$$a_k = \left.\frac{d^k v_{out}}{dv_{in}^k}\right|_{v_{in}=0} \quad (k^{th} - \text{output}) \qquad 2\text{-}6$$

Table 2.4: Intermodulation (IMD) products

Component	Formula
DC component	$0.5 \cdot a_2(\mathbf{A}_1^2 + \mathbf{A}_2^2)$
Fundamentals (First harmonic)	$a_1\mathbf{A}_1 \cdot cos(2\pi f_1 t + \varphi_1)$ $a_1\mathbf{A}_2 \cdot cos(2\pi f_2 t + \varphi_2)$
Second harmonic	$(0.5 \cdot a_2\mathbf{A}_1^2) \cdot cos(2 \cdot 2\pi f_1 t + 2\varphi_1)$ $(0.5 \cdot a_2\mathbf{A}_2^2) \cdot cos(2 \cdot 2\pi f_2 t + 2\varphi_2)$
Second-order IMD products	$a_2\mathbf{A}_1\mathbf{A}_2 \cdot cos(2\pi(f_1 - f_2)t + \varphi_1 - \varphi_2)$ $a_2\mathbf{A}_1\mathbf{A}_2 \cdot cos(2\pi(f_1 + f_2)t + \varphi_1 + \varphi_2)$
Third harmonic	$0.25 \cdot a_3\mathbf{A}_1^3 \cdot cos(3 \cdot 2\pi f_1 t + 3\varphi_1)$ $0.25 \cdot a_3\mathbf{A}_2^3 \cdot cos(3 \cdot 2\pi f_2 t + 3\varphi_2)$
Third-order IMD products	$0.75 \cdot a_3\mathbf{A}_1^2\mathbf{A}_2 \cdot cos(2\pi(2f_1 + f_2)t + 2\varphi_1 + \varphi_2)$ $0.75 \cdot a_3\mathbf{A}_1^2\mathbf{A}_2 \cdot cos(2\pi(2f_1 - f_2)t + 2\varphi_1 - \varphi_2)$ $0.75 \cdot a_3\mathbf{A}_1\mathbf{A}_2^2 \cdot cos(2\pi(2f_2 + f_1)t + 2\varphi_2 + \varphi_1)$ $0.75 \cdot a_3\mathbf{A}_1\mathbf{A}_2^2 \cdot cos(2\pi(2f_2 - f_1)t + 2\varphi_2 - \varphi_1)$

Figure 2.11 illustrates IMD products and their relative frequencies [79]. The order of IMD products corresponds to the sum of the orders of the components involved. For instance, for the product at the frequency of $2f_1 - f_2$, the order can be calculated as 2 + 1 = 3.

Linearity performance of reconfigurable antennas can be investigated in terms of a few other parameters which have been reported and investigated in open literature. Previous works which are discussed in Section 2.13 have listed the following as crucial parameters when it comes to nonlinearity measurements and are illustrated further in Figure 2.12.

i. Third-order intermodulation distortion (IMD3) products

ii. Third-order input intercept point (IIP3)

iii. Third-order output intercept point (OIP3)

iv. 1-dB gain compression point ($P_{1\text{-dB}}$)

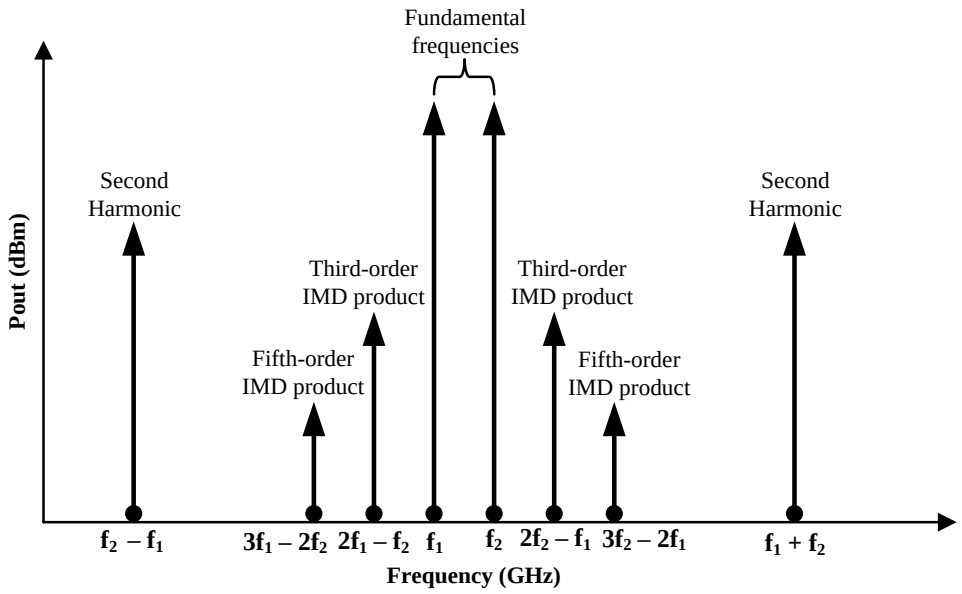

Figure 2.11: The locations of IMD products with respect to their fundamental frequencies [79]

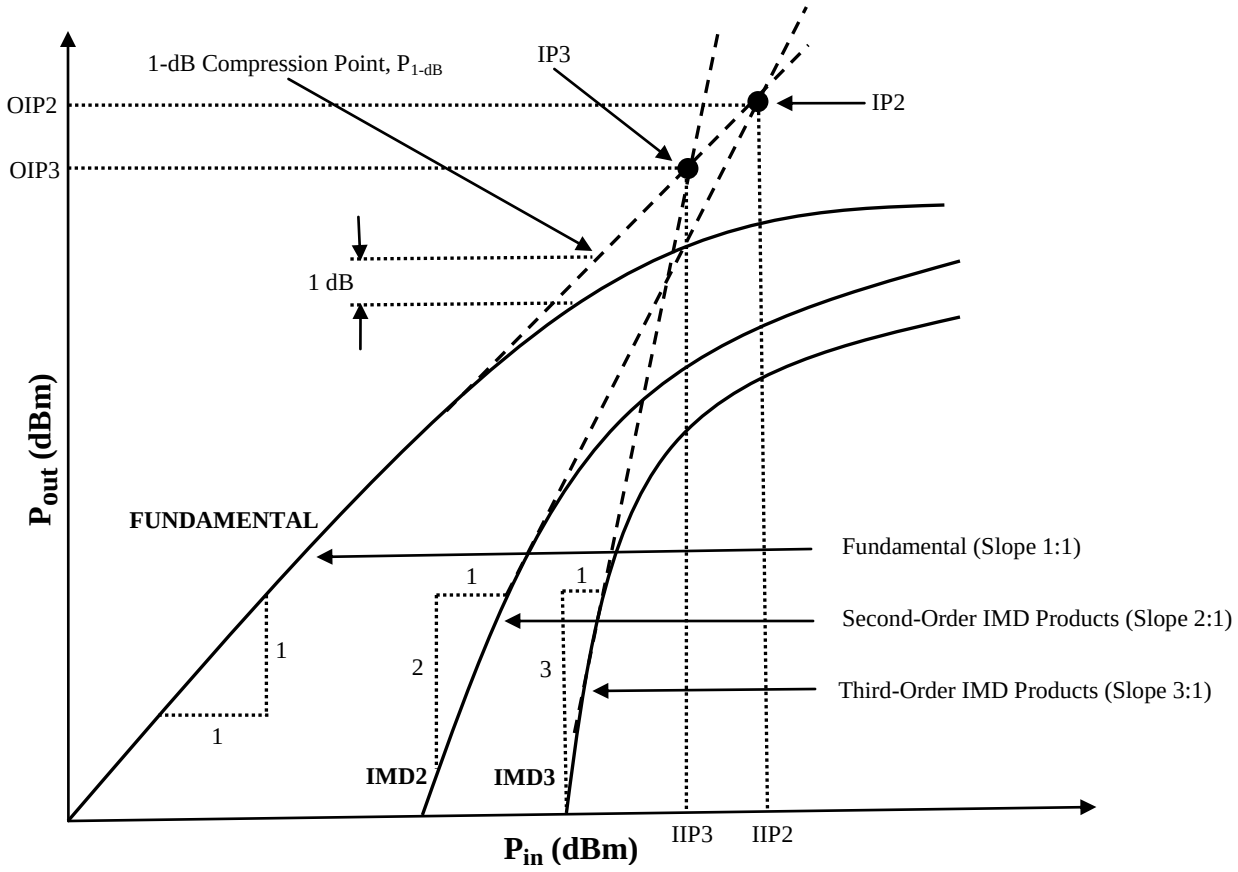

Figure 2.12: Crucial parameters in nonlinearities measurement [82]

From Figure 2.12, if the input and output power of a two-tone signal are applied to reconfigurable antennas and their IMD products are graphed on a log-log scale, the fundamental tone will have a slope of 1, the second-order IMD products will have a slope of 2 and the third-order IMD products will have a slope of 3. Within its linear region, the output power, P_{out} of the fundamental tone will increase at the same rate as the input power, P_{in}. However, P_{out} will not be able to keep pace with the linear increase of P_{in} beyond the linear region. The point at which P_{out} is reduced by 1-dB from the expected value is called the 1-dB compression point, $P_{1\text{-dB}}$ [81]. It is also known as the 1-dB gain compression point. By extending the lines, the second and third-order intercept

points (IP2 and IP3, respectively) can be located. The points at which IP2 and IP3 are located are being introduced for global characterization [80]. These are fictitious points where the P_{out} of the fundamental tone, second and third-order IMD products are having the same values. If they are referred to the P_{in} of the horizontal axis, they are called the input intercept points of IIP2 and IIP3 whereas if they are referred to the P_{out} of the vertical axis, they are called the output intercept points of OIP2 and OIP3.

From the industrial point of view, linearity performance of RF antenna switch is becoming a crucial specification. This results from the requirement to reduce intermodulation and cross-modulation from one or more receiver and transmitter paths. The Third Generation Partnership Project (3GPP) Mobile Broadband standard is used by the industry to determine the degree of switch linearity which is evaluated from the specification of third-order input intercept point (IIP3) [3].

Each new generation of cellular network requires progressively higher linearity. This is evident from Table 2.5 provided by Intel Mobile Corporation (2012) which stated that the Second Generation (2G) requirement for switch linearity was an IIP3 of 55 dBm, the Third Generation (3G) switch requirement was 65 dBm while the Long Term Evolution (LTE) switch IIP3 requirement was set to 72 dBm.

Table 2.5: Cellular network linearity requirements from Intel Mobile Corporation (2012)

Network	IIP3 of Switch Linearity Specification (dBm)
2G	55
3G	65
3.9G	72
4G	≈ 90

2.12.2 Measuring Linearity of Reconfigurable Antennas

The following formulas are applied to calculate IMD products based on the measurement results. If f_1 and f_2 are the frequencies of the two tones, the third-order IMD products will occur on both sides of these tones at $2f_2 - f_1$ and $2f_1 - f_2$. Figure 2.13 shows the output spectrum of a nonlinear circuit with two-tone input signal at f_1 and f_2 [80]. By assuming that the power levels of the two tones are equal, IMD3 is the difference between the power of the fundamental signals and the third-order IMD products. This is also known as third-order intermodulation suppression, IMD3. It can be defined as in Equation 2-7 below:

$$IMD3 = P_{out} - P_{out3} \text{ (dBc)} \qquad 2\text{-}7$$

Where: P_{out} is the power level of one of the fundamental tones

P_{out3} is the power level of one of the output of IMD3 products

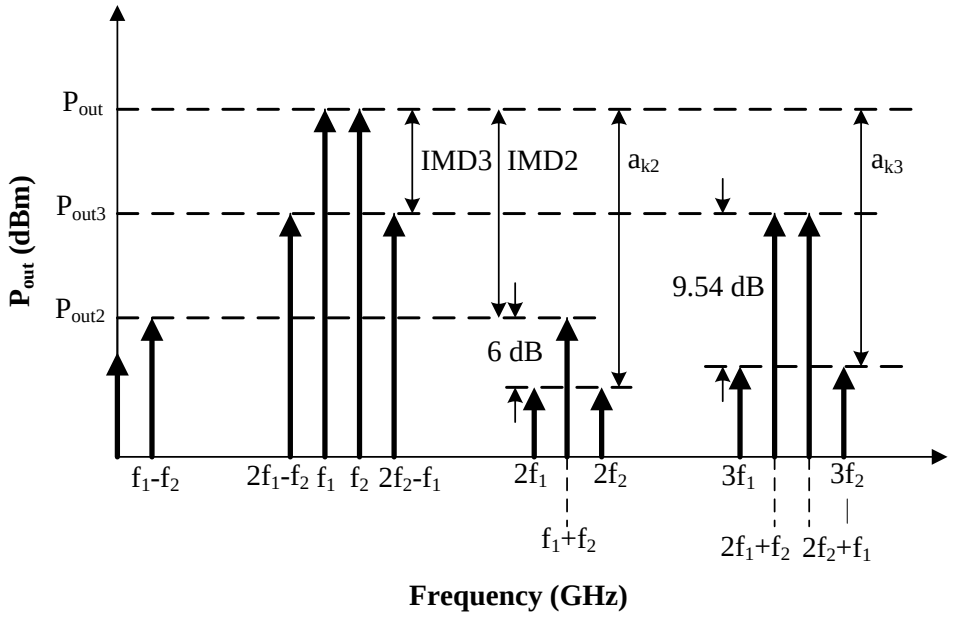

Figure 2.13: Output spectrum of a nonlinear circuit with two-tone input signal at f_1 and f_2 [66]

Once the value of IMD3 has been obtained, the output third-order intercept point (OIP3) can be calculated by using Equation 2-8 :

$$OIP3 = \frac{IMD3}{2} + P_{out} = \frac{1}{2}(3P_{out} - P_{out3}) \text{ (dBm)} \quad 2\text{-}8$$

From Equation 2-8, the input third-order intercept point (IIP3) can be obtained from Equation 2-9 below:

$$IIP3 = OIP3 - G \text{ (dBm)} \quad 2\text{-}9$$

Where: G is the gain of reconfigurable antenna

From Figure 2.13, the second-order intermodulation distortion (IMD2), second harmonic suppression (a_{k2}) and third harmonic suppression (a_{k3}) can also be calculated. The IIP3 value quantifies third-order linearity of the antenna. The two tones injected into the device under test (DUT) or in this case, the reconfigurable antenna must be free from any third-order products. A three or four-port vector network analyzer based on multiple source concept is capable of simultaneously generating the f_1 and f_2 frequencies with two internal generators [83]. Network analyzers that only have one internal generator will require an external signal generator for this application. These two tones will then be combined before the DUT input and as such, they must be well isolated. If they are not well isolated, the signals will intermodulate with each other and cause mutual intermodulation distortion at the output stage of the generators.

For this purpose, an internal combiner is available in some network analyzers. If it is not the case, the following devices are suitable for this purpose and can be applied externally:

(i) Power divider / Splitter / Combiner

(ii) Directional coupler

The broadband bandwidth of a power divider is an advantage of its usage. However, a note must be taken that it has an insertion loss of 6 dB [80]. A directional coupler, on the other hand, can be configured to have an insertion loss of about 3 dB. In addition, such a device offers significantly better decoupling of both generators when properly designed. Typical circuit diagrams of power divider and directional coupler can be seen in Figure 2.14

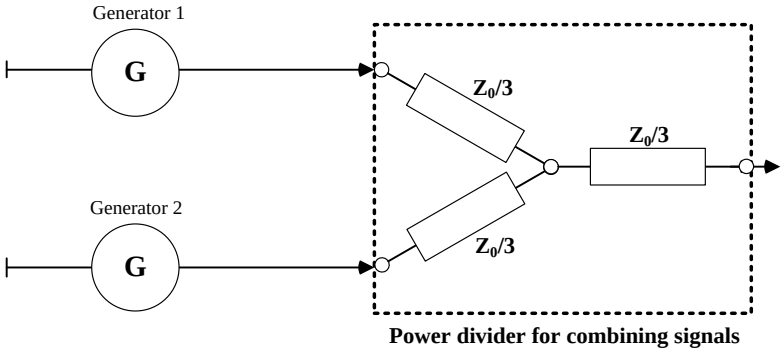

(a)

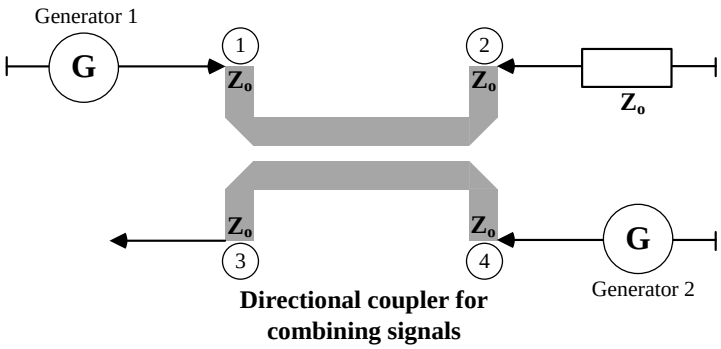

(b)

Figure 2.14: Combination of two generator signals;
(a) Power divider (b) Directional coupler [80]

2.13 Previous Work on Nonlinearity Performance Measurements

To date, there are fairly a limited number of papers in the open literature that have reported on full wave analysis of linearity performance and nonlinearity measurements of active-switch reconfigurable antennas. Instead, most of the available papers that contain nonlinearities discussion in some parts of the publication are diverted to active tuning devices. The varactor diode is one particular example. Thus, the next few paragraphs will discuss the previous works on nonlinearity measurements performed on varactor-controlled reconfigurable antennas.

A few papers have been reported that performed measurements of radiated and received IMD products when varactor diodes are integrated in their tunable antennas [84-86]. Work in [85] has provided the initial study of harmonic generation and IMD products when two reverse biased varactor diodes are integrated on a 1.4 GHz microstrip patch antenna for automatic detuning. It is evident from their work that the use of active nonlinear devices for detuning will lead to some signal distortion problems. Figure 2.15 illustrates their experimental setup to measure the IMD products for power levels similar to those transmitted by a mobile handset. In the transmitting mode, the presence of product levels will be much higher than when the handset is in the receiving mode but in this case, they serve to illustrate the effect.

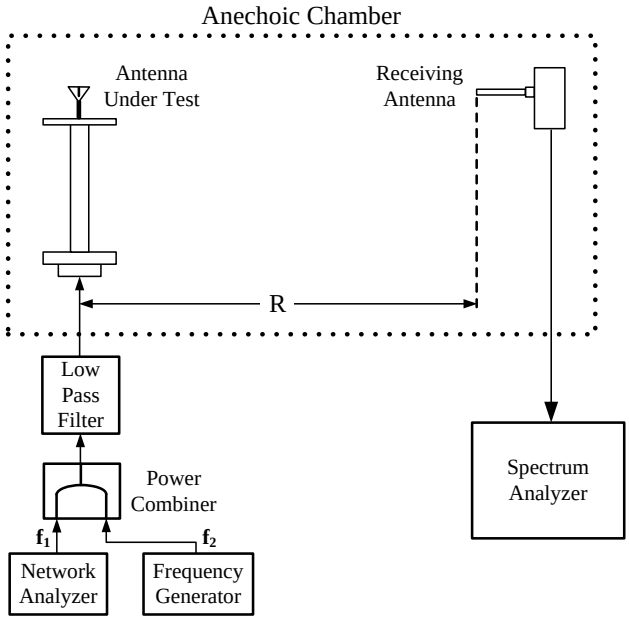

Figure 2.15: Experimental arrangement for measurement of IMD products [85]

Figure 2.16 shows the measured received spectrum which has been normalized to the level of the highest signal received at the distant antenna. The third-order IMD products are found at about 40 dB down on the peak signal. The fundamental signals are separated by 50 MHz at 1.325 and 1.375 GHz.

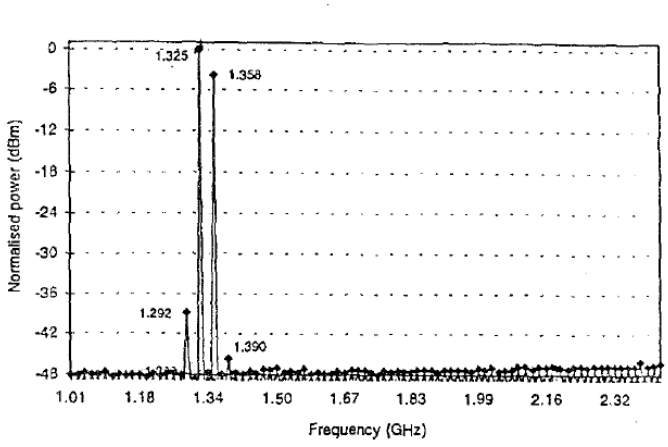

Figure 2.16: Measured received spectrum in the transmit mode in [85]

Work done by Kaliakis and Hall in [87] has investigated the power generated by harmonics in a quarter and a half-wavelength long frequency reconfigurable varactor-tuned antennas by means of harmonic isotropic radiated power (HIRP). This has been identified as the first work to demonstrate a full wave analysis to address the problem of harmonic generation due to varactor loading for half-wavelength and quarter-wavelength patches. During that particular time of the work is conducted, quarter wavelength microstrip antennas and variations were gaining popularity as system elements due to their small size. The experimental setup for the measurement of harmonic radiated power is depicted in Figure 2.17.

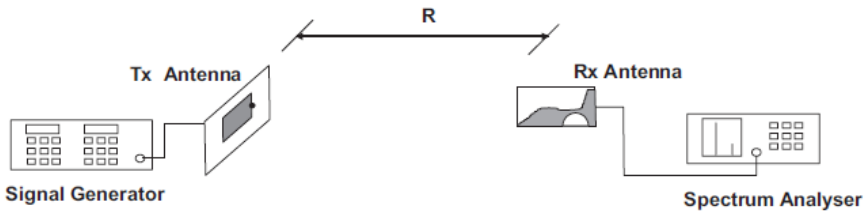

Figure 2.17: Harmonic radiated power for measurement setup in [87]

At the same time, radiation patterns at second harmonic for both quarter and half-wavelength antennas have been calculated and compared with experimental radiation patterns for different bias voltages. Patterns are measured by exciting the antenna at its second resonance. This is also the first work that has been reported in the literature. The radiation patterns are obtained and illustrated in Figure 2.18 and Figure 2.19.

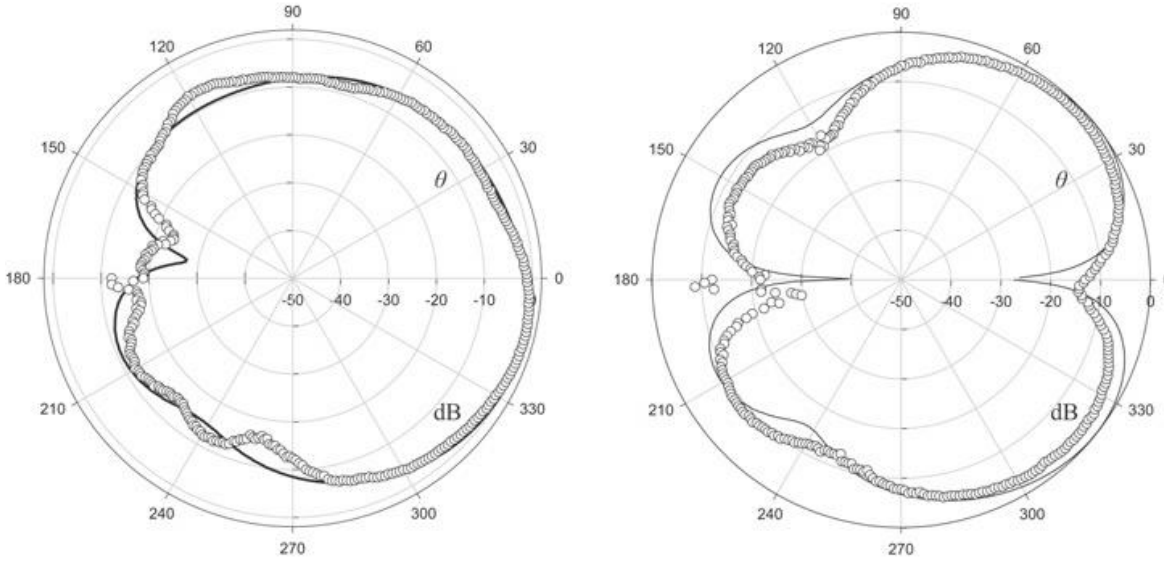

(a) (b)

Figure 2.18: Radiation patterns for a varactor loaded quarter-wavelength antenna at second harmonic with bias voltage of -2.5 V along; (a) E-plane (b) H-plane [87]

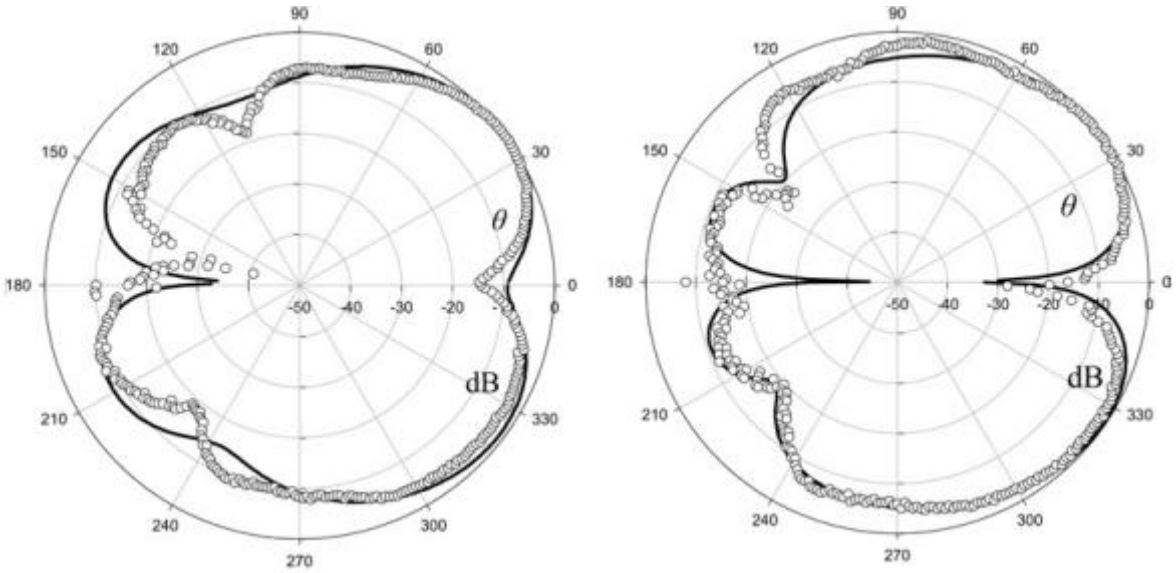

(a) (b)

Figure 2.19: Radiation patterns for a varactor loaded half-wavelength antenna at second resonance with bias voltage of -2.5 V along; (a) E-plane (b) H-plane [87]

From both figures, for the quarter- and half-wavelength antennas, the agreements are very good for the front lobe but there are slight disruptions for the back lobe due to the existence of a DC power supply in a form of metal case with feeding wires at the back of the ground plane.

White and Rebeiz [88] in their work have provided the measurement of 1-dB gain compression and input third order intercept point (IIP3) in the transmit mode. The measurement setup to measure IIP3 can be viewed in Figure 2.20. The experiment setup for $P_{1\text{-dB}}$ measurement is the same as in the setup to measure IIP3 except that only a single source is used at f_o. Therefore, there is no need to include a power combiner in the arrangement. $P_{1\text{-dB}}$ is measured by feeding a slot-ring antenna with a continuous-wave (CW) source and measuring the signal at one angle with a ridge-horn antenna and a spectrum analyzer. For IIP3 measurement, two CW sources separated by 100 kHz are combined with a power combiner. From the nonlinearity measurements, it can be concluded that reflection loss contributed significantly to the gain compression of the antenna at f_o due to a shift in the resonance frequency. This can be observed in the reflection coefficient graph of the antenna at 2 V bias voltage with different power levels as in Figure 2.21. The resonance frequency decreases with increased power levels because as the voltage swing across the diodes increases, the effective capacitance will also increase. For that reason, it can be concluded that $P_{1\text{-dB}}$ can be further improved by increasing the bias voltage as the power level is increased.

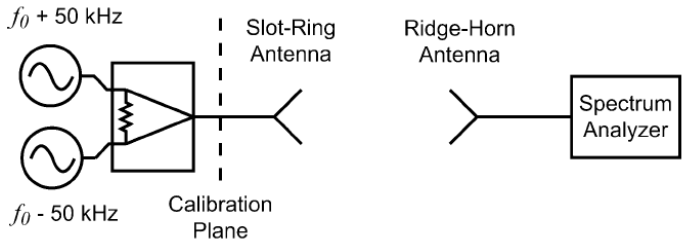

Figure 2.20: Experimental setup for IIP3 measurement in [88]

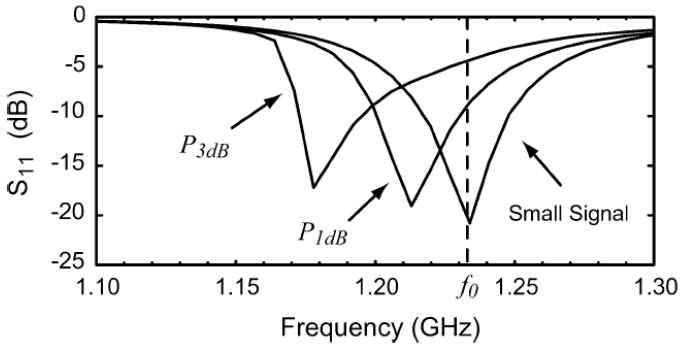

Figure 2.21: Measured reflection coefficient when V_b = 2 V at three different power levels: the small signal region (-20dBm) and the 1 and 3 dB compression points (1.2 and 5.4 dBm) [88]

Previous work done in [89] has conducted a comprehensive analysis of nonlinear effects of varactor diodes on their reconfigurable patch antenna. The effects of radiated, received and reflected IMD products on antenna performance have been studied. This is the first reported work of reflected IMD products measurement on reconfigurable antenna. In order to do so, two different varactor diodes - one is for reduced power consumption (SMV 1233) and the other one is for improved linearity (SMV 1235) - are used for comparison purposes and to examine the trade-offs between power consumption and linearity of the antennas. Further measurements have been made which are $P_{1\text{-dB}}$ and realized gain at varying input power levels which are measured from the co-polar radiated patterns along the *E*-plane. The radiation pattern measurements have

been performed to study the current distribution on the antenna as the gain compresses. From the radiation patterns in Figure 2.22, it can be observed that the measured gain decreases uniformly at all angles as the input power exceeds -6 dBm. Further investigation is performed which is the measurement of co- and cross-polarization radiated fields along *E* and *H* planes. From the measurement, the same trend is observed which suggest that the difference in current magnitude yields gain compression although the relative current distribution remains constant with varying input power levels. This can be viewed in Figure 2.23.

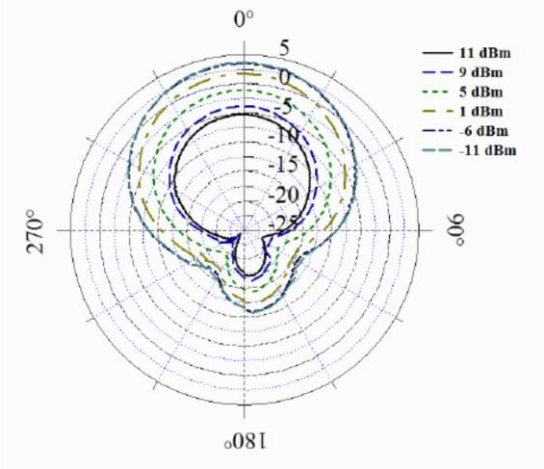

Figure 2.22: Measured realized gain along E-plane at 1.175 GHz with varying input power of reconfigurable antenna in [89]

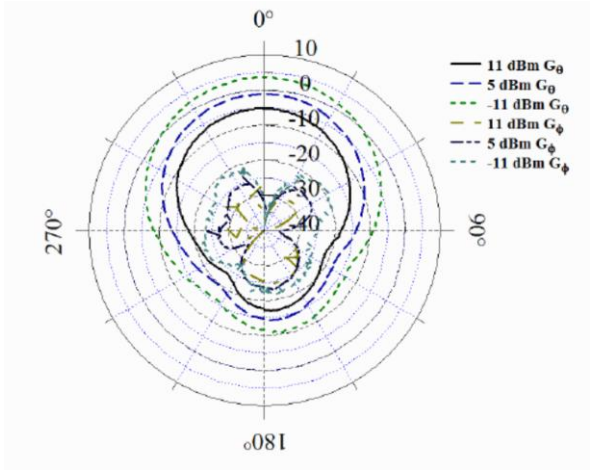

(a)

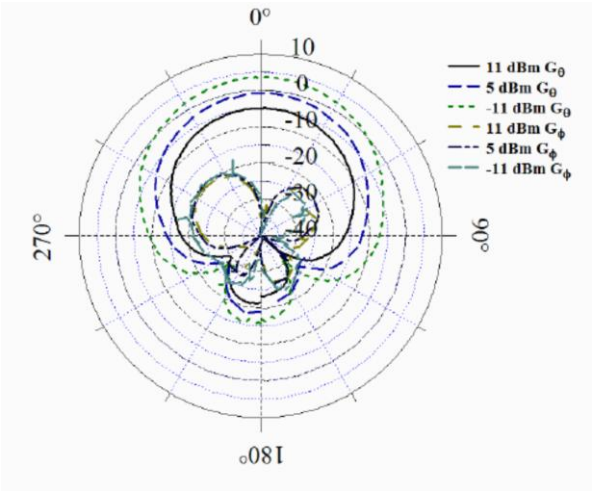

(b)

Figure 2.23: Co- and Cross-polar radiation patterns at 1.175 GHz with varying input power for reconfigurable antenna in; (a) Along E-plane (b) Along H-plane [89]

Recent work in [90] has investigated the maximum input power from the 1-dB compression point measurements of their reconfigurable antenna. From that measurement, they found that maximum input power of BB833 varactor diodes is limited to 17.6 dBm at 700 MHz. This has placed a constraint on the input power to achieve a linear operation with sufficient low power level of IMD components and lower diode self-biasing. Consequently, this behaviour will limit the

antenna to be used in some high power applications. Thus, a varactor diode with higher power rating and larger tuning range is required for long range cognitive radio communications. For that reason, they suggested that reconfigurable antennas which use active components should have an IIP3 specification to be placed on them. Schematic diagrams of the experimental arrangement to measure $P_{1\text{-}dB}$ and IIP3 in the transmit mode can be viewed in Figure 2.24.

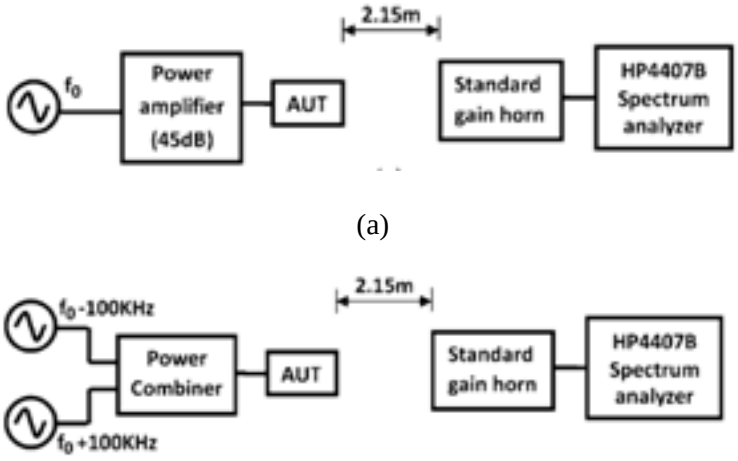

Figure 2.24: Experimental setup for; (a) $P_{1\text{-}dB}$ measurement (b) IIP3 measurement, both in [90]

Until recently, there is only one work which has been identified that performed an analysis of harmonic distortions generated by their PIN diode wideband planar antenna having reconfigurable omnidirectional and directional patterns [91]. This paper discusses IMD products when nonlinear active switches are introduced into the antenna structure to allow pattern reconfigurability. The IMD products are evaluated using harmonic balance (HB) simulation as a part of a 2 x 2 MIMO system. This can be viewed in Figure 2.25. In a MIMO system, mutual coupling will exist when multiple antennas are integrated together which must be taken into account. The wide operation bandwidth has served as a motivation to evaluate the IMD products

that might be present in-band when the two antennas operate at different centre frequencies. They have shown that, in both omnidirectional and directional operation of their antenna, the quality of the signal is not significantly affected by the nonlinearity of the PIN diodes. This is due to the fact that the distortions generated are still below -110 dBm noise floor for higher mutual couplings (worst case). For low coupling, the third-order IMD products are out-of-band. This can be further illustrated by the graphs in Figure 2.26.

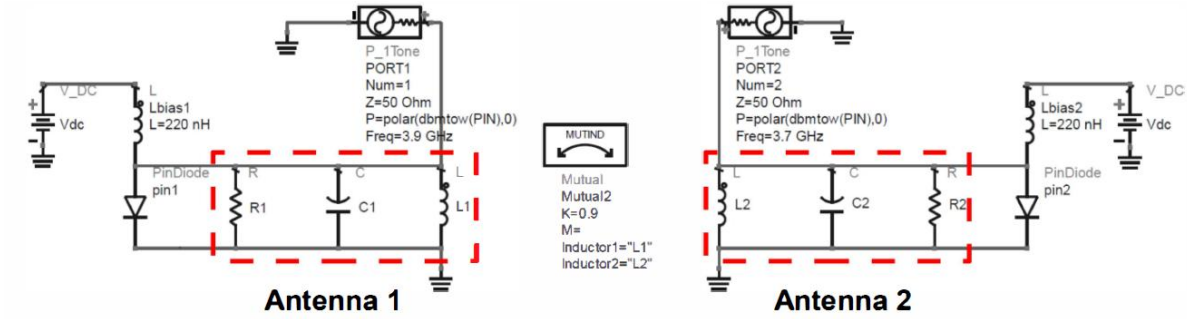

Figure 2.25: Circuit schematic of two reconfigurable omni-directional antennas which emulates coupling in 2 x 2 MIMO antenna system in [91]

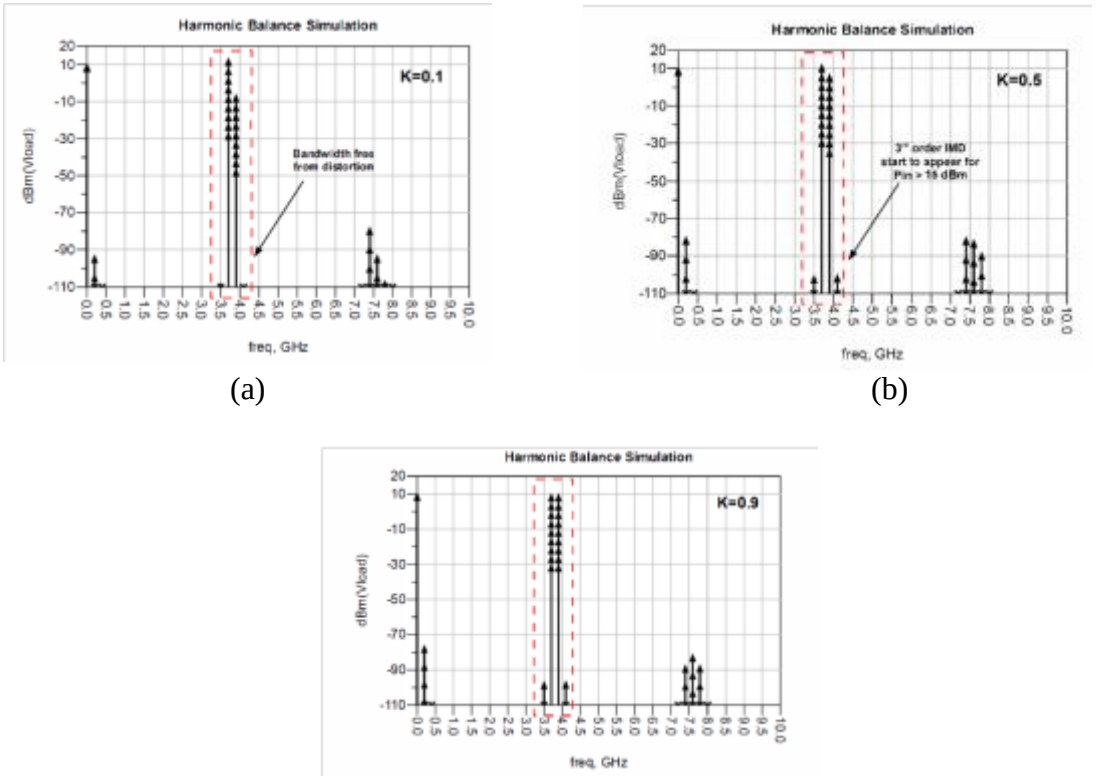

Figure 2.26: Harmonic balance simulation with both antennas in omni-directional mode: (a) Low coupling, k = 0.1 (b) High coupling, k = 0.5 (c) Very high coupling, k = 0.9 [91]

As far as RF MEMS switch is concerned, there is no work available in the open literature that reported on linearity performance of RF MEMS-based reconfigurable antennas. Most of the work discussing linearity measurements of RF MEMS switches were performed on other reconfigurable microwave devices other than antennas such as tunable filters [92-94] , phase shifters [95] and power amplifiers [96].

Only one previous work has been identified in the literature which involved the design and fabrication of reconfigurable antenna for cognitive radio (CR) applications using GaAs FET switches [97]. However, nonlinearity measurements are not conducted in their work. As a result,

they have successfully reconfigured an ultra-wideband (UWB) antenna to work in multiple frequency bands using two GaAs FET switches to connect and disconnect four stubs of different lengths to the main feed line of the circular monopole antenna. Four main frequency bands have been reconfigured and they are 2.1 – 2.6 GHz, 3.4 – 3.6 GHz, 2.8 – 3.4 GHz and 4.9 – 5.8 GHz. The antenna configuration can be seen in Figure 2.27.

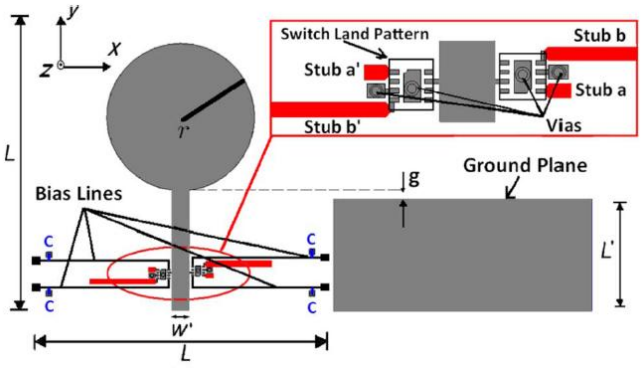

(a) (b)

Figure 2.27: Reconfigurable UWB monopole antenna in; (a) Top view (b) Bottom view [97]

Previous work involving nonlinearity measurements has been further summarized and can be viewed in Table 2.6.

Table 2.6: Previous work on nonlinearity measurement of reconfigurable

Work	Application	Frequency	Active Device	Nonlinearity Measurements	Full Wave Analysis
[84]	Varactor tunable antenna	470 – 702MHz (DVB-H)	Varactor diode	IMD products in transmit mode	NO
[85]	Microstrip patch antenna	1.4 GHz	Varactor diodes	IMD products in transmit mode	NO
[86]	Leaky-wave antenna	3.33 GHz	Varactor diodes	IMD products in transmit and receive modes	NO
[87]	Quarter-wavelength and half-wavelength microstrip antenna	• 1.2 – 1.65 GHz for quarter-wavelength antenna • 1.48 – 1.75 GHz for half-wavelength antenna	Varactor diodes	• Power generated at second harmonics • Radiation patterns plotted at second harmonics	YES
[88]	Single and dual-polarized tunable slot-ring antenna	0.95 – 1.8 GHz	Varactor diodes	• 1-dB compression point, $P_{1\text{-}dB}$ • IIP3 (Both in transmit mode)	NO
[89]	Microstrip slot antenna	1.1625 – 1.185 GHz	Varactor diodes	• IMD products in transmit, receive and reflect modes • 1-dB compression point, $P_{1\text{-}dB}$ in transmit mode and realized gain at varying input power • Single tone radiation patterns at varying input power to study the relative current distribution and current magnitude that cause gain compression	YES
[90]	Printed Yagi-Uda dipole antenna	478 – 741 MHz (UHF TV band)	Varactor diodes	• 1-dB compression point, P_{1dB} • IIP3 (Both on transmit mode)	NO
[91]	Microstrip antenna	• Omnidirectional mode centered at 3.8 GHz • Directional mode centered at 3.8 GHz	PIN diode	Harmonic balance (HB) simulations in 2×2 MIMO system to investigate the third order IMD products in the transmit mode	YES
[97]	UWB monopole antenna	• 2.1 – 2.6 GHz • 3.6 – 4.6 GHz • 2.8 – 3.4 GHz • 4.9 – 5.8 GHz	GaAs FET	No nonlinearity measurements	NO

Based on the previous works reviewed and the summary from Table 2.6, there are a few gaps in the open literature which has yet to be filled and foresee the need to be addressed. They are listed as follows:

i. Papers on full wave analysis on nonlinearity measurements of reconfigurable antennas in the open literature are still lacking. Most of the papers identified are using varactor diodes to tune the frequency bands with brief analysis on nonlinear distortions which left a broad gap for research work involving reconfigurable antennas with active switches. To date, there are no papers in the literature discussing nonlinearity of reconfigurable antennas using FET and RF MEMS switches. Only one full paper has been identified which discusses the nonlinearity of PIN diodes on their reconfigurable antennas in terms of IMD3 products in transmit mode [91]. However, the outcomes are solely based on the simulation (harmonic balance) results. There are no experimental measurements involved.

ii. The paper identified do not include comprehensive nonlinearity measurements of their reconfigurable antennas. The nonlinearity measurements are only discussed in brief as part of the full paper. Only three previous works have been identified so far that have provided a full wave analysis of nonlinearity issues faced in their reconfigurable antennas. Two of which using varactor diodes to reconfigure the antennas [87, 89] and one using PIN diodes to reconfigure the pattern reconfigurable antenna [91].

iii. There are no measurements of radiation patterns at IMD frequencies have been performed on the reconfigurable antennas in the previous works. However, work in [87]

has measured the radiation patterns at the first and second harmonics. Single tone radiation patterns at various input power have been included in [89] to study the relative current distribution and current magnitude that are responsible in causing gain compression.

2.14 Conclusion

Based on the findings in this chapter, the topic of nonlinearity in reconfigurable antennas can be considered as another branch of research in the field of Antennas and Propagation. As can be concluded from the reviewed literature, the number of papers discussing nonlinear characteristics of active-switching reconfigurable antennas is still lacking. From the reconfiguration technology point of view, solid state switches such as PIN diode and FET switches have a good switching speed, they suffer from poor linearity performance at high frequencies. On the other hand, RF MEMS switch have gained much interest due to their excellent linearity performance but high cost will become an impending factor apart from the slow switching speed if they are to be used in mass production of reconfigurable antennas. Thus, the study of nonlinearity in reconfigurable antennas was conducted to further understanding and clarifies the nonlinear effects of active switches to the performance of reconfigurable antennas. Crucial parameters to measure the nonlinearity performance of the antennas have been identified and were performed. The results obtained from the nonlinearity measurements of the reconfigurable antennas were analyzed and compared with the reference antennas that employ copper bridges as linear interconnection.

CHAPTER 3

3. RECONFIGURABLE PIFA WITH BAR50-02V PIN DIODE

3.1 Introduction

A reconfigurable multiband PIFA with positive-intrinsic-negative (PIN) diode switching and the nonlinearity measurements are discussed in this chapter. A preliminary study was conducted to observe the antenna characteristics before the complete structure of switchable reconfigurable antenna with PIN diode was simulated and fabricated. The antenna geometry and dimensions are similar for all reconfigurable antennas in this research work but with different biasing circuits. In fact, one of the challenges lies in the design of the biasing circuit itself. Due to the sensitivity of the switch, the biasing circuit must be designed in such a way as not to adversely affect the performance of the switch. In addition, a proper biasing circuit will avoid any physical damage to the PIN diode. The fundamentals of PIN diodes are discussed briefly in the next section.

3.1.1 Fundamentals of PIN Diodes

Based on the references in the literature, the PIN diode is a widely used solid state RF and microwave switch to reconfigure the antennas. Since 1960s until the present time, the PIN diode has remained an efficient and exhaustively-studied solid state semiconductor switch [55]. There are various types of PIN diode in the market nowadays. Depending on the application, a suitable candidate can be selected. In general, the performance of a PIN diode is primarily dependent on chip geometry and the nature of semiconductor material in the finished diode, particularly in the I-layer [98]. A good PIN diode should have a long carrier lifetimes (τ) and very well controlled

I-layer thickness [55]. These characteristics will enhance the ability to control RF signals with minimum distortion while at the same time still using much smaller levels of direct current (DC) excitation.

To summarize, the PIN diode is a P-N junction with a wide intrinsic I-layer sandwiched between the P and N-layers. The I-layer acts as an insulator which determines the performance of a particular PIN diode. In terms of material used, the I-layer can be made from a wafer of almost intrinsically pure silicon [98]. Figure 3.1 shows the construction of a PIN diode. A PIN diode takes the advantage of a lightly doped I-layer sandwiched in between the highly doped P and N-layers which allow the PIN diode to act as a switch [99]. The PIN diode cross-section [55] can be viewed in Figure 3.2.

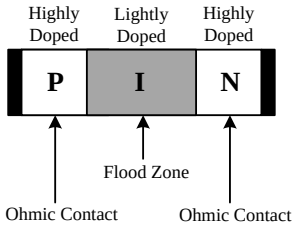

Figure 3.1: PIN diode construction [99]

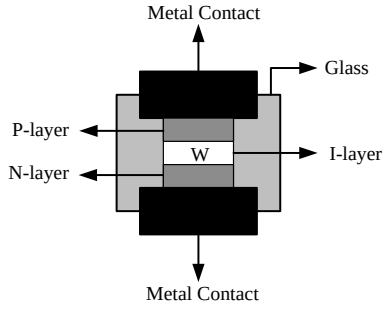

Figure 3.2: PIN diode cross-section [55]

The P-contact is the anode and the N-contact is the cathode during forward biased operation which can be seen in Figure 3.3. The highly doped layers preserve the low ohmic resistance since these are the contact points for the switch. During forward biased operation, the P and N-layers are charged and this will cause a high-level of carrier injection to take place in the I-layer. As a result, the diode will be flooded with electrons and holes to the point where it acts as a nearly perfect linear resistor. The electrons and holes will coexist in the I-layer for τ seconds where τ is the lifetime of charge carriers. The greater the τ in the I-region, the lower the frequency signals (commonly near 1 MHz) that the PIN diode is capable of handling. The more charge carriers, Q are injected into the I-layer, the greater the forward bias current, I_F that could pass through the PIN diode, the lower the forward bias resistance, R_S to the frequency signals. Thus, a PIN diode behaves like a variable resistor in forward biased operation [81]. In reverse bias, the diode is nonconductive. In this state, the depletion layer becomes fully depleted or in other words, the charge carriers do not get injected into I-layer [55]. Thus, the diode capacitance is independent of the level of bias since there is only a little remaining net charge in the I-layer. Furthermore, the depletion layer thickness is almost constant in reverse bias

because it is set by the I-layer thickness and this is the main reason for the constant value of the capacitance.

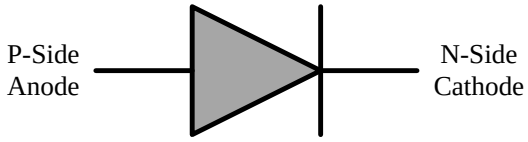

Figure 3.3: Schematic of PIN diode in forward biased

3.2 Preliminary Investigation

Prior to the design and fabrication stage of reconfigurable PIFA with BAR50-02V PIN diode, a few preliminary stages have been performed to investigate the reconfigurable PIFA characteristics in terms of reflection coefficient, current distribution, radiation patterns, realized gain, directivity and efficiency which will be elaborated further in this section.

3.2.1 Preliminary Study - Antenna Design with Copper Bridge

In the early stage to study the reconfigurable PIFA, a copper bridge was used to investigate the antenna's characteristics. The idea is to use copper bridge to connect the main and additional radiating planes to get a general understanding of the antenna's behaviour. The generic structure of the antenna is shown in Figure **3.4**. The radiating structure of the antenna with and without copper bridge can be viewed in Figure 3.4(e) and (f). The whole structure of the reconfigurable PIFA is also included for reference purpose. Detailed geometry and dimensions of the reconfigurable PIFA are discussed in Section 3.3.

The copper bridge was connected between the first and second radiating planes to represent the ON state. The copper bridge was then removed in the OFF state. Although its representation is not practical as it does not take into account the degradation of the switch to the performance of the antenna, the proof of concept is vital for comparison purpose with the readily available commercial switches in the market.

(a)

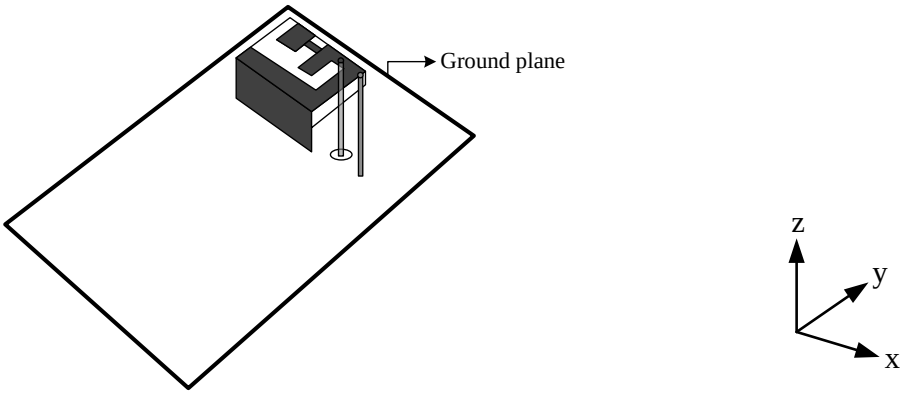

(b)

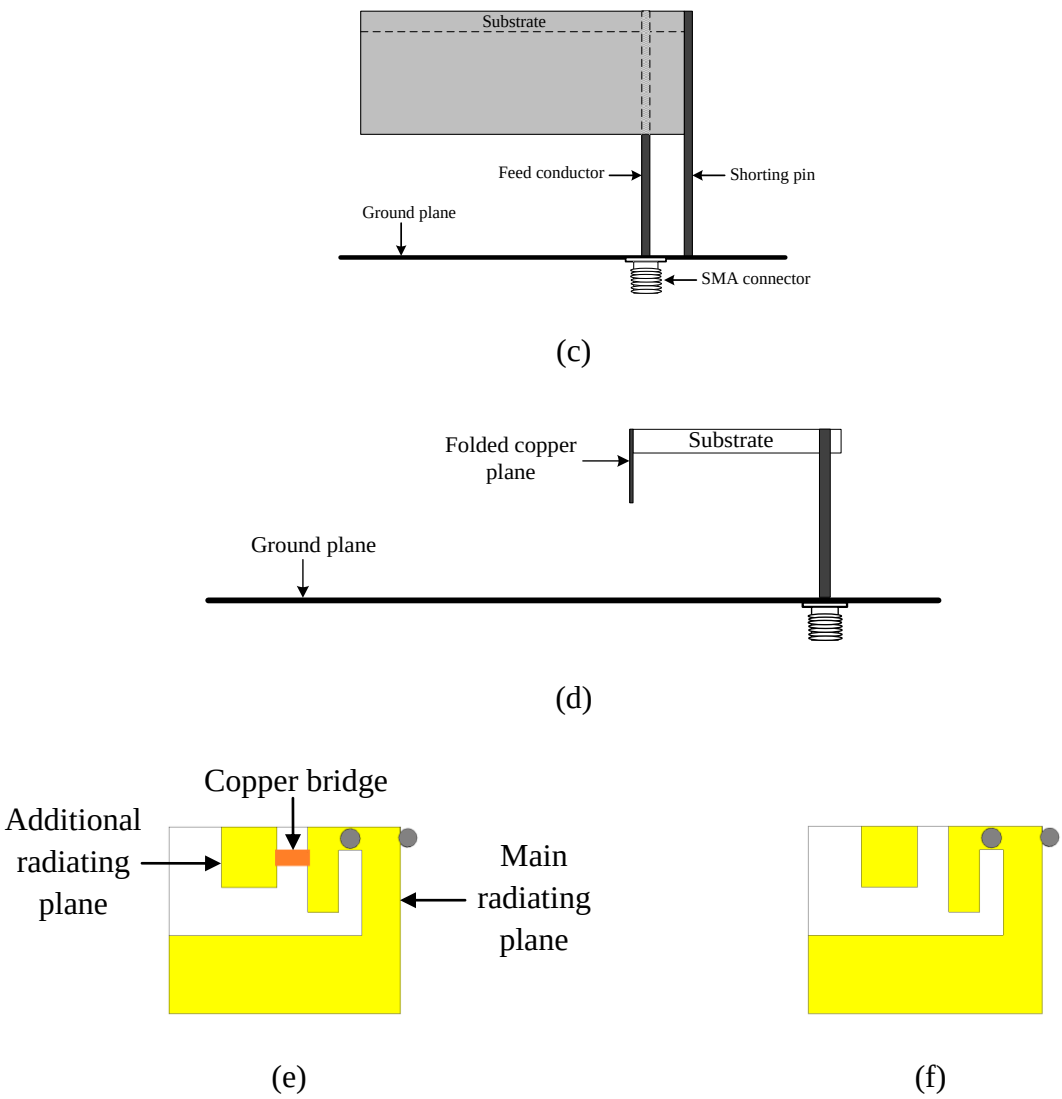

Figure 3.4: Structure of reconfigurable PIFA;
(a) Radiating planes (b) Top view (c) Front view (d) Side view
(e) With copper bridge to represent ON state (f) Without copper bridge to represent OFF state

3.2.1.1 Reflection Coefficient

The simulations were performed in CST MWS platform and the simulated reflection coefficients in both cases can be seen in Figure 3.5. Resonant frequency performance of the reconfigurable

PIFA with and without the copper bridge is further summarized in Table 3.1. From the table, when the copper bridge was connected between the planes to represent ON state, electrical current flows through the copper bridge and the copper resonant frequency is reduced to 4.03 GHz. The upper resonant frequency increases to 5.65 GHz when the copper bridge was removed in OFF state. In both states, the lower resonant frequency remains the same at 2.01 GHz.

This is consistent with the concept of electrical current length which dictates the location of each resonant frequency. The longer the electrical current path takes to complete the loop on the radiating structure of an antenna, the lower the resonant frequency. The case is the same during the presence of a copper bridge to interconnect the main and the second radiating planes. The copper bridge allows the current to flow through it from the main to the second radiating planes. Hence, the longer current path decreases the resonant frequency. Without the copper bridge, the current is mainly confined within the main radiating plane. Thus, the electrical current path is shorter which increases the resonant frequency.

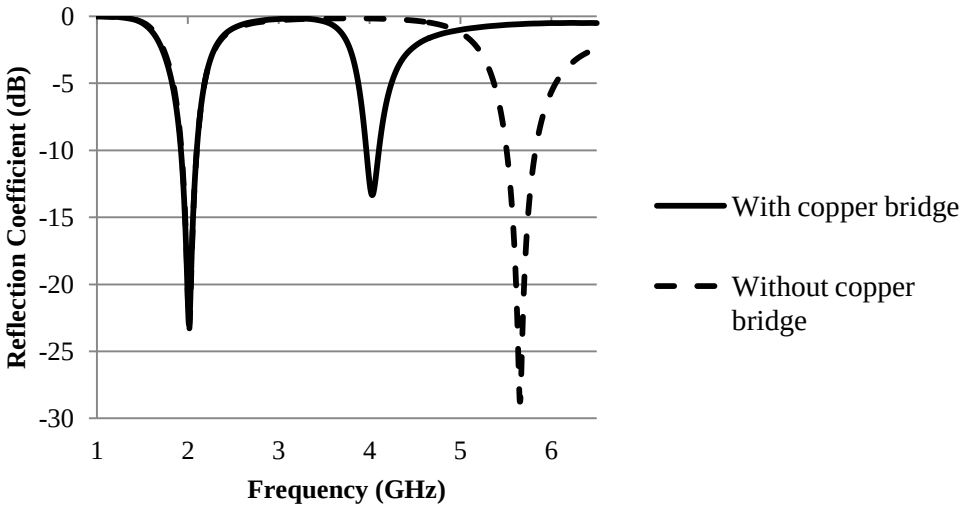

Figure 3.5: Reflection coefficient of reconfigurable PIFA with copper bridge (ON state) and without (OFF state) copper bridge

Table 3.1: Resonant frequency performance of reconfigurable PIFA with and without copper bridge

	Reconfigurable PIFA	
	With Copper Bridge	**Without Copper Bridge**
First resonant frequency, f_{r1} (GHz)	2.01	2.01
Second resonant frequency, f_{r2} (GHz)	4.03	5.65
6-dB Lower Bandwidth, BW_1 (MHz)	2.1601 – 1.8549 = **305.2**	2.1606 – 1.8652 = **295.4**
6-dB Upper Bandwidth, BW_2 (MHz)	4.2003 – 3.8986 = **301.7**	5.9776 – 5.4082 = **569.4**

3.2.1.2 Current Distribution

Current distributions on the radiating structure of the antenna were simulated to investigate their attributes to the resonant frequencies on the reflection coefficient graphs. Radiation patterns of an antenna are inherently related to the distributions of the currents on its surface [100]. Therefore, predetermination of these current paths allows prediction of radiation patterns at various

frequencies of operation. The current distributions were simulated in CST MWS software and can be divided into two parts which can be viewed in Figure 3.6 and Figure 3.7.

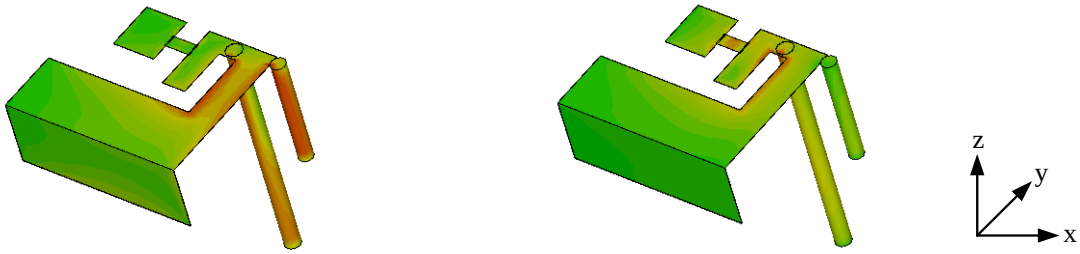

(a) (b)

Figure 3.6: Current distribution on the radiating structure of reconfigurable PIFA with copper bridge to represent ON state at; (a) 2.01 GHz (b) 4.03 GHz

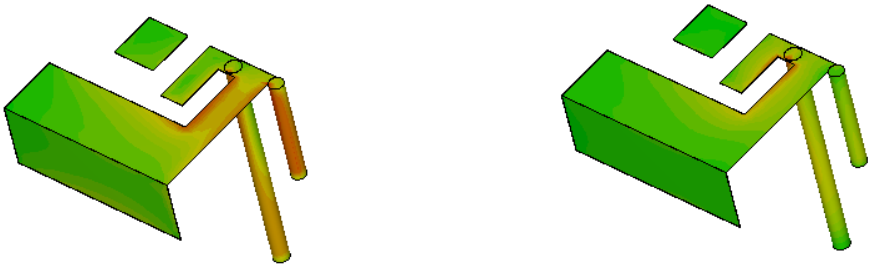

(a) (b)

Figure 3.7: Current distribution on the radiating structure of reconfigurable PIFA without copper bridge to represent OFF state at; (a) 2.01 GHz (b) 5.65 GHz

From Figure 3.6(a), the maximum current is concentrated on the edge of the main radiating plane, the feed line and the shorting pin at 2.01 GHz. In the upper resonant frequency of 4.03 GHz, the maximum current is further elongated to the copper bridge area and on the additional radiating plane which can be viewed in Figure 3.6(b). Thus, it is evident that in ON state (with copper bridge), the electrical current path travels from the main to additional radiating planes and this in

return, decreases the upper resonant frequency. A similar concentration of maximum current is observed on the folded part of the antenna at 2.01 GHz in OFF state (without copper bridge) as can be seen in Figure 3.7(a). At the upper resonant frequency of 5.65 GHz, the maximum current is concentrated mainly around the edge of the main radiating plane – the one which is close to the feed point as in Figure 3.7(b). Hence, the current path is shorter and as a result, the upper resonant frequency increases.

From the simulation results, it is evident that the placement of copper bridge in the radiating structure of the antenna to replace the switch will decrease the upper resonant frequency considerably if it is to be compared with the antenna without copper bridge to represent the OFF state. This knowledge is crucial before the reconfigurable PIFA with an actual active switch are simulated and fabricated.

3.2.1.3 Radiation Pattern

The co-polar radiation patterns in xy-, xz- and yz- planes of the reconfigurable antenna with copper bridge across the main and additional radiating planes to represent the ON state and without copper bridge to represent the OFF state can be viewed in Figure 3.8.

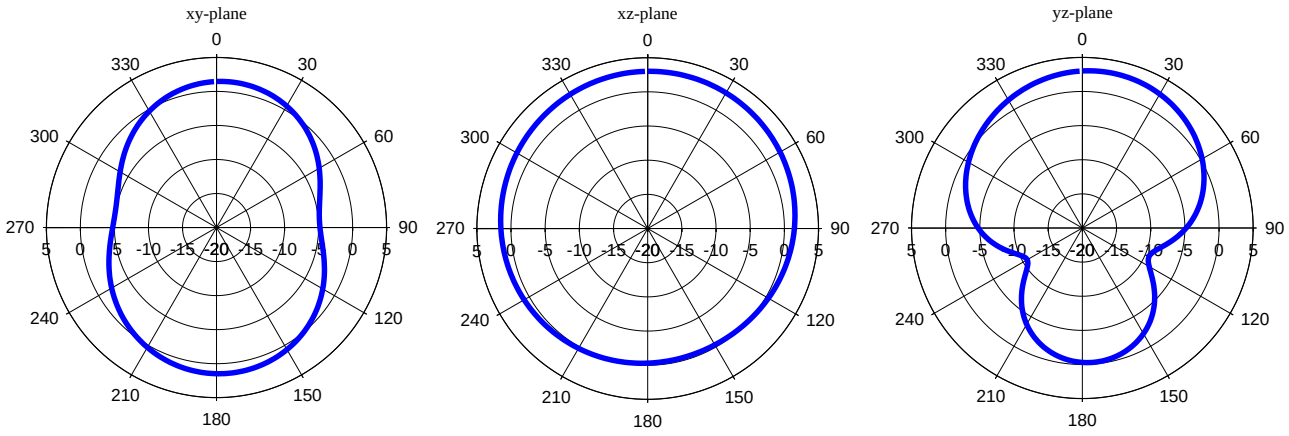
xy-plane
xz-plane
yz-plane
0
30
60
90
120
150
180
210
240
270
300
330
5 0 -5 -10 -15 -20 -15 -10 -5 0 5

(a)

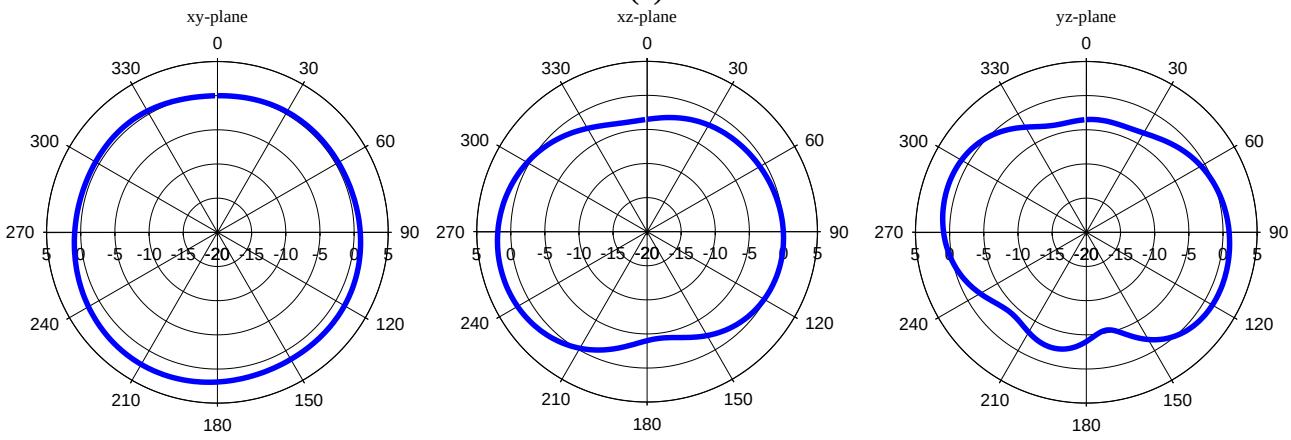
xy-plane
xz-plane
yz-plane
0
30
60
90
120
150
180
210
240
270
300
330
5 0 -5 -10 -15 -20 -15 -10 -5 0 5

(b)

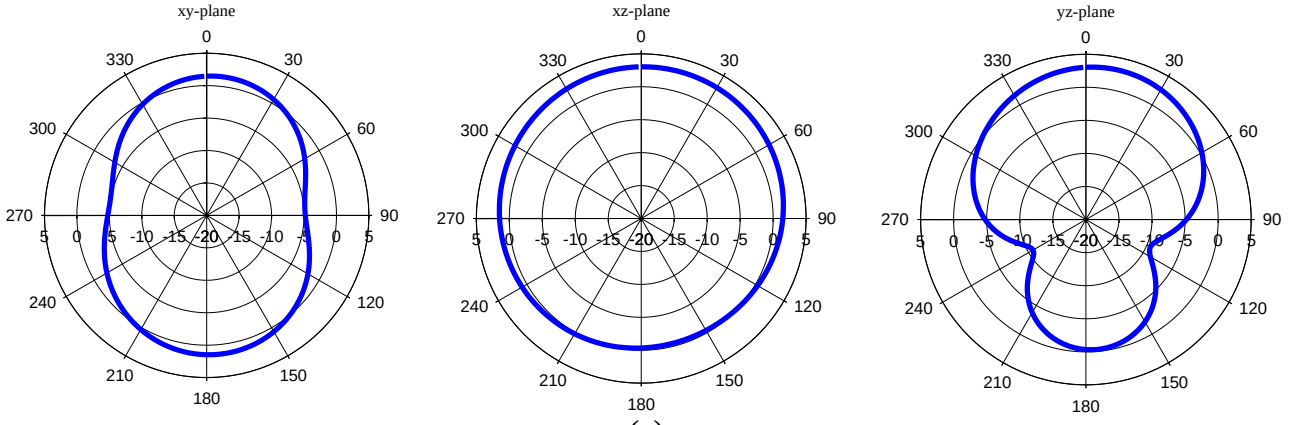
xy-plane
xz-plane
yz-plane
0
30
60
90
120
150
180
210
240
270
300
330
5 0 -5 -10 -15 -20 -15 -10 -5 0 5

(c)

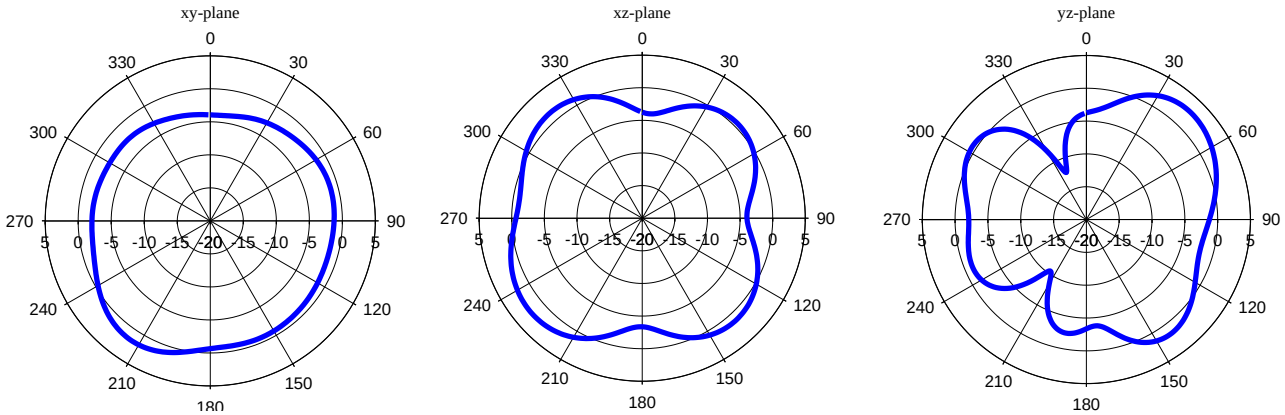

(d)

Figure 3.8: Co-polar radiation patterns in xy-, xz- and yz- planes of PIFA with copper bridge (ON state) at; (a) 2.01 GHz (b) 4.03 GHz and without copper bridge (OFF state) at; (c) 2.01 GHz (d) 5.65 GHz

3.2.1.4 Realized Gain, Directivity and Efficiency

The realized gain, directivity and efficiency of the reconfigurable PIFA are further summarized in Table 3.2. From the table, it can be observed that the gain, directivity and efficiency are consistently good at each resonant frequency. However, the efficiency at 4.03 GHz is 96.2% which is slightly lower. This can explained from the reflection coefficient graph of the reconfigurable PIFA with copper bridge in Figure 3.5. From the figure, the reflection coefficient at 4.03 GHz is slightly mismatched at -13.3 dB and this has reduced the radiation efficiency.

Table 3.2: Realized gain, directivity and efficiency of reconfigurable PIFA with copper bridge (ON state) and without copper bridge (OFF state)

	Reconfigurable PIFA			
	With Copper Bridge		**Without Copper Bridge**	
	f_{r1} = 2.01 GHz	f_{r2} = 4.03 GHz	f_{r1} = 2.01 GHz	f_{r2} = 5.65 GHz
Realized Gain, G (dB)	3.053	1.968	3.059	3.076
Directivity, D (dBi)	3.118	2.344	3.139	3.187
Efficiency, η (%)	99	96.2	98.7	97.5

3.2.2 Antenna Design with Only the Main Radiating Plane

The next simulation performed in CST MWS software involved the main radiating plane which was connected directly to the feed network. The main radiating plane consists of planar and folded parts. This simulation was performed to see the contribution of the main radiating plane to the frequency reconfiguration of the antenna and how the additional radiating plane will affect the reflection coefficient. The main radiating plane of the antenna can be seen in Figure 3.9.

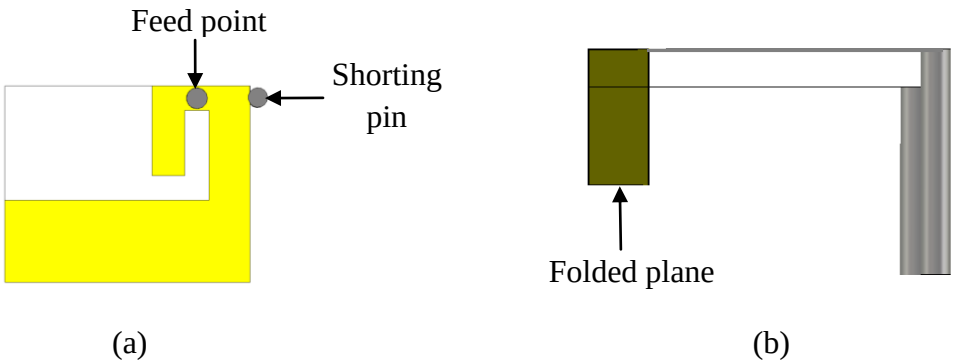

Figure 3.9: The main radiating plane of reconfigurable PIFA; (a) Front view (b) Side view

3.2.2.1 Reflection Coefficient

The simulated reflection coefficient for the antenna with only the main radiating plane can be viewed in Figure 3.10. From observation, the reflection coefficient is almost similar with the antenna without copper bridge as in the previous Figure 3.5. Only a small increment is seen in the upper resonant frequency. The reflection coefficient for both cases (antenna without copper bridge and antenna with only the main radiating plane) can be viewed in Figure 3.11.

Table 3.3 summarizes the resonant frequency performance of the antennas. From the table, the upper resonant frequency is reduced from 5.74 GHz to 5.65 GHz with the presence of an additional radiating plane. The small frequency difference suggested that an additional radiating patch on the radiating structure has introduced some reactive loading to the antenna which in return reduces the resonant frequency. However, the shifting in frequency is not considerably huge which implies that the additional radiating plane does not affect the reflection coefficient performance of the antenna. Thus, in the next section, an active switch was placed in between the radiating planes to study the shifting of the upper resonant frequency. If the upper resonant frequency is reduced considerably, the structure would be selected as the best platform to introduce active switches to reconfigure the frequency.

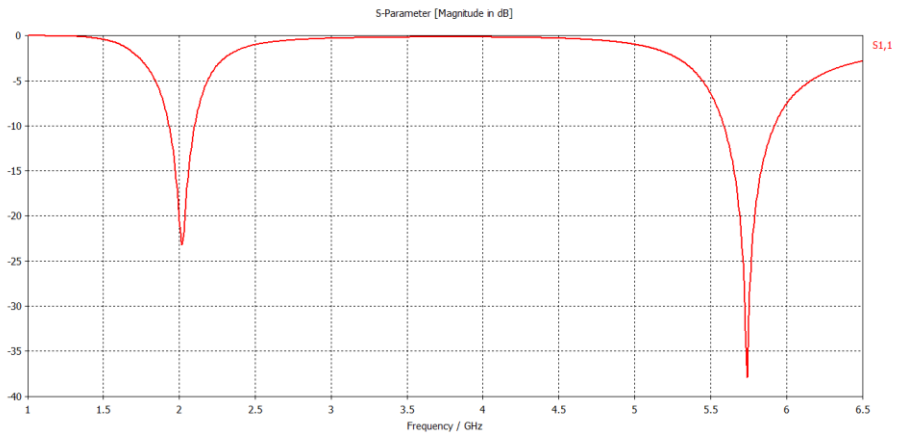

Figure 3.10: Reflection coefficient of the reconfigurable antenna with the main radiating plane

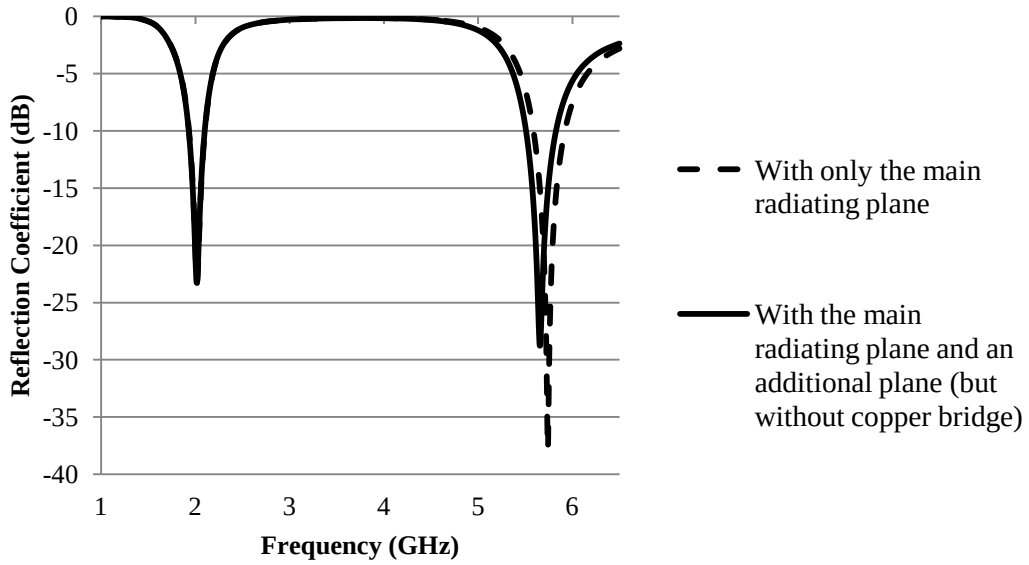

Figure 3.11: Reflection coefficient comparison between reconfigurable PIFAs with only the main radiating plane and the main radiating plane with an additional plane (but without copper bridge)

Table 3.3: Resonant frequency performance comparison of reconfigurable PIFAs with a single and two radiating planes

	Radiating Structure of Reconfigurable PIFA	
	Only the Main Radiating Plane	**The Main Radiating Plane and an Additional Plane (Without Copper Bridge)**
First resonant frequency, f_{r1} (GHz)	2.01	2.01
Second resonant frequency, f_{r2} (GHz)	5.74	5.65
6-dB Lower Bandwidth, BW_1 (MHz)	2.1625 – 1.868 = **294.5**	2.1606 – 1.8652 = **295.4**
6-dB Upper Bandwidth, BW_2 (MHz)	6.0822 – 5.4861 = **596.1**	5.9776 – 5.4082 = **569.4**

3.2.2.2 Current Distribution

Current distributions on the main radiating plane were simulated and can be viewed in Figure 3.12. From Figure 3.12(a), maximum current concentration is observed on the edge of the

main radiating plane, the feed line and the shorting pin at 2.01 GHz whereas at the upper resonant frequency of 5.74 GHz, the maximum current is very noticeable around the edge of the main radiating plane – the one which is close to the location of the feed point as in Figure 3.12(b). The locations of maximum current at both frequencies are similar to the locations of maximum current of the antenna in Figure 3.7.

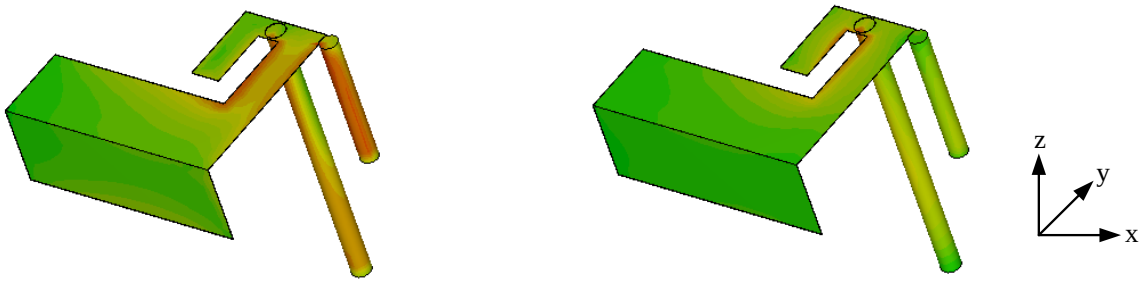

(a) (b)

Figure 3.12: Current distribution of reconfigurable PIFA with only a main radiating plane at; (a) 2.01 GHz (b) 5.74 GHz

3.2.2.3 Radiation Pattern

The co-polar radiation patterns in xy-, xz- and yz- planes of the antenna were simulated in CST MWS software and can be viewed in Figure 3.13.

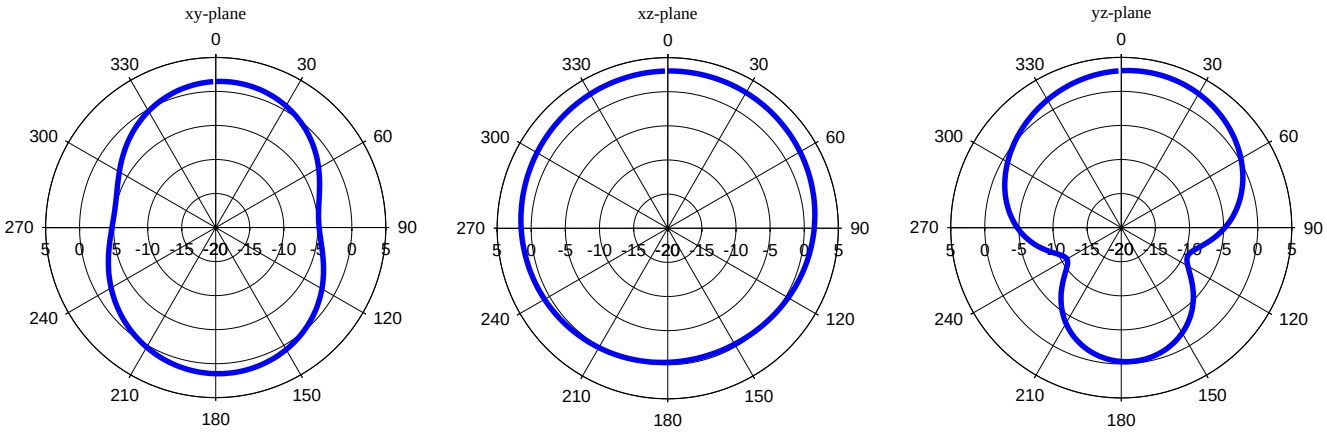

(a)

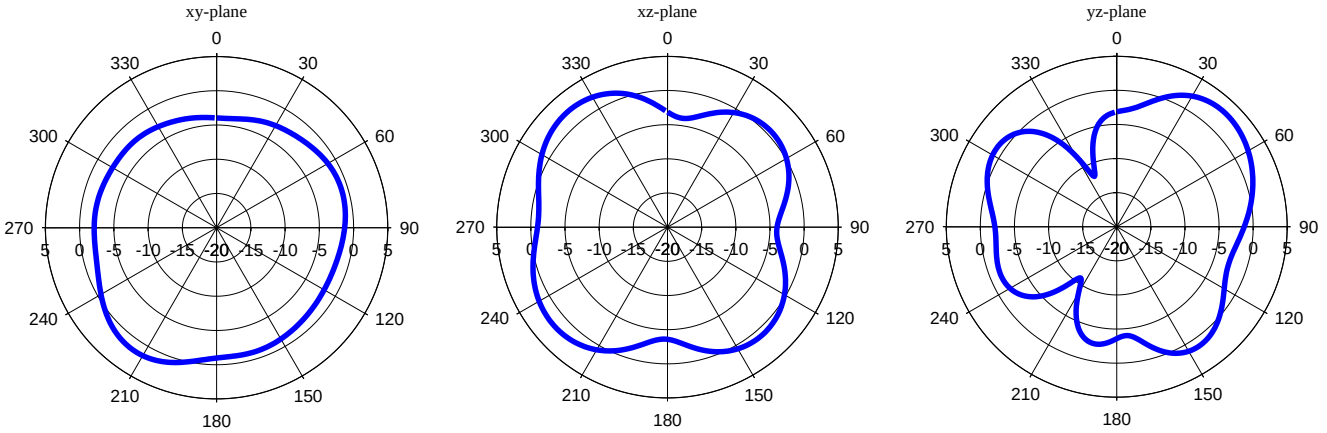

(b)

Figure 3.13: Co-polar radiation patterns in xy-, xz- and yz- planes of reconfigurable PIFA with a main radiating plane at; (a) 2.01 GHz (b) 5.74 GHz

3.2.2.4 Realized Gain, Directivity and Efficiency

Table 3.4 summarizes the realized gain, directivity and efficiency of the antenna with only the main radiating plane in comparison with the same antenna but with an additional radiating plane. From the table, an additional radiating plane has increased the realized gain, G from 2.931 to 3.076 dB and directivity, D from 3.031 to 3.187 dB of the upper resonant frequency. However,

the efficiency remains similar. Those values imply that by adding an additional radiating plane, the performance of the antenna is not affected and by connecting the main to additional radiating planes, the antenna can be reconfigured to increase and decrease the upper resonant frequency depending on the state of the respective switch.

Table 3.4: Realized gain, directivity and efficiency of reconfigurable PIFA with respect to the radiating planes

	Radiating Plane			
	Only the Main Radiating Plane		**The Main Radiating Plane and an Additional Plane (Without Copper Bridge)**	
	f_{r1} = 2.01 GHz	f_{r2} = 5.74 GHz	f_{r1} = 2.01 GHz	f_{r2} = 5.65 GHz
Realized Gain, G (dB)	3.066	2.931	3.059	3.076
Directivity, D (dBi)	3.148	3.031	3.139	3.187
Efficiency, η (%)	98.7	97.7	98.7	97.5

3.3 Reconfigurable PIFA with BAR50-02V PIN Diode

In this section, the copper bridge was replaced with an active switch. It has been decided that the first switch will be a PIN diode. Before that, a careful selection of the PIN diode was performed from the commercially available PIN diodes in the market. After serious consideration which has taken into account the switch repetitions in the reviewed literature, the BAR50-02V PIN diode from Infineon Technologies [101] was selected.

The respective PIN diode is housed in SC-79 surface mount plastic package with a frequency range from 10 MHz to 6 GHz. This frequency range fulfills the requirement of the intended frequency range in this research work which foresees the applications in wireless mobile communication. BAR50-02V PIN diode as a switch has allowed an isolation of 18 dB and a low

insertion loss of 0.2 dB. Although the switch linearity is not specified, it has a very low capacitance (typical value of 0.15 pF) at frequencies above 1 GHz with zero voltage reverse bias. The value of this capacitance has no dependence on microwave voltage. Thus, it is capable of operating with minimum nonlinear distortions.

A lumped-element equivalent circuit for the PIN diode in ON and OFF states can be seen in Figure 3.14. The switch is represented as a resistor in the ON state and a series capacitor in the OFF state [48].

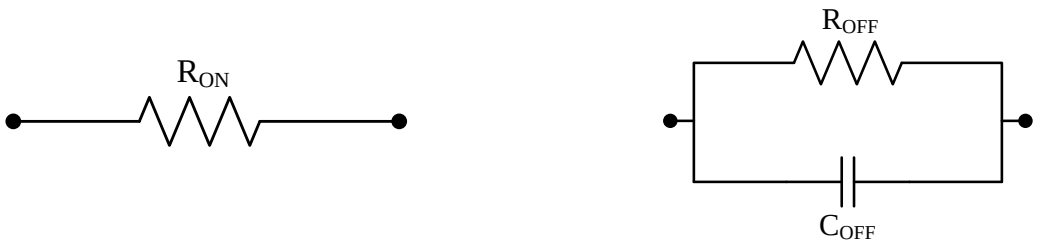

Figure 3.14: PIN diode lumped element equivalent circuit in; (a) ON state (b) OFF state [48]

The equivalent lumped elements circuit models in the ON and OFF states were simulated in CST MWS software to give the correct values of R and C. The simulations were performed without the surface mounting effect since CST simulation tool cannot apply a complex RLC model [72]. Based on the simulations, the values of R and C are listed in Table 3.5.

Table 3.5: Lumped element values of BAR50-02V PIN diode in ON and OFF states

	BAR50-02V PIN Diode	
	ON State	**OFF State**
Resistance (Ω)	3	25k
Capacitance (pF)	-	0.15

There are two ways to simulate the actual PIN diode in CST MWS software. Firstly, based on the lumped element values in the table, the BAR50-02V PIN diode can be modeled in its ON state as a 3 Ω resistance and as a 0.15 pF capacitance in its OFF state [102]. However, the 3 Ω resistance is only valid for 10 mA forward current. Secondly, the Touchstone 2-port S-parameters (*.s2p) file which can be obtained from the manufacturer can be used as an exact switch model to simulate the antenna. The advantage of using the Touchstone .s2p file format from the manufacturer is that it has included the package parasitic effect. Thus, the latter option was adopted and implemented on this reconfigurable antenna. In order to increase the accuracy of the simulation results, a metal rod (to represent a feed-through capacitor) and copper pad were also included as can be seen in Figure 3.15 (refer forward to Table 3.6 for dimensions). The datasheet of BAR50-02V PIN diode from Infineon Technologies can be found in Appendix A.

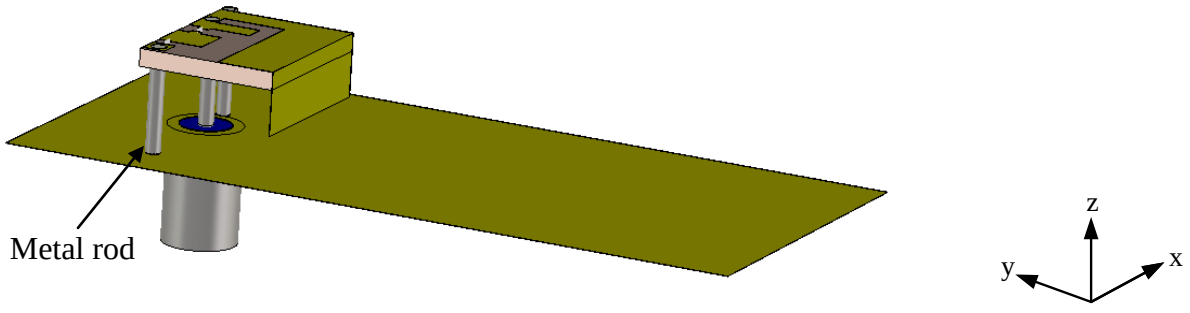

Figure 3.15: Reconfigurable PIFA with metal rod to represent feed-through capacitor

3.3.1 Antenna Geometry and Dimensions

This section discusses the geometry and dimensions of the reconfigurable PIFA with BAR50-02V PIN diode in CST MWS software. The integration of CST MWS with other modules of CST STUDIO SUITE allows for a straightforward coupling of EM simulation and circuit simulation. Thus, for each CST MWS structure, two fundamental views of the model exist. The Standard view is the 3D model representation which is visible by default. At the same time, a Schematic view can be activated by selecting the corresponding tab under the standard view. Once this view is activated, a schematic canvas is shown where the 3D structure is represented by a single block (MWS block) with terminals. The terminals have a one-to-one correspondence with the 3D structure (in this case, the reconfigurable antenna) and discrete ports. The Schematic view allows for easy addition of external circuit elements to the terminals of the 3D structure. The connection of these arbitrary networks to CST MWS can either be realized as a standard or a transient EM/circuit co-simulation.

In CST MWS software, the switch is represented by a discrete port in the 3D model. Figure 3.16 shows the top view of the radiating structure with a discrete port to connect the main radiating plane to an additional plane. In the schematic view, the discrete port is represented by a Touchstone block (TS block) which contains the *.s2p file of the PIN diode. There are two separate *.s2p files of the PIN diode in ON and OFF states. The schematic view of the reconfigurable PIFA in the ON and OFF states can be viewed in Figure 3.17. Further illustration of the geometry and dimensions of the antenna can be viewed in Figure 3.18. Table 3.6 listed the values of each dimension of the antenna structure.

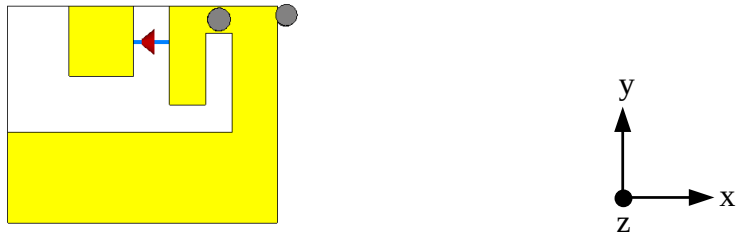

Figure 3.16: Top view of reconfigurable PIFA with a discrete port connecting the radiating planes

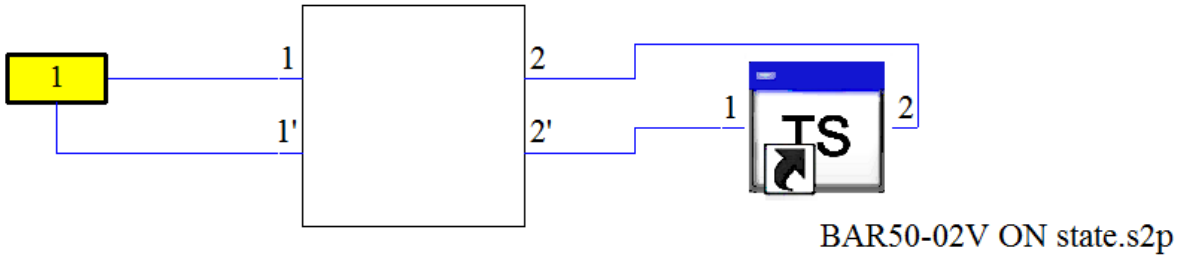

(a)

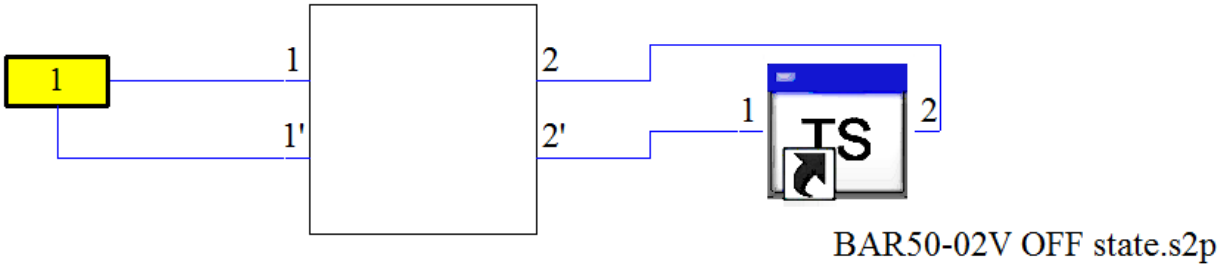

(b)

Figure 3.17: Schematic view of reconfigurable PIFA with PIN diode in;
(a) ON state (b) OFF state

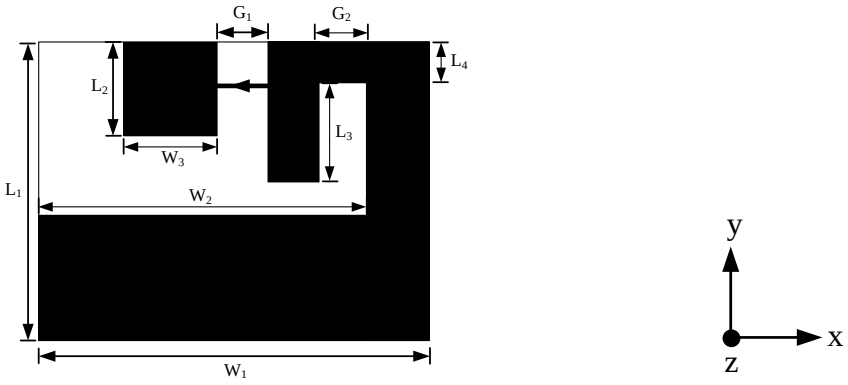
G1
G2
L4
L2
L3
W3
L1
W2
W1
y
x
z

(a)

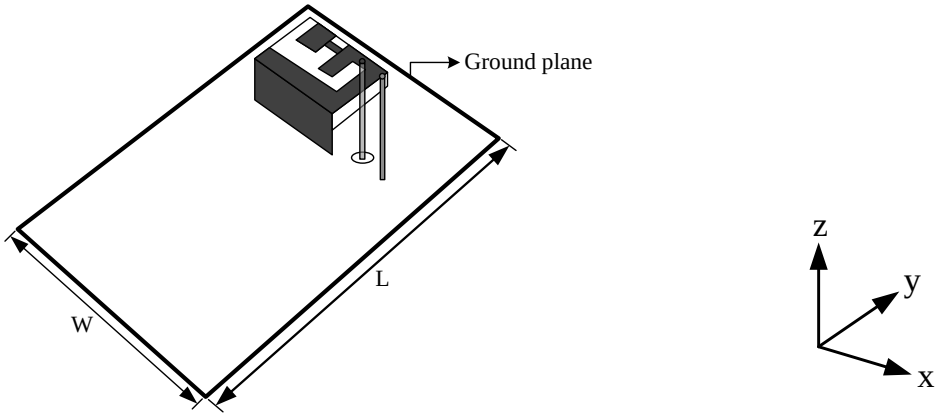
Ground plane
L
W
z
y
x

(b)

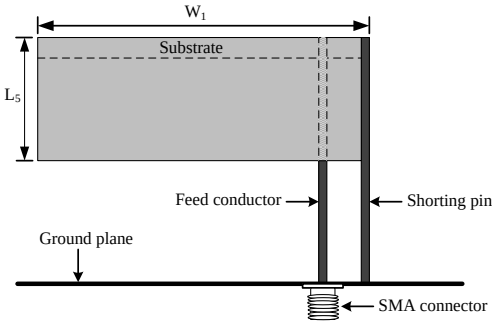
W1
Substrate
L5
Feed conductor
Shorting pin
Ground plane
SMA connector

(c)

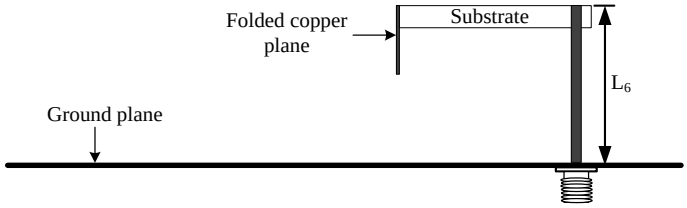

(d)

Figure 3.18: Detailed dimensions of reconfigurable PIFA with PIN diode which is represented by a discrete port;
(a) Radiating planes (b) Top view (c) Front view (d) Side view

Table 3.6: Dimensions of the whole structure of reconfigurable PIFA with PIN diode

Dimension	Value (in mm)
L	65
L_1	12
L_2	3.9
L_3	4
L_4	1.5
L_5	5.5
L_6	9
W	32
W_1	15
W_2	12.5
W_3	3.6
G_1	2
G_2	1.5

3.3.2 Reflection Coefficient

The reflection coefficients were simulated and the switching capability of the PIN diode was demonstrated, allowing the upper resonant frequency of the reconfigurable PIFA to be reconfigured when it is switched ON and OFF. In both cases, the first resonant frequency remains unchanged regardless of the switching states. The simulated reflection coefficient in ON and OFF

states can be seen in Figure 3.19. Table 3.7 summarizes the resonant frequency performance of the antenna. In the OFF state, there will be no current passing through the PIN diode to the second radiating plane. Thus, the current length is shorter which increases the upper resonant frequency to 5.16 GHz. In the ON state, the PIN diode lets the current to pass through it from the main radiating plane to the additional plane. The longer current path reduces the resonant frequency from 5.16 to 3.67 GHz. The first resonant frequencies have remained similar in both states at 2.01 GHz. The reconfigurable PIFA is designed to have the lower resonant frequency at 2.01 GHz based on the fact that there are a lot of wireless communication bands at around 2 GHz [103]. Among the related wireless communication bands are the USPCS (1.85 – 1.99 GHz), WCDMA (1.92 – 2.18 GHz) and UMTS (1.92 – 2.17 GHz) bands. At 3.67 GHz, the m-WiMAX (3.4 – 3.6 GHz) band is supported and the UNII-1 (5.15 – 5.25 GHz) band, which is a sub-band of the 5-GHz ISM band, is covered at 5.16 GHz. The reflection coefficient comparison in the ON and OFF states can be viewed in Figure 3.19.

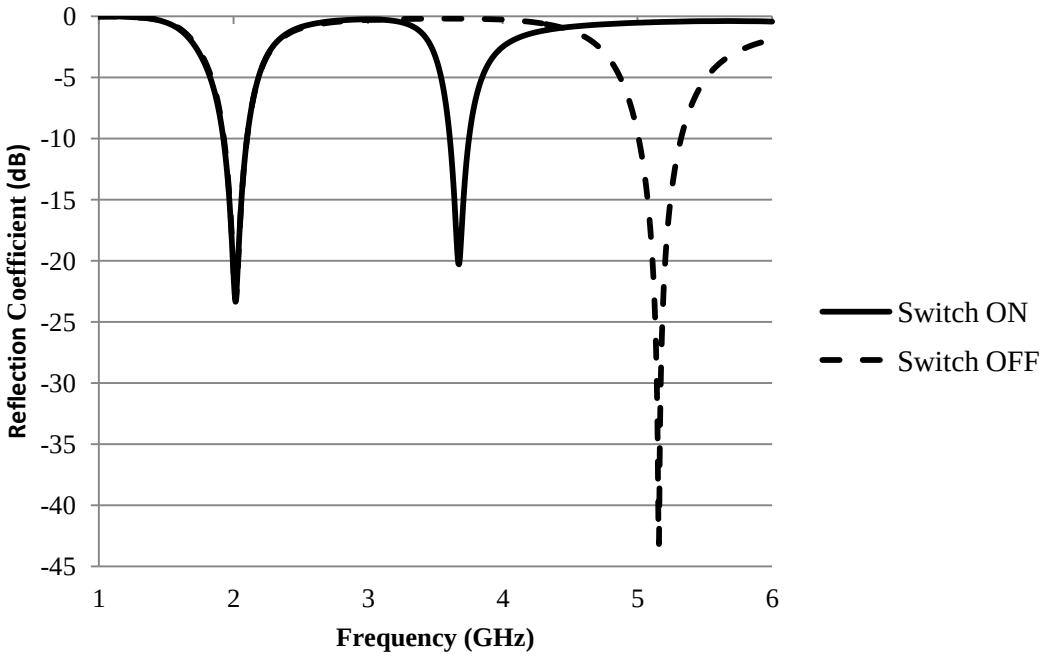

Figure 3.19: Reflection coefficient comparison of reconfigurable PIFA with PIN diode in ON and OFF states

Table 3.7: Resonant frequency performance of reconfigurable PIFA with PIN diode in ON and OFF states

	Reconfigurable PIFA with BAR50-02V PIN Diode	
	ON State	**OFF State**
First resonant frequency, f_{r1} (GHz)	2.01	2.01
Second resonant frequency, f_{r2} (GHz)	3.67	5.16
6-dB Lower Bandwidth, BW_1 (MHz)	2.1618 – 1.8544 = **307.4**	2.1618 – 1.8625 = **299.3**
6-dB Upper Bandwidth, BW_2 (MHz)	3.8171 – 3.5595 = **257.6**	5.4551 – 4.9103 = **544.8**

3.3.3 Current Distribution

Current distributions on the radiating structure of the reconfigurable PIFA were extracted from CST MWS and can be seen in Figure 3.20 and Figure 3.21 in ON and OFF states. As previously discussed, the location of maximum current dictates the location of a particular resonant frequency. From Figure 3.20(a) and Figure 3.21(a), the maximum current is concentrated on the edge of the main radiating plane, the feed line and the shorting pin at the first resonant frequency of 2.01 GHz. From Figure 3.20(b), at 3.67 GHz, the maximum current is concentrated on the edge of the main radiating plane close to the feed point and further elongated to the additional plane where the maximum current is seen to be concentrated on the edge of the plane. This behaviour suggested that the current electrical path is longer which decreases the upper resonant frequency. From Figure 3.21(b), it is observed that the maximum current is concentrated on the edge of the main radiating plane which is close to the feed point. Thus, the current path is shorter which in return increases the upper resonant frequency to 5.16 GHz in the OFF state.

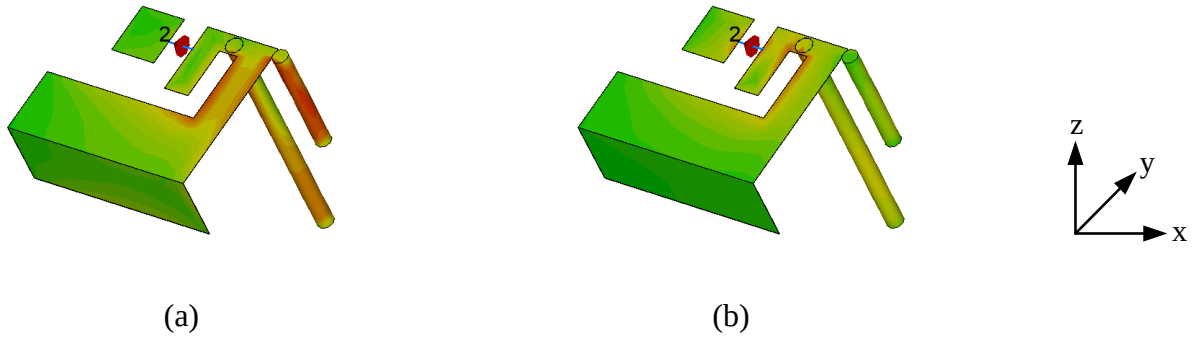

(a) (b)

Figure 3.20: Current distribution of reconfigurable PIFA with PIN diode in ON state at; (a) 2.01 GHz (b) 3.67 GHz

(a) (b)

Figure 3.21: Current distribution of reconfigurable PIFA with PIN diode in OFF state at; (a) 2.01 GHz (b) 5.16 GHz

3.3.4 Radiation Pattern

The co-polar radiation patterns in xy-, xz- and yz- planes have been simulated and observed to determine the antenna's performance. Similar radiation patterns at lower resonant frequency of 2.01 GHz can be viewed from Figure 3.22(a) and (c). In those figures, the radiation patterns in the xy- ($\theta = 90°$) and xz- ($\phi = 0°$) planes have a doughnut-shaped pattern cutting across the plane. In the yz- ($\phi = 90°$) plane, the radiation pattern is directional with minimum back lobe. From Figure 3.22(b) at 3.67 GHz in the ON state, omnidirectional and dipole-like radiation patterns can be observed in the xy- and xz- planes. In the yz-plane, there are several nulls in the radiation pattern. Similar radiation patterns are observed in Figure 3.22(d) in the OFF state at 5.16 GHz.

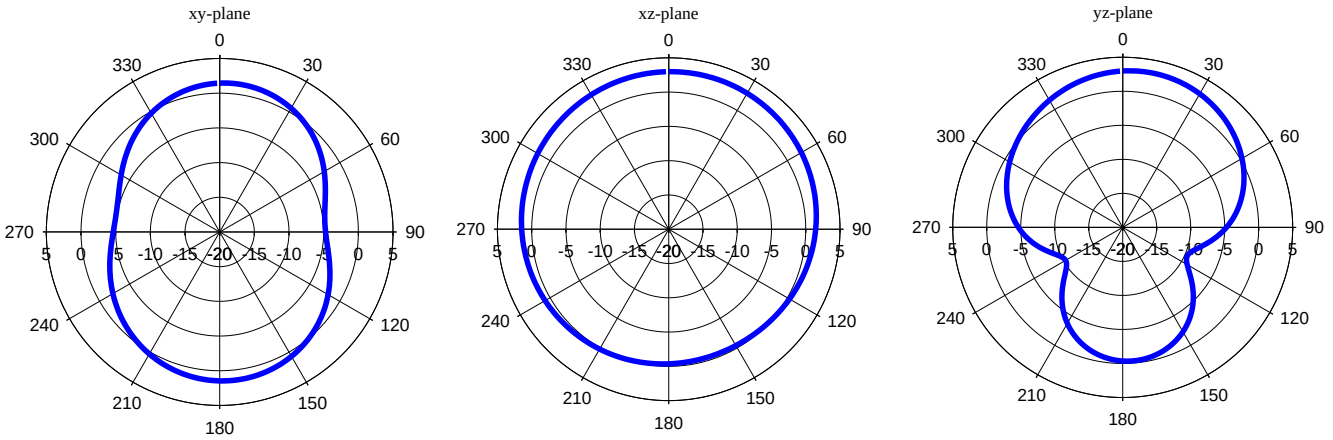
xy-plane
xz-plane
yz-plane
0
30
60
90
120
150
180
210
240
270
300
330
5 0 -5 -10 -15 -20 -15 -10 -5 0 5

(a)

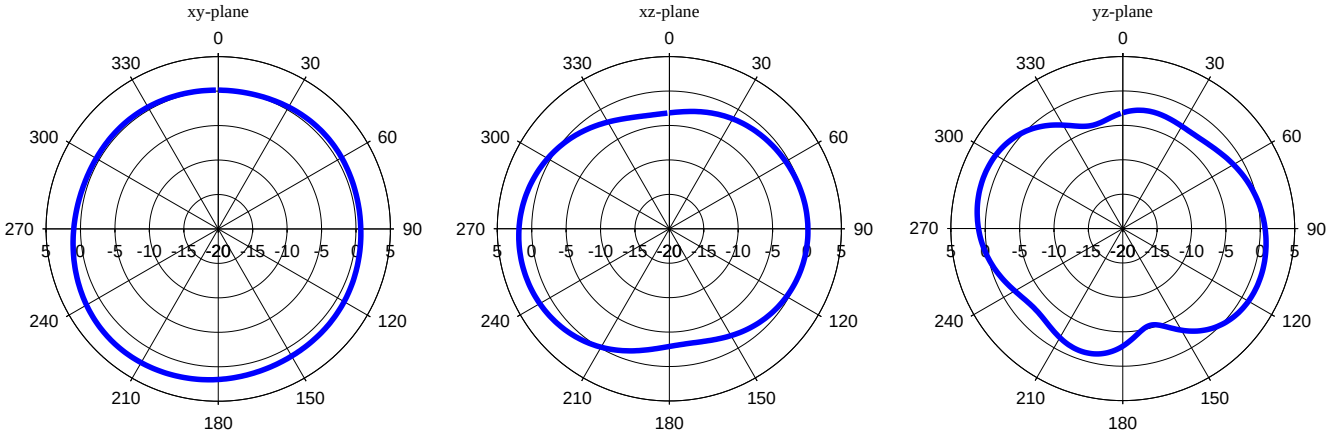
xy-plane
xz-plane
yz-plane
0
30
60
90
120
150
180
210
240
270
300
330
5 0 -5 -10 -15 -20 -15 -10 -5 0 5

(b)

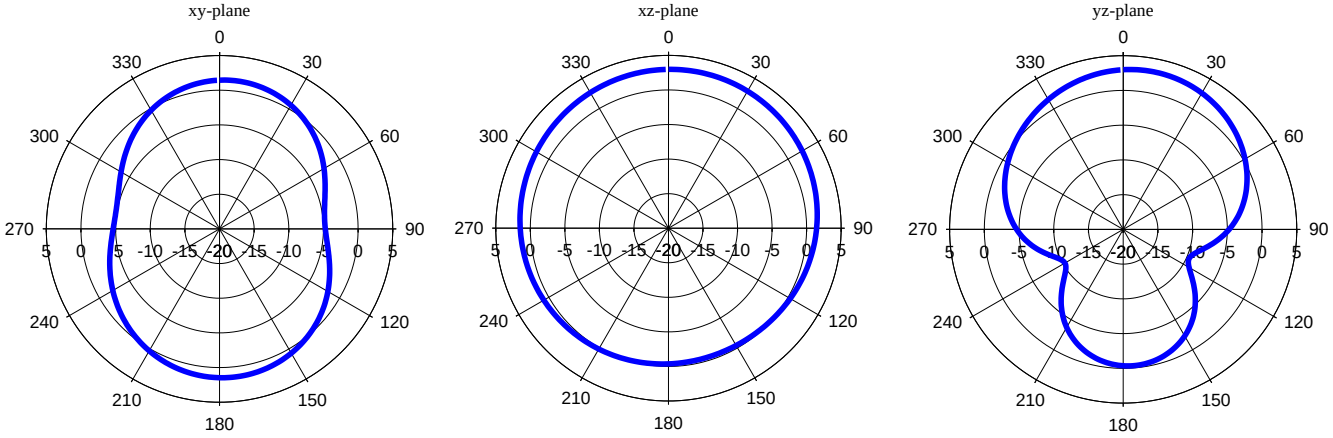
xy-plane
xz-plane
yz-plane
0
30
60
90
120
150
180
210
240
270
300
330
5 0 -5 -10 -15 -20 -15 -10 -5 0 5

(c)

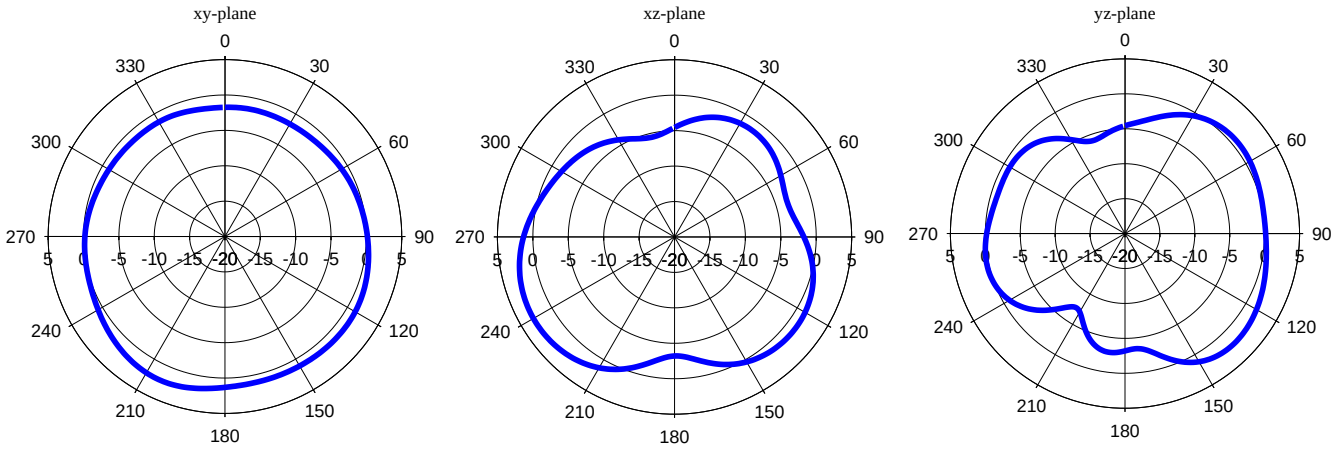

(d)

Figure 3.22: Co-polar radiation patterns in xy-, xz- and yz- planes of reconfigurable PIFA with PIN diode in ON state at; (a) 2.01 GHz (b) 3.67 GHz and OFF state at; (c) 2.01 GHz (d) 5.16 GHz

3.3.5 Realized Gain, Directivity and Efficiency

Table 3.8 summarizes the realized gain, directivity and efficiency of the reconfigurable PIFA. From the table, they are consistently good at all resonant frequencies in both ON and OFF states. However, at 3.67 GHz, the efficiency is only 64.8%. The reduced efficiency can explained from the reflection coefficient graph in Figure 3.19. From the figure, the reflection coefficient at 3.67 GHz is -20 dB which is lower than other reflection coefficient at the other resonant frequencies. This contributes to the reduction in efficiency. In addition, a forward bias DC current in the ON state is one of the drawbacks of the PIN diode as it can also reduce the radiation efficiency.

Table 3.8: Realized gain, directivity and efficiency of reconfigurable PIFA with PIN diode in ON and OFF states

	Reconfigurable PIFA with BAR50-02V PIN Diode			
	ON State		**OFF State**	
	f_{r1} = 2.01 GHz	f_{r2} = 3.67 GHz	f_{r1} = 2.01 GHz	f_{r2} = 5.16 GHz
Realized Gain, G (dB)	3.056	0.5149	3.073	2.412
Directivity, D (dBi)	3.127	2.437	3.146	3.308
Efficiency, η (%)	98.9	64.8	98.8	81.4

Figure 3.23 and Figure 3.24 show the variations in gain and efficiency of the reconfigurable PIFA within the lower and upper resonant frequencies in the ON state.

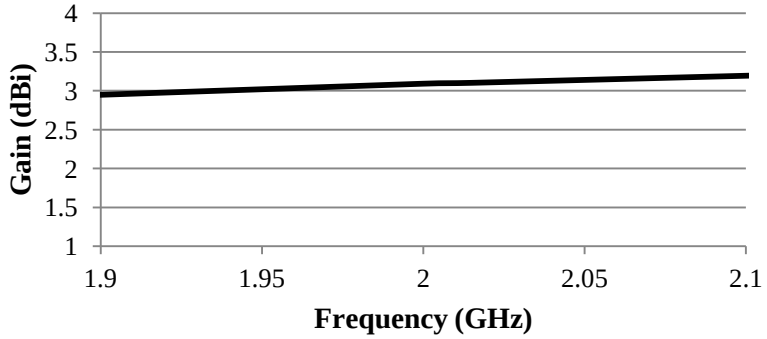

(a)

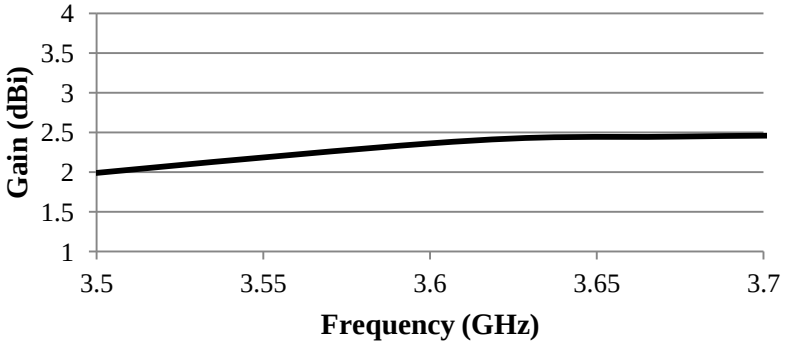

(b)

Figure 3.23: Gain of reconfigurable PIFA with PIN diode in ON state within;
(a) Lower frequency band (b) Upper frequency band

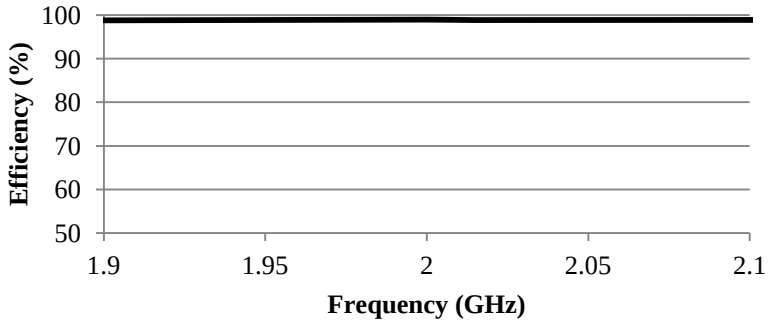

(a)

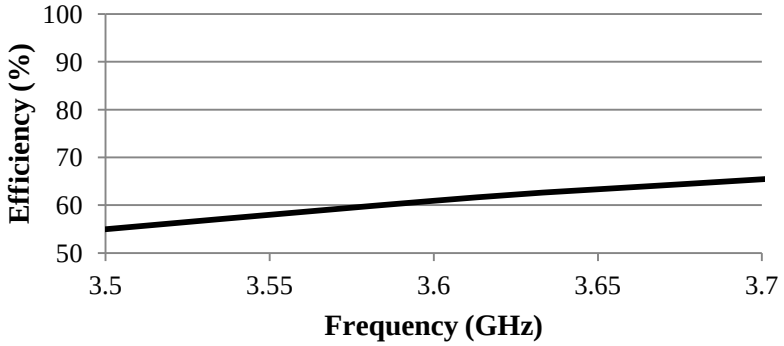

(b)

Figure 3.24: Efficiency of reconfigurable PIFA with PIN diode in ON state within;
(a) Lower frequency band (b) Upper frequency band

Figure 3.25 and Figure 3.26 show the gain and efficiency graphs of the reconfigurable PIFA within the lower and upper frequency bands in the OFF state.

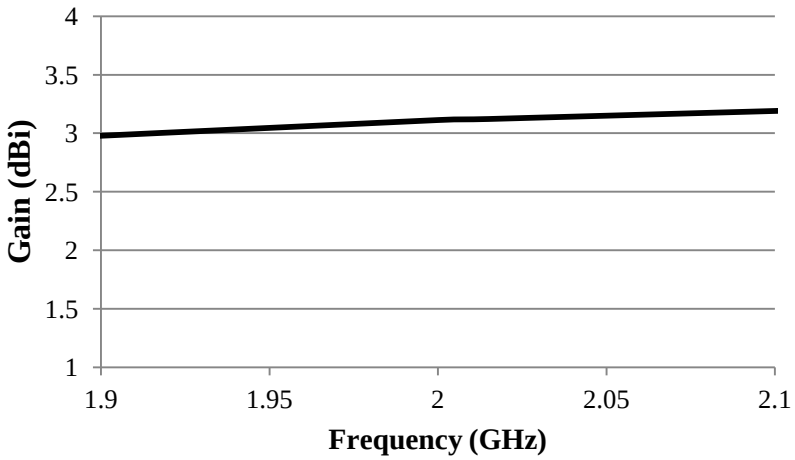

(a)

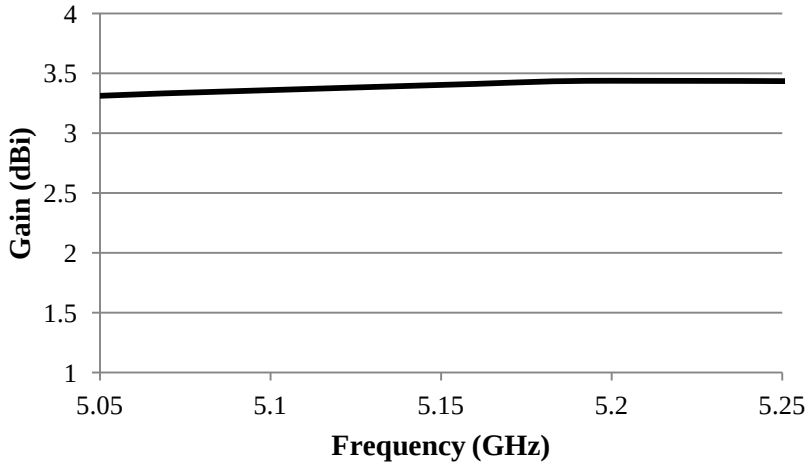

(b)

Figure 3.25: Gain of reconfigurable PIFA with PIN diode in OFF state within;
(a) Lower frequency band (b) Upper frequency band

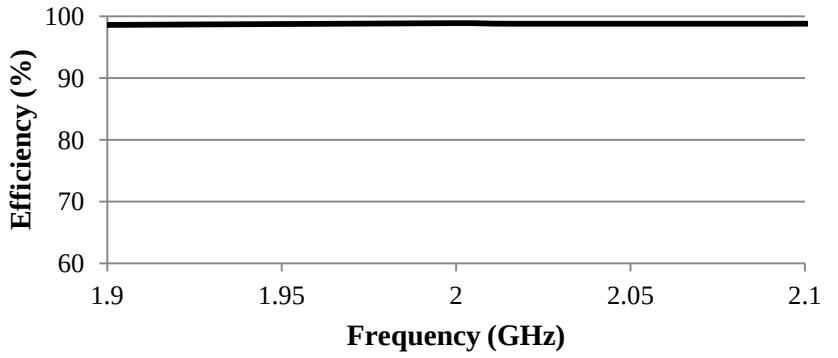

(a)

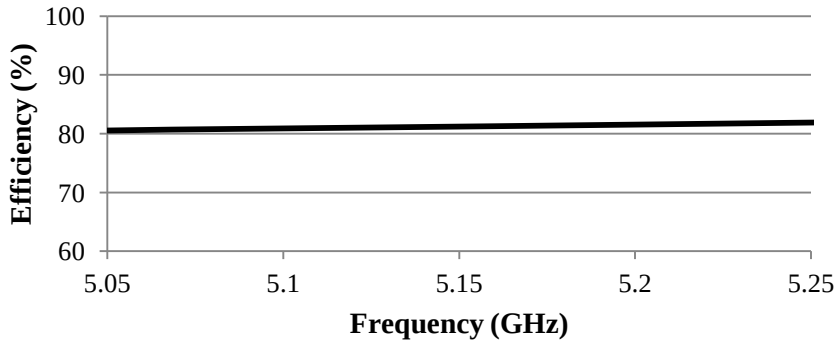

(b)

Figure 3.26: Efficiency of reconfigurable PIFA with PIN diode in OFF state within; (a) Lower frequency band (b) Upper frequency band

3.4 Antenna Fabrication and Measurement

The reconfigurable PIFA with PIN diode was fabricated on Taconic RF-35 substrate with relative permittivity, ε_r of 3.5, loss tangent, tan δ of 0.0018 and substrate thickness, t of 1.52 mm. Copper with an electrical conductivity, σ of 5.8×10^7 S/m was used as the conducting material. The radiating plane is mounted at 9 mm above a copper ground plane with a thickness of 0.5 mm. The feed line is a coaxial with the outer conductor connected to the ground plane and the inner

(centre) conductor emerged from beneath the ground plane to contact the first radiating plane. The fabricated antenna can be viewed in Figure 3.27.

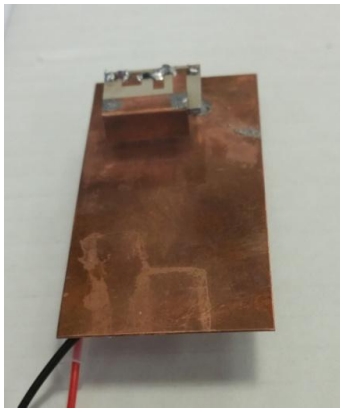

(a)

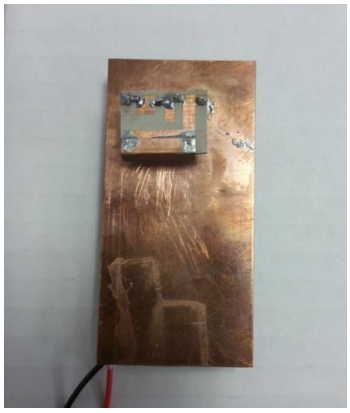

(b)

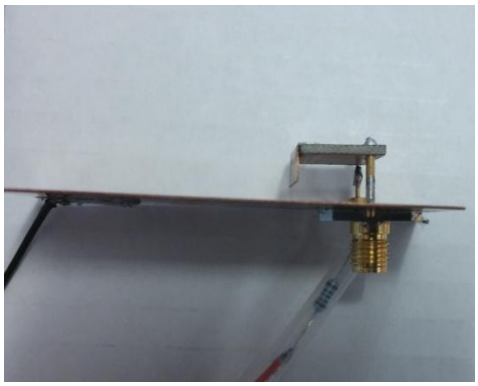

(c)

Figure 3.27: Fabricated reconfigurable PIFA with PIN diode;
(a) Front view (b) Top view (c) Side view

The biasing circuit to switch the PIN diode into ON and OFF states consists of a feed-through capacitor with a capacitance, C of 1200 pF, an RF choke inductor with an inductance, L_1 of 16 nH with a self-resonant frequency, SRF of 3.3 GHz and an isolating resistor with a resistance, R of 1.1 kΩ in order to achieve a 10 mA forward current. L_2 is a low value of

inductance from the shorting pin. A voltage supply of +12 V is fed from the power supply to the antenna via feed-through capacitor to switch on the PIN diode. The power supply is switched off in the OFF state. The DC biasing circuit setup of the reconfigurable PIFA can be seen in Figure 3.28. The location of the PIN diode is 2 mm from the edge which gives the best result of reflection coefficient. The circuit diagram of biasing circuit of the antenna is shown in Figure 3.29.

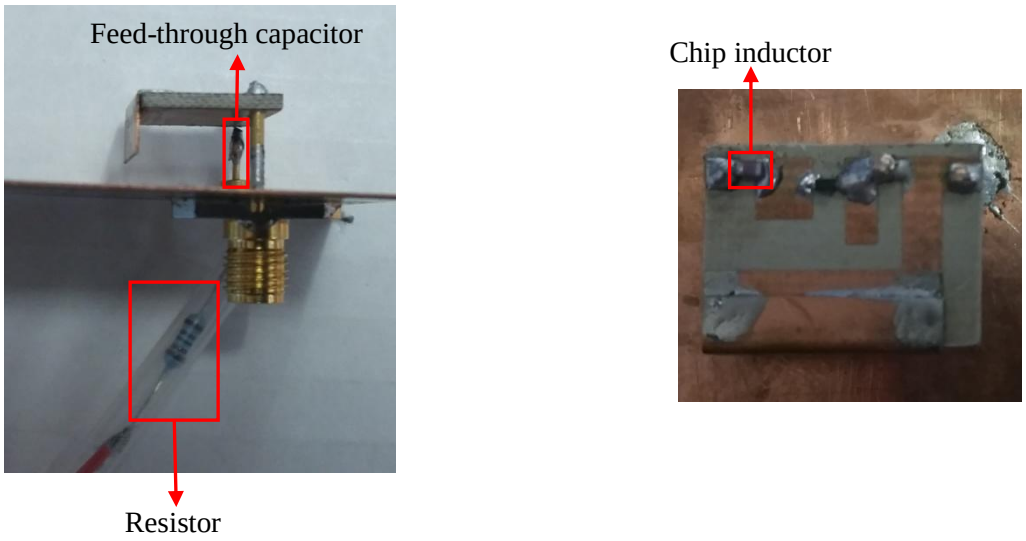

(a) (b)

Figure 3.28: DC bias setup for reconfigurable PIFA measurement;
(a) 1200-pF feed-through capacitor and 1.1-kΩ resistor (b) 16-nH chip inductor

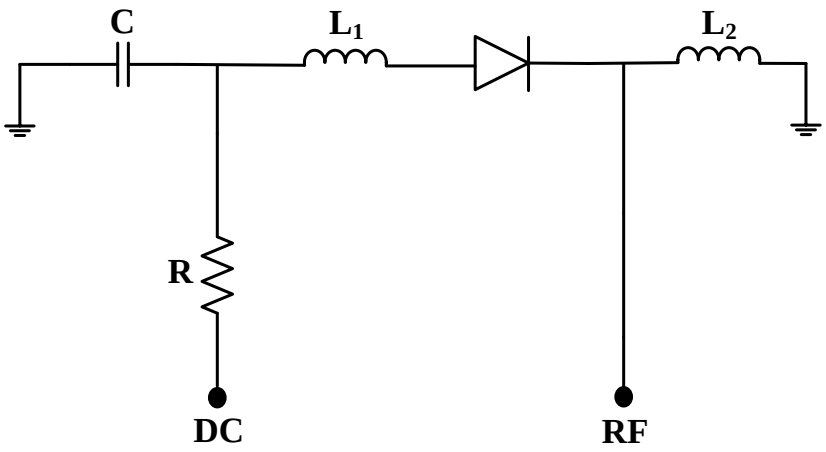

Figure 3.29: Biasing circuit of BAR50-02V PIN diode

3.4.1 Reflection Coefficient Measurement

Reflection coefficient measurements of the antenna in the ON and OFF states were performed on 8720ES Agilent S-parameter Network Analyzer (50 MHz – 20 GHz). The antenna was connected to the VNA via a coaxial bias tee for safety precaution. The ZX85-12G+ coaxial bias tee from Mini-Circuits has a wideband frequency ranging from 0.2 to 12 GHz, low insertion loss of 0.6 dB and high current capability of 400 mA. Due to its small size, the bias tee was housed in a metal case. The bias tee can be viewed in Figure 3.30. The measurement setup to measure the reflection coefficient of the reconfigurable PIFA can be viewed in Figure 3.31.

Figure 3.30: ZX85-12G+ Coaxial Bias Tee from Mini-Circuits

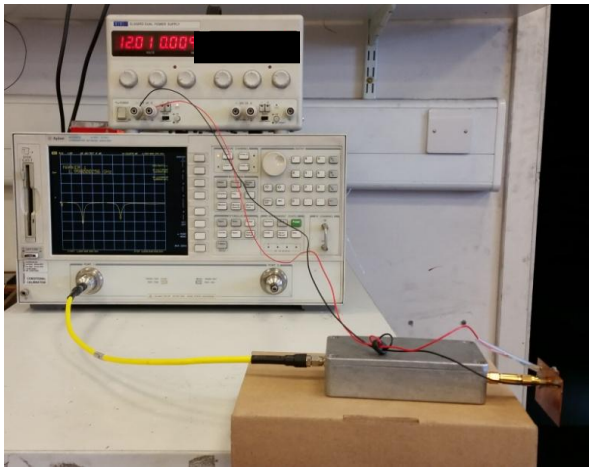

Figure 3.31: Measurement setup of reconfigurable PIFA with PIN diode

3.5 Active Switch Performance and Antenna Analysis

The reflection coefficient in the ON and OFF states were measured and compared with the simulation results. Figure 3.32 shows the comparison of the measured and simulated reflection coefficient in the ON state while the comparison in the OFF state can be viewed in Figure 3.33. From both figures, it is observed that there is an agreement between the simulation and measurement results. However, from the measurement result of the reflection coefficient in the OFF state, a new resonance is seen to appear at 1.4 GHz. Thus, further investigation was conducted to study the cause of its appearance. The overall comparison in the ON and OFF states is depicted in Figure 3.34.

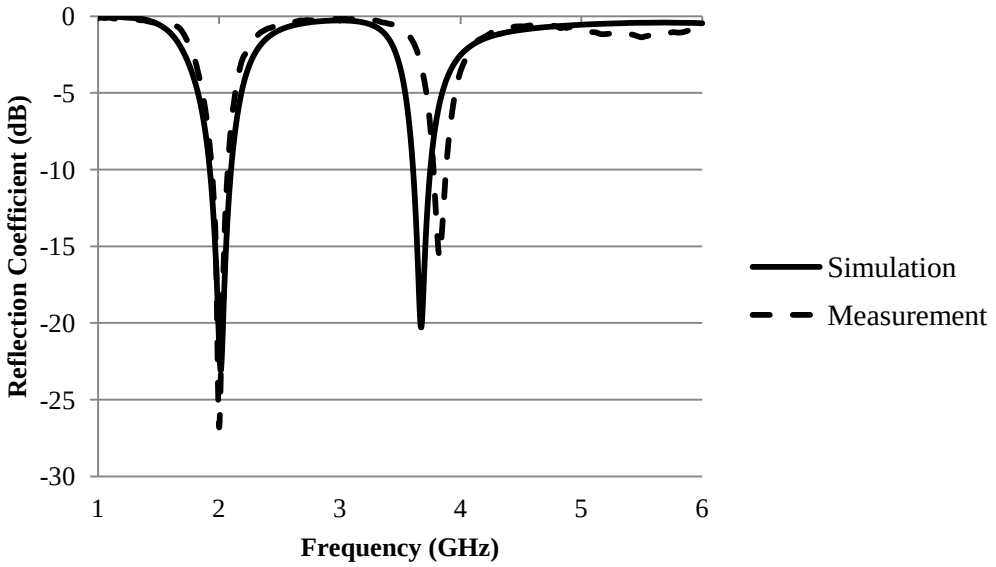

Figure 3.32: Measured reflection coefficient of reconfigurable PIFA with PIN diode in ON state

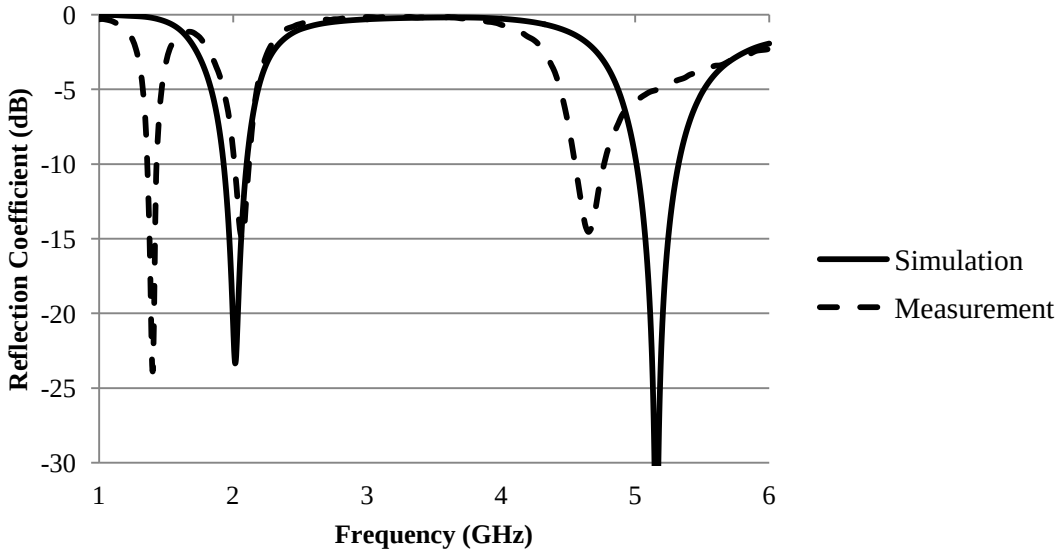

Figure 3.33: Measured reflection coefficient of reconfigurable PIFA with PIN diode in OFF state

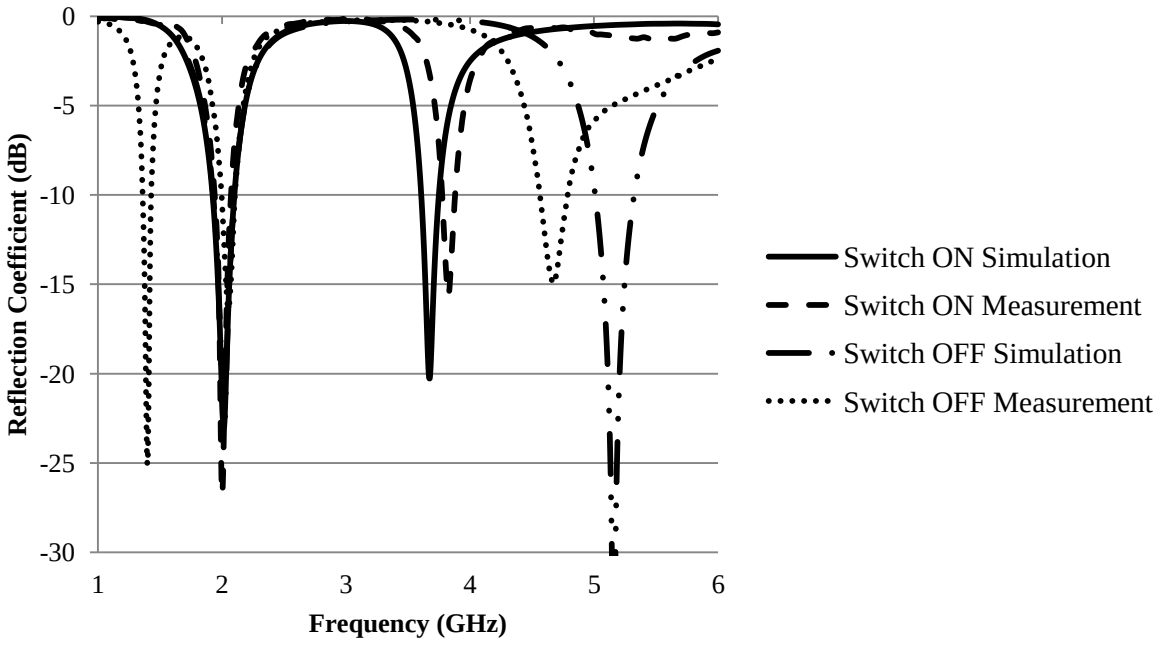

Figure 3.34: Comparisons of simulated and measured reflection coefficient of reconfigurable PIFA with PIN diode

3.5.1 Further Investigation on the Appearance of the New Resonant Frequency

This section discusses the tasks that were performed to investigate the appearance of the new resonance at 1.4 GHz in the OFF state. The tasks are outlined as below:

i. Identify the components used in the biasing circuit of the antenna which are not included in the simulation with CST MWS software

There are two components in the biasing circuit of the reconfigurable PIFA namely the 1200-pF feed-through capacitor and 16-nH RF choke inductor. It was found that the inductor was not included in the simulation of the antenna on the Schematic view of CST MWS software as can be viewed in Figure 3.18. Therefore, the Touchstone (*.s2p) file of the 16-nH inductor was obtained from the manufacturer and was included in the new simulation. The feed-through capacitor was

modelled as a metal rod which has been included in the previous simulation as can be seen in Figure 3.15.

ii. New simulation of reflection coefficient

New simulations of reflection coefficients in ON and OFF states were performed on the schematic view of CST MWS software as can be seen in Figure 3.35. From the figure, the Touchstone (*.s2p) file of the 16-nH RF choke inductor has been included. The measured reflection coefficients are compared with the new simulations.

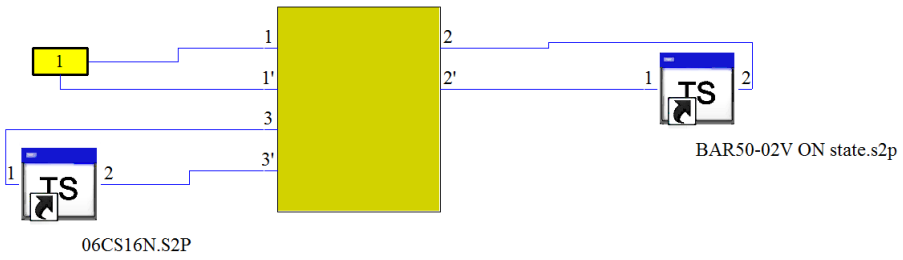

(a)

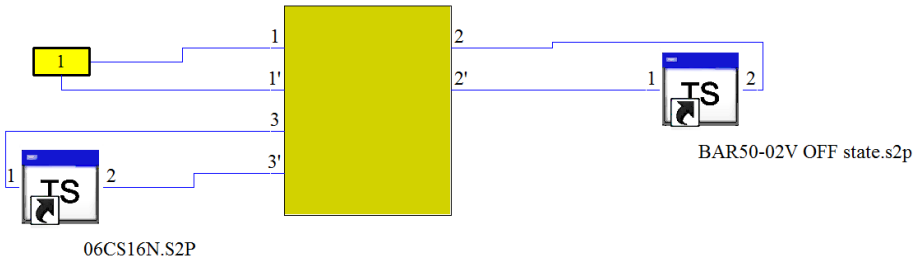

(b)

Figure 3.35: Schematic view of the new simulation of reconfigurable PIFA with PIN diode in; (a) ON state (b) OFF state

iii. Reflection coefficient analysis in OFF state

The comparison between the simulated and measured reflection coefficients of the reconfigurable PIFA can be viewed in Figure 3.36. From the figure, it is observed that in both states, the simulation results are very similar with the measurements. In addition, it can be seen clearly from Figure 3.38(b) that a new resonance has appeared at 1.4 GHz in the simulation which agrees really well with the measurement. Thus, it can be concluded that the appearance of the new resonance at 1.4 GHz is caused by the 16-nH bias inductor.

Table 3.9 summarizes the resonant frequency performance of the reconfigurable PIFA. From the table, the resonant frequencies are shifted slightly to 2.05 and 3.65 GHz in the ON state. The shift of resonant frequencies is more pronounced in the upper resonant frequency in the OFF state which observed a reduction from 5.16 to 4.75 GHz.

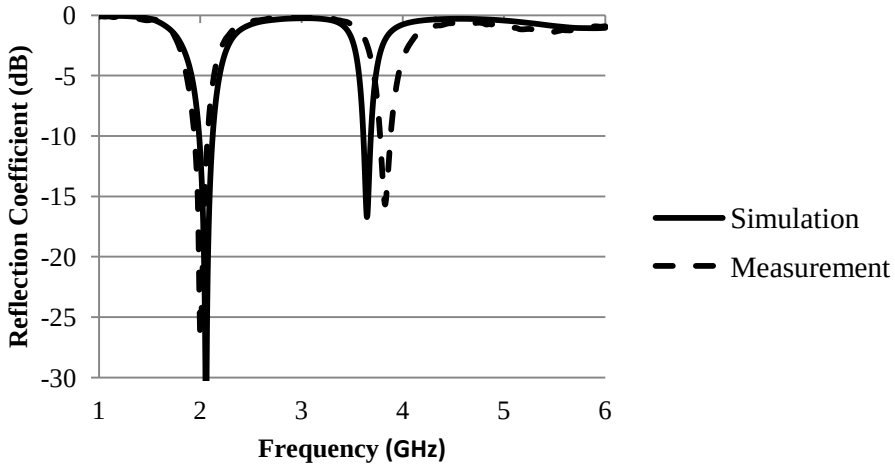

(a)

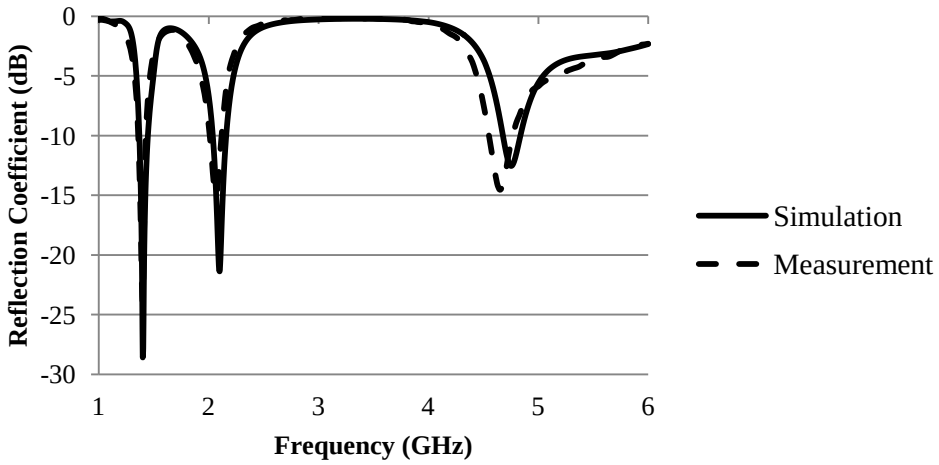

(b)

Figure 3.36: New simulation of reflection coefficient of reconfigurable PIFA with PIN diode and comparison with the measurement result in; (a) ON state (b) OFF state

Table 3.9: Resonant frequency performance of reconfigurable PIFA with PIN diode (include the 16-nH RF choke inductor and 1200-pF feed-through capacitor)

	Reconfigurable PIFA with BAR50-02V PIN Diode (include bias inductor and feed-through capacitor)	
	ON State	**OFF State**
First resonant frequency, f_{r1} (GHz)	2.05	1.4
Second resonant frequency, f_{r2} (GHz)	3.65	2.1
Third resonant frequency, f_{r3} (GHz)	-	4.75
6-dB Lower Bandwidth, BW_1 (MHz)	2.1701 – 1.9359 = **234.2**	1.4859 – 1.3495 = 136.4
6-dB Middle Bandwidth, BW_2 (MHz)	-	2.2074 – 1.9895 = 217.9
6-dB Upper Bandwidth, BW_3 (MHz)	3.7191 – 3.5801 = **139**	4.9760 – 4.5882 = **387.8**

iv. Radiation patterns of the reconfigurable PIFA with PIN diode

The radiation patterns of the antenna were simulated in xy-, xz- and yz- planes at its respective resonant frequencies to investigate any changes and are shown in Figure 3.37 and Figure 3.38.

In the ON state, it can be observed that the radiation patterns of the new simulations at 2.05 GHz are similar to the previous simulations. Slight differences can be seen at 3.65 GHz but they are still acceptable. In the OFF state, the comparison at 2.1 GHz shows that the radiation patterns are similar.

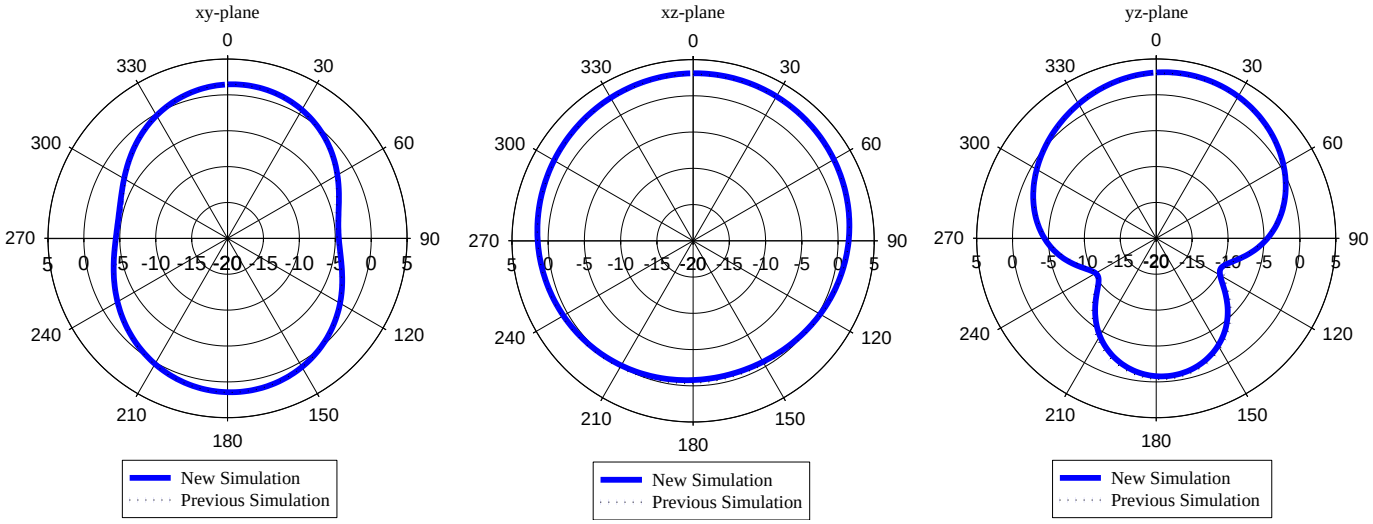

(a)

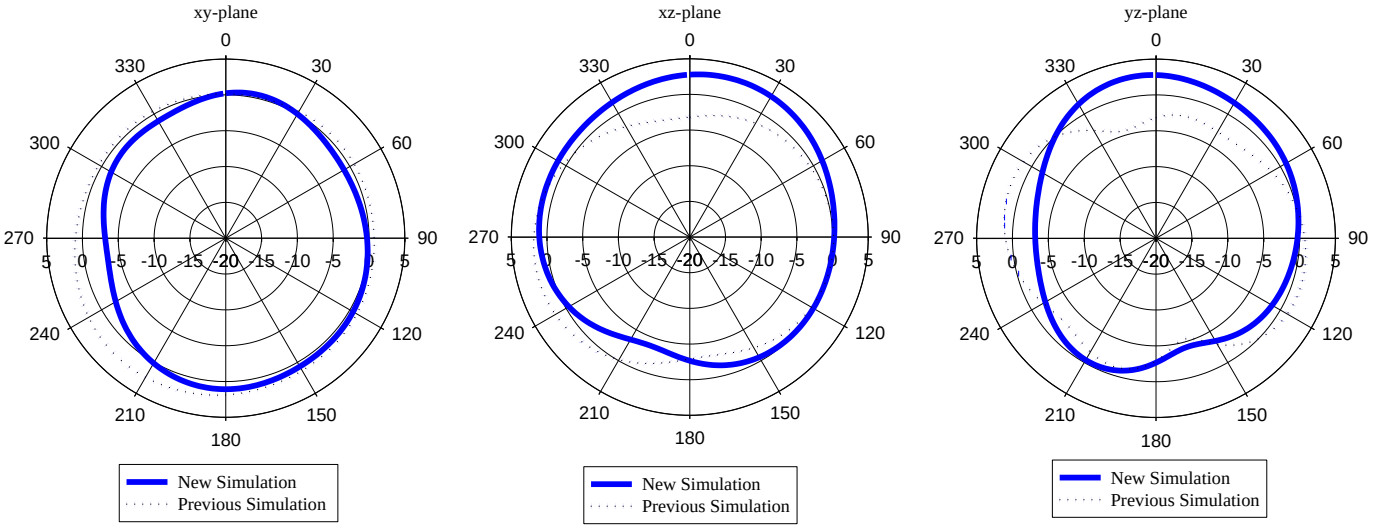

(b)

Figure 3.37: Radiation patterns of reconfigurable PIFA with PIN diode (include the bias RF choke inductor and feed-through capacitor) in ON state at; (a) 2.05 GHz (b) 3.65 GHz

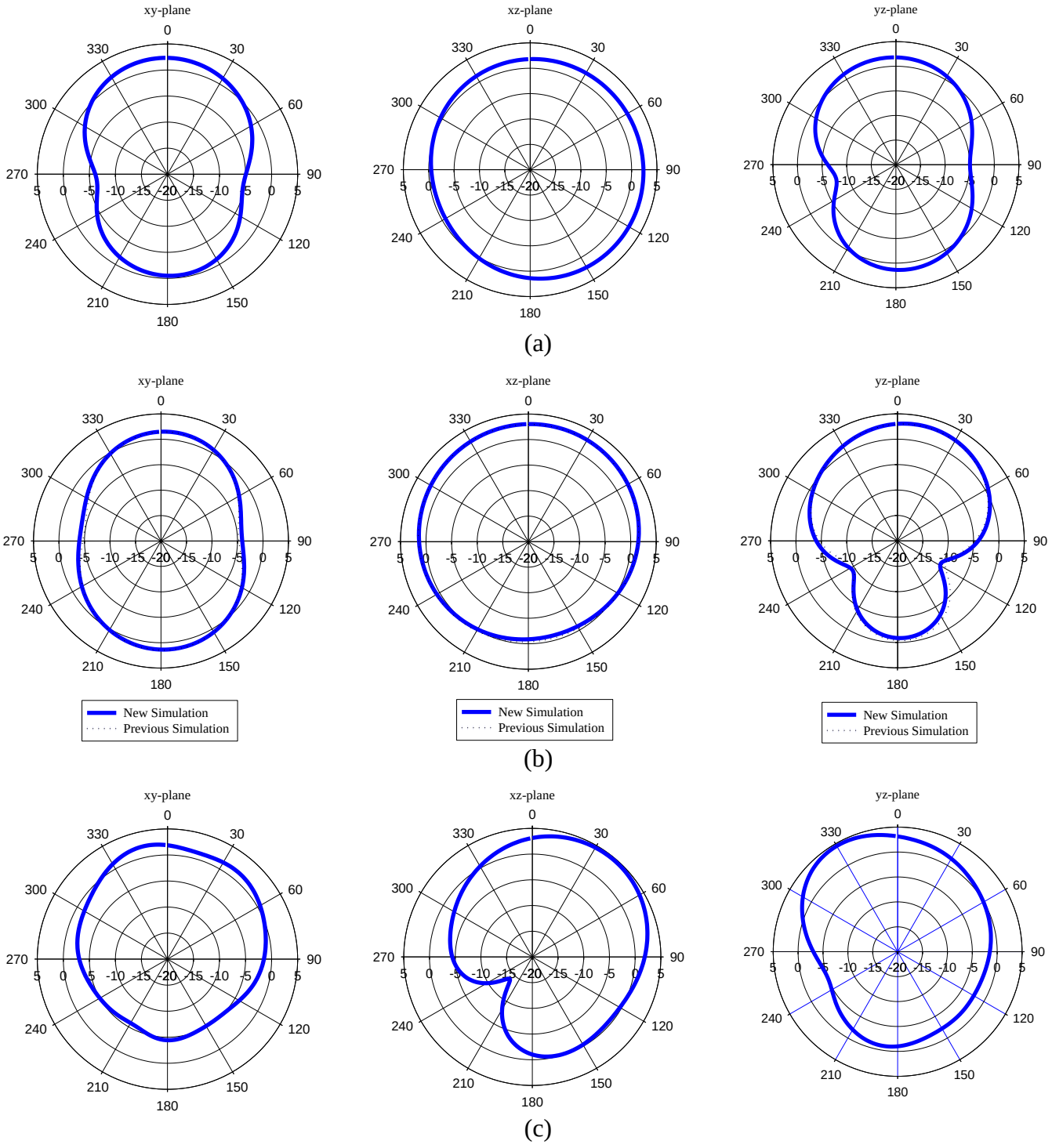

Figure 3.38: Radiation patterns of reconfigurable PIFA with PIN diode (include the bias RF choke inductor and feed-through capacitor) in OFF state at;
(a) 1.4 GHz (b) 2.1 GHz (c) 4.75 GHz

v. Realized Gain, Directivity and Efficiency

Table 3.10 summarizes the simulated realized gain, directivity and efficiency of the reconfigurable PIFA. From the table, the realized gain, G and the radiation efficiency, η at 1.4 GHz are -14.05 dB and 57.8 %. These values are very low which suggests that operation at 1.4 GHz may not be viable.

Table 3.10: Realized gain, directivity and efficiency of reconfigurable PIFA with PIN diode in ON and OFF states

	Reconfigurable PIFA with BAR50-02V PIN Diode				
	ON State		**OFF State**		
	f_{r1} = 2.05 GHz	f_{r2} = 3.65 GHz	f_{r1} = 1.4 GHz	f_{r2} = 2.1 GHz	f_{r3} = 4.75 GHz
Realized Gain, G (dB)	3.166	-0.5951	-14.05	2.928	3.792
Directivity, D (dBi)	3.248	2.978	2.478	3.213	5.147
Efficiency, η (%)	99.4	89.5	57.8	98.8	97.7

3.6 Reconfigurable PIFA with BAR50-02V PIN Diode (Gap, G_1 = 5 mm)

From the previous design of reconfigurable PIFA with PIN diode, the gap between the main radiating and additional planes is fixed to 2 mm due to the smaller size of the PIN diode. However, when it comes to the E-PHEMT switch, the bigger size of the transistor has seen the need to increase the gap between the radiating planes to 5 mm. An increase in the gap has enabled the transistor and other biasing components to be included in the gap. Thus, another reconfigurable PIFA with PIN diode was fabricated. The geometry and dimensions of this particular reconfigurable PIFA are similar to the reconfigurable PIFA with E-PHEMT switch. Since the dimensions of the PIN diode is too small with respect to the gap of 5 mm, two traces of

transmission lines were introduced into the gap to connect the switch to both planes. Figure 3.39 illustrates the changes that were made to the radiating structure of the antenna. Table 3.11 listed the changes in dimensions of the antenna.

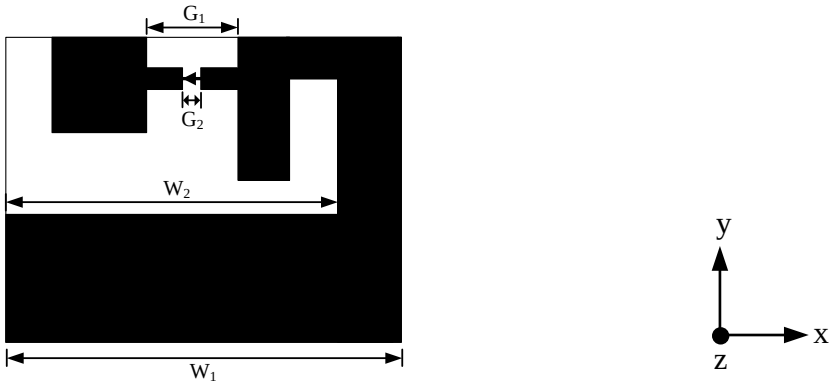

Figure 3.39: Top view of reconfigurable PIFA with PIN diode
(Gap, G_1 is increased from 2 mm to 5 mm)

Table 3.11: Changes in dimensions of reconfigurable PIFA with PIN diode (Gap, G_1 = 5 mm)

Dimension	Value (in mm)
G_1	5 (from 2)
G_2	1
W_1	18 (from 15)
W_2	15.5 (from 12.5)

3.6.1 Reflection Coefficient

The reflection coefficient of the reconfigurable PIFA that were simulated in CST MWS software is shown in Figure 3.40. Table 3.12 shows the resonant frequency performance of the antenna. From the table, the first resonant frequency in both states is reduced to 1.825 GHz as compared to 2.01 GHz when the Gap, G_1 is 2 mm. The upper resonant frequencies are also decrease to 3.13 GHz from 3.67 GHz (ON state) and to 4.705 GHz from 5.16 GHz (OFF state). The reduction in frequency is expected since an increase in the gap has increased the distance of

current travelled from the main to additional planes. Figure 3.41 shows the comparison of reflection coefficient for both reconfigurable PIFA with gap, G_1 of 2 and 5 mm.

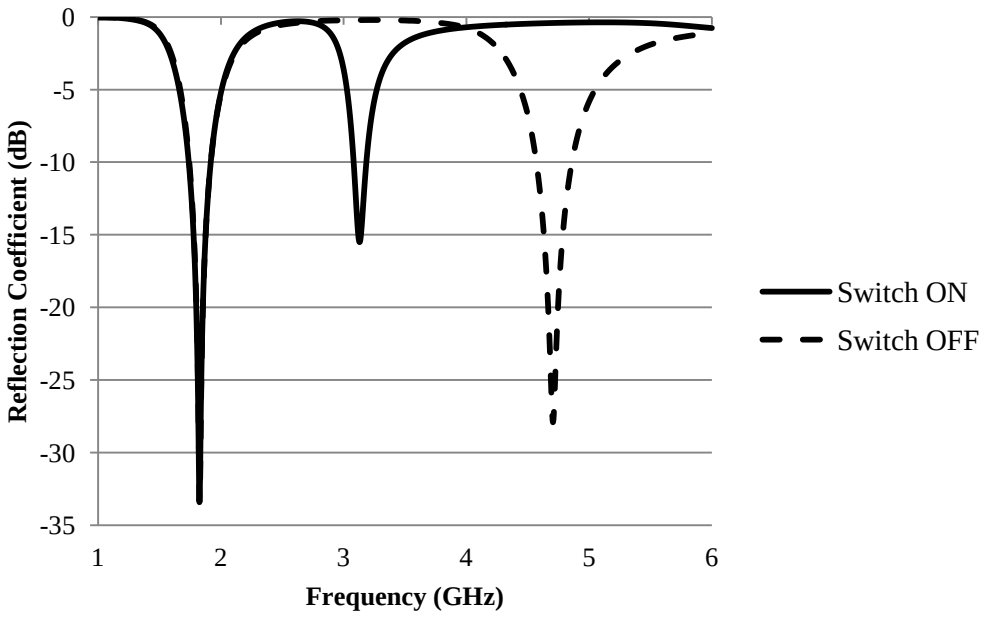

Figure 3.40: Reflection coefficient of reconfigurable PIFA with PIN diode (Gap, G_1 = 5 mm) in ON and OFF states

Table 3.12: Resonant frequency performance of reconfigurable PIFA with PIN diode (Gap, G_1 = 5 mm)

	BAR50-02V PIN Diode (Gap, G_1 = 5 mm)	
	ON State	**OFF State**
First resonant frequency, f_{r1} (GHz)	1.825	1.825
Second resonant frequency, f_{r2} (GHz)	3.13	4.705
6-dB Lower Bandwidth, BW_1 (MHz)	1.9816 – 1.6819 = **299.7**	1.9833 – 1.6891 = **294.2**
6-dB Upper Bandwidth, BW_2 (MHz)	3.2444 – 3.0416 = **202.8**	4.9883 – 4.4772 = **511.1**

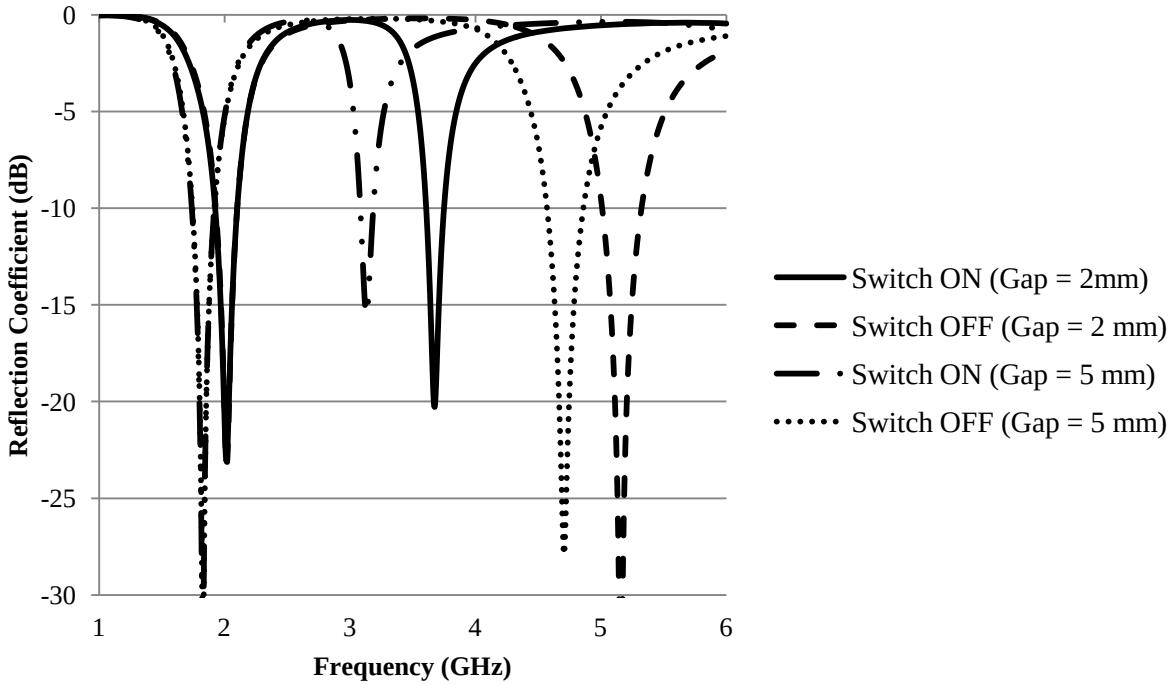

Figure 3.41: Reflection coefficient comparison of reconfigurable PIFAs with PIN diode (variations in Gap, G_1 of 2 and 5 mm)

3.6.2 Current Distribution

Current distributions on the radiating planes of the reconfigurable PIFA were simulated in CST MWS software. In either ON or OFF state, the maximum current is seen to be concentrated on the edge of the main radiating plane, the feed line and the shorting pin at 1.825 GHz. These can be viewed from Figure 3.42(a) and Figure 3.43(a). From Figure 3.42(b), the maximum current is concentrated on the edge of the main radiating plane close to the feed point and on the extra transmission lines connecting the main and additional radiating planes via the PIN diode in the ON state at 3.13 GHz. The elongation of current path from the main to the additional radiating planes increases the distance travelled which in return decreases the resonant frequency. The concentration of maximum current is observed on the edge of the main radiating plane close

to the feed point at 4.705 GHz as can be seen in Figure 3.43(b). The shorter current path implies that the resonant frequency is further increased.

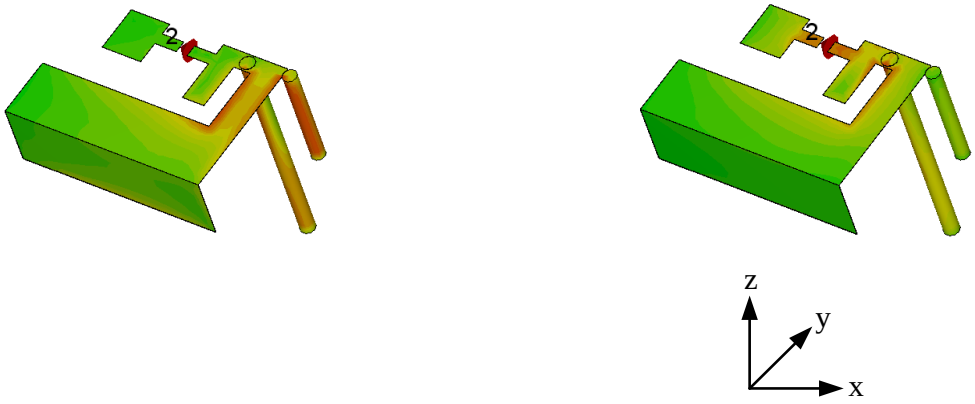

(a) (b)

Figure 3.42: Current distribution on the radiating planes of reconfigurable PIFA with PIN diode (Gap, G_1 = 5 mm) in ON state at; (a) 1.825 GHz (b) 3.13 GHz

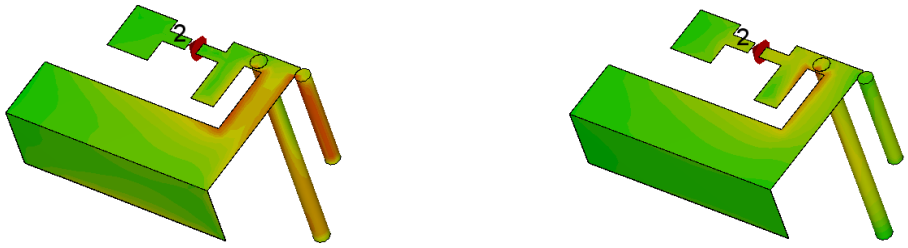

(a) (b)

Figure 3.43: Current distribution on the radiating plane of reconfigurable PIFA with PIN diode (Gap, G_1 = 5 mm) in OFF state at; (a) 1.825 GHz (b) 4.705 GHz

3.6.3 Radiation Pattern

The co-polar radiation patterns of the reconfigurable PIFA with PIN diode (Gap, G_1 = 5 mm) in xy-, xz- and yz- planes were simulated in CST MWS software at their respective resonant frequencies in ON and OFF states and are shown in Figure 3.44. The radiation patterns are similar to the radiation patterns of reconfigurable PIFA with Gap, G_1 of 2 mm (Figure 3.22).

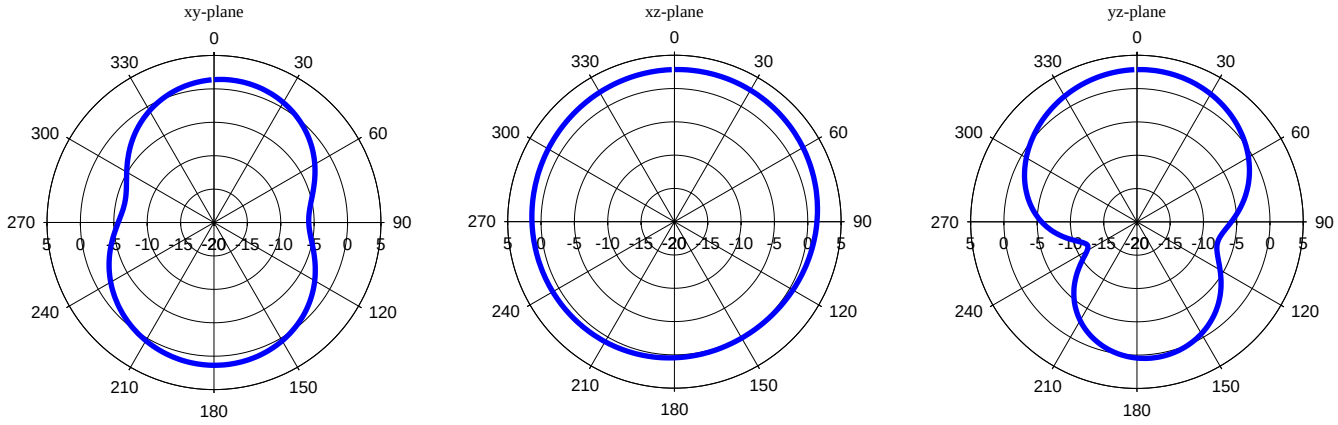

(a)

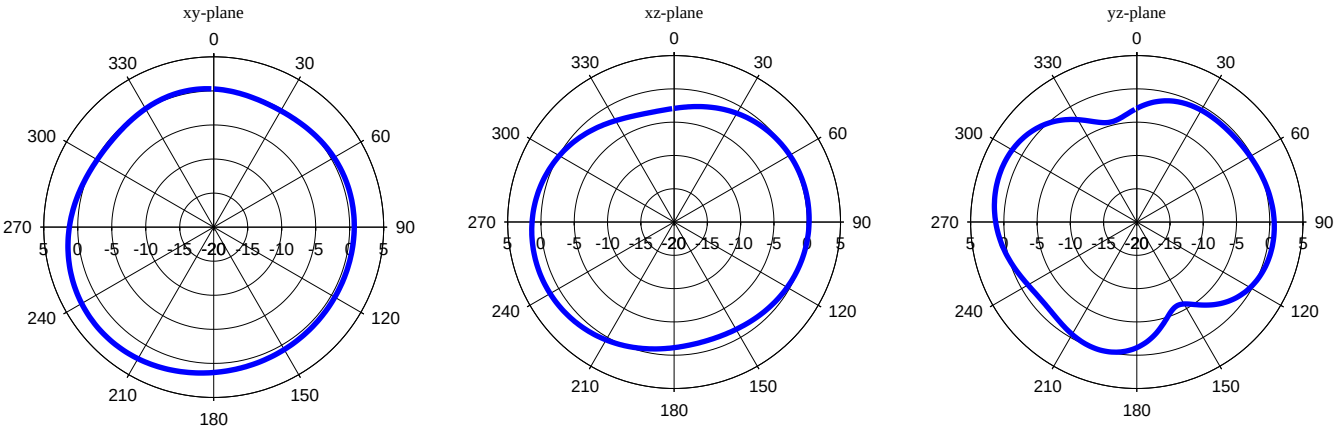

(b)

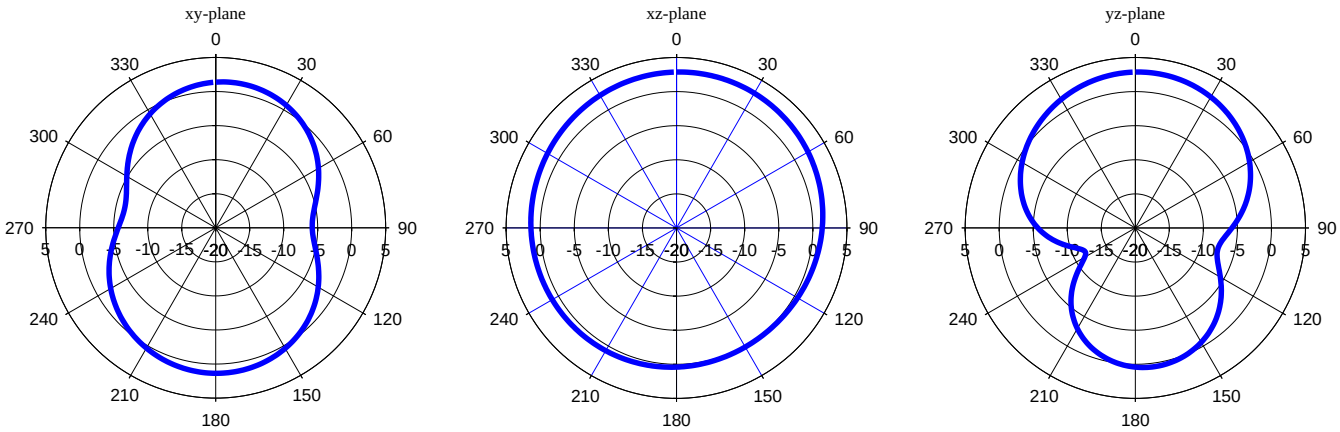

(c)

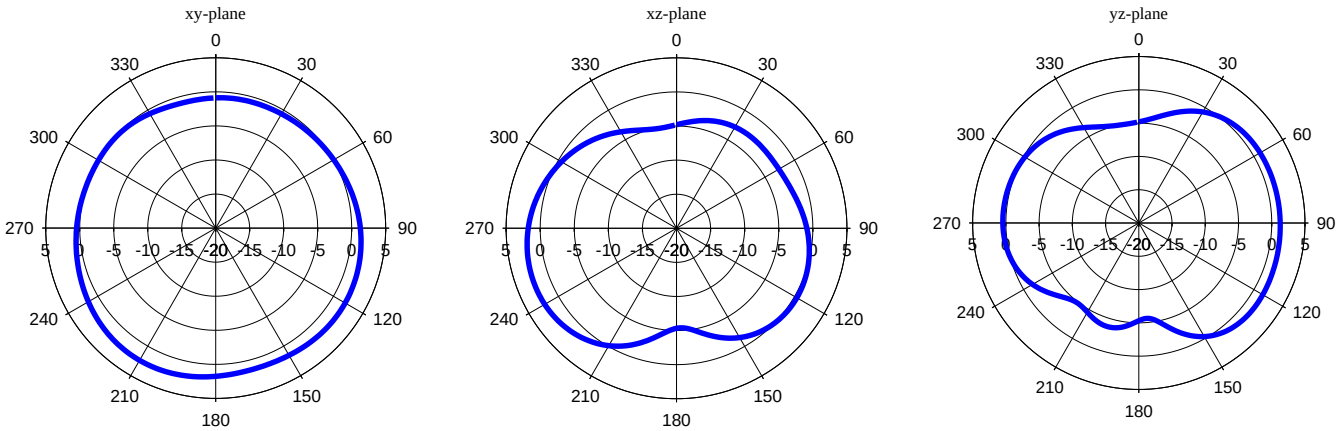

(d)

Figure 3.44: Co-polar radiation patterns in xy-, xz- and yz- planes of reconfigurable PIFA with PIN diode (Gap, G_1 = 5 mm) in ON state at; (a) 1.825 GHz (b) 3.13 GHz and OFF state at; (c) 1.825 GHz (d) 4.705 GHz

3.6.4 Realized Gain, Directivity and Efficiency

The performance of the antenna in terms of realized gain, directivity and efficiency is summarized in Table 3.13. The radiation efficiency is only 65% at 3.13 GHz which is caused by the 10 mA forward bias DC current in the ON state.

Table 3.13: Realized gain, directivity and efficiency of reconfigurable PIFA with PIN diode (Gap, G_1 = 5 mm)

	Reconfigurable PIFA with BAR50-02V PIN diode (Gap, G_1 = 5 mm)			
	ON State		**OFF State**	
	f_{r1} = 1.825 GHz	f_{r2} = 3.13GHz	f_{r1} = 1.825 GHz	f_{r2} = 4.705 GHz
Realized Gain, G (dB)	2.877	0.5528	2.890	1.494
Directivity, D (dBi)	2.917	2.555	2.933	2.730
Efficiency, η (%)	99.1	65	99.1	75.4

The gain and efficiency variations within the lower and upper frequency bands of the antenna in the ON state can be seen in Figure 3.45 and Figure 3.46.

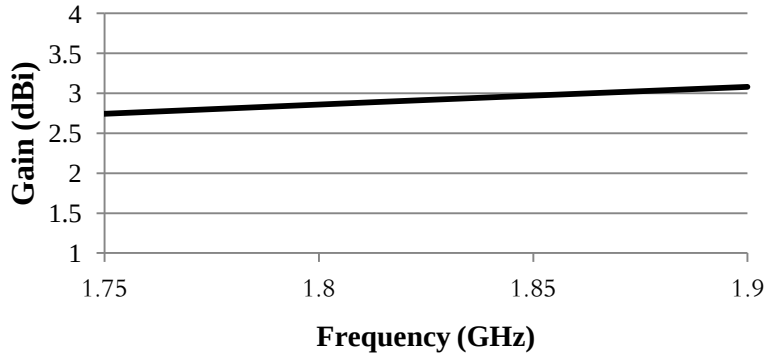

(a)

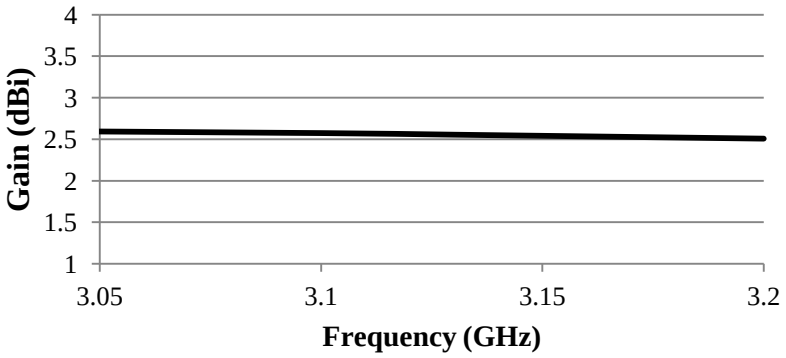

(b)

Figure 3.45: Gain of reconfigurable PIFA with PIN diode (Gap, G_1 = 5 mm) in ON state within; (a) Lower frequency band (b) Upper frequency band

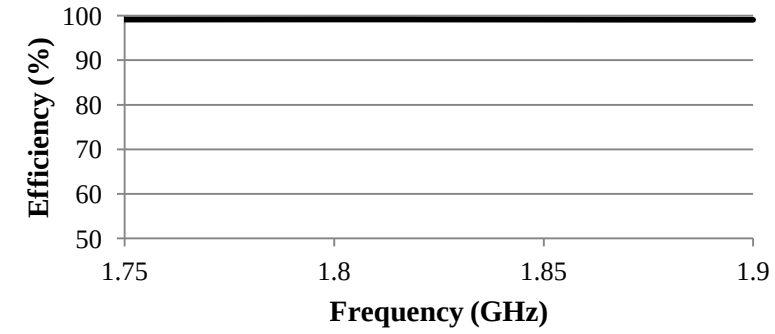

(a)

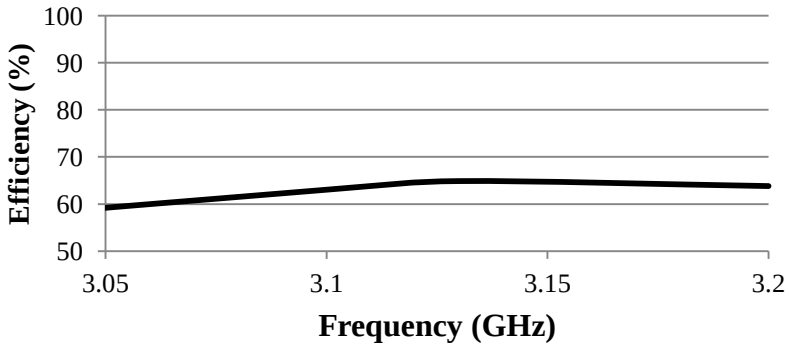

(b)

Figure 3.46: Efficiency of reconfigurable PIFA with PIN diode (Gap, G_1 = 5 mm) in ON state within; (a) Lower frequency band (b) Upper frequency band

Figure 3.47 and Figure 3.48 shows the gain and efficiency of the antenna within the lower and upper frequency bands in the OFF state.

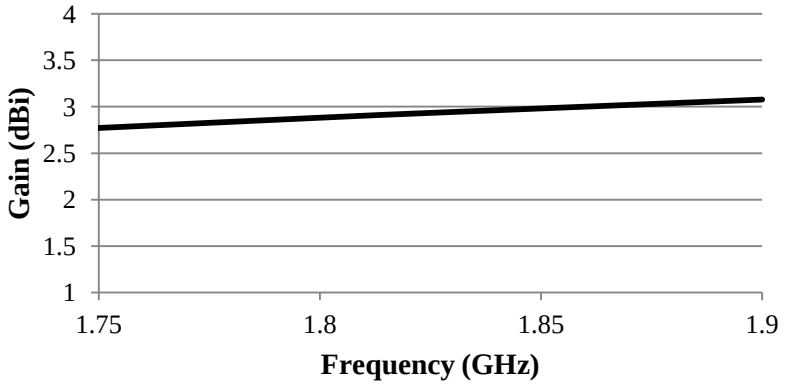

(a)

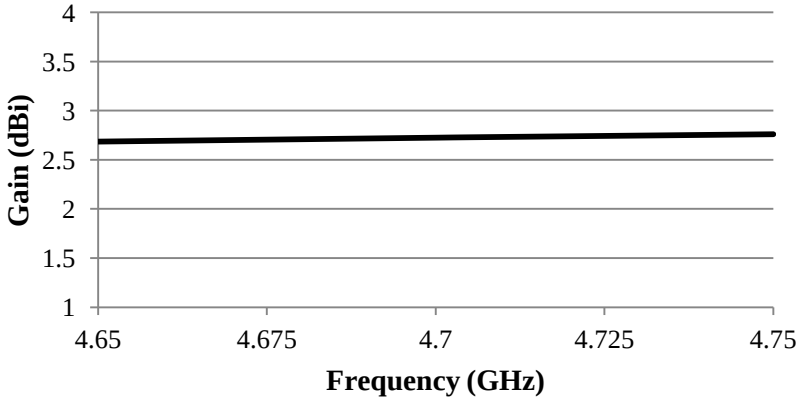

(b)

Figure 3.47: Gain of reconfigurable PIFA with PIN diode (Gap, G_1 = 5 mm) in OFF state within; (a) Lower frequency band (b) Upper frequency band

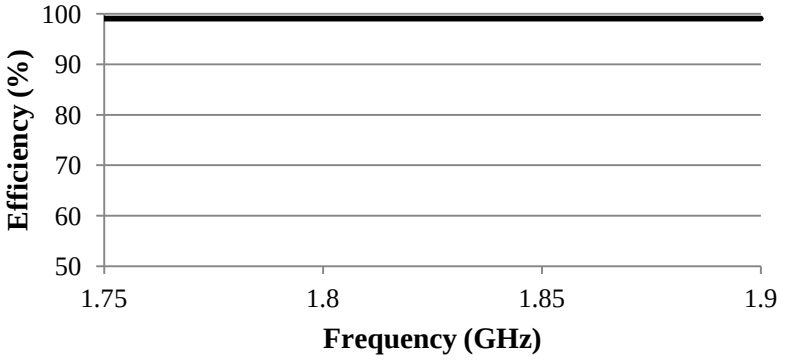

(a)

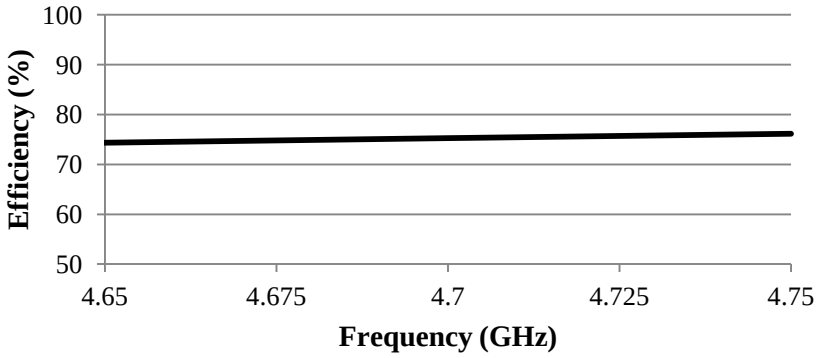

(b)

Figure 3.48: Efficiency of reconfigurable PIFA with PIN diode (Gap, G_1 = 5 mm) in OFF state within; (a) Lower frequency band (b) Upper frequency band

3.7 Antenna Fabrication and Measurement

The reconfigurable PIFA with PIN diode (Gap, G_1 = 5 mm) was fabricated using the same technique to fabricate the previous antenna. The same bias voltage, V_b of 12 V was applied to switch the PIN diode in its ON state with a current limiting resistor, R of 1.1 kΩ which allows only 10 mA of forward bias current to pass through. The power supply was removed in the OFF state. The fabricated antenna from multiple views can be viewed in Figure 3.49 while Figure 3.50 shows the biasing setup of the reconfigurable PIFA.

(a) (b)

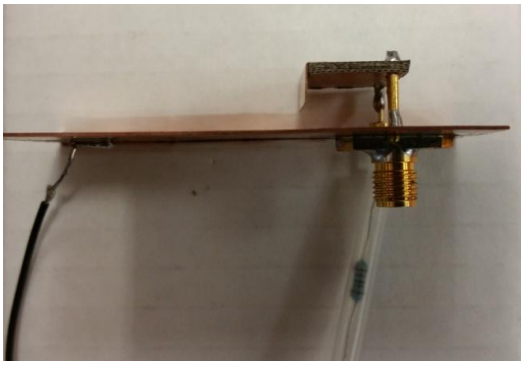

(c)

Figure 3.49: Fabricated reconfigurable PIFA with PIN diode (Gap, G_1 = 5 mm);
(a) Front view (b) Top view (c) Side view

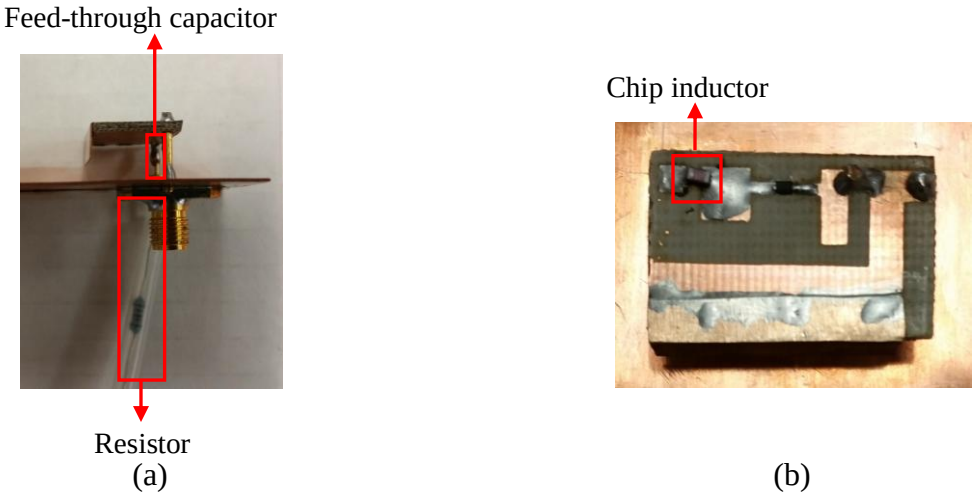

(a) (b)

Figure 3.50: DC bias setup for reconfigurable PIFA measurement;
(a) 1200-pF feed-through capacitor and 1.1-kΩ resistor (b) 16-nH chip inductor

3.7.1 Reflection Coefficient Measurement

The same experimental setup to measure the reflection coefficient of previous antenna was applied to this antenna as can be seen in Figure 3.51.

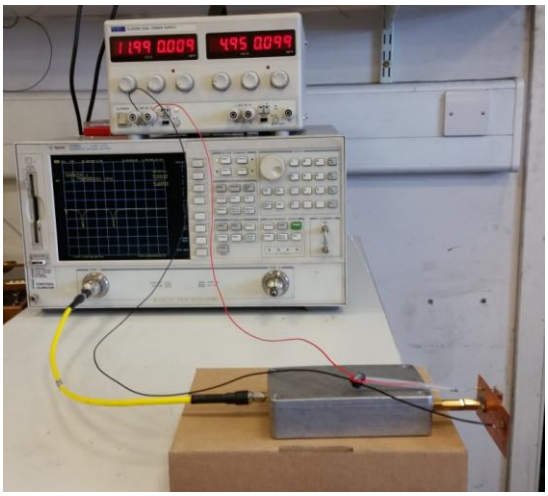

Figure 3.51: Measurement setup of reconfigurable PIFA with PIN diode (Gap, G_1 = 5 mm)

3.8 Active Switch Performance and Antenna Analysis

The measured reflection coefficients for both states of the reconfigurable PIFA were compared with the simulated results in CST MWS software. The comparison in the ON and OFF states is shown in Figure 3.52 and Figure 3.53. It is apparent that a new resonance is seen in the OFF state. From the investigation conducted previously, it is caused by the bias inductor.

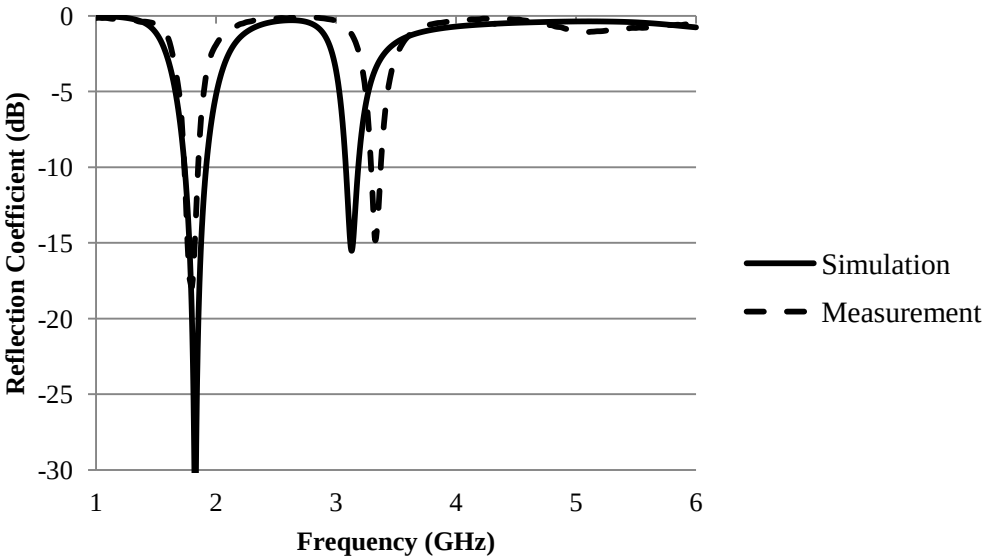

Figure 3.52: Measured reflection coefficient of reconfigurable PIFA with PIN diode (Gap, G_1 = 5 mm) in ON state

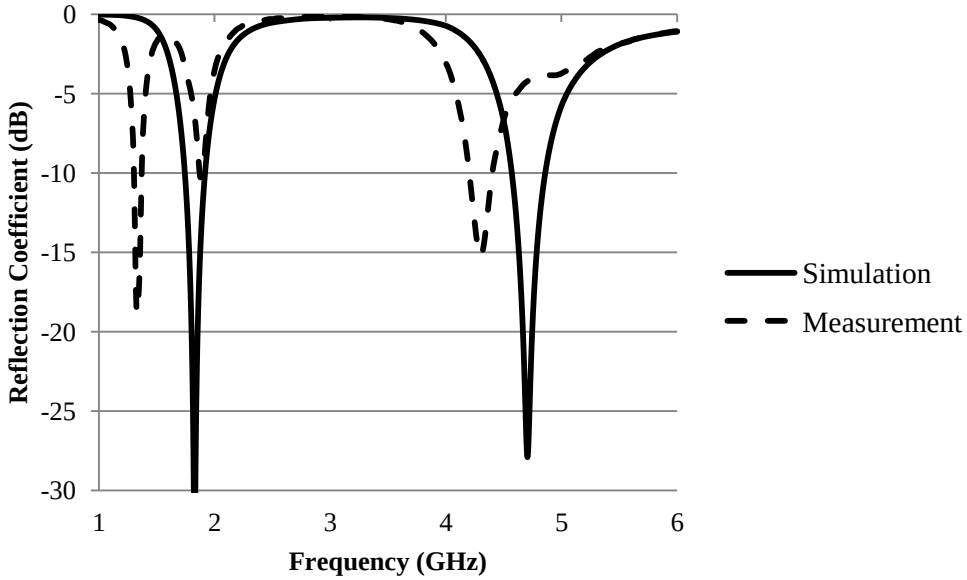

Figure 3.53: Measured reflection coefficient of reconfigurable PIFA with PIN diode (Gap, G_1 = 5 mm) in OFF state

3.9 Conclusion

In this chapter, a preliminary investigation was conducted to examine the nature of the PIFA before an active switch was introduced on the radiating structure of the antenna to reconfigure the frequency. Two reconfigurable PIFAs with PIN diodes (Gap, G_1 = 2 and 5 mm) were successfully designed, simulated and fabricated. The variations in the gap are necessary to accommodate the size of the active switch. Initially, the reconfigurable PIFA with the 2 mm gap between the main and additional radiating planes was designed to fit the smaller size of the PIN diode ($\approx 1 \times 1$ mm^2). However, the gap has to be increased to 5 mm to cater for the bigger size of the E-PHEMT ($\approx 2.25 \times 2.40$ mm^2) and its biasing components. Two resonant frequencies are generated in each state of the PIN diode. The first resonant frequency is similar in both ON and OFF states of the PIN diode. The second resonant frequency is being switched to the lower frequency in the ON state and to the upper frequency in the OFF state. This behaviour can be explained from the relation of the current path with respect to the reduction or increment in the resonant frequencies. From the measurement result in the OFF state, a new resonance is observed before the first resonant frequency for both antennas. Thus, further investigation was conducted to clarify the behaviour before a conclusion was made that it was caused by the chip inductor as one of the biasing components.

CHAPTER 4

4. RECONFIGURABLE PIFA WITH ATF 54143 E-PHEMT SWITCH

4.1 Introduction

In this chapter, a field-effect transistor (FET) switch will be introduced into the PIFA radiating structure to reconfigure the resonant frequencies. There are several variations of FET switches in the market depending on the technology to manufacture them. Metal-semiconductor FET (MESFET) and pseudomorphic high-electron mobility transistor (PHEMT) are the two variations of transistors that are widely used as switches in mobile communication applications. The comparisons of the two switches are listed in Table 4.1 [2]. The characteristics of the transistors as switching elements are briefly discussed in the next section.

Table 4.1: Comparison of MESFET and PHEMT in switching configurations

	1 µm MESFET Switch	**0.25 µm PHEMT Switch**
Number of terminals	3	3
Typical ON resistance	1.5 Ω/mm	1.2 Ω/mm
Typical OFF capacitance	0.40 pF/mm	0.32 pF/mm
Figure-of-Merit	265 GHz	414 GHz
Breakdown voltage	15 V	8 V
Lower frequency limit	DC	DC
Driver circuit complexity	Low	Low
Driver requirements	0 V (ON); -5 V (OFF)	+0.5 V (ON); -5 V (OFF)

4.1.1 Characteristics of Switching Transistors

In general, a FET is a three terminal device denoted by Gate (G), Source (S) and Drain (D). The transistor can be reconfigured to act as a switch with a proper biasing. A structure of a FET [81] can be seen in Figure 4.1. Electrons are drawn from the source to the drain by the positive V_{ds} supply voltage. The majority electron carriers will then be modulated by an input signal voltage on the gate which produces voltage amplification. The gate length will limit the maximum frequency of operation. Commonly, the manufactured FETs have gate lengths on the order of 0.3 to 0.6 μm with corresponding upper frequency limits of 100 to 50 GHz.

The equivalent circuit of the FET in the ON and OFF states can be viewed in Figure 4.2. From the figure, the channel between the source and drain will act as a conducting path for the RF signal to flow. Gate port will control whether the RF signal will be blocked or passed through depending on the states of the switch. In the ON and OFF states, the channel may be represented by small impedance, R_{ON} and capacitance, C_{OFF}. Voltage and current characteristic with negative current and voltage segments when the FET is in the ON and OFF states is illustrated in Figure 4.3.

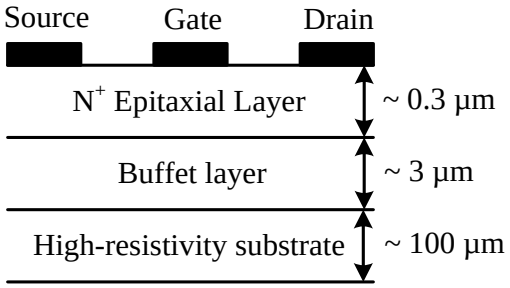

Figure 4.1: Cross section of a Field Effect Transistor (FET) [81]

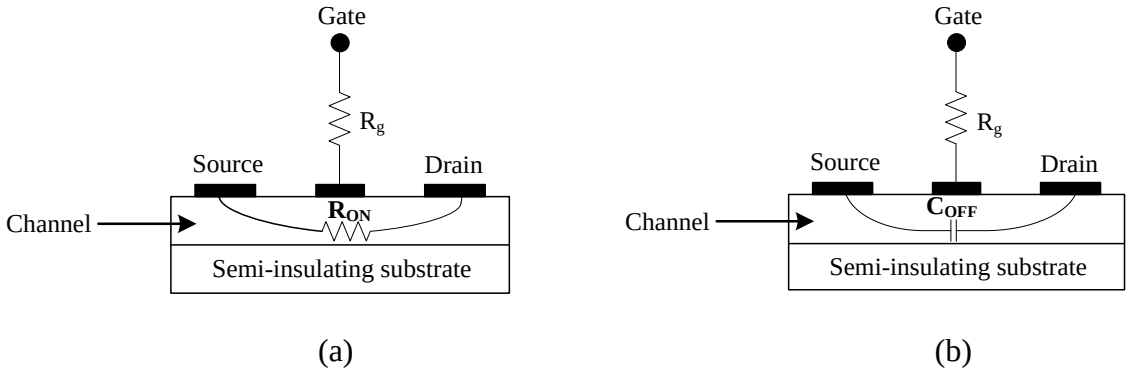

Figure 4.2: FET equivalent circuit in the; (a) ON state (b) OFF state

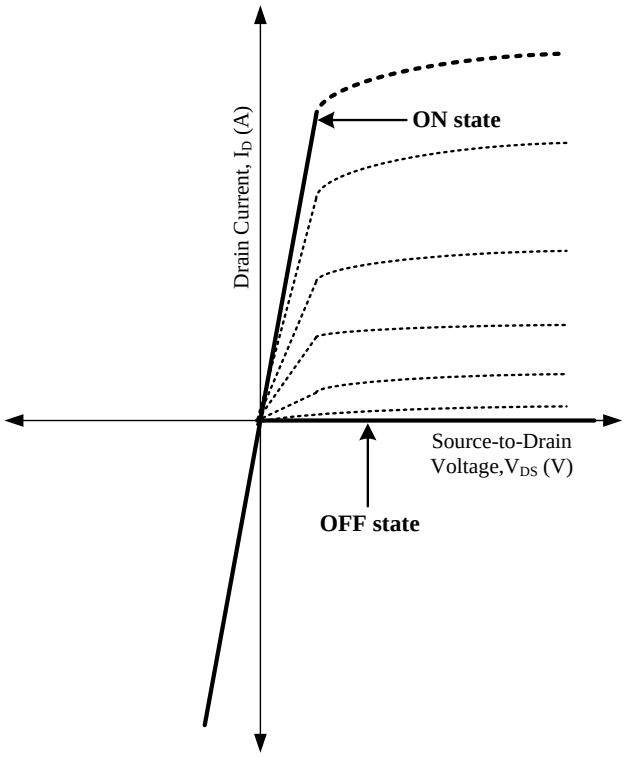

Figure 4.3: Voltage-Current characteristic when FET is in ON and OFF states

4.2 Low Noise Pseudomorphic Enhancement Mode High-Electron Mobility Transistor (E-PHEMT) by Avago Technologies

In this work, the ATF 54143 E-PHEMT by Avago Technologies was used to reconfigure the antenna. The advantage of enhancement mode technology is that it only requires a single positive voltage source, V_{gs}. Thus, the need for negative gate voltage associated with the conventional depletion mode devices has been eliminated in this technology. ATF 54143 E-PHEMT is a combination of high gain, high linearity and low noise transistor with a frequency range from 450 MHz to 6 GHz. This transistor is housed in a miniature 4-lead SC-70 (SOT-343) surface mount plastic package. The pin connections can be seen in Figure 4.4. The datasheet of the transistor can be viewed in Appendix B.

(a) (b)

Figure 4.4: ATF 54143 E-PHEMT;
(a) Surface mount package (b) Pin connections and package marking

In order to analyse the switching action of the ATF 54143 transistor, it was modeled in AWR Microwave Office (MWO) software with a proper biasing circuit. The model was then simulated to look at the specific behaviour of the S-parameters in the ON and OFF states. Instead of modeling the transistor in lumped elements, a Modelithic™ model of the ATF 54143 transistor in AWR MWO has been obtained from the manufacturer. The advantage of a Modelithic™ model

is that it includes package parasitic effect and this will generate more accurate simulation results. The next task is to design the biasing circuit so that the transistor can be used as a switch. For that reason, the required lumped elements are connected to the Gate, Source and Drain of the transistor to supply the voltage and current in ON state and to block them in OFF state. The main objective is to reduce the insertion loss in the ON state and to improve the isolation in the OFF state. The circuit diagrams of the proposed biasing circuits for the ATF 54143 E-PHEMT in the ON and OFF states can be viewed in Figure 4.5. From the figure, two different bias voltages are applied to the gate to switch the transistor. A bias voltage of +1 V is applied to switch ON the transistor and a negative bias voltage of -1 V to switch it OFF. A 1.6 pF chip capacitor is connected in series with the Source pin to improve the impedance matching of the lower frequency range in the ON state and the higher frequency range in the OFF state.

The results of the best compromise between high isolation and low insertion loss of the simulated S-parameters in AWR MWO software can be seen in Figure 4.6. From Figure 4.6(a), the insertion loss, S_{21} at 4 GHz is approximately 0.66 dB which means that only a small amount of power is dissipated. Thus, the reconfigurable PIFA efficiency will not be affected by the switch. Meanwhile, the reflected signal, S_{11} of the switch is -12.3 dB. From Figure 4.6(b), the isolation in the OFF state is 11.6 dB at 2 GHz. The reflected signal on the other hand is -0.37 dB which is considerably low.

The S-parameters of the ATF 54143 E-PHEMT switch in the ON and OFF states was then converted to Touchstone (*.s2p) files which contain all the two-port S-parameters data. These Touchstone files were exported to the Schematic view of CST MWS software and connected to the discrete port of the reconfigurable PIFA before being simulated to get the required results.

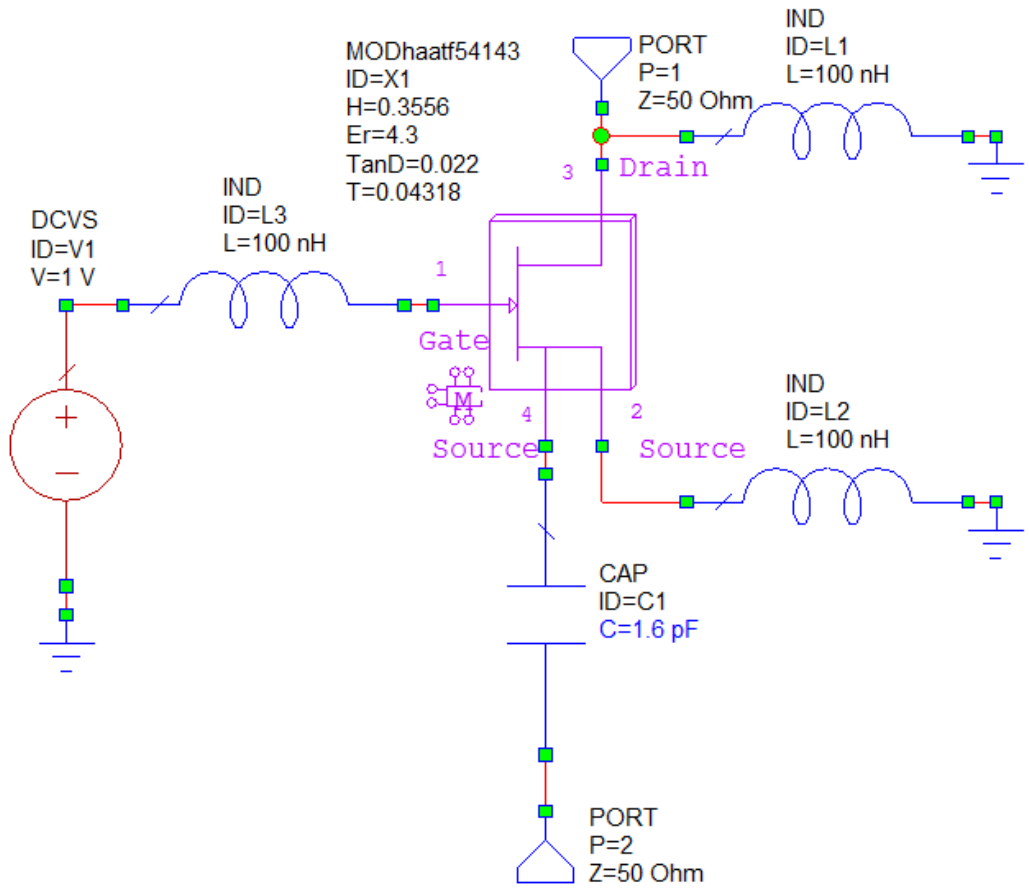

Figure 4.5: Circuit diagram of E-PHEMT switch in ON state. In OFF state, a bias voltage of -1 V is applied to the gate of the transistor

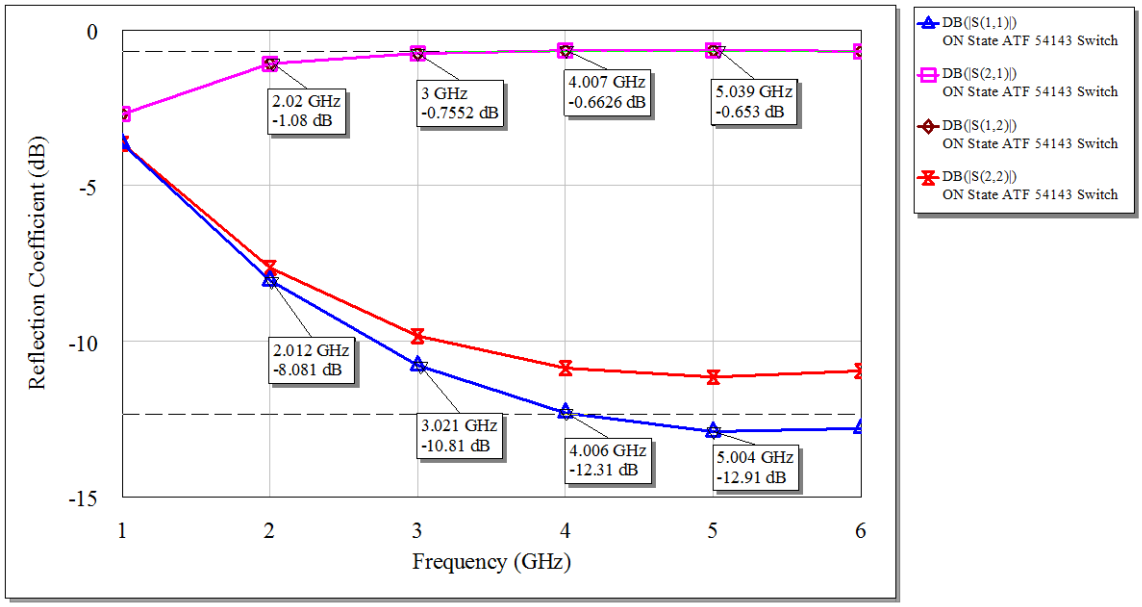

(a)

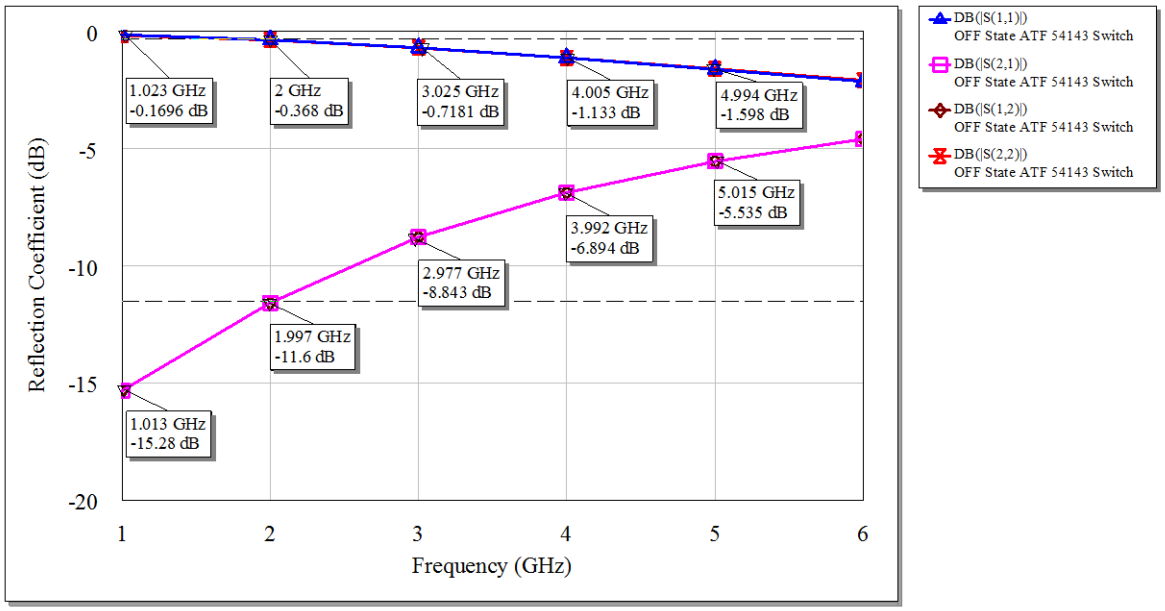

(b)

Figure 4.6: Simulated reflection loss, S_{11} and insertion loss, S_{21} of E-PHEMT switch in; (a) ON state (b) OFF state

The switch can also be represented by lumped element circuit models in the ON and OFF states. This can be done by adopting a simplified RLC equivalent circuit without having to include the surface mounting effect. The lumped element equivalent circuits of the E-PHEMT switch in the ON and OFF states are shown in Figure 4.7.

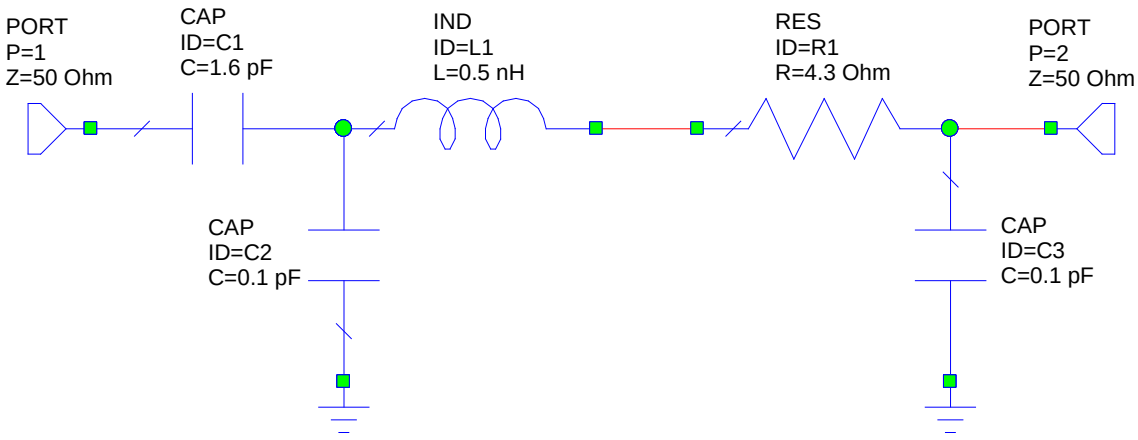

(a)

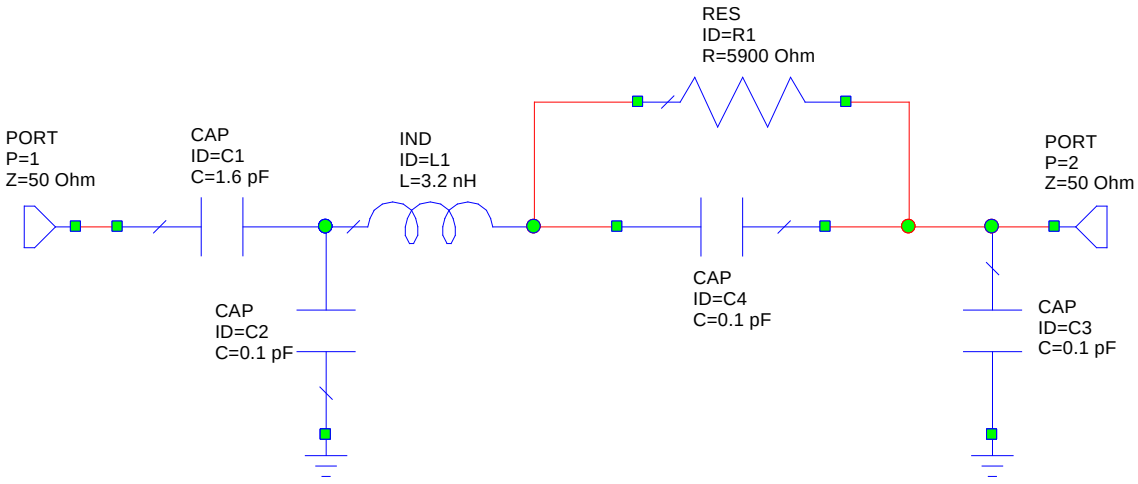

(b)

Figure 4.7: Lumped element equivalent circuit of E-PHEMT switch in;
(a) ON state (b) OFF state

The lumped element values of R, L and C in the ON and OFF states of the E-PHEMT switch were optimized in AWR MWO software and are listed in Table 4.2. In the optimization process, the circuit models in Figure 4.7 were constructed and the S_{11} and S_{21} results obtained were compared with the simulation results of the ATF 54143 E-PHEMT as a switch (Figure 4.6). The comparison was performed on the Smith Chart as shown in Figure 4.8.

Table 4.2: The lumped element values of ATF 54143 E-PHEMT switch in ON and OFF states

	ATF 54143 E-PHEMT Switch	
	ON State	**OFF State**
R1 (Ω)	4.3	5900
L1 (nH)	0.5	3.2
C1 (pF)	1.6	1.6
C2 (pF)	0.1	0.1
C3 (pF)	0.1	0.1
C4 (pF)	-	0.1

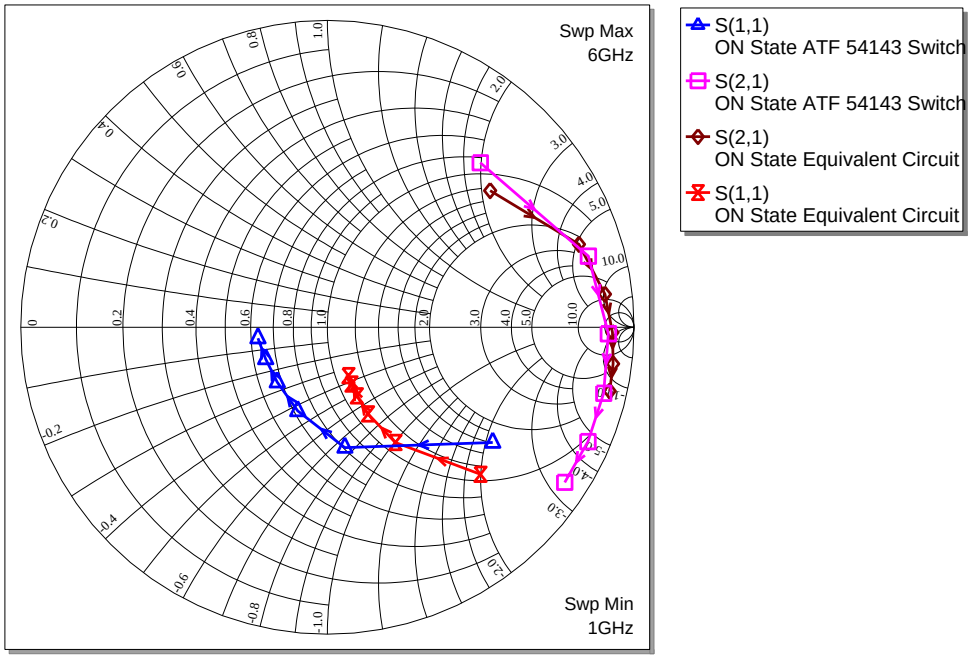

(a)

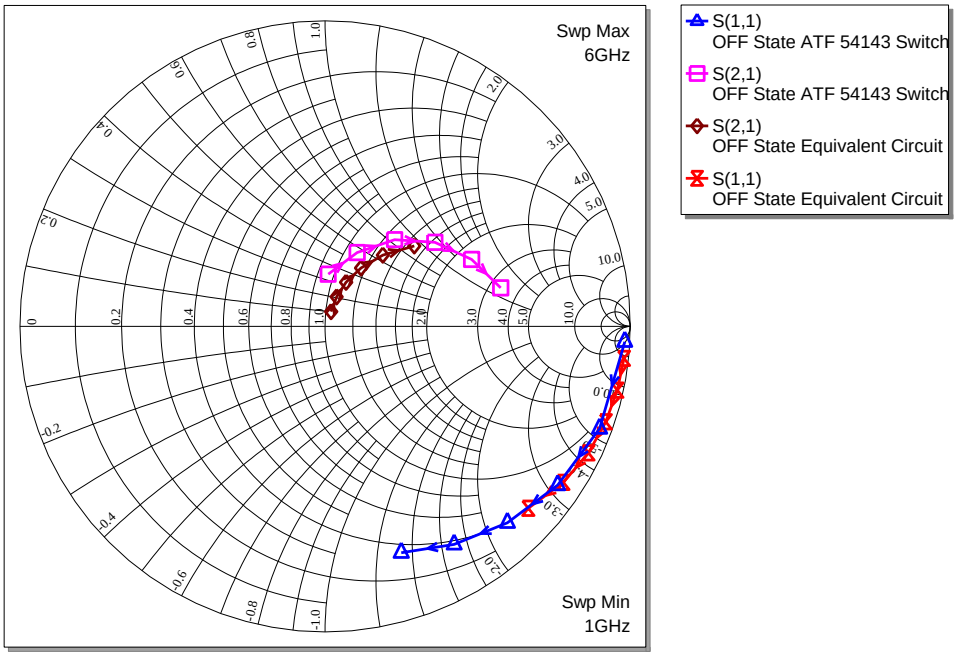

(b)

Figure 4.8: S_{11} and S_{21} of lumped element equivalent circuit and S_{11} and S_{21} of simulated ATF 54143 E-PHEMT switch in; (a) ON state (b) OFF state

4.3 Antenna Geometry and Dimensions

The geometry and dimensions of the reconfigurable PIFA with E-PHEMT switch are similar to the reconfigurable PIFA with PIN diode (Gap, G_1 = 5 mm). Figure 4.9 shows the location of the switch on the radiating structure of the antenna. The switch is represented by a discrete port in CST MWS software.

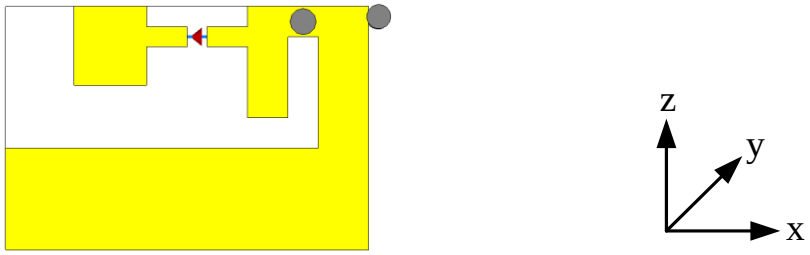

Figure 4.9: Location of a discrete port to represent the ATF 54143 E-PHEMT switch

4.4 Antenna Design and Configuration

The idea of reconfiguring the PIFA with E-PHEMT switch is demonstrated in this section. The Touchstone 2-port S-parameters (*.s2p) files of the switch in the ON and OFF states which were previously simulated in AWR MWO software were exported to CST MWS software and were used to simulate the antenna in its ON and OFF states. The ability of CST MWS software to simulate the Touchstone files in its Schematic canvas has been utilized to get the desired results. The Schematic view of the reconfigurable PIFA in the ON and OFF states can be viewed in Figure 4.10.

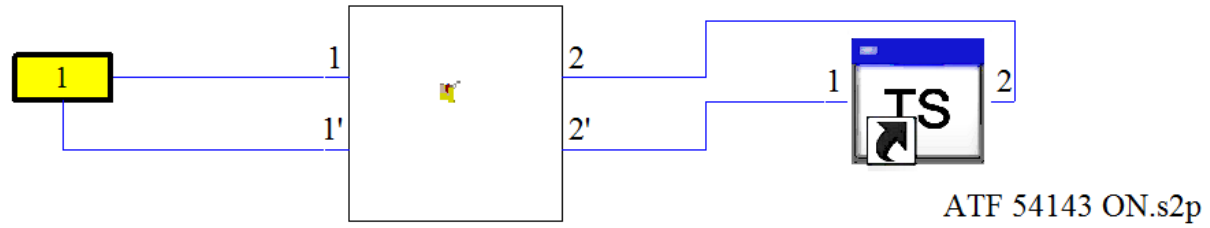

(a)

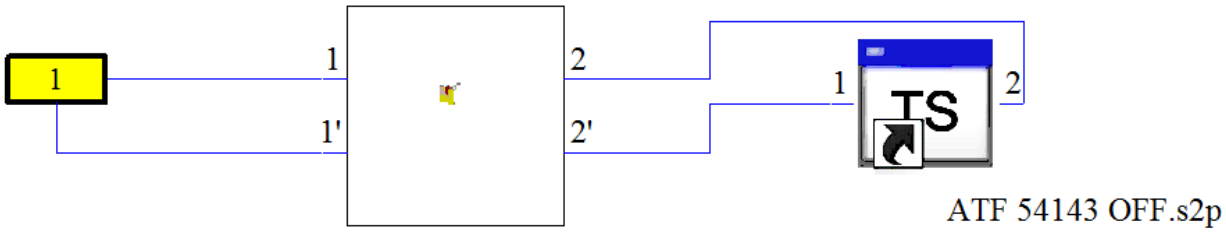

(b)

Figure 4.10: Schematic view of reconfigurable PIFA with E-PHEMT switch in;
(a) ON state (b) OFF state

4.4.1 Reflection Coefficient

The simulated reflection coefficients of the reconfigurable PIFA in the ON and OFF states can be viewed in Figure 4.11. From the figure, the first resonant frequency remains similar regardless of the state of the switch. The second resonant frequency is being switched from the upper to the lower frequency or vice versa depending on the state of the switch. This behaviour is similar to the previous reconfigurable PIFA with PIN diode.

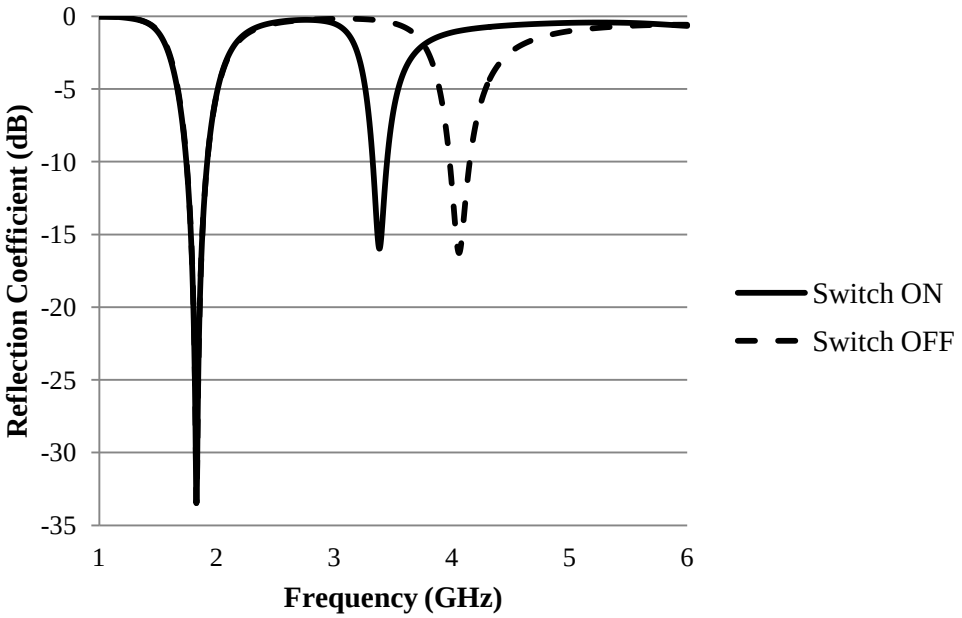

Figure 4.11: Reflection coefficient comparison of reconfigurable PIFA with E-PHEMT switch in ON and OFF states

Table 4.3 summarizes the resonant frequency performance of the antenna. From the table, it can be seen that the first resonant frequency remains similar at 1.825 GHz in both states of the switch. In the ON state, the upper resonant frequency is reduced to 3.38 GHz from 4.06 GHz in the OFF state.

Table 4.3: Resonant frequency performance of reconfigurable PIFA with E-PHEMT switch

	Reconfigurable PIFA with ATF 54143 E-PHEMT Switch	
	ON State	**OFF State**
First resonant frequency, f_{r1} (GHz)	1.825	1.825
Second resonant frequency, f_{r2} (GHz)	3.38	4.06
6-dB Lower Bandwidth, BW_1 (MHz)	1.9819 – 1.6837 = **298.2**	1.9829 – 1.6875 = **295.4**
6-dB Upper Bandwidth, BW_2 (MHz)	3.5134 – 3.2793 = **234.1**	4.2437– 3.9163 = **327.4**

4.4.2 Current Distribution

Current distributions on the radiating structure of the reconfigurable PIFA with E-PHEMT switch can be viewed in Figure 4.12 and Figure 4.13. A clear similarity is observed at 1.825 GHz in both states of the switch. At that particular frequency, the maximum current is seen to be concentrated on the edge of the main radiating plane, the feed line and the shorting pin. In the upper resonant frequency of 3.38 GHz in the ON state, the maximum current is concentrated on edge of the main radiating plane close the feed point and the extra transmission lines connecting the main and additional planes via the switch. This suggested that the electrical current path is elongated from the main to additional radiating planes. Thus, the path is longer which reduces the resonant frequency.

In the OFF state, the same concentration of maximum current can also be seen on the edge of the main radiating plane and extra transmission lines but with less intensity as compared to the ON state as can be observed in Figure 4.13(b). This suggested that some of the current is passing through the switch increases the electrical current path but it is still shorter than the current path in the ON state based on the density.

The fact that the upper resonant frequency in the OFF at 4.06 GHz is close to 3.38 GHz (only differ by 680 MHz) suggested that there is not much frequency switching behaviour and has complied with the current distribution observation. On another note, a logical explanation to this behaviour can also be explained from the low isolation in the upper frequency range of the OFF state as can be referred from Figure 4.6(b).

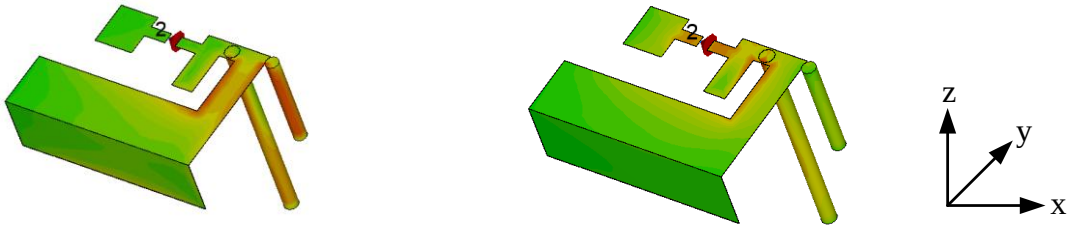

(a) (b)

Figure 4.12: Current distributions on the radiating structure of reconfigurable PIFA with E-PHEMT switch in ON state at; (a) 1.825 GHz (b) 3.38 GHz

(a) (b)

Figure 4.13: Current distributions on the radiating structure of reconfigurable PIFA with E-PHEMT switch in OFF state at; (a) 1.825 GHz (b) 4.06 GHz

4.4.3 Radiation Pattern

The co-polar radiation patterns in xy-, xz- and yz- planes of the reconfigurable PIFA were simulated in CST MWS to determine the performance of the antenna. The radiation patterns in the ON and OFF states of the antenna can be viewed in Figure 4.14. The radiation patterns in the xy-plane ($\theta = 90°$) at 1.825 GHz have a doughnut-shaped pattern cutting across the plane. In the xz- ($\phi = 0°$) and yz- ($\phi = 90°$) planes, omnidirectional and directional radiation patterns with minimum back lobes have been observed. At the upper resonant frequencies, similar radiation patterns have been observed in both states. In the xy- and xz- planes, the radiation patterns are

dipole-like and omnidirectional. However, in yz- plane, the radiation patterns have nulls in several directions.

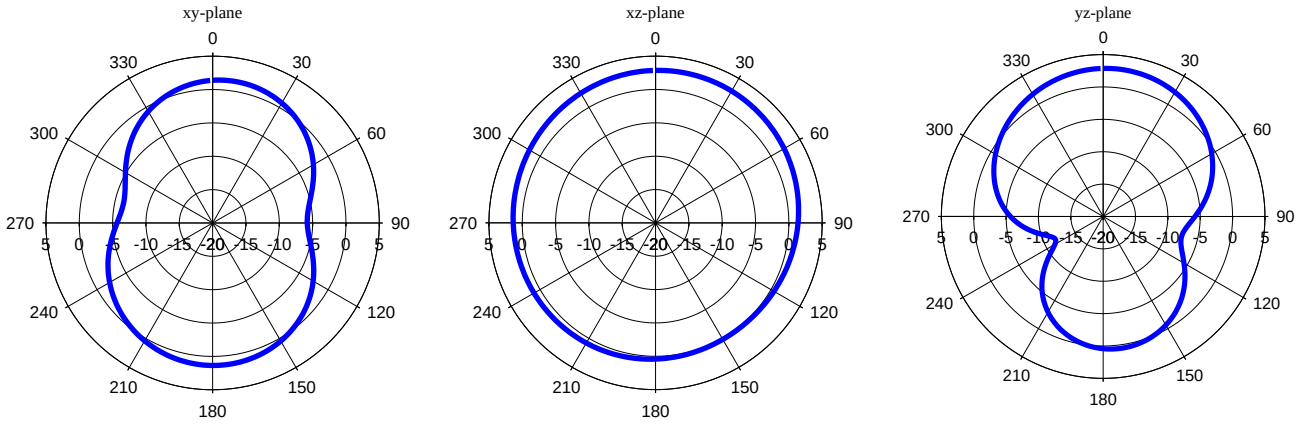

(a)

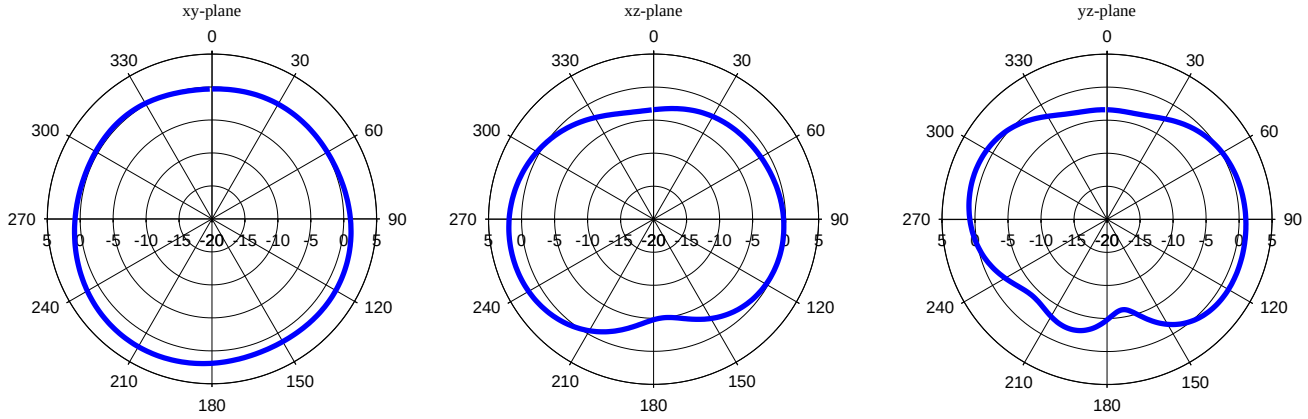

(b)

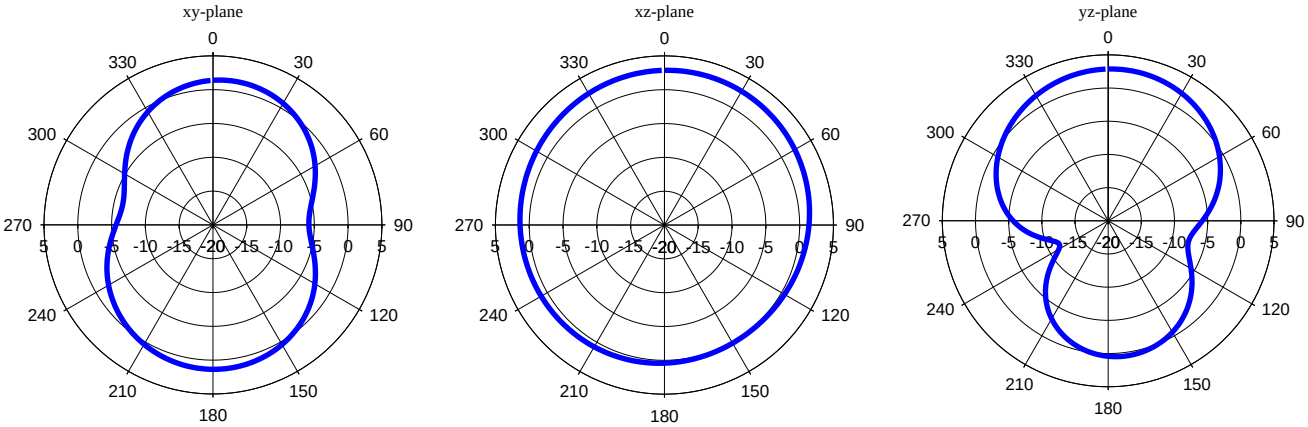

(c)

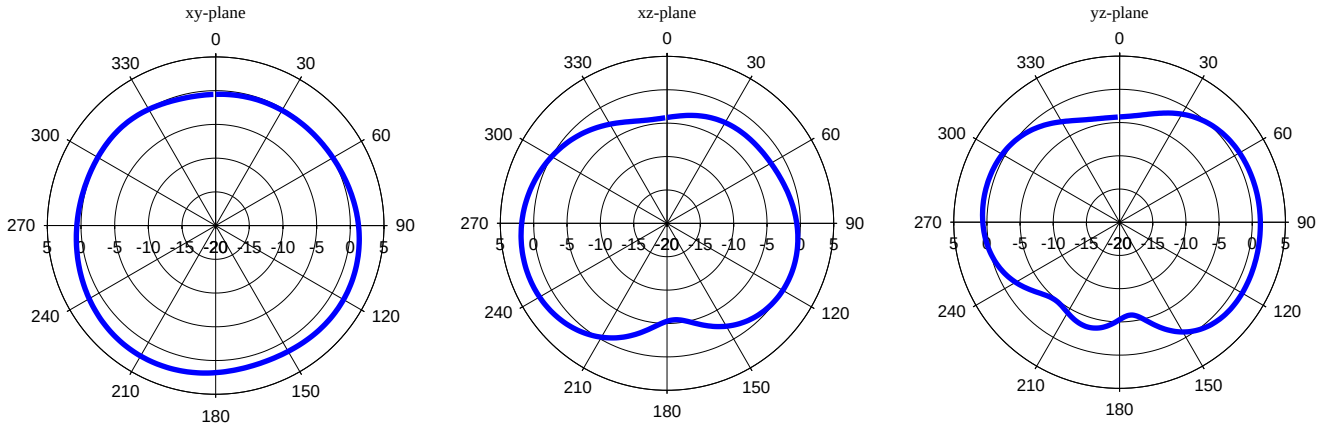

(d)

Figure 4.14: Co-polar adiation patterns in xy-, xz- and yz- planes of reconfigurable PIFA with E-PHEMT switch in ON state at; (a) 1.825 GHz (b) 3.38 GHz and OFF state at; (c) 1.825 GHz (d) 4.06 GHz

4.4.4 Realized Gain, Directivity and Efficiency

The realized gain, directivity and efficiency of the reconfigurable PIFA are summarized in Table 4.4. From the table, it can be seen that the realized gain, directivity and efficiency are consistently good at all resonant frequencies except at 3.38 GHz where the efficiency is considerably low.

Table 4.4: Realized gain, directivity and efficiency of reconfigurable PIFA with E-PHEMT switch in ON and OFF states

	Reconfigurable PIFA with ATF 54143 E-PHEMT Switch			
	ON State		**OFF State**	
	f_{r1} = 1.825 GHz	f_{r2} = 3.38 GHz	f_{r1} = 1.825 GHz	f_{r2} = 4.06 GHz
Realized Gain, G (dB)	2.881	0.9002	2.881	1.614
Directivity, D (dBi)	2.921	2.587	2.929	2.416
Efficiency, η (%)	99.1	69.6	99.1	85.1

The gain and efficiency variations within the lower and upper frequency bands of the antenna in the ON state can be viewed in Figure 4.15 and Figure 4.16.

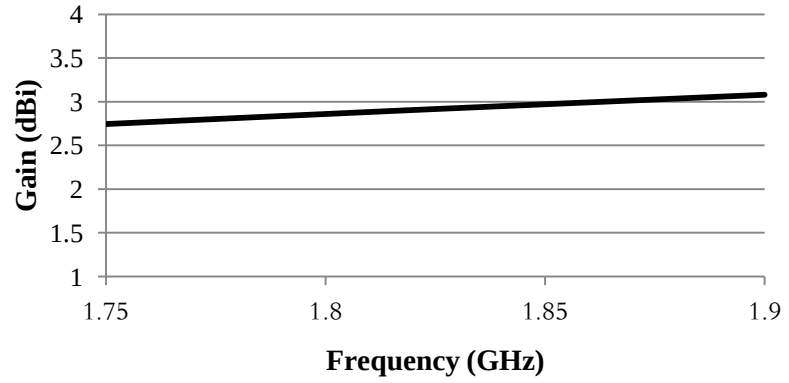

(a)

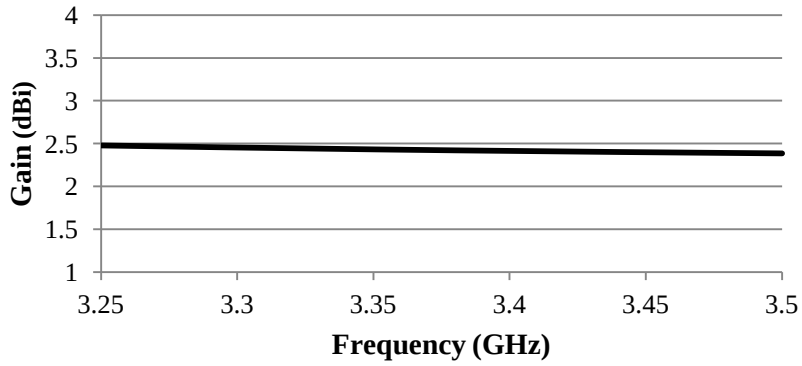

(b)

Figure 4.15: Gain of reconfigurable PIFA with E-PHEMT switch in ON state within;
(a) Lower frequency band (b) Upper frequency band

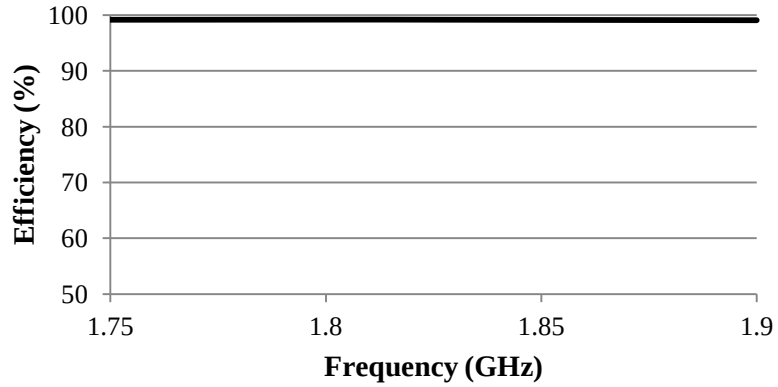

(a)

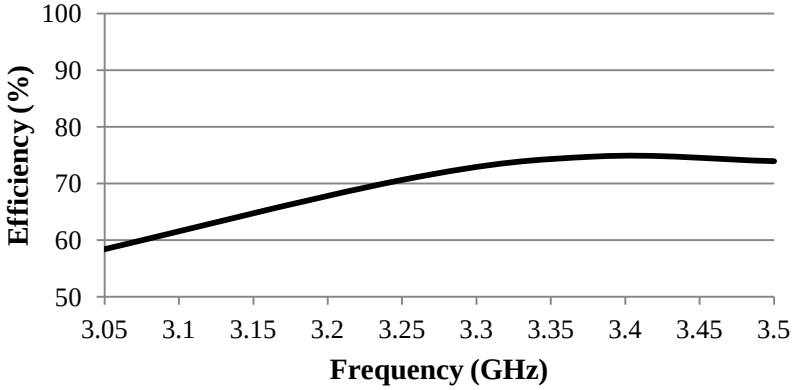

(b)

Figure 4.16: Efficiency of reconfigurable PIFA with E-PHEMT switch in ON state within; (a) Lower frequency band (b) Upper frequency band

Figure 4.17 and Figure 4.18 shows the gain and efficiency of the antenna within the lower and upper frequency bands in the OFF state.

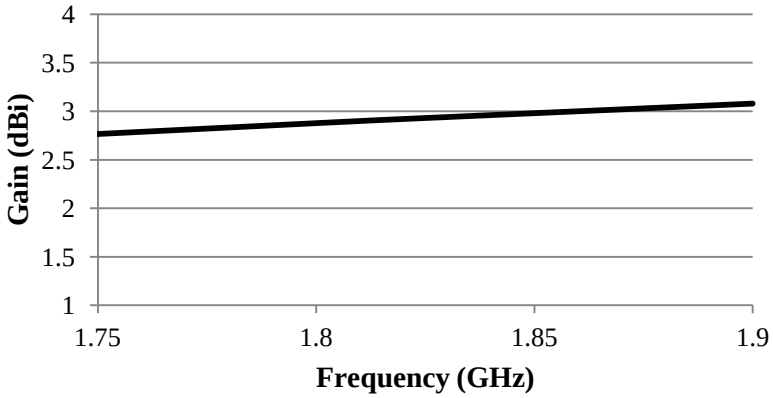

(a)

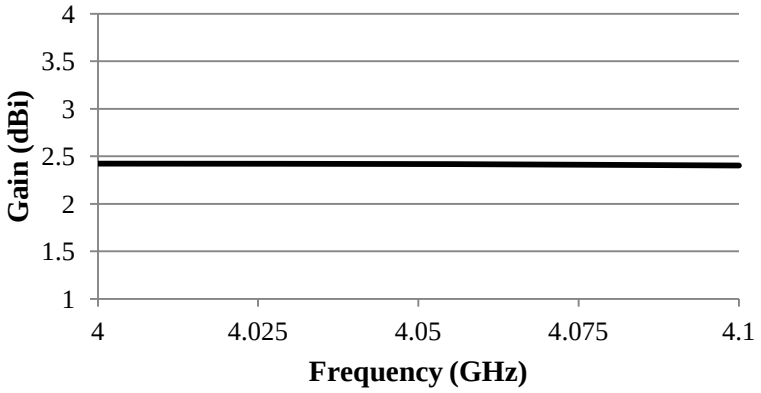

(b)

Figure 4.17: Gain of reconfigurable PIFA with E-PHEMT switch in OFF state within; (a) Lower frequency band (b) Upper frequency band

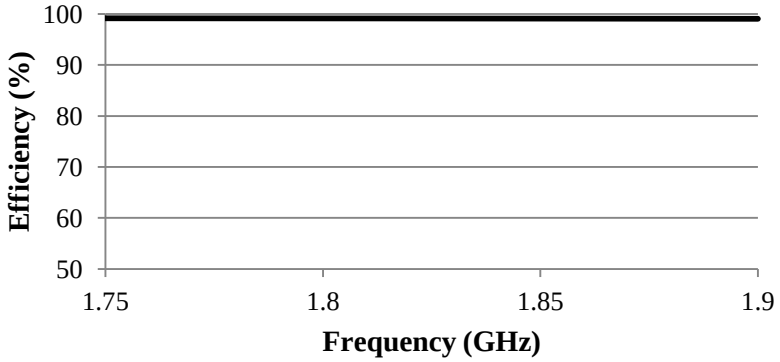

(a)

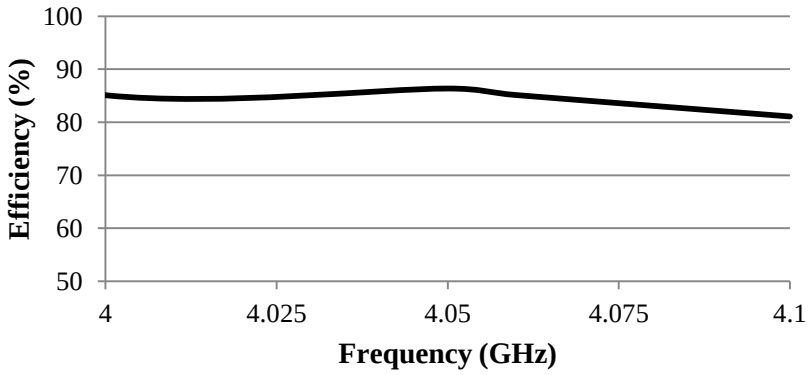

(b)

Figure 4.18: Efficiency of reconfigurable PIFA with E-PHEMT switch in OFF state within; (a) Lower frequency band (b) Upper frequency band

4.5 Antenna Fabrication and Measurement

The reconfigurable PIFA was fabricated on the same substrate as the previous antennas. The substrate is Taconic RF-35 with relative permittivity, ε_r of 3.5, loss tangent, tan δ of 0.0018 and substrate thickness, t of 1.52 mm. Copper with an electrical conductivity, σ of 5.8×10^7 S/m was used as the conducting material. The fabricated antenna from different perspectives can be seen in Figure 4.19. The biasing circuit was fabricated based on the previous schematic in AWR MWO software (Figure 4.5). The same biasing circuit was capable to switch the transistor in the ON and OFF states with two distinct bias voltages.

(a)

(b)

(c)

Figure 4.19: Fabricated reconfigurable PIFA with E-PHEMT switch;
(a) Front view (b) Top view (c) Side view

Figure 4.20 shows the biasing circuit of the reconfigurable PIFA with E-PHEMT switch. From the figure, the resistor, R is used as a current limiter to limit the bias current passing through the switch to avoid any physical damages. In the ON state, there must be an electrical connection between the Source and Drain. This is the opposite for the OFF state. For that reason, the Source and Drain are shorted to the ground plane of the antenna. The chip inductors, L_1 and L_2 are used as RF chokes to provide low impedance for DC signals and high impedance for RF signals. The SRF of the chip inductors is 6.9 GHz which is outside the frequency range of this antenna. The DC block chip capacitor, C on the other hand, is used to prevent the DC signal from flowing

to the main feed line by allowing only RF signals to pass through. Table 4.5 listed the values of the biasing components.

Table 4.5: Biasing components of ATF 54143 E-PHEMT switch

Biasing Component	Value
R	1000 Ω
C	1.6 pF
L_1	3.9 nH
L_2	3.9 nH

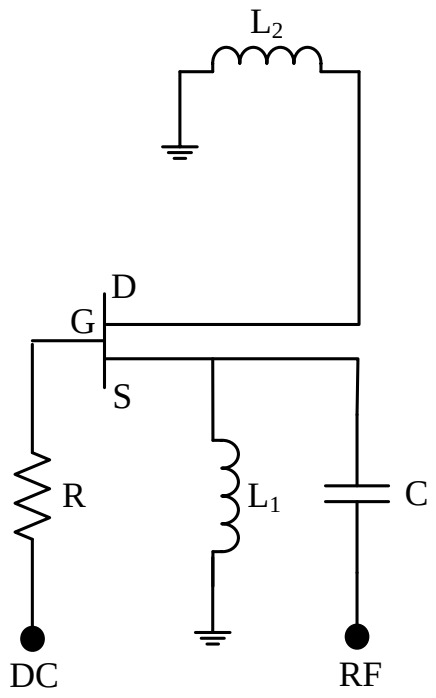

Figure 4.20: Biasing circuit of ATF 54143 E-PHEMT switch

4.5.1 Reflection Coefficient Measurement

The reflection coefficient measurement was performed on 8720ES Agilent VNA. The experimental setup was similar to the previous antennas. The bias tee is positioned at the

receiving end of the coaxial cable during the measurement process to block any unwanted return current to the VNA. The measurement setup can be seen in Figure 4.21. It was found that the bias voltage has to be increased to 3.5 V in the ON state to allow the current to flow through the switch. The same negative voltage of -3.5 V was applied to the Gate of the transistor in the OFF state. The measurement results are shown in Figure 4.22 and Figure 4.23. From the figure, there is a good agreement between the measurement and simulation results in the ON state. However, there are three spurious resonances at 1, 2.7 and 5.7 GHz with reflection coefficients that are less than -10 dB. The same behaviour is observed in the OFF state of the previous antennas with PIN diode. Thus, it is safe to conclude that the occurrences of these spurious are caused by the presence of the two bias inductors (L_1 and L_2) as the biasing components.

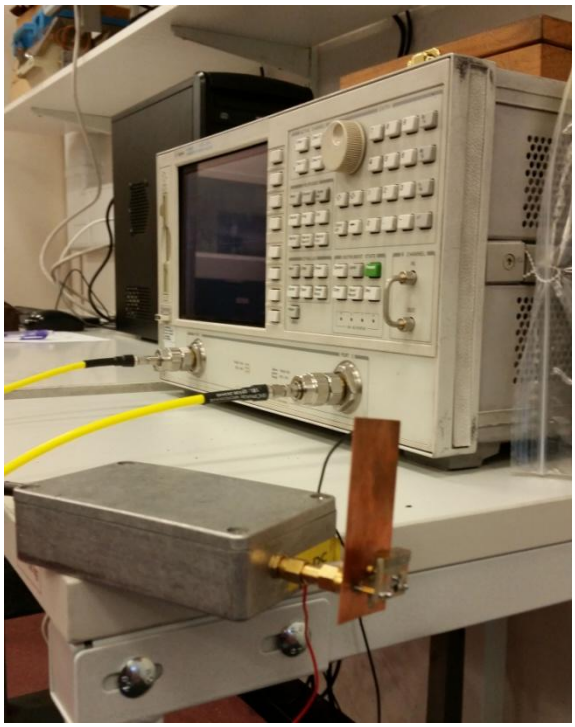

Figure 4.21: Measurement setup of reconfigurable PIFA with E-PHEMT switch

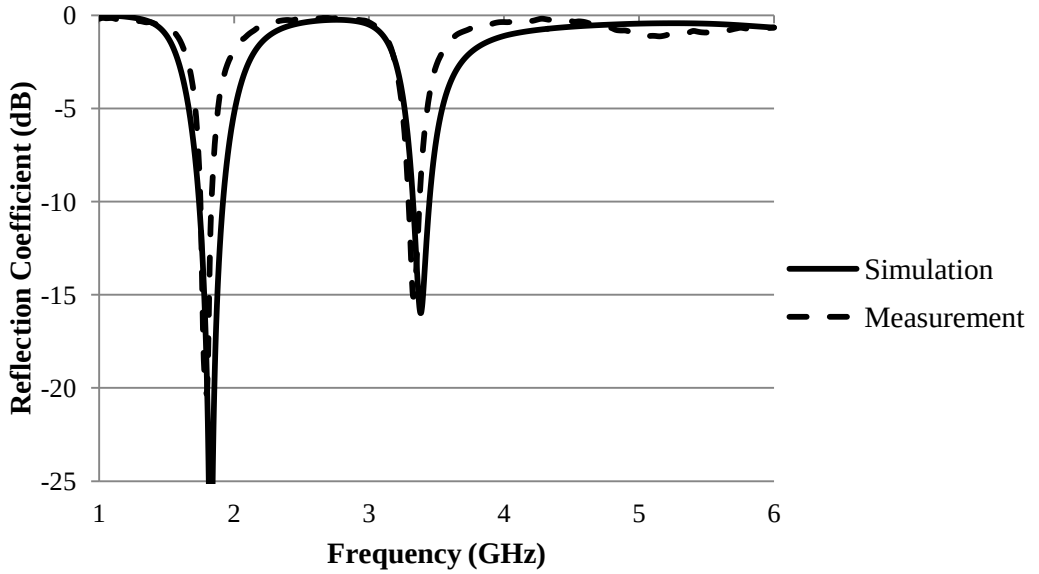

Figure 4.22: Measured reflection coefficient of reconfigurable PIFA with E-PHEMT switch in ON state

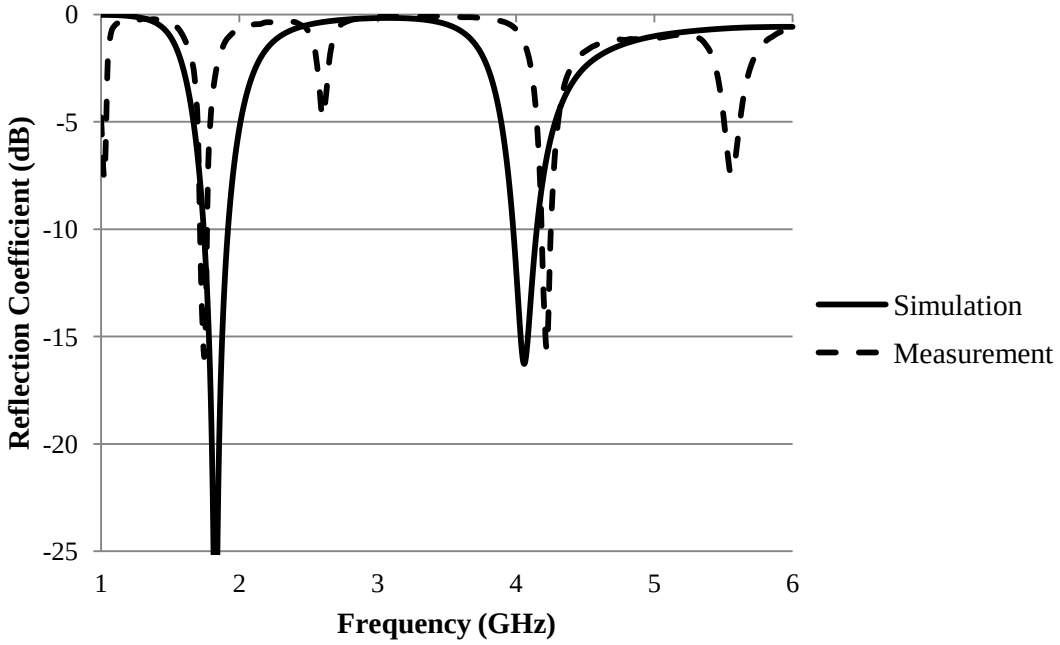

Figure 4.23: Measured reflection coefficient of reconfigurable PIFA with E-PHEMT switch in OFF state

4.6 Conclusion

In this chapter, a reconfigurable PIFA with E-PHEMT switch was successfully designed, simulated and fabricated. The antenna was measured and the results agree well with the simulations. The biasing circuit of the antenna was designed and simulated in AWR MWO software to find a reasonable agreement between the insertion loss and isolation in the ON and OFF states. The Touchstone files were then exported to the Schematic view of CST MWS software and were connected to the differential port of the reconfigurable antenna before the simulations can be performed. From the resonant frequency performance, the first resonant frequency in both states of the switch is at 1.825 GHz. The second resonant frequency is reduced to 3.38 GHz in the ON state from 4.06 GHz in the OFF state. The switching difference in the upper resonant frequencies is only 680 MHz which can be explained from the current distribution behaviour and the low isolation in the upper frequency range of the OFF state. The IMD properties of the E-PHEMT switch are generally worse than those of the PIN diode and the copper bridge. In terms of CR, it would be problematic if the IMD properties of the switch are too high because high levels of IMD outputs could interfere with CR users of adjacent channels. Spurious resonances are observed in the measured reflection coefficient in the OFF state of the switch. Since the behaviour is similar as in the previous antennas, it can be concluded that the attributes are from the presence of the inductors in the biasing circuit.

CHAPTER 5

5. PIFA WITH COPPER BRIDGE AS REFERENCE ANTENNA

5.1 Introduction

Two PIFAs with copper bridges were designed and fabricated for comparison purposes. The width, W of the copper bridges are 2 mm and 5 mm to connect the main radiating plane to the additional plane. The length, L is fixed to 1 mm. A copper bridge serves as a linear interconnection and for that reason, it is used to replace the active switch for a linear comparison. As explained previously (in Chapter 2), the 2 mm gap between the radiating planes is sufficient to accommodate the smaller size of the PIN diode. However, due to the bigger size of the E-PHEMT, the gap between the planes was increased to 5 mm as it is not possible to fit the transistor and all components of the biasing circuit into the 2 mm gap. Thus, two copper bridges with dimensions of $W \times L = 2 \times 1$ mm^2 and 5×1 mm^2 respectively were constructed and each of them was introduced on the radiating structure of the PIFA. The PIFA with 2×1 mm^2 copper bridge is included in this chapter for reference purpose and comparison with the PIFA with 5×1 mm^2 copper bridge.

5.2 PIFA with 2 × 1 mm^2 Copper Bridge

5.2.1 Antenna Geometry and Dimensions

The 2 × 1 mm^2 copper bridge on the radiating structure can be seen in Figure 5.1. The geometry and dimensions are similar to the reconfigurable PIFA with PIN diode (Gap, G_1 = 2 mm).

Figure 5.1: Top view of PIFA with 2 × 1 mm^2 copper bridge

5.2.2 Reflection Coefficient

The simulated reflection coefficient of the antenna was simulated in CST MWS software and the graph is depicted in Figure 5.2. It can be seen that the first resonant frequency at 2.01 GHz is similar to the reconfigurable PIFA with PIN diode (Gap, G_1 = 2 mm). However, the second resonant frequency at 4.03 GHz is higher as compared to 3.67 GHz from the previous antenna. Table 5.1 compares the resonant frequencies of both antennas.

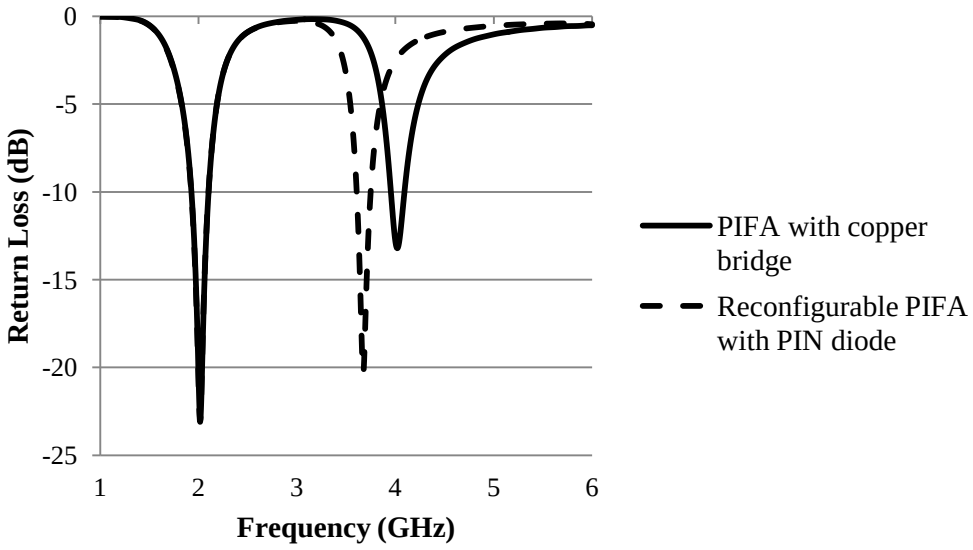

Figure 5.2: Reflection coefficient comparison between PIFA with 2 × 1 mm^2 copper bridge and reconfigurable PIFA with PIN diode (Gap, G_1 = 2 mm) in ON state

Table 5.1: Resonant frequency performance of PIFA with 2 × 1 mm^2 copper bridge and reconfigurable PIFA with PIN diode in ON state

	PIFA	
	With 2 × 1 mm^2 Copper Bridge	**With BAR50-02V PIN Diode (ON State)**
First resonant frequency, f_{r1} (GHz)	2.01	2.01
Second resonant frequency, f_{r2} (GHz)	4.03	3.67
6-dB Lower Bandwidth, BW_1 (MHz)	2.1622 – 1.8565 = **305.77**	2.1618 – 1.8544 = **307.4**
6-dB Upper Bandwidth, BW_2 (MHz)	4.1915 – 3.8875 = **303.95**	3.8171 – 3.5595 = **257.6**

5.2.3 Current Distribution

Current distributions on the radiating structure of PIFA were simulated in CST MWS software to study the current behavior at the specified resonant frequency. Figure 5.3 shows the current concentration on the antennas at 2.01 and 4.03 GHz. From the observation, the maximum current is concentrated on the edge of the main radiating plane, the feed line and the shorting pin at the lower resonant frequency. At higher resonant frequency, the maximum current is concentrated on the edge of the main radiating plane close to the feed point and on the copper bridge itself. A similar behaviour can also be observed in the previous antenna with PIN diode.

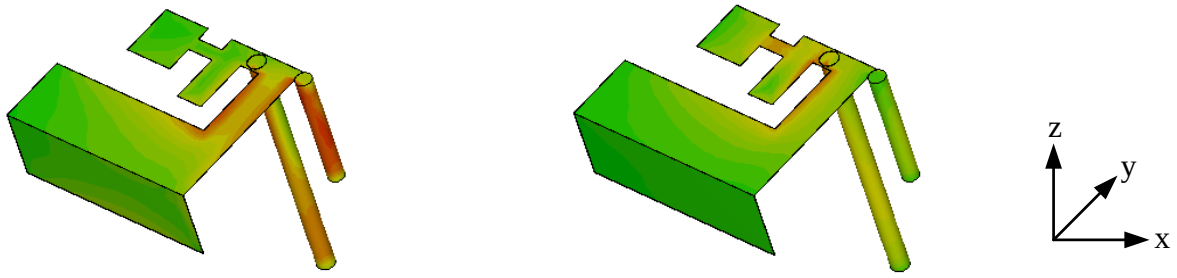

(a) (b)

Figure 5.3: Current distribution of PIFA with 2 × 1 mm^2 copper bridge at;
(a) 2.01 GHz (b) 4.03 GHz

5.2.4 Radiation Pattern

The co-polar radiation patterns in xy-, xz- and yz- planes were extracted from CST MWS software can be viewed in Figure 5.4. From the figures, the radiation patterns are similar to the radiation patterns of the reconfigurable PIFA with PIN diode (Gap, G_1 = 2 mm) at 2.01 GHz.

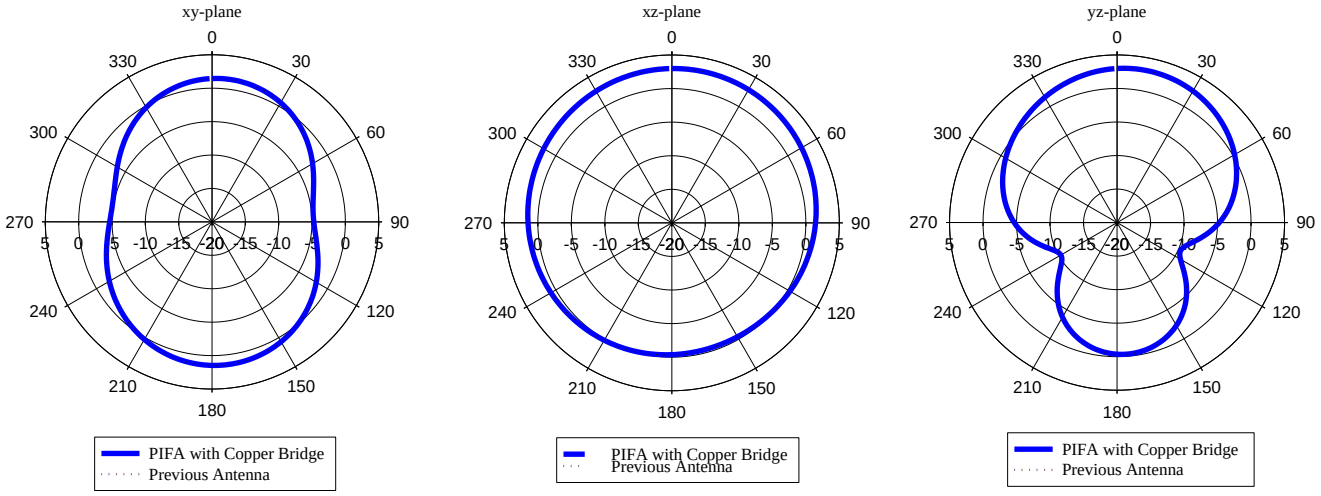

(a)

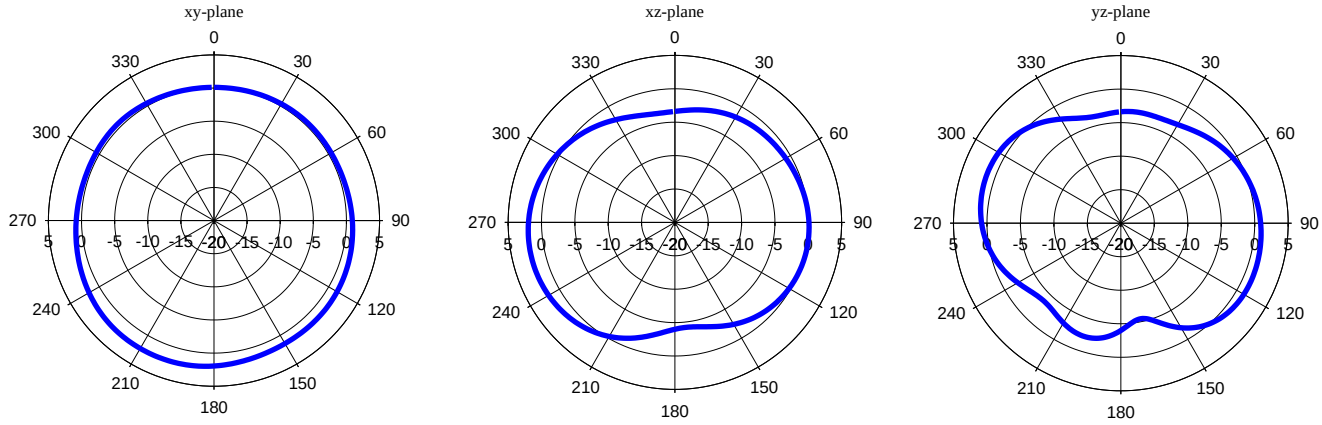

(b)

Figure 5.4: Co-polar radiation patterns in xy-, xz- and yz- planes of PIFA with 2 × 1 mm^2 copper bridge at; (a) 2.01 GHz (b) 4.03 GHz

5.2.5 Realized Gain, Directivity and Efficiency

Table 5.2 shows the realized gain, directivity and efficiency of the PIFA. From the table, each of them is consistently good in their respective resonant frequency. Separate graphs for gain and efficiency at lower and upper resonant frequency bands were simulated in CST MWS software which can be seen in Figure 5.5 and Figure 5.6.

Table 5.2: Realized gain, directivity and efficiency of PIFA with 2 × 1 mm^2 copper bridge (Gap, G_1 = 2 mm)

	PIFA with 2 × 1 mm^2 Copper Bridge (Gap, G_1 = 2 mm)	
	f_{r1} = 2.01 GHz	f_{r2} = 4.03 GHz
Realized Gain, G (dB)	3.072	1.984
Directivity, D (dBi)	3.137	2.358
Efficiency, η (%)	99.02	96.35

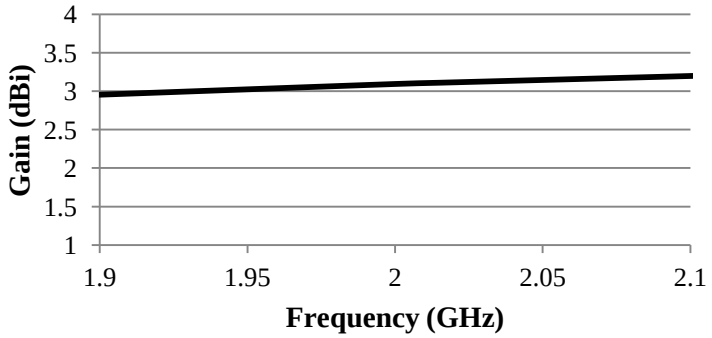

(a)

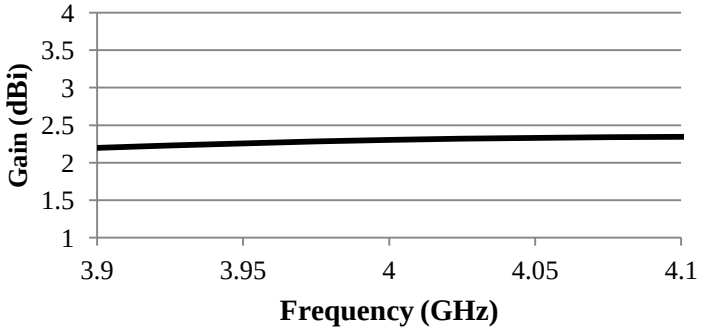

(b)

Figure 5.5: Gain of PIFA with 2 × 1 mm^2 copper bridge in;
(a) Lower resonant frequency band (b) Upper resonant frequency band

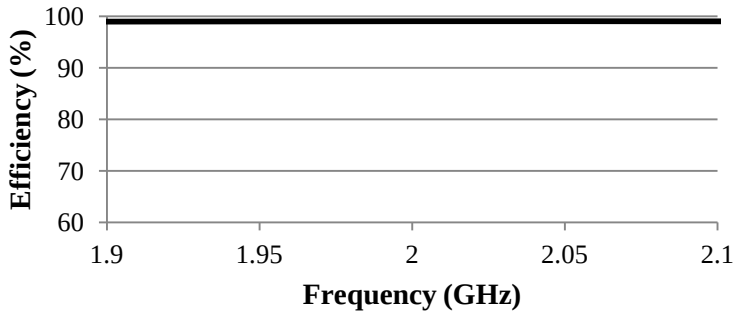

(a)

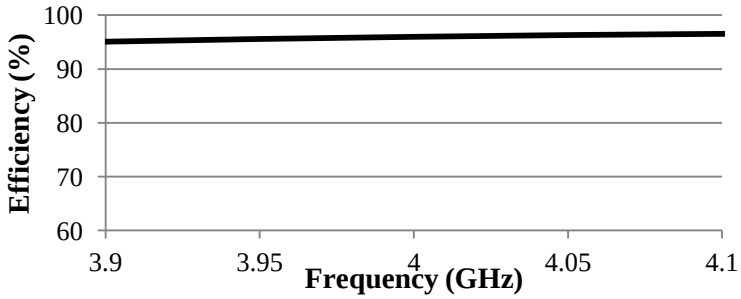

(b)

Figure 5.6: Efficiency of PIFA with 2×1 mm^2 copper bridge in;
(a) Lower resonant frequency band (b) Upper resonant frequency band

5.2.6 Antenna Fabrication and Measurement

The antenna was fabricated on the same substrate as the predecessor which is Taconic RF-35 with relative permittivity, ε_r of 3.5, loss tangent, tan δ of 0.0018 and substrate thickness, t of 1.52 mm. Copper with an electrical conductivity, σ of 5.8×10^7 S/m was used as the conducting material. The radiating plane is mounted at 9 mm above a copper ground plane measuring 31×65 mm^2. The fabricated antenna is illustrated in Figure 5.7.

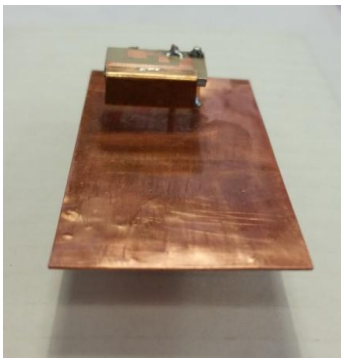

(a)

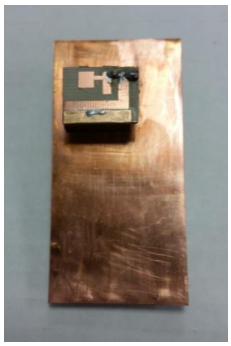

(b)

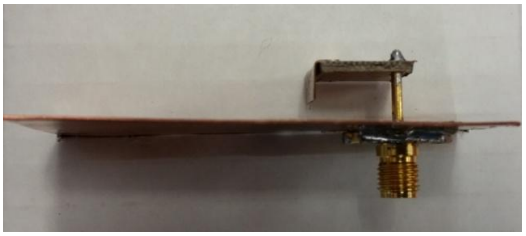

(c)

Figure 5.7: PIFA with 2 × 1 mm^2 copper bridge;
(a) Front view (b) Top view (c) Side view

5.2.7 Reflection Coefficient Measurement

The reflection coefficient measurement was performed on the antenna to come to an agreement with the simulation. The measurement setup can be viewed in Figure 5.8. Although there is no biasing voltage that needs to be supplied to the antenna, the bias tee is still positioned to connect the antenna to the VNA. The measured reflection coefficient can be viewed in Figure 5.9.

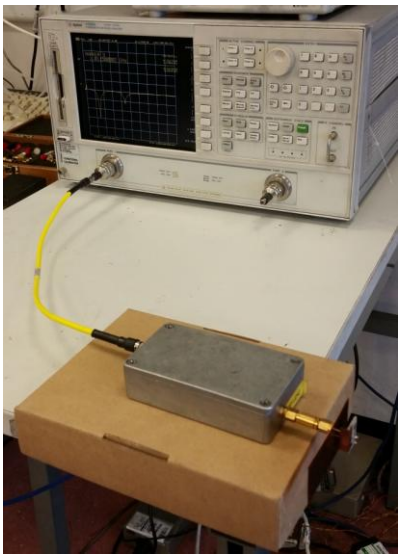

Figure 5.8: Reflection coefficient measurement of PIFA with 2 × 1 mm^2 copper bridge

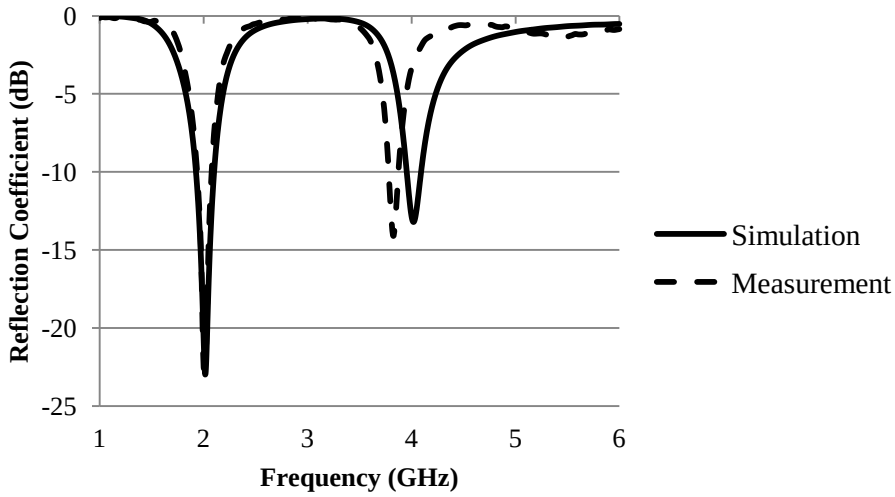

Figure 5.9: Comparison of reflection coefficient from measurement and simulation of PIFA with 2 × 1 mm^2 copper bridge

5.3 PIFA with 5 × 1 mm^2 Copper Bridge

5.3.1 Antenna Geometry and Dimensions

The geometry and dimensions of the antenna is similar to the reconfigurable PIFA with BAR50-02V PIN diode (Gap, G_1 = 5 mm) and the reconfigurable PIFA with ATF 54143 E-PHEMT switch. The radiating planes from the top view are shown in Figure 5.10.

Figure 5.10: Dimensions of PIFA with 5 × 1 mm^2 copper bridge

5.3.2 Reflection Coefficient

The simulated reflection coefficient of the antenna can be viewed in Figure 5.11. The result was compared with the reflection coefficient of reconfigurable PIFA with PIN diode (Gap, G_1 = 5mm) and E-PHEMT switch. Table 5.3 compares the resonant frequency performance of the antennas. From the table, it is observed that the resonant frequency of the antenna at 1.825 GHz is similar to the previous antennas. However, the second resonant frequency is shifted to 3.33 GHz which is slightly higher than 3.13 GHz (reconfigurable PIFA with PIN diode) and almost identical to 3.38 GHz (reconfigurable PIFA with E-PHEMT switch).

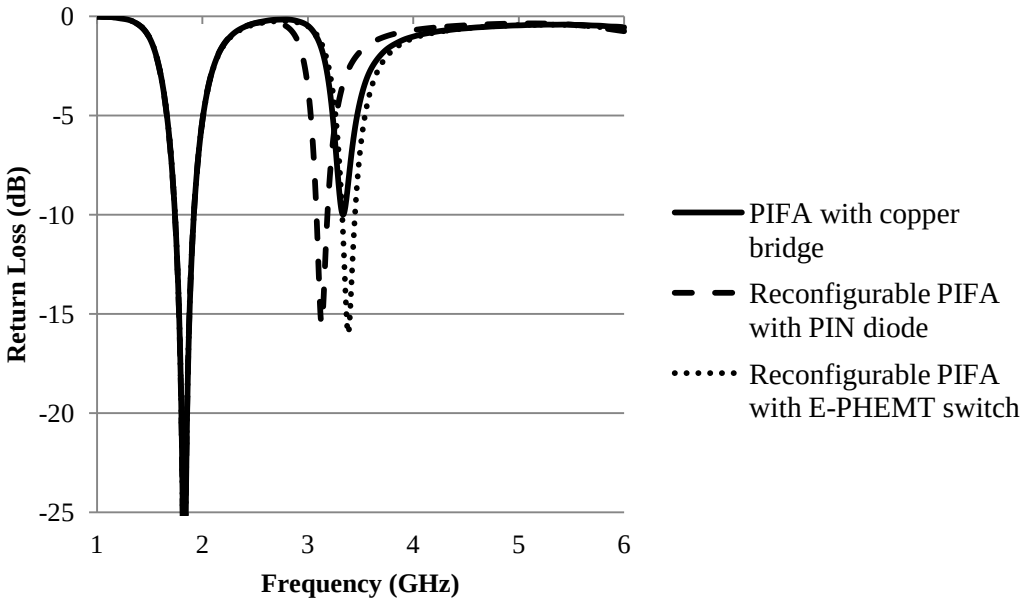

Figure 5.11: Reflection coefficient comparison of PIFA with 5 × 1 mm^2 copper bridge and reconfigurable PIFA with PIN diode (Gap, G_1 = 5 mm) and E-PHEMT switch in ON state

Table 5.3: Resonant frequency performance of PIFA with 5 × 1 mm^2 copper bridge and reconfigurable PIFA with PIN diode (Gap, G_1 = 5 mm) and E-PHEMT switch in ON state

	Reconfigurable PIFA		
	With 5 × 1 mm^2 Copper Bridge	**With PIN Diode (ON State)**	**With E-PHEMT switch (ON State)**
First resonant frequency, f_{r1} (GHz)	1.825	1.825	1.825
Second resonant frequency, f_{r2} (GHz)	3.33	3.13	3.38
6-dB Lower Bandwidth, BW_1 (MHz)	1.9817 – 1.683 = **298.69**	1.9816 – 1.6819 = **299.7**	1.9819 – 1.6837 = **298.2**
6-dB Upper Bandwidth, BW_2 (MHz)	3.4369 – 3.2523 = **184.53**	3.2444 – 3.0416 = **202.8**	3.5134 – 3.2793 = **234.1**

5.3.3 Current Distribution

Current distributions on the radiating surface of the antenna were simulated at each respective resonant frequency. Figure **5.12** shows the current distribution at 1.825 and 3.33 GHz.

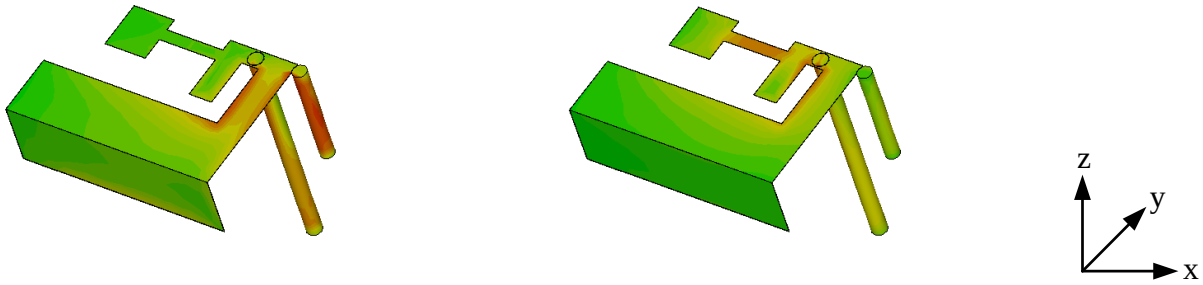

(a) (b)

Figure 5.12: Current distribution of PIFA with 5 × 1 mm^2 copper bridge at;
(a) 1.825 GHz (b) 3.33 GHz

5.3.4 Radiation Pattern

The co-polar radiation patterns in xy-, xz- and yz-planes were generated in CST MWS software at 1.825 and 3.33 GHz. The radiation patterns in the xy-, xz- and yz- planes are shown in Figure 5.13. The radiation patterns are similar with the previous antennas at the lower resonant frequency.

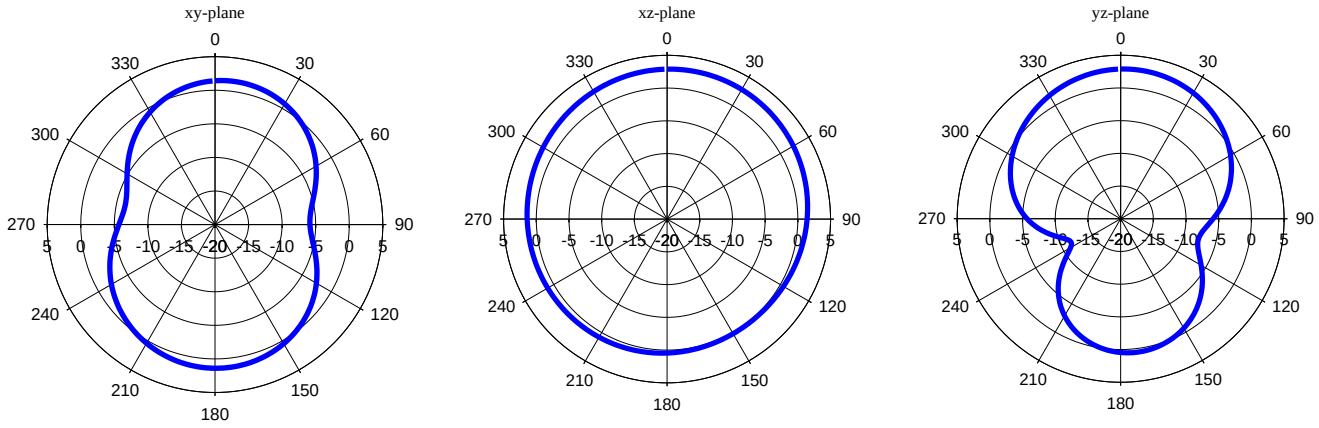

(a)

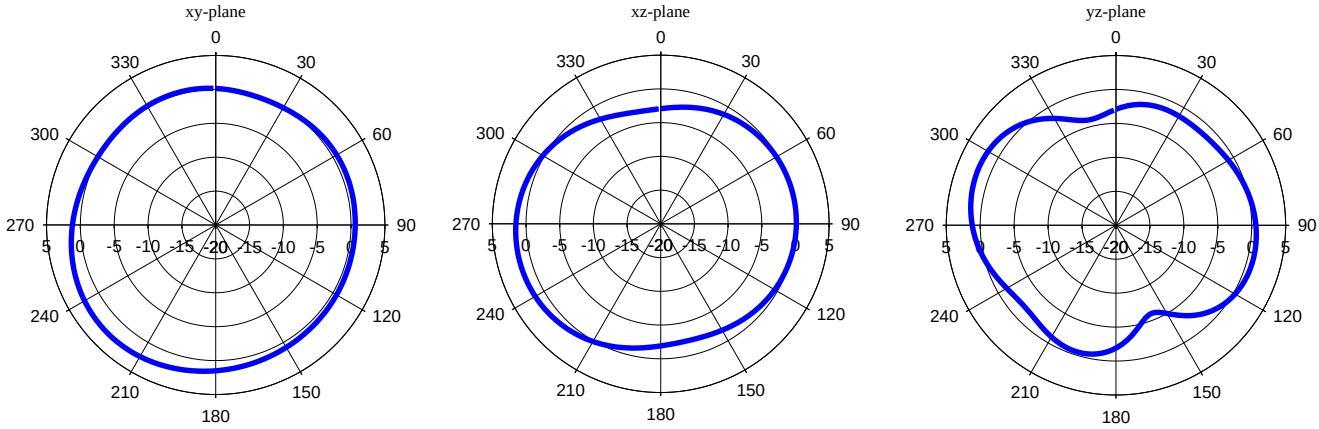

(b)

Figure 5.13: Co-polar radiation patterns in xy-, xz- and yz- planes of PIFA with 5 × 1 mm^2 copper bridge at; (a) 1.825 GHz (b) 3.33 GHz

5.3.5 Realized Gain, Directivity and Efficiency

The realized gain, directivity and efficiency of the antenna are summarized in Table 5.4. The values are consistently good at each resonant frequency of 1.825 and 3.33 GHz which are further illustrated from the gain and efficiency graphs in Figure 5.14 and Figure 5.15.

Table 5.4: Realized gain, directivity and efficiency of PIFA with 5 × 1 mm^2 copper bridge

	PIFA with 5 × 1 mm^2 Copper Bridge	
	f_{r1} = 1.825 GHz	f_{r2} = 3.33 GHz
Realized Gain, G (dB)	2.887	1.870
Directivity, D (dBi)	2.924	2.551
Efficiency, η (%)	99.17	94.9

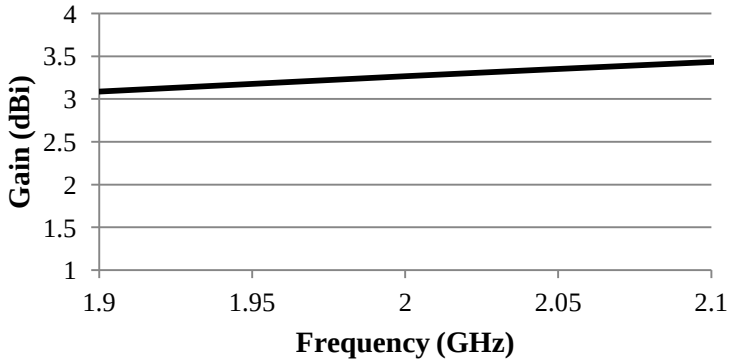

(a)

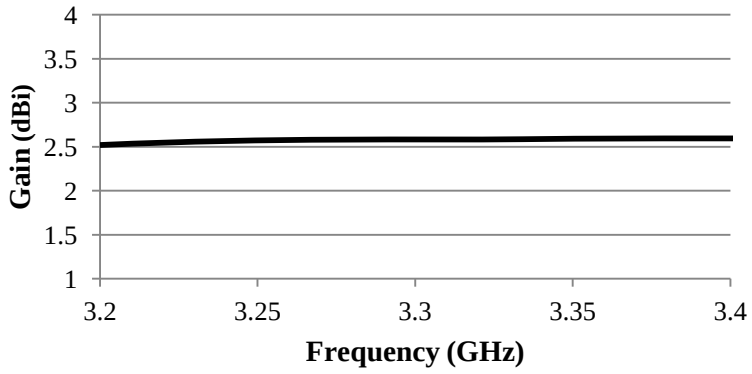

(b)

Figure 5.14: Gain of PIFA with 5 × 1 mm^2 copper bridge in;
(a) Lower resonant frequency band (b) Upper resonant frequency band

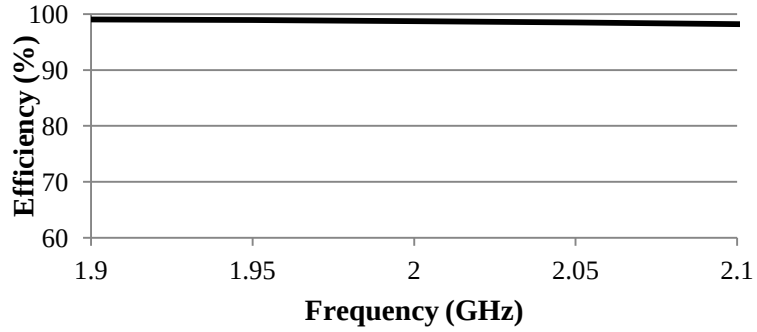

(a)

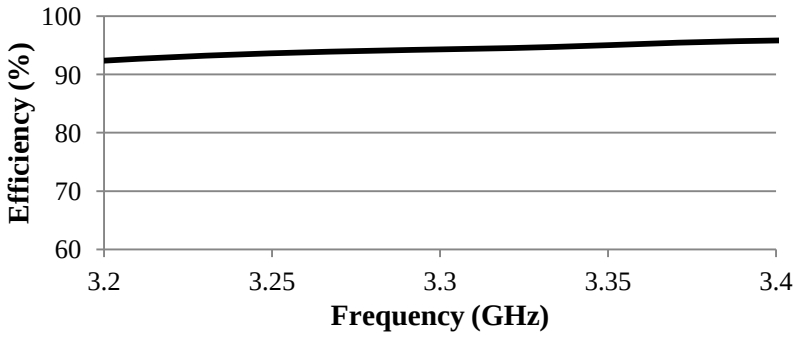

(b)

Figure 5.15: Efficiency of PIFA with 5 × 1 mm^2 copper bridge in;
(a) Lower resonant frequency band (b) Upper resonant frequency band

5.3.6 Antenna Fabrication and Measurement

The antenna were fabricated and assembled to produce a complete structure as can be viewed in Figure 5.16. The same substrate was used as in the previous antenna.

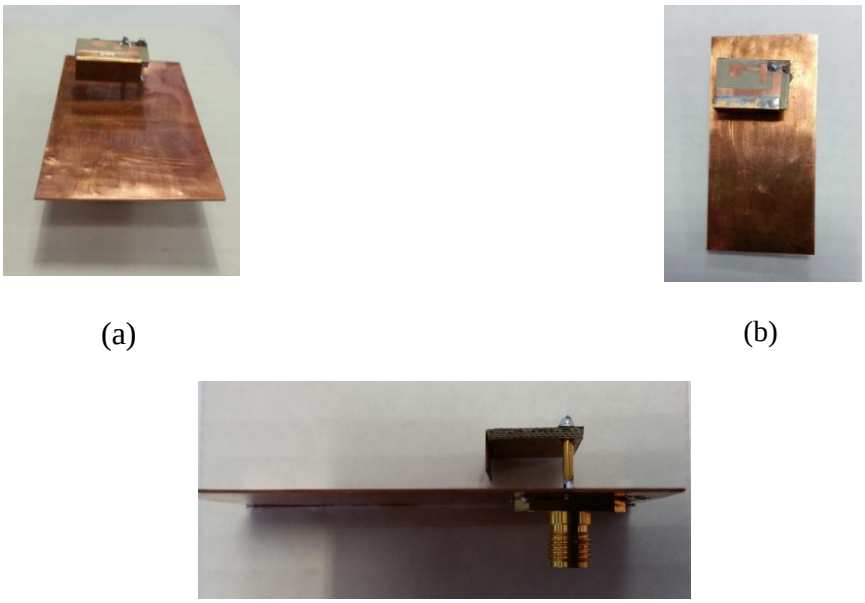

(a) (b)

(c)

Figure 5.16: PIFA with 5 × 1 mm^2 copper bridge;
(a) Front view (b) Top view (c) Side view

5.3.7 Reflection Coefficient Measurement

The experimental setup to measure reflection coefficient of the PIFA with 5 × 1 mm^2 copper bridge can be viewed in Figure 5.17. The comparison of reflection coefficients from the measurement and simulation results was performed to ensure that they agree well with each other. It shows that an agreement is achieved from Figure 5.18.

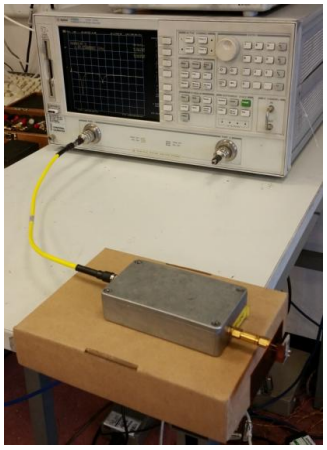

Figure 5.17: Experimental setup to measure reflection coefficient of reconfigurable PIFA with 5×1 mm^2 copper bridge

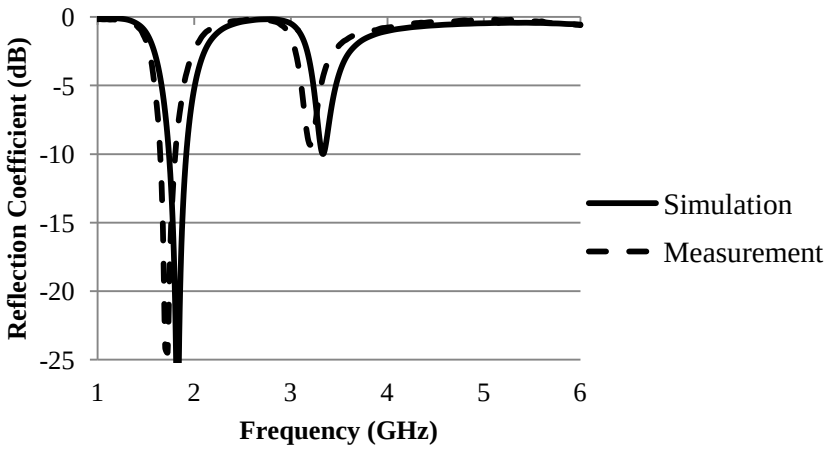

Figure 5.18: Comparison of reflection coefficient from measurement and simulation of PIFA with 5×1 mm^2 copper bridge

5.4 Conclusion

In this chapter, two PIFAs with copper bridges were fabricated as reference antennas. The copper bridge as a linear interconnection was constructed to replace the nonlinear active switch. Two types of active switches were implemented on the previous reconfigurable PIFAs namely PIN diode and E-PHEMT switch. The characteristics of the previous antennas were compared to the PIFAs with copper bridges. It is observed that the upper resonant frequencies of the PIFAs are slightly higher than the previous antennas with similar geometry and dimensions. However, the upper resonant frequency of the reconfigurable PIFA with E-PHEMT switch is almost identical with the PIFA with 5×1 mm^2 copper bridge. The next chapter will discuss the methodology and the nonlinearity measurements performed on the reconfigurable PIFAs with active switches and PIFAs with copper bridges.

CHAPTER 6

6. NONLINEARITY MEASUREMENTS OF RECONFIGURABLE PIFAs WITH ACTIVE SWITCHES AND PIFAs WITH COPPER BRIDGES

6.1 Introduction

This chapter investigates the nonlinearity of the reconfigurable PIFAs with active switches and the PIFAs with copper bridges. Two active switches with different linearity performances were introduced on each of the reconfigurable PIFA. For comparison purposes, two PIFAs with copper bridges were constructed. A set of nonlinearity measurements was identified from the reviewed literature and were performed to investigate the nonlinearity performance of the antennas in the transmit mode.

6.2 Methodology

The new experimental setups to measure the nonlinearity of the active antennas were designed based on the information from the literature and facilities available in the research laboratory. The parameters that were measured are listed as follows:

i. Fundamental two-tone signals at device output (Lower and Upper tones)

ii. Third-order intermodulation distortion (IMD3) products at device output

iii. Variations of the IMD3 products against the tone distance

iv. Ratio of the third-order intermodulation distortion (IMD3) products to the fundamental signals

v. IMD3 products asymmetry

vi. Third-order input intercept point (IIP3) at the device output

vii. 1-dB gain compression point ($P_{1\text{-dB}}$) at device output

6.2.1 Measurement of Third-Order Intermodulation Distortion (IMD3) Products

The experimental setups to measure the IMD3 products are discussed in this section. The locations of the IMD3 products are very close to the fundamental signals or also known as the two-tone signals. As a result, the products are impossible to be filtered out and it is crucial to measure the magnitudes to ensure no disruptions to the output signals.

6.2.1.1 Experimental Setup in Transmit Mode

Figure 6.1 shows the block diagram to measure the IMD3 products when the antenna is transmitting signals. The measurement setup was initially proposed but due to the available facility in the research laboratory, some of the components were omitted and replaced by the 4-port model ZVA67 Rohde & Schwarz (R&S) VNA. However, the experimental setups can be used as another alternative in the occasion where the VNA is not available.

The two-tone signals measurements consist of two-tone signals from Port 1 and Port 2 of the VNA. These two signals flow through the signal generators, low pass filters and isolators before

being combined in the power combiner. The low pass filter prevents harmonics of the second-order and above produced by the signal generators from entering the measurement system. The purpose of isolators is to prevent the generation of IMD3 products from the interaction of the fundamental input tones from both generators. In this particular experiment, the power combiner must possess a good isolation between the input ports to ensure the signal from one port is not coupled into the other port. In addition, adequate isolation is crucial to measure the low level readings of IMD3 products. However, IMD3 products are not critical in the power combiner as it is insignificant with the present state of transformer technology [80].

In the transmit mode, the third port of the directional coupler is terminated with a 50-Ω load to obtain a minimal insertion loss. In this measurement setup, a directional coupler with high directivity was selected.

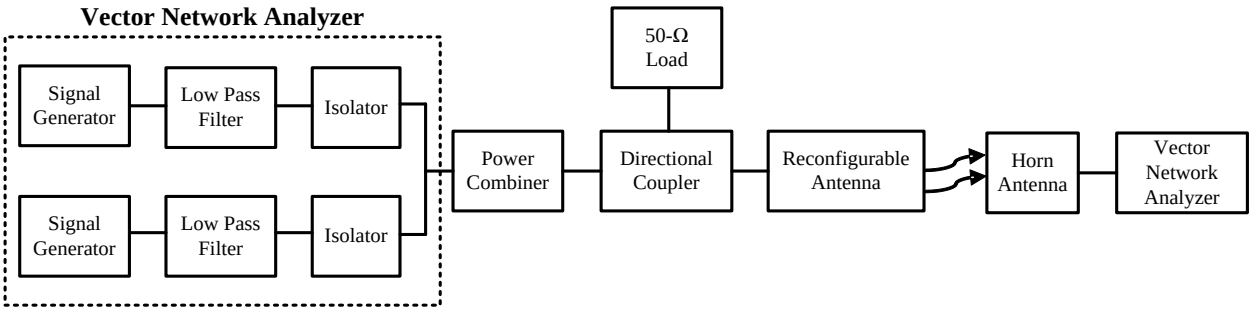

Figure 6.1: Block diagram for measurement of IMD3 products when the antenna is transmitting signals

Table 6.1 lists the components in the experimental setups. The actual photos of the components are shown in Figure 6.2.

Table 6.1: List of components in IMD3 product measurements

Equipment	Manufacturer	Part Number	Specification
Signal generator 1 Signal generator 2 Low pass filter Isolator	The function of these three components was replaced by ZVA67 Rohde & Schwarz VNA	ZVA67	• Frequency range: 10 MHz – 67 GHz • Number of ports: 4
Power combiner	Mini-Circuits	ZN2PD2-63-S+	• Wideband frequency range: 0.35 – 6 GHz • Typical isolation: 25 dB • Typical insertion loss: 0.6 dB
Directional coupler	Mini-Circuits	ZHDC-16-63-S+	• Wideband frequency range: 50 MHz – 6 GHz • High directivity: 32 dB • Flat coupling: ±0.45 dB • Good VSWR: 1.20 : 1
Top-hat dipole	*Not available*	*Not Available*	• Frequency range: 1 – 6 GHz

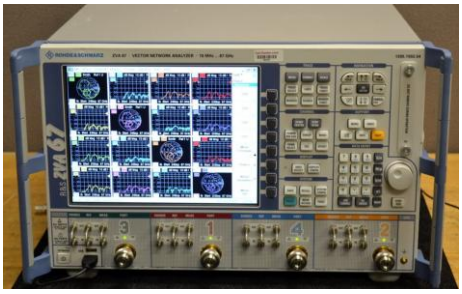

(a)

(b)

(c)

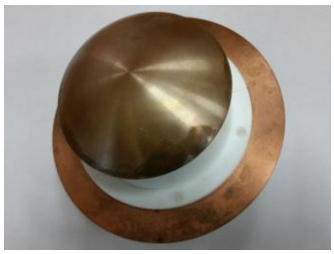

(d)

Figure 6.2: Components involved in experimental setup to measure IMD3 products;
(a) ZVA67 vector network analyzer (b) ZN2PD2-63-S+ power combiner
(c) ZHDC-16-63-S+ Directional coupler (d) Top-hat dipole

6.2.2 Simplified Experimental Setup to Measure IMD3 Products

The ZVA67 R&S VNA was used to perform the nonlinearity measurements. The high-end model of ZVA67 is an ideal choice for demanding measurements of nonlinearity on reconfigurable antennas. The availability of the four ports has further simplified the initial experimental setup proposed in Figure 6.1. The new simplified version of the nonlinear measurements is based on the configuration shown in Figure 6.3. The configuration was obtained from the operation manual of the ZVA67 [80]. From the figure, the intermodulation quantities can be measured at the DUT input (wave a_1) or output (wave b_2). The DUT in this case is the reconfigurable antenna.

Thus, based on the configuration, a few modifications from the original experimental setups are necessary and discussed in this paragraph. Firstly, the signal generators, low pass filters and isolators were omitted as the VNA has the capability to generate the two-tone signals from two of its four ports. Secondly, the directional coupler was also removed as the VNA is capable to superimpose the two signals that are available from one of its test port.

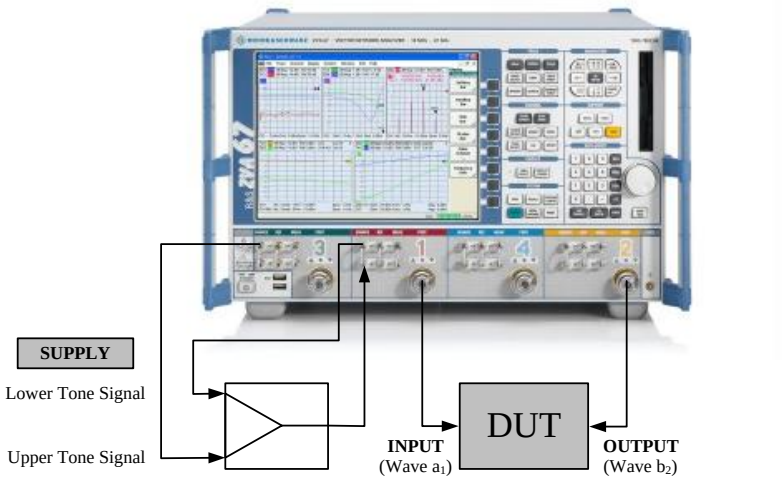

Figure 6.3: The configuration of nonlinear measurements from operating manual of ZVA67 R&S VNA [80]

6.2.2.1 Simplified Experimental Setup in Transmit Mode

The new, simplified experimental setups can be viewed in Figure 6.4 based on the modifications discussed in the previous section. The lower tone signal is generated at Port 1 and the upper tone is provided by a second SOURCE OUT at Port 3. Both signals are then combined with the power combiner and fed to the SOURCE IN connector at Port 1. As a result, the superimposed signals that are available at test Port 1 are ready to be supplied to the input of the reconfigurable PIFA. The radiated signals are then transmitted to the reference antenna (top-hat dipole) that is connected to Port 2. The waveforms of the transmitted IMD3 products are measured at the output of the reference antenna.

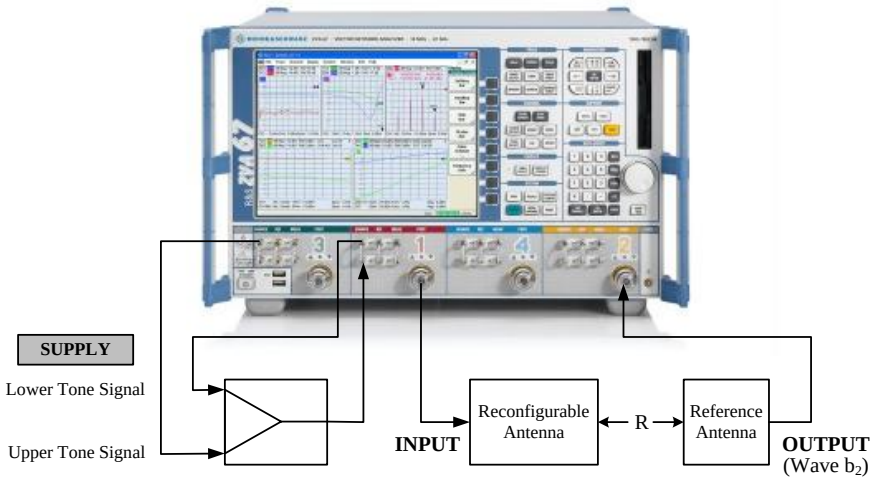

Figure 6.4: Simplified experimental setups of IMD3 products measurement in transmit mode

6.2.3 Measurement of Ratio of IMD3 Products to Carrier

The ratio of the IMD products to carrier is another measure of nonlinearity performance of the reconfigurable PIFA with an active switch. The idea is to observe whether the ratio changes from different angles of radiation when the antenna is transmitting signals. The ratio was measured at each radiation angle as illustrated in Figure 6.5. From the figure, the radiation angle is varied from -90° to 90° with a maximum radiation occurs at 0°.

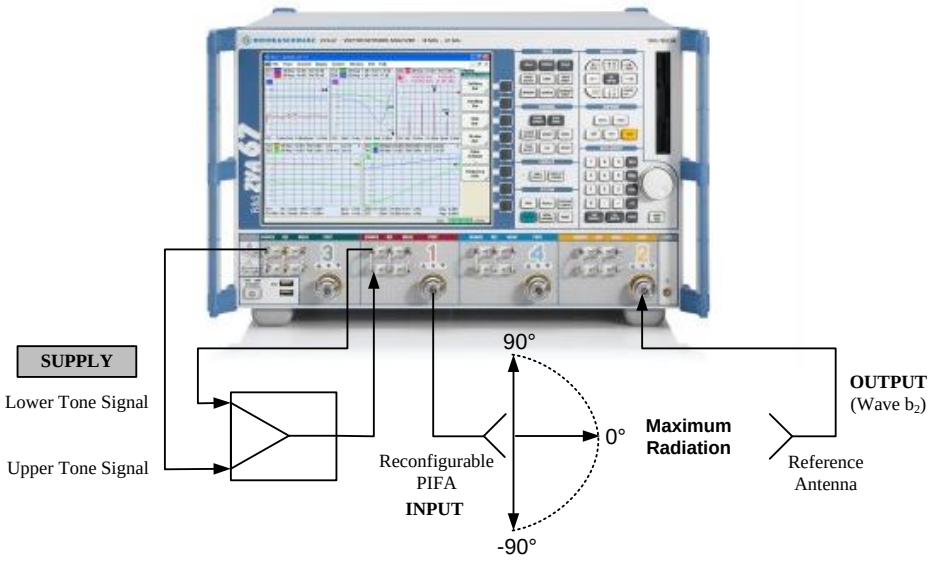

Figure 6.5: Experimental setup to measure ratio of IMD3 products to carrier in transmit mode

6.2.4 Measurement of Third-Order Input Intercept Point (IIP3)

Another measure of nonlinearity can be expressed in terms of the IIP3. The experimental setup to measure IIP3 is similar to the experimental setups to measure IMD3 products (Figure 6.4). In this measurement, the input power is swept from 0 to 20 dBm at a specific IMD3 frequency and the output power of the two-tone signals and IMD3 products were measured. The IIP3 can be located from the graph of output power against input power in dBm from the intersection between two linear regression lines of the fundamental tones (1:1 slope) and IMD3 products (3:1 slope).

6.2.5 Measurement of 1-dB Gain Compression Point ($P_{1\text{-dB}}$)

The $P_{1\text{-dB}}$ is another measurement of nonlinearity introduced to the reconfigurable antenna system due to the presence of active switch. The experimental setup for the measurement is the same as the setup used to measure the IMD3 products but in this particular measurement, only a

single-tone signal is used instead of two-tone signals. Thus, the power combiner is no longer needed. The experimental setups to measure the $P_{1\text{-dB}}$ can be viewed in Figure 6.6. From the figure, the S_{21} of the transmitted signals are generated across a swept of input power from -10 to 20 dBm at the specific IMD3 frequency. The $P_{1\text{-dB}}$ can be determined at the point where the output power dropped by 1 dB from the graph of S_{21} against input power in dBm.

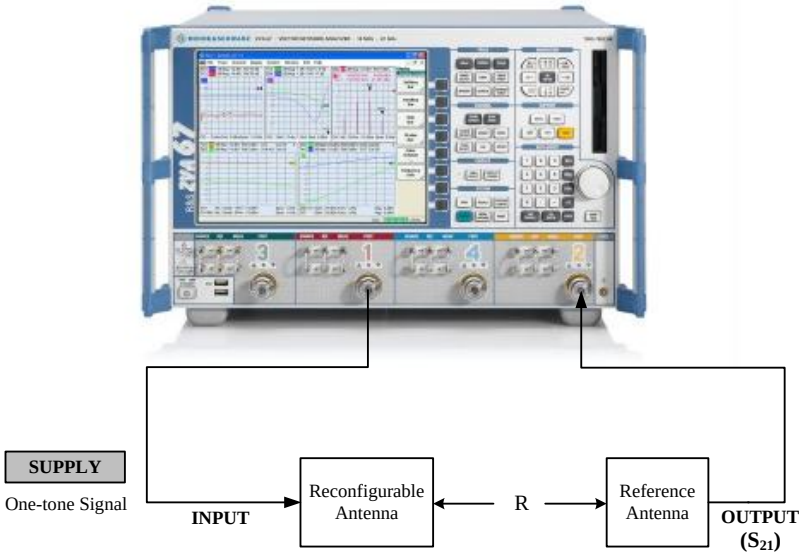

Figure 6.6: Experimental setup for 1-dB gain compression measurement in transmit mode

6.3 Nonlinearity Measurements of Reconfigurable PIFAs with Active Switches

The nonlinearity measurements were performed on the antennas fabricated in this work. The results are presented in this section. Initial investigations were conducted to determine the location of the IMD3 products on the reconfigurable PIFA with PIN diode. This was performed by varying the RF input power on the VNA. It was found that the IMD3 products were the strongest at 20 dBm with a noise floor of -80 dBm. Therefore, all the measurements were carried

out at the input power of 20 dBm and noise floor of -80 dBm. The experimental setup for the nonlinearity measurements in the laboratory is shown in Figure 6.7.

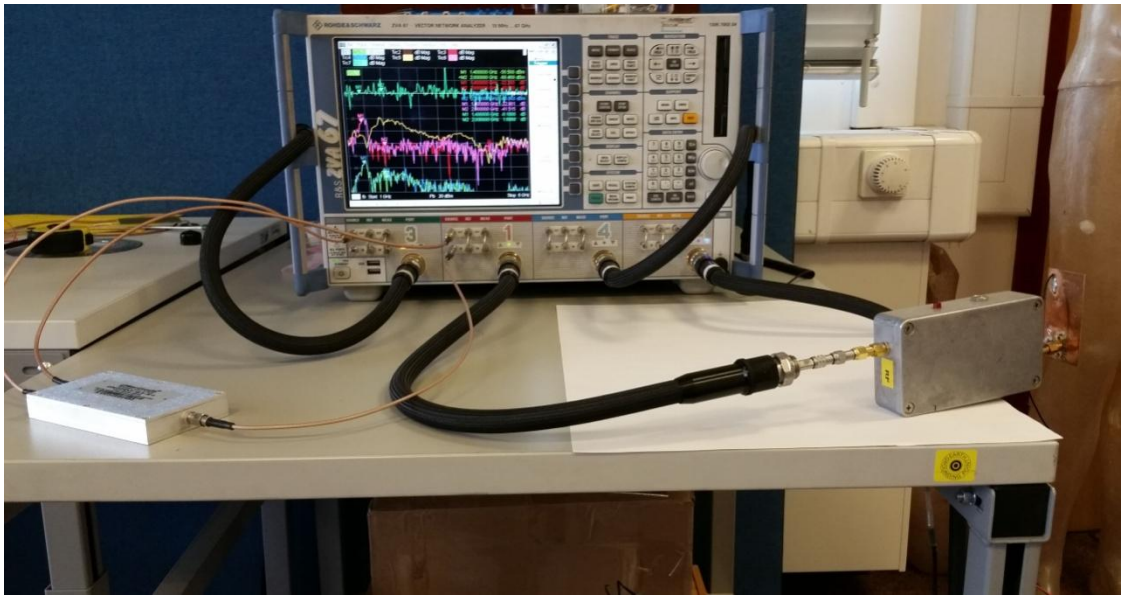

Figure 6.7: Experimental setup for nonlinearity measurements

The next critical task is to select the best tone distance and measured bandwidth (BW) of the signals on the VNA. Theoretically, the measured bandwidth determines how fast the signals will be processed and does not play any roles in changing the waveforms. Early investigation reveals that a 1 kHz of measured bandwidth (BW) is the most suitable value since the waveforms are processed in a reasonable speed. Thus, the measured BW is fixed to 1 kHz and the attention was being paid to the tone distance. The task was accomplished by plotting the variations of the IMD3 products frequencies of the reconfigurable PIFAs with PIN diodes against tone distance. The plotted graphs are shown in Figure 6.8, Figure 6.9 and Figure 6.10. The figures are distinguished between the reconfigurable PIFA with PIN diode (Gap, G_1 = 2 and 5 mm) and the PIFA with copper bridge (2 × 1 mm^2 and 5 × 1 mm^2) for comparison purposes. From the figures, it is

noticeable that at the tone distance of 1 MHz, the effects of IMD3 products are more pronounced. In addition, it is evident that in the ON state of the PIN diode, the IMD3 products are significantly visible at 2 GHz which is the first resonant frequency of the reconfigurable PIFA (Gap, G_1 = 2 mm) from the reflection coefficient graph. However, in the OFF state, there are two occurrences of significant IMD3 products at 1.4 and 2 GHz with the 1.4 GHz being the most pronounced. Similarly, the same behaviour is observed for the reconfigurable PIFA with PIN diode (Gap, G_1 = 5 mm). In the ON state, the IMD3 products is the worst at 1.85 GHz while in the OFF state, two significant IMD3 products can clearly be seen at 1.35 GHz and 1.85 GHz with the strongest IMD3 products being at 1.35 GHz. In the case of the PIFA with copper bridges, there are no signs of IMD3 products as all the signals fall below the noise floor. Thus, the tone distance of 1 MHz and the measured BW of 1 kHz were selected for all the nonlinearity measurements in this work.

Furthermore, it can be concluded from the two tasks performed on the reconfigurable PIFA with PIN diode (Gap, G_1 = 2 mm and 5 mm) that the IMD3 products are the most significant at the first resonant frequency of the antennas in the ON state. In the OFF state, two distinct IMD3 products can be observed at the first resonant frequency and at the new resonance. As previously mentioned in Chapter 3, the new resonance was caused by the bias inductor of the biasing circuit.

For the sake of simplicity, the nonlinear parameters in the legend of each graph are listed below for quick reference:

i. LTO – Lower tone at the Device Output

ii. UTO – Upper tone at the Device Output

iii. IMD3LO – Third-order IMD products of the Lower tone at the Device Output

iv. IMD3UO – Third-order IMD products of the Upper tone at the Device Output

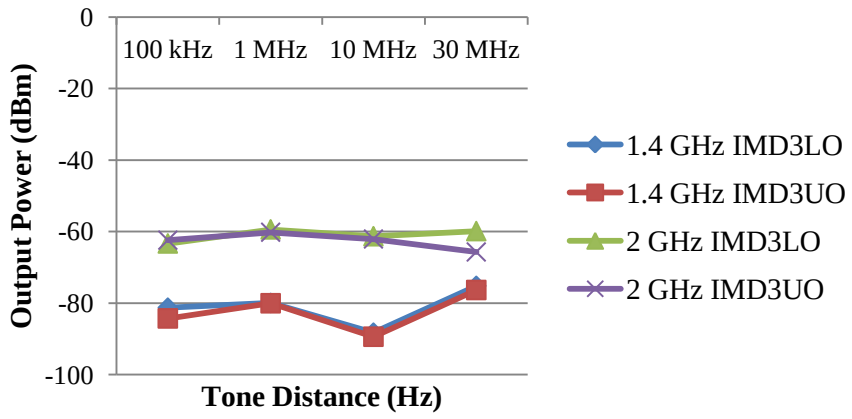

(a)

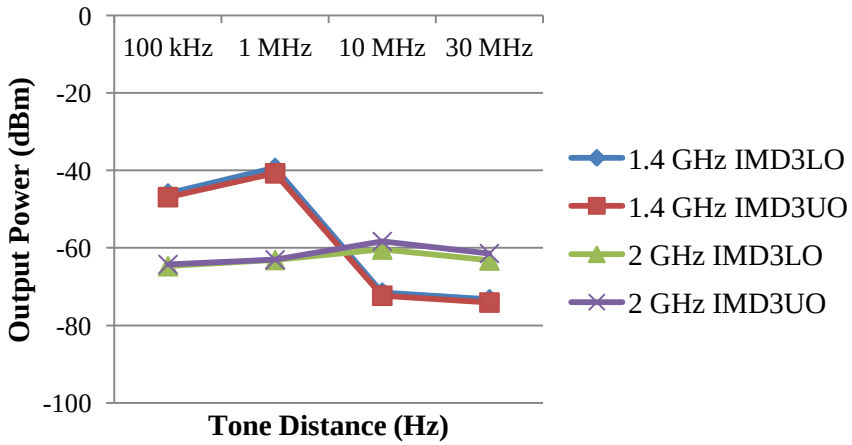

(b)

Figure 6.8: IMD3 frequencies variation with tone distance of reconfigurable PIFA with PIN diode (Gap, G_1 = 2 mm); (a) ON state (b) OFF state

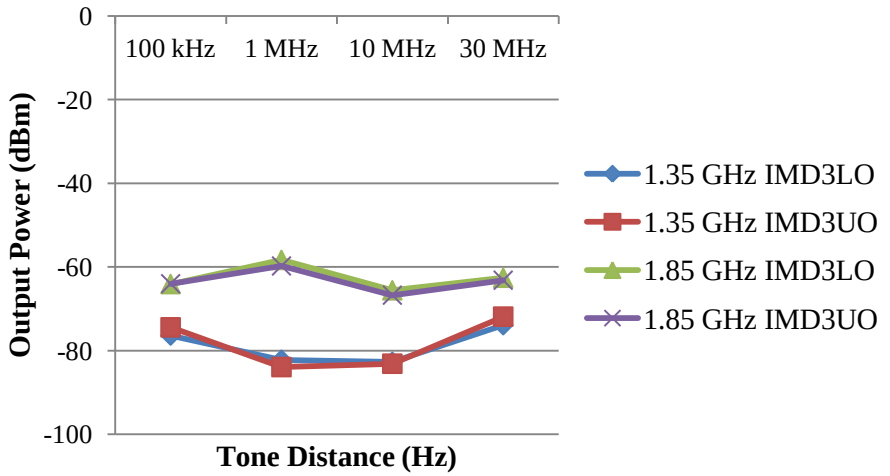

(a)

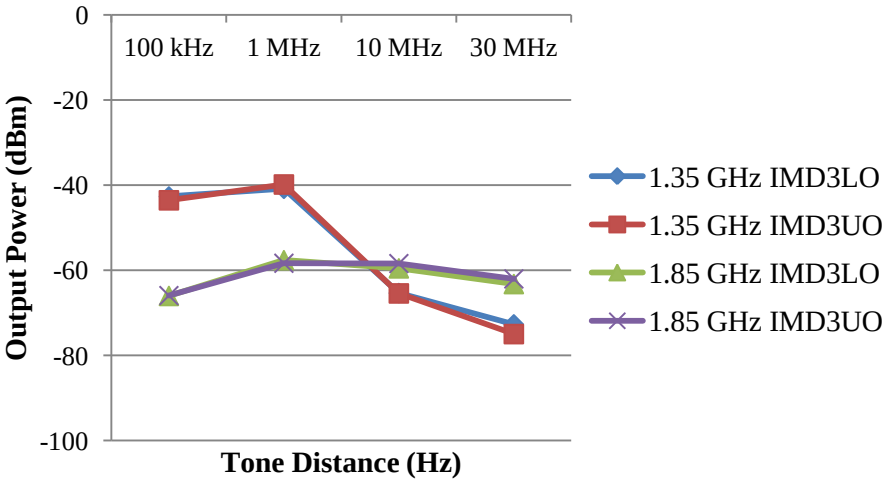

(b)

Figure 6.9: IMD3 frequencies variation with tone distance of reconfigurable PIFA with PIN diode (Gap, G_1 = 5 mm); (a) ON state (b) OFF state

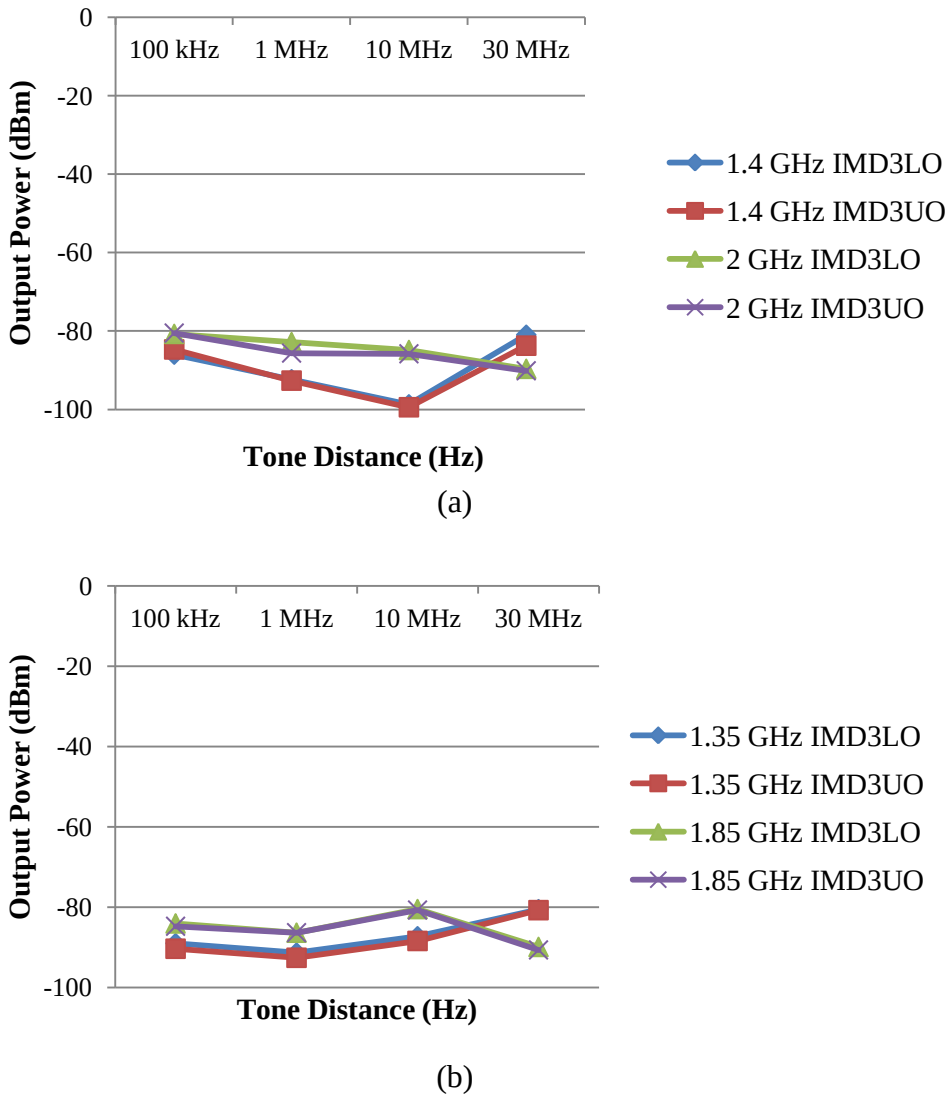

Figure 6.10: IMD3 frequencies variation with tone distance of PIFA with copper bridge; (a) 2 × 1 mm^2 (b) 5 × 1 mm^2

6.3.1 Reconfigurable PIFA with BAR50-02V PIN Diode (Gap, G_1 = 2 mm)

The nonlinear measurements conducted on the reconfigurable PIFA with BAR50-02V PIN diode (Gap, G_1 = 2 mm) are discussed in this section.

6.3.1.1 PIN Diode in ON State

6.3.1.1.1 Measurement of IMD3 Products

The IMD3 products were measured when the reconfigurable PIFA is transmitting signals at the device output. The measurements obtained are organized as follows in this section and will apply to the same section for the next antenna. Firstly, the plot of the transmitted IMD3 products together with the lower and upper tones is displayed at each radiation angle from -90° to 90°. Next, the ratio of the IMD3 products to carrier are displayed with the respective IMD3 products across the radiation angles to study the variations. The outcomes are useful in predicting the IMD3 products radiation patterns. The results are shown in each state of the PIN diode.

As previously discussed, in the ON state of PIN diode, the IMD3 products are more pronounced at 2 GHz. For that reason, all the measurements were conducted at 2 GHz. Figure 6.11 shows the transmitted IMD3 products and fundamental tones with varying radiation angles from -90° to 90°. From previously mentioned, maximum radiation occurs at 0°. From the figure, the measured IMD3 products for the lower and upper tones are approximately 47 dB below the fundamental tones in the direction of maximum radiation. The ratios of the IMD3 products to carrier in the lower and upper tones are plotted in Figure 6.12. It shows that the ratios are stable from -50° to 50° radiation angles. However, outside the range, the IMD3 products levels fall below the noise floor. Thus the ratios are unreliable.

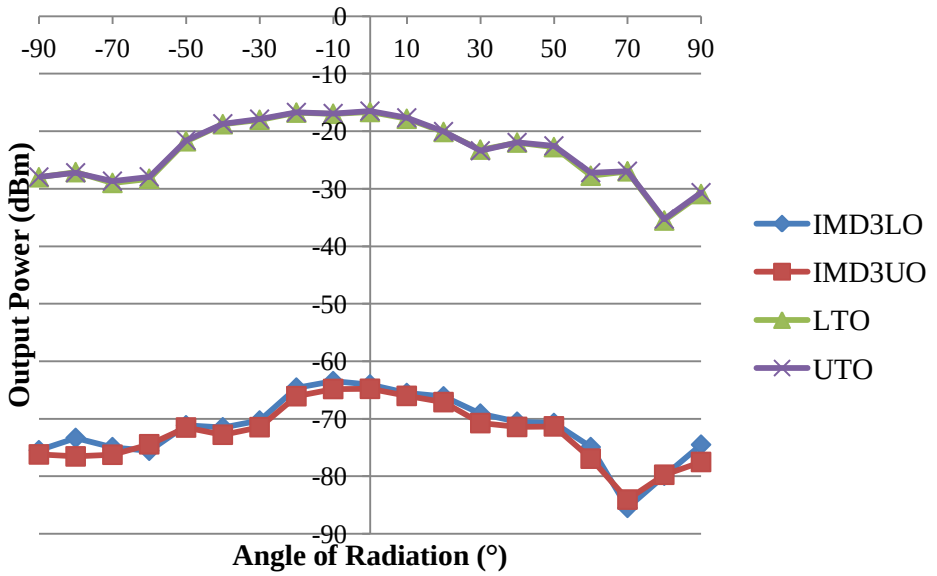

Figure 6.11: Transmitted IMD3 products of reconfigurable PIFA with PIN diode (Gap, G_1 = 2 mm) in ON state at 2 GHz

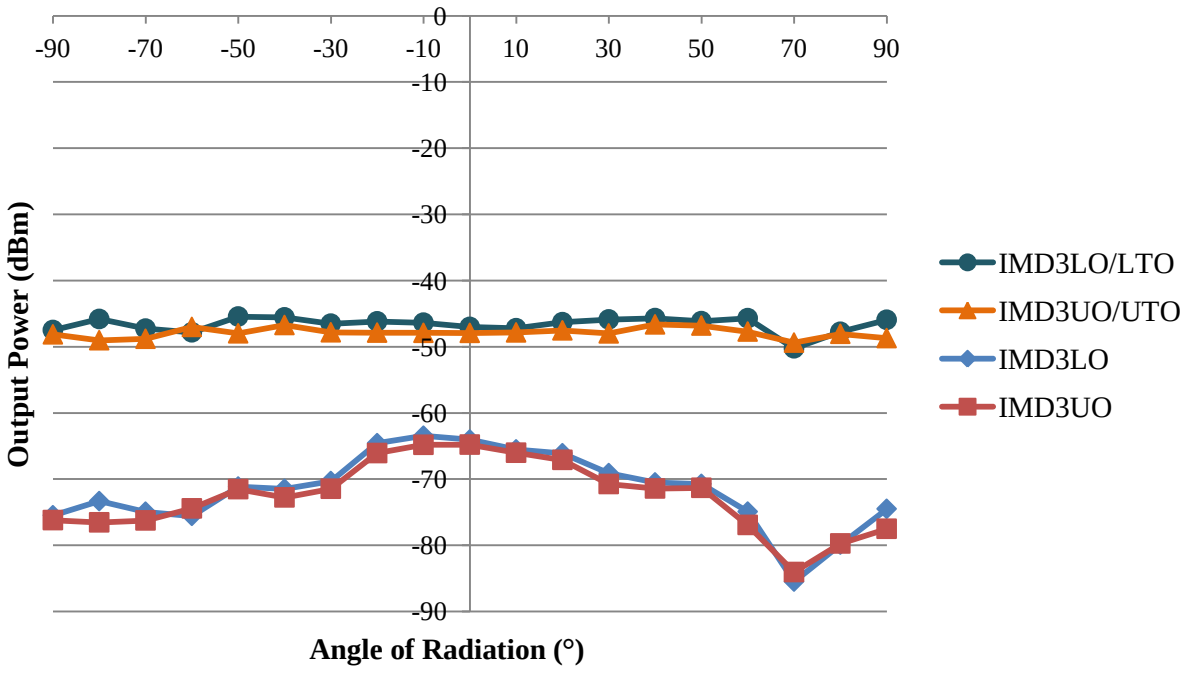

Figure 6.12: Ratio of IMD3 products to carrier in transmit mode of reconfigurable PIFA with PIN diode (Gap, G_1 = 2mm) in ON state at 2 GHz

6.3.1.1.2 Measurement of IMD3 Products Asymmetry

IMD3 products asymmetry across the radiation angles are plotted with the IMD3 products in the lower and upper tones. The IMD3 products asymmetry is the ratio of the IMD3 products in the upper tone to IMD3 products in the lower tone. In other words, it is the measure of the difference between IMD3UO and IMD3LO. This measurement is imperative to investigate its implication to memory effect in the reconfigurable PIFA or any nonlinear devices. Any significant memory effect will demand the application of complicated and more expensive predistortion device. On the other hand, if the ratios remain small with respect to 0 dB, then the device is said to be memoryless. In this particular case, simple and inexpensive predistortion technique can be applied to linearize the device. The IMD3 products asymmetry of the reconfigurable PIFA in the ON state at 2 GHz is plotted in Figure 6.13. From the figure, the ratios are close to 0 dB which suggests that the memory effects are small. Hence, it can be concluded that the device is almost memoryless in the ON state at 2 GHz.

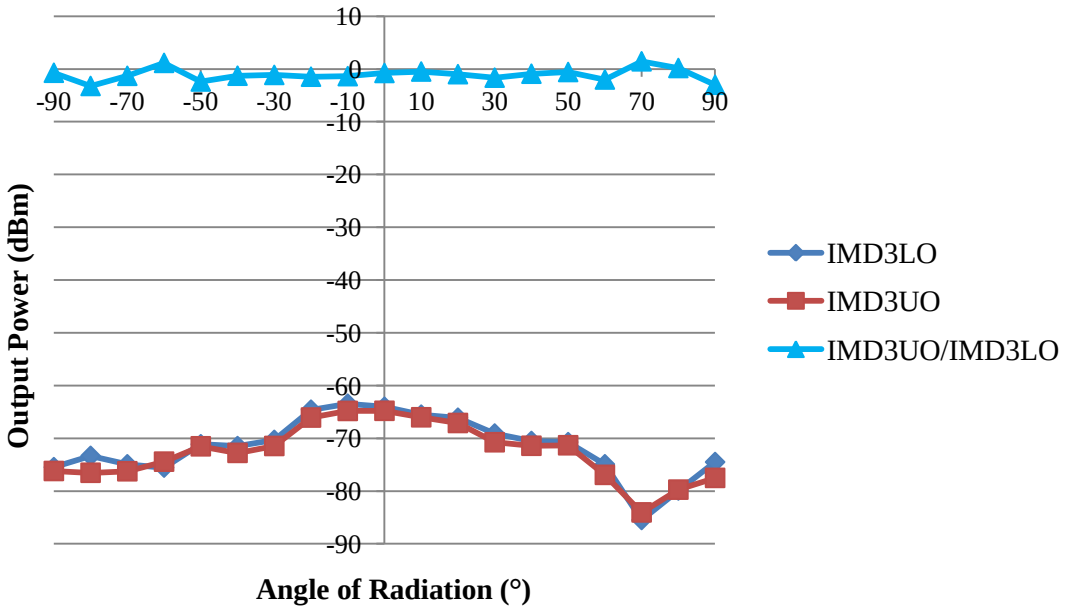

Figure 6.13: Intermodulation asymmetry of reconfigurable PIFA with PIN diode (Gap, G_1 = 2 mm) in ON state at 2 GHz

6.3.1.1.3 Measurement of IIP3

The IIP3 in the ON state of the PIN diode is shown in Figure 6.14. The point can be located at the intersection of the linear regression lines projected from measurements of output power taken at the fundamental tones (1:1 slope) and IMD3 products (3:1 slope). From the two figures, the IIP3 is approximately at 44 dBm with respect to the input power.

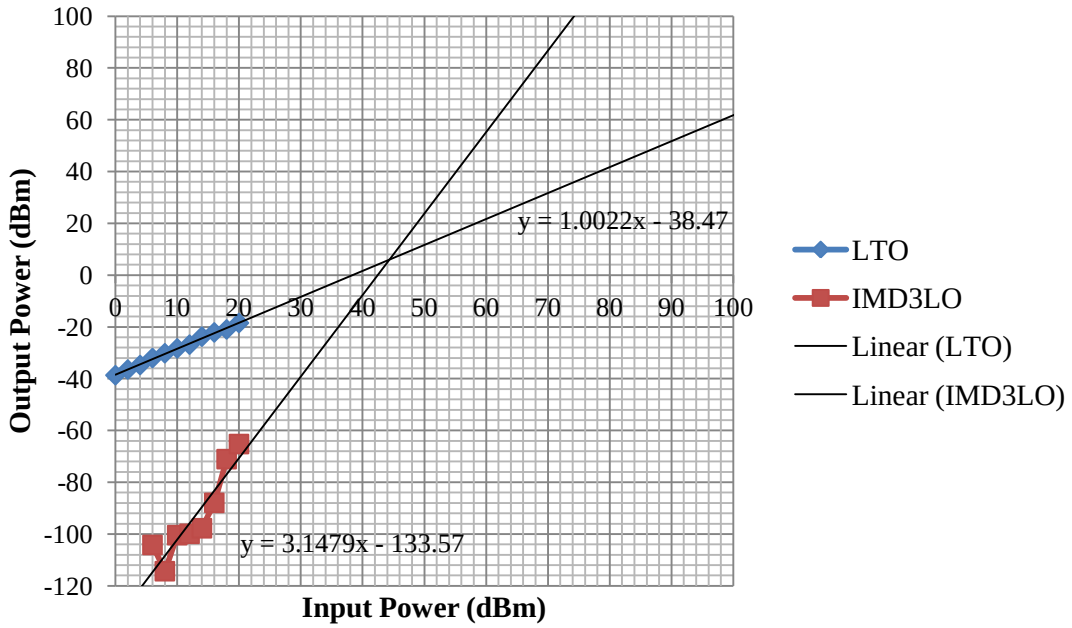

(a)

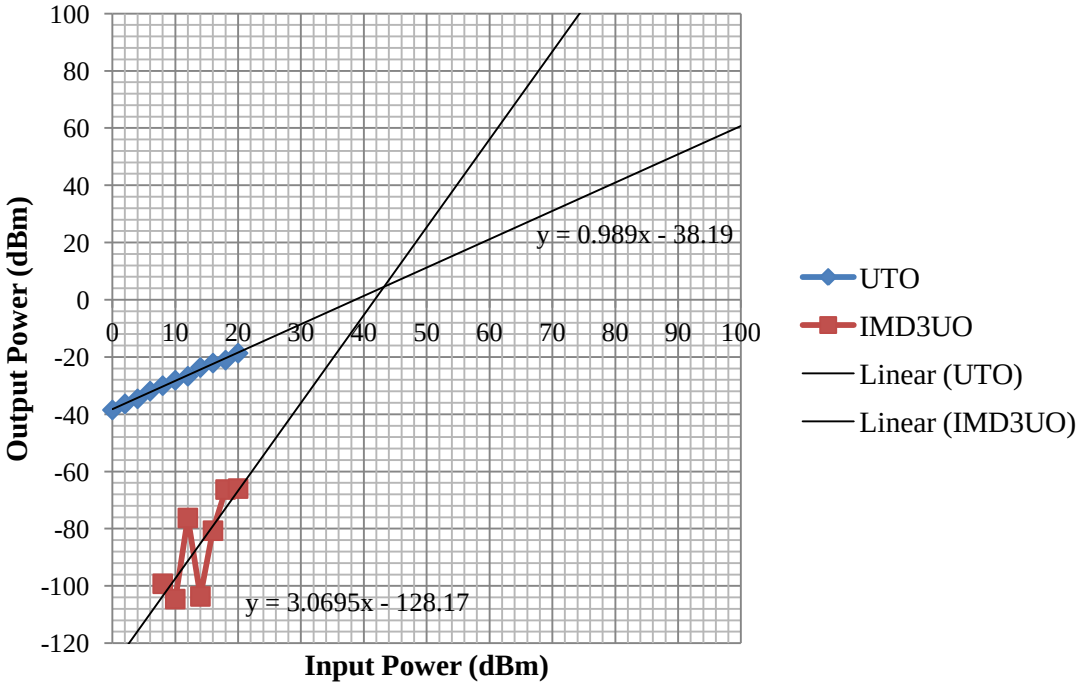

(b)

Figure 6.14: IIP3 of reconfigurable PIFA with PIN diode (Gap, G_1 = 2 mm) in ON state at 2 GHz for; (a) Fundamental and lower tones (b) Fundamental and upper tones

6.3.1.1.4 Measurement of $P_{1\text{-}dB}$

The $P_{1\text{-}dB}$ can be located from the plot of S_{21} against input power that was varied from -10 to 20 dBm. From the measurement, the point could not be located which suggests that the antenna behave linearly within the range of input power. The IIP3 at this frequency is 44 dBm and theoretically, the $P_{1\text{-}dB}$ is located at 34 dBm of input power. Figure 6.15 shows the transmission loss compression plot of the antenna.

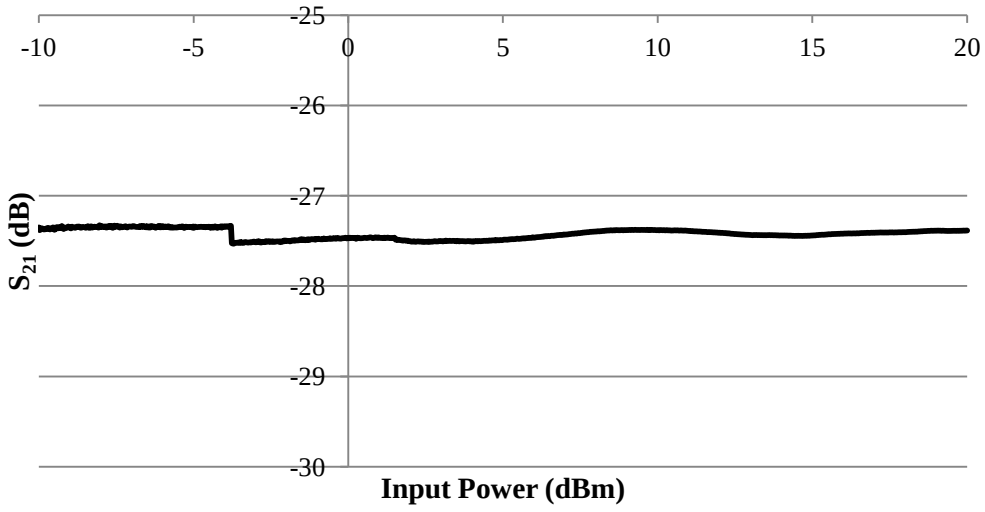

Figure 6.15: Transmission loss compression plot of reconfigurable PIFA with PIN diode (Gap, G_1 = 2 mm) in ON state at 2 GHz

6.3.1.2 PIN Diode in OFF State

6.3.1.2.1 Measurement of IMD3 Products

In the OFF state of the PIN diode, the IMD3 products can be observed significantly at 1.4 GHz. From the reflection coefficient graph of the PIN diode, the appearance of this resonance was

caused by the 16-nH bias inductor. At the same time, considerable IMD3 products are observed at 2 GHz. The transmitted IMD3 products and fundamental tones at the respective frequencies are shown in Figure 6.16. From Figure 6.16(a), the measured IMD3 products for the upper and lower tones are located at approximately 19 dB below the fundamental tones at 1.4 GHz. At 2 GHz, the IMD3 products suppression is approximately 41 dBc in the direction of maximum radiation which implies that at this particular frequency, the signal is more linear as compared to its counterpart at 1.4 GHz. The ratios of the IMD3 products to the carrier are shown in Figure 6.17. From the figure, small variations are observed from -50° to 40° radiation angles.

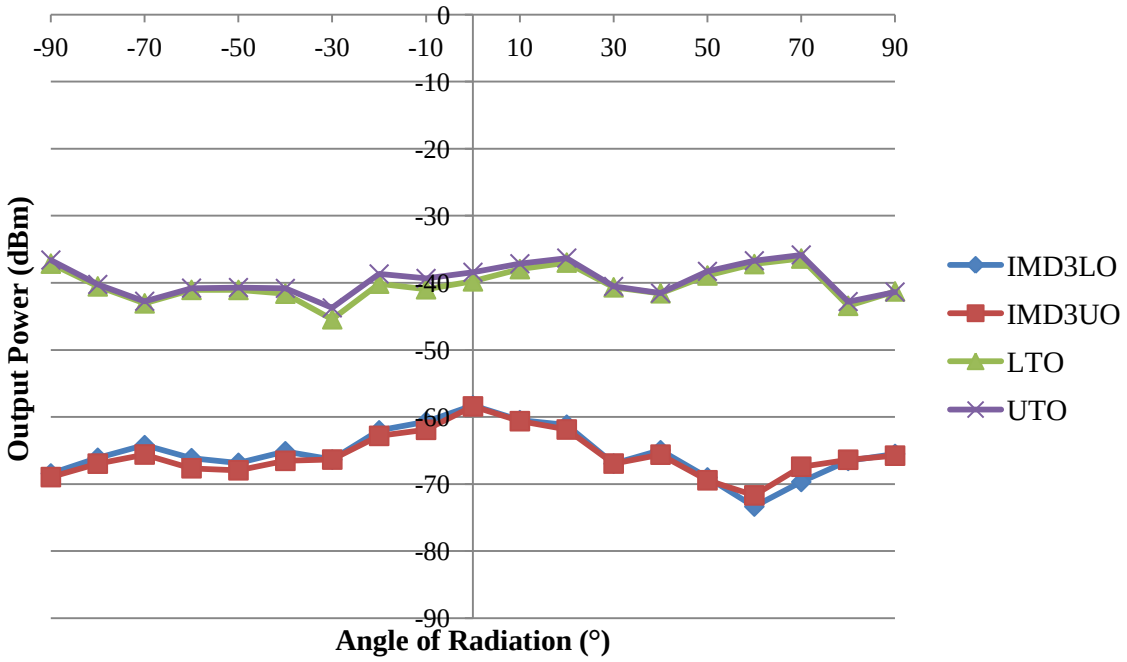

(a)

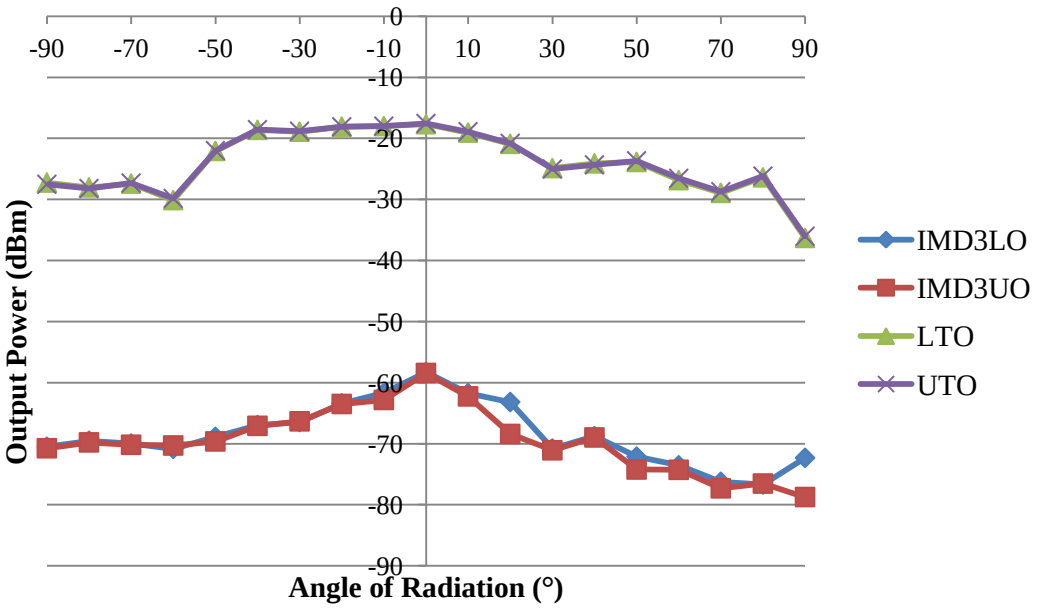

(b)

Figure 6.16: Transmitted IMD3 products of reconfigurable PIFA with PIN diode (Gap, G_1 = 2 mm) in OFF state at; (a) 1.4 GHz (b) 2 GHz

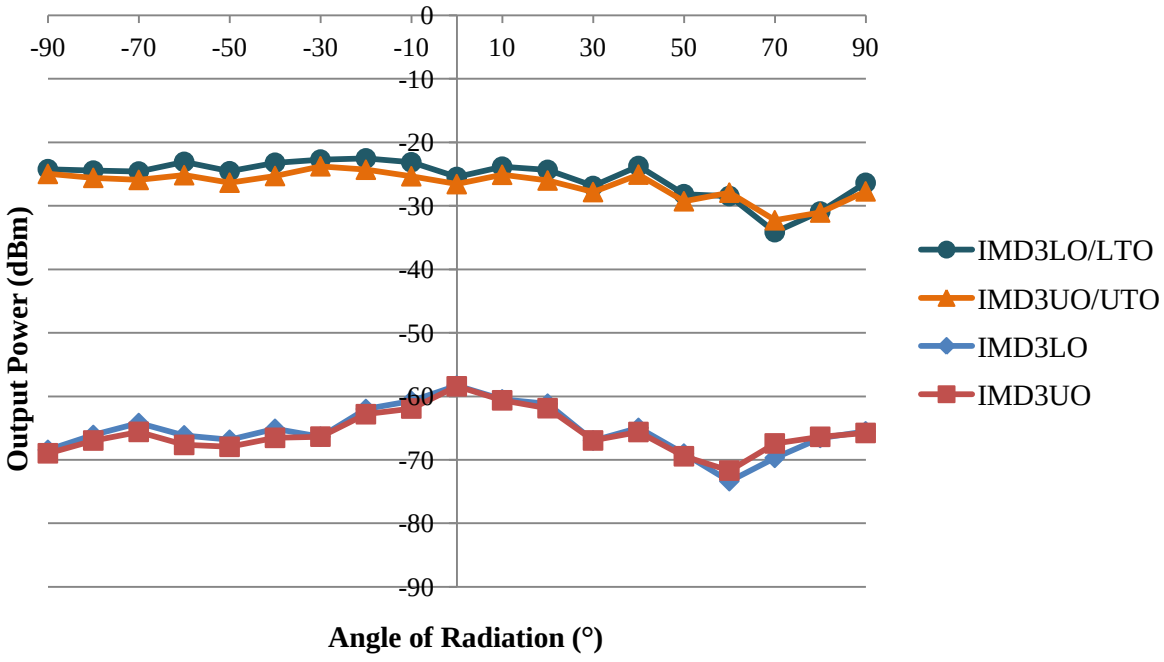

(a)

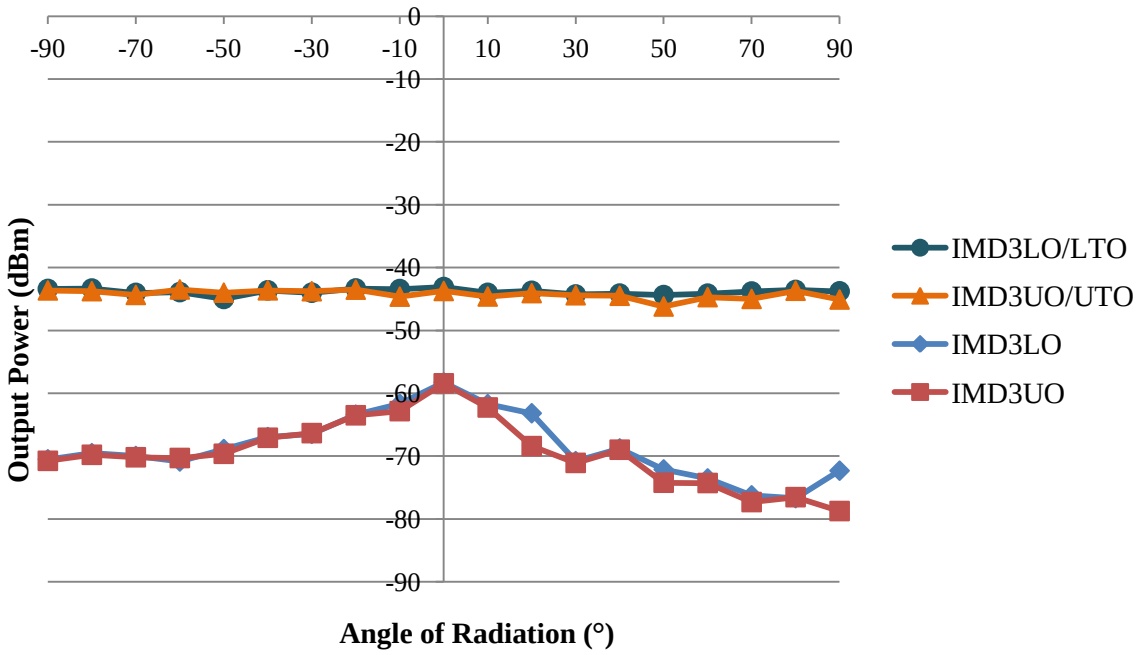

(b)

Figure 6.17: Ratio of IMD3 products to carrier in transmit mode of reconfigurable PIFA with PIN diode (Gap, G_1 = 2mm) in OFF state at; (a) 1.4 GHz (b) 2 GHz

6.3.1.2.2 Measurement of IMD3 Products Asymmetry

The plots of the IMD3 products asymmetry can be viewed in Figure 6.18. From the figures, it can be observed that the ratios of the IMD3UO to IMD3LO at both frequencies are close to 0 dB which means that there is no significant difference between both IMD3 products. Therefore, the reconfigurable PIFA is still almost memoryless in the OFF state of the PIN diode.

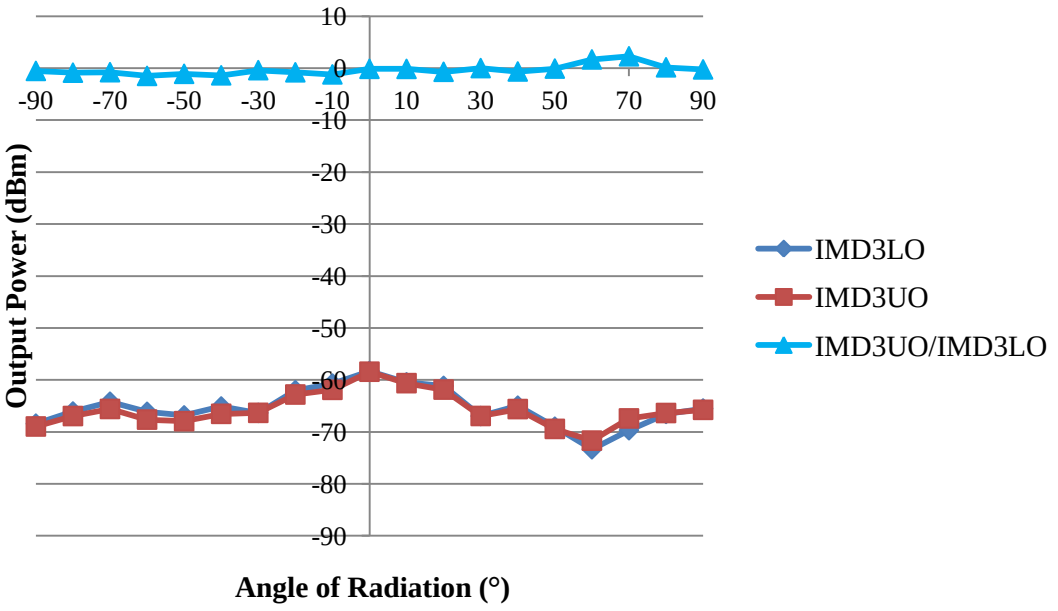

(a)

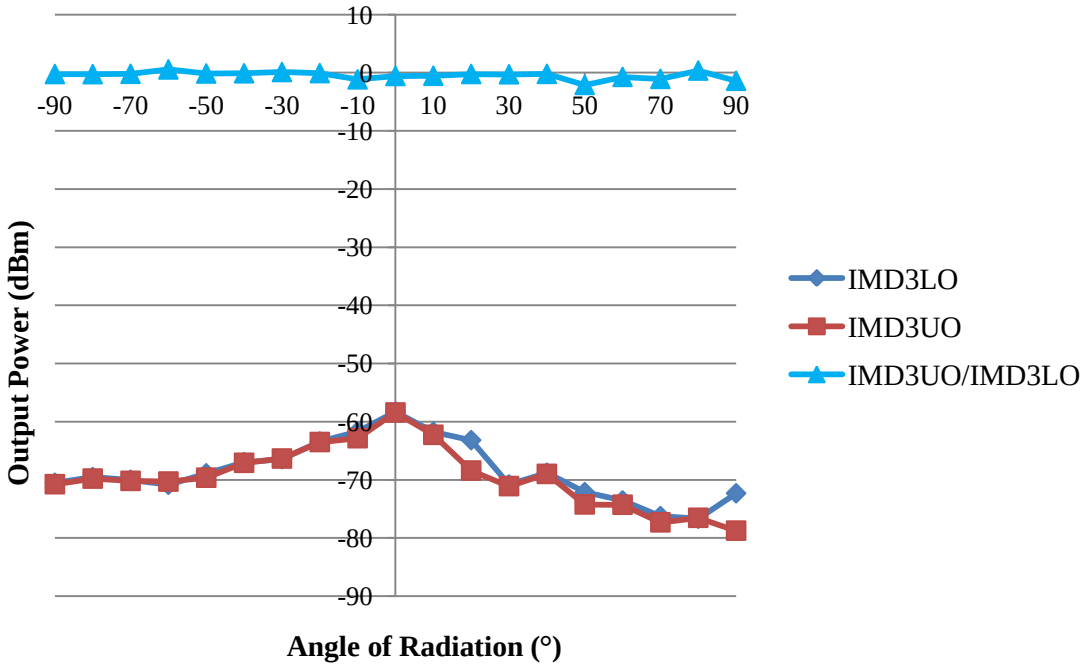

(b)

Figure 6.18: Intermodulation asymmetry of reconfigurable PIFA with PIN diode (Gap, G_1 = 5 mm) in OFF state at; (a) 1.4 GHz (b) 2 GHz

6.3.1.2.3 Measurement of IIP3

Figure 6.19 and Figure 6.20 show the location of the IIP3 in the OFF state of the reconfigurable PIFA at 1.4 and 2 GHz. The results are plotted separately for the lower and upper tones. From the figure, the IIP3 at 1.4 GHz is approximately 27 dBm with respect to the input power while at 2 GHz, the IIP3 is approximately at 44 dBm.

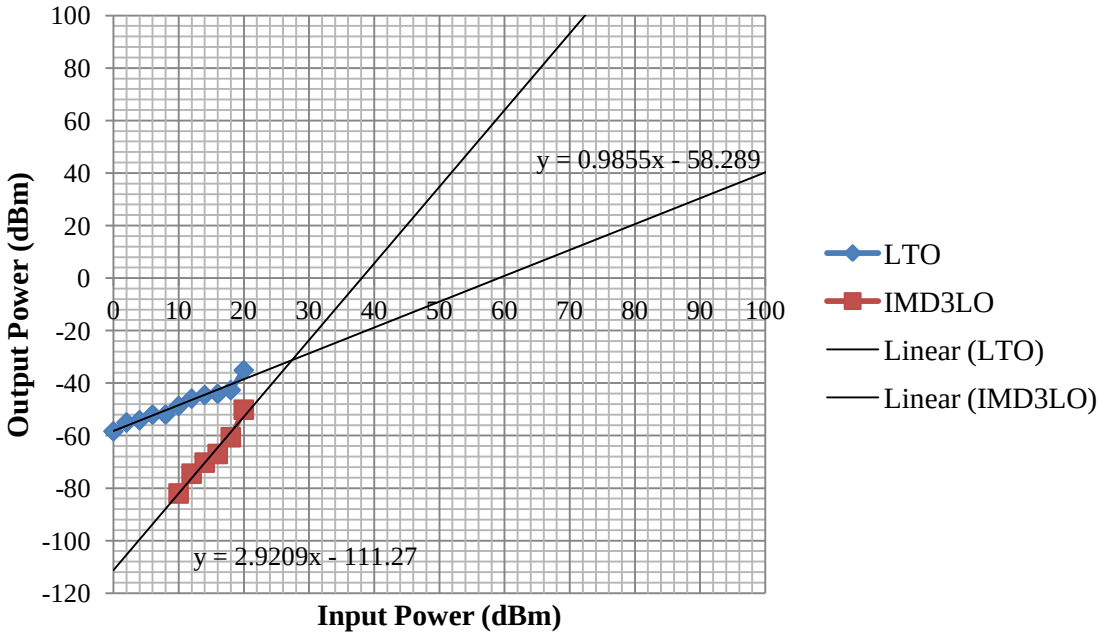

(a)

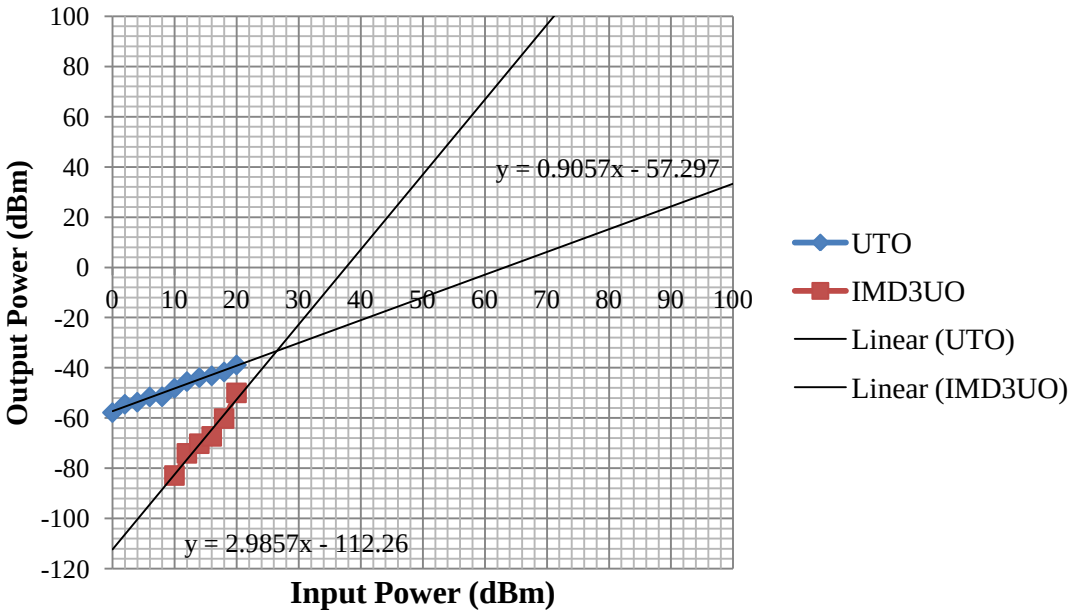

(b)

Figure 6.19: IIP3 of reconfigurable PIFA with PIN diode (Gap, G_1 = 2 mm) in OFF state at 1.4 GHz for; (a) Fundamental and lower tones (b) Fundamental and upper tones

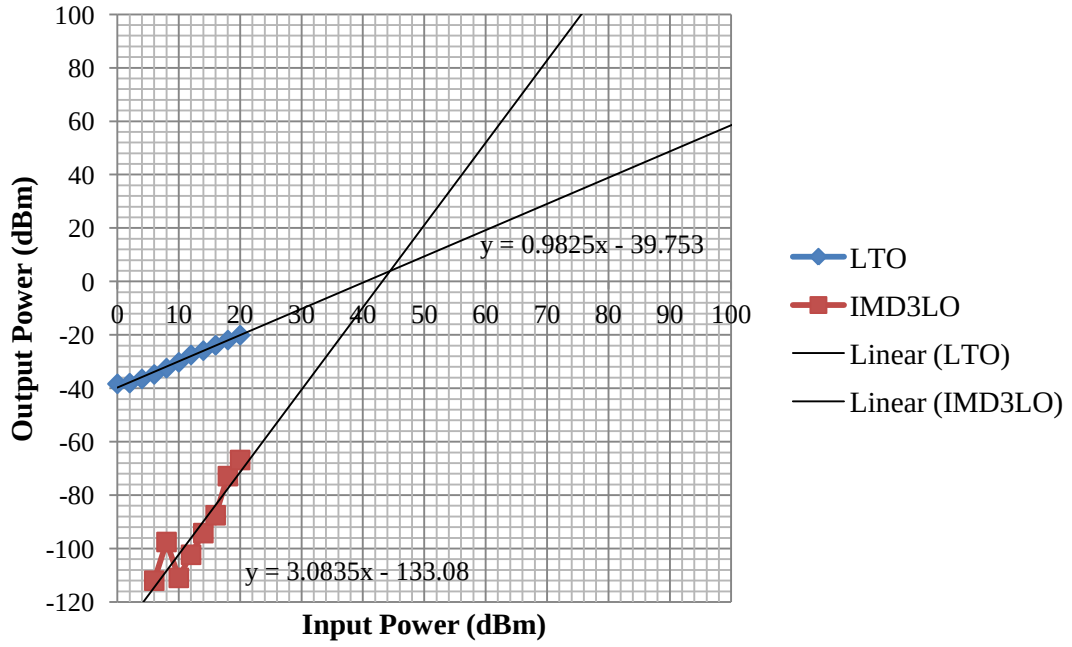

(a)

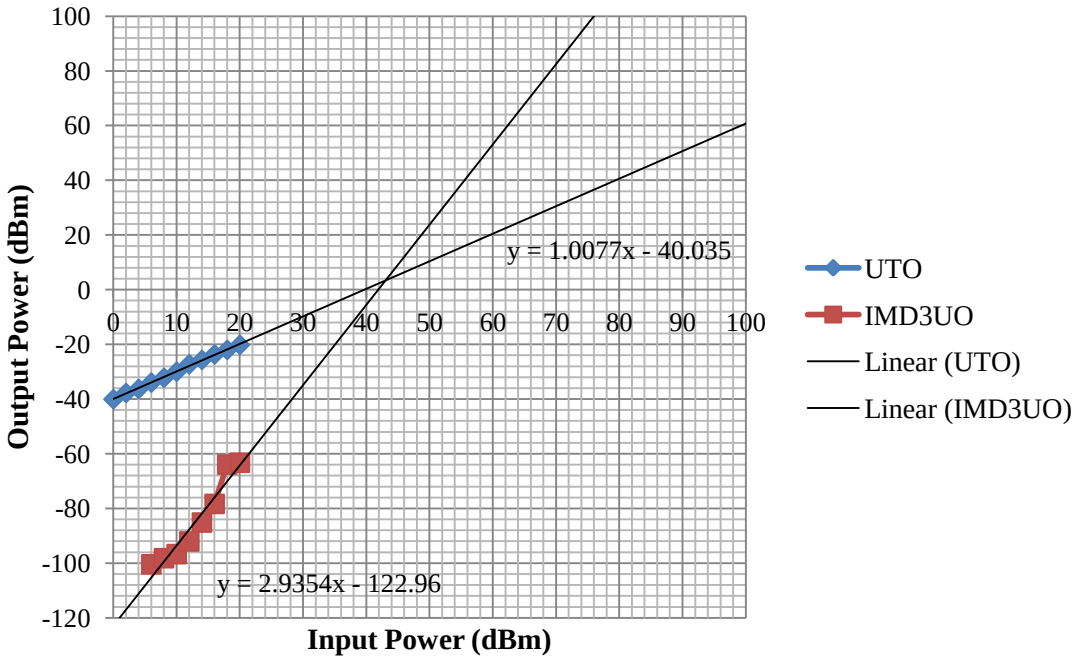

(b)

Figure 6.20: IIP3 of reconfigurable PIFA with PIN diode (Gap, G_1 = 2 mm) in OFF state at 2 GHz for; (a) Fundamental and lower tones (b) Fundamental and upper tones

6.3.1.2.4 Measurement of $P_{1\text{-dB}}$

The $P_{1\text{-dB}}$ of the reconfigurable PIFA in the OFF state was measured at 1.4 and 2 GHz. Figure 6.21 shows the $P_{1\text{-dB}}$ location at its respective frequency. From the figure, the gain compression could not be located at 2 GHz which implies that the point lies outside the range of input power. On the other hand, the point can be located within the stipulated range at 1.4 GHz. From Figure 6.21(a), the $P_{1\text{-dB}}$ is located at 17.7 dBm from the reading on ZVA67 VNA. Based on the IIP3 value of 27 dBm at the same frequency, the gain compression is predicted to be located at 17 dBm which is at very close approximation to the measured $P_{1\text{-dB}}$ at 17.7 dBm.

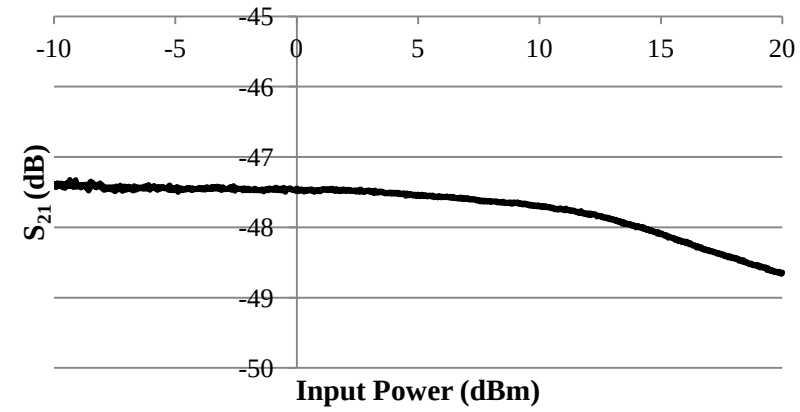

(a)

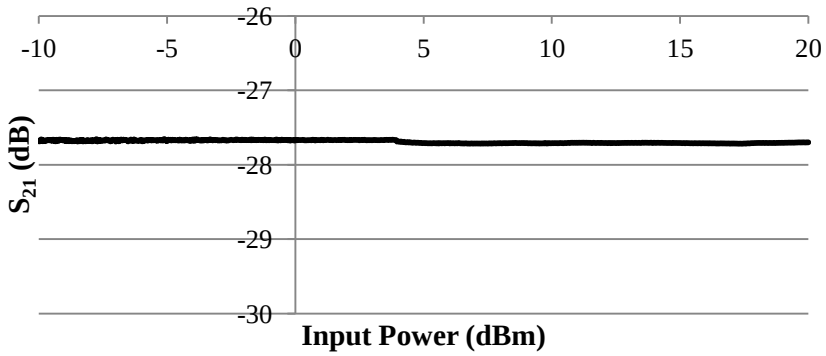

(b)

Figure 6.21: Transmission loss compression plot of reconfigurable PIFA with PIN diode (Gap, G_1 = 2 mm) in OFF state at; (a) 1.4 GHz (b) 2 GHz

6.3.2 Reconfigurable PIFA with BAR50-02V PIN Diode (Gap, G_1 = 5 mm)

The nonlinearity measurements performed on the reconfigurable PIFA with BAR50-02V PIN diode (Gap, G_1 = 5 mm) are presented in this section.

6.3.2.1 PIN Diode in ON State

6.3.2.1.1 Measurement of IMD3 Products

In the ON state, the IMD3 products can be located at 1.85 GHz. The plot of IMD3 products in the lower and upper tones with fundamental tones can be seen in Figure 6.22. From the figure, the IMD3 products are at approximately 43 dB below the fundamental tones in the direction of maximum radiation as compared to 47 dB from the previous antenna. The ratio of the IMD3 products to carrier can be viewed in Figure 6.23. From the figure, the ratios are stable between -50° to 50° of radiation angles. The IMD3 product levels fall below the noise floor outside the range. Thus, the ratios are not reliable.

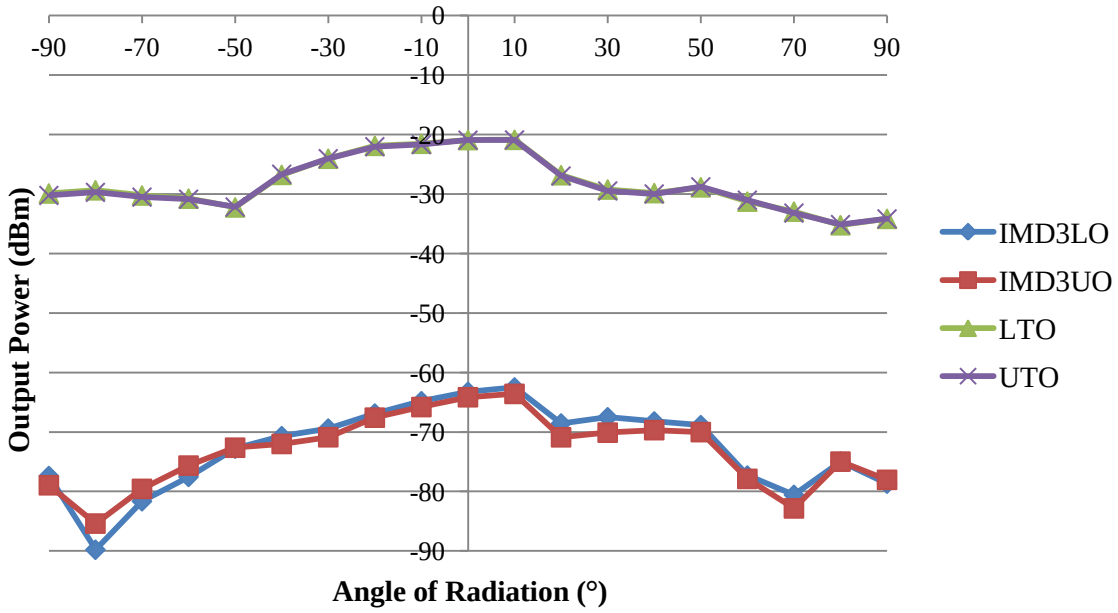

Figure 6.22: Transmitted IMD3 products of reconfigurable PIFA with PIN diode (Gap, G_1 = 5 mm) in ON state at 1.85 GHz

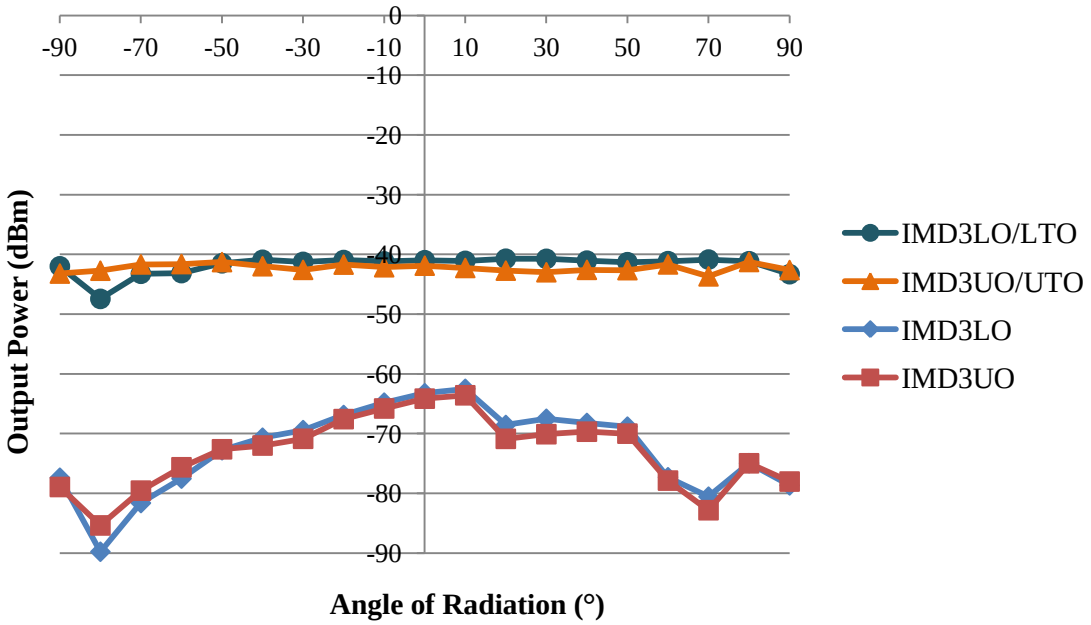

Figure 6.23: Ratio of IMD products to carrier in transmit mode of reconfigurable PIFA with PIN diode (Gap, G_1 = 5 mm) in ON state at 1.85 GHz

6.3.2.1.2 Measurement of IMD3 Products Asymmetry

The IMD3 products asymmetry of the antenna is plotted in Figure 6.24. From the figure, the differences between the IMD3 products in the upper and lower tones are small from -50° to 50° radiation angles. The wide angle demonstrates that the IMD3 products asymmetry can still be considered almost memoryless, similar to the previous antenna.

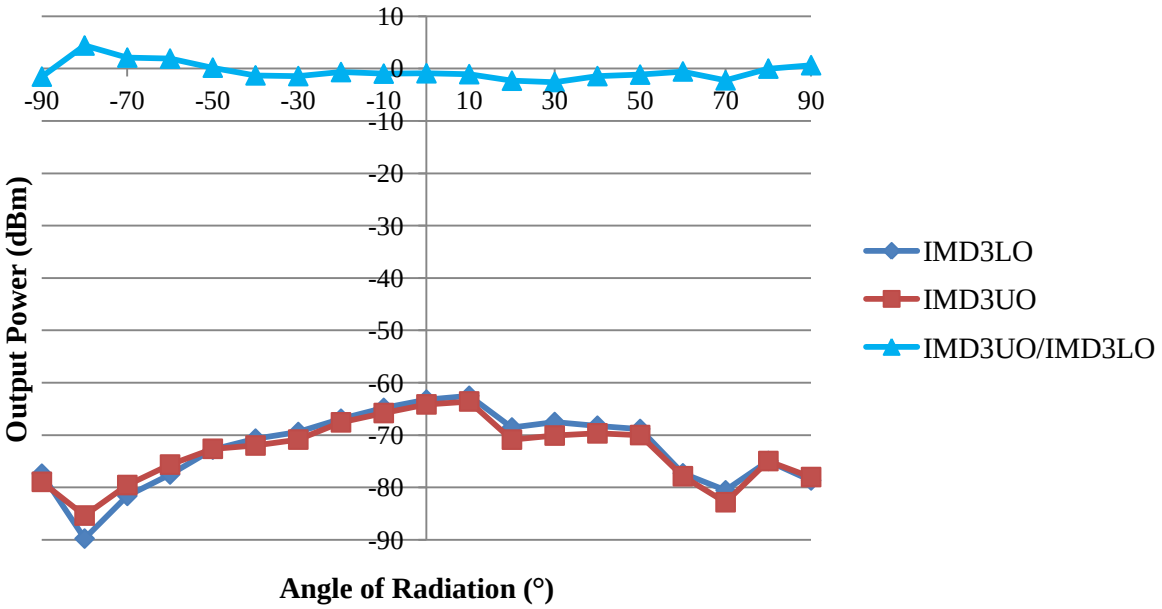

Figure 6.24: Intermodulation asymmetry of reconfigurable PIFA with PIN diode (Gap, G_1 = 5 mm) in ON state at 1.85 GHz

6.3.2.1.3 Measurement of IIP3

The IIP3 of the reconfigurable PIFA can be located from the graphs in Figure 6.25. It can be seen clearly that the location of the IIP3 from both graphs is at approximately 42 dBm with respect to the input power.

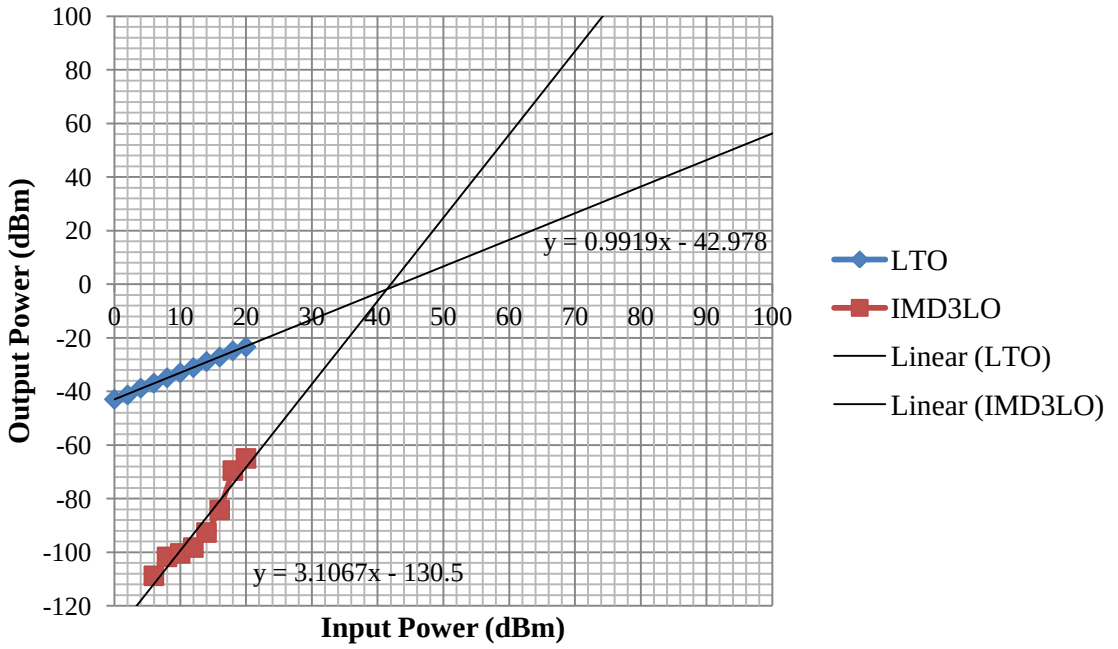

(a)

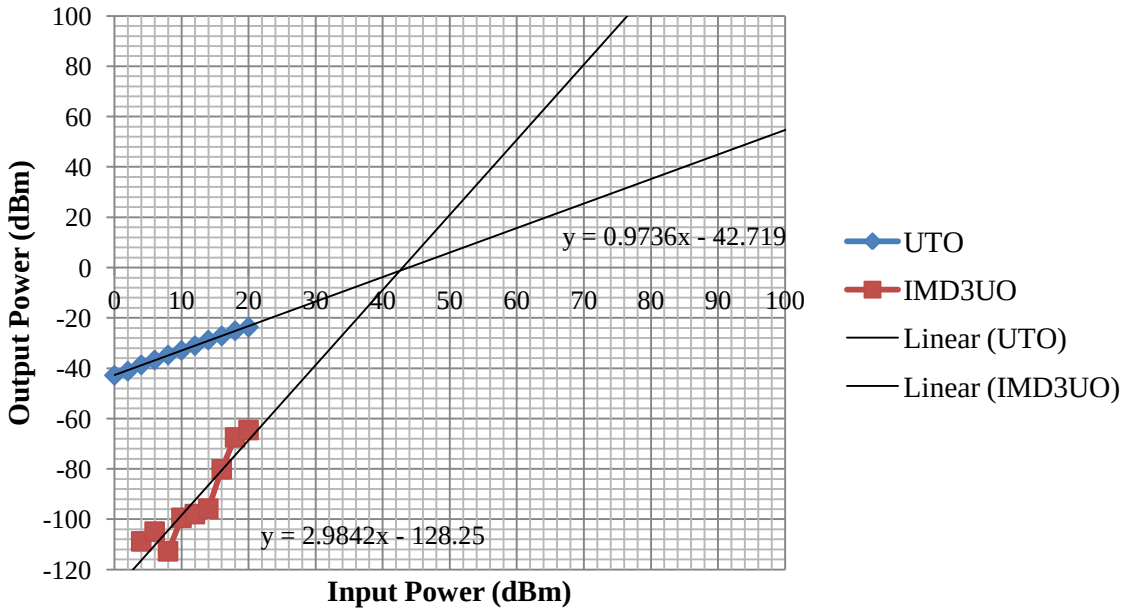

(b)

Figure 6.25: IIP3 of reconfigurable PIFA with PIN diode (Gap, G_1 = 5 mm) in ON state at 1.85 GHz for; (a) Fundamental and lower tones (b) Fundamental and upper tones

6.3.2.1.4 Measurement of $P_{1\text{-}dB}$

The measurement of $P_{1\text{-}dB}$ was performed at 1.85 GHz in the ON state of the antenna as can be viewed in Figure 6.26. However, the gain compression could not be located from the graph which implies that it is greater than 20 dBm. From the measured IIP3 of the antenna, the $P_{1\text{-}dB}$ is predicted at 32 dBm which confirms that the measurement is reliable.

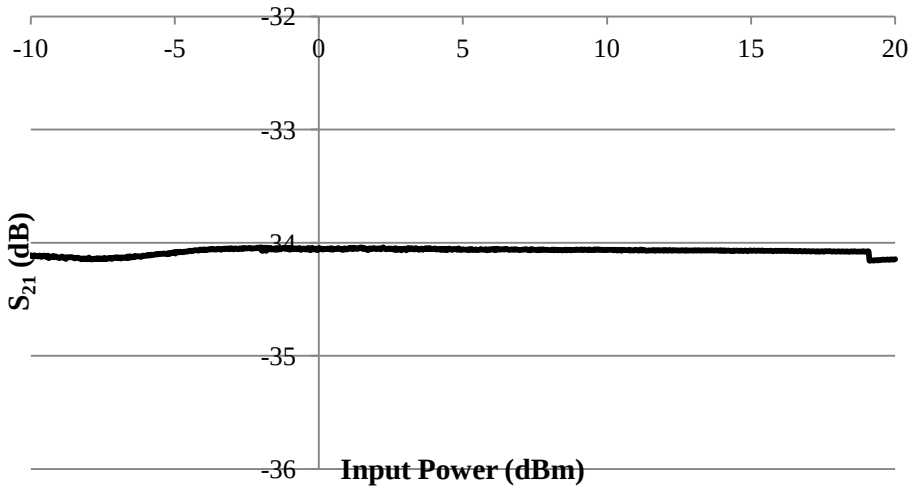

Figure 6.26: Transmission loss compression plot of reconfigurable PIFA with PIN diode (Gap, G_1 = 5 mm) in ON state at 1.85 GHz

6.3.2.2 PIN Diode in OFF State

6.3.2.2.1 Measurement of IMD3 Products

The IMD3 products in the OFF state are measured at 1.35 and 1.85 GHz since the IMD3 products are significantly noticeable at these frequencies. The transmitted IMD3 products can be viewed in Figure 6.27. From the figure, the IMD3 products suppression is approximately 15 dBc in the direction of maximum radiation at 1.35 GHz. This suggested that the reconfigurable PIFA is

highly nonlinear at that particular frequency. As previously mentioned, the new resonance from the bias inductor occurred at 1.35 GHz. On the other hand, at 1.85 GHz, the suppression is approximately 43 dBc which implies that the signals are highly linear at that particular frequency. The ratios of the IMD3 products to carrier at its respective frequencies are displayed in Figure 6.28. From the figures, the ratios at 1.35 GHz are stable from -50° to 50° angles. On the contrary, at 1.85 GHz, the ratios are only reliable from -60° to 60° because outside the range, the IMD3 products are approaching the noise floor.

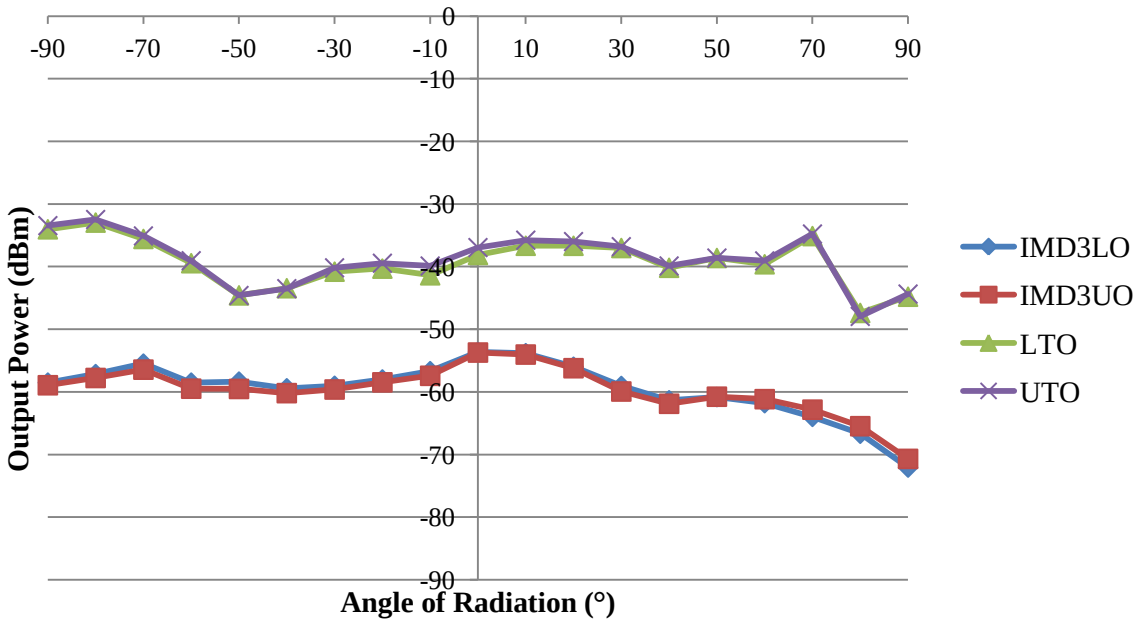

(a)

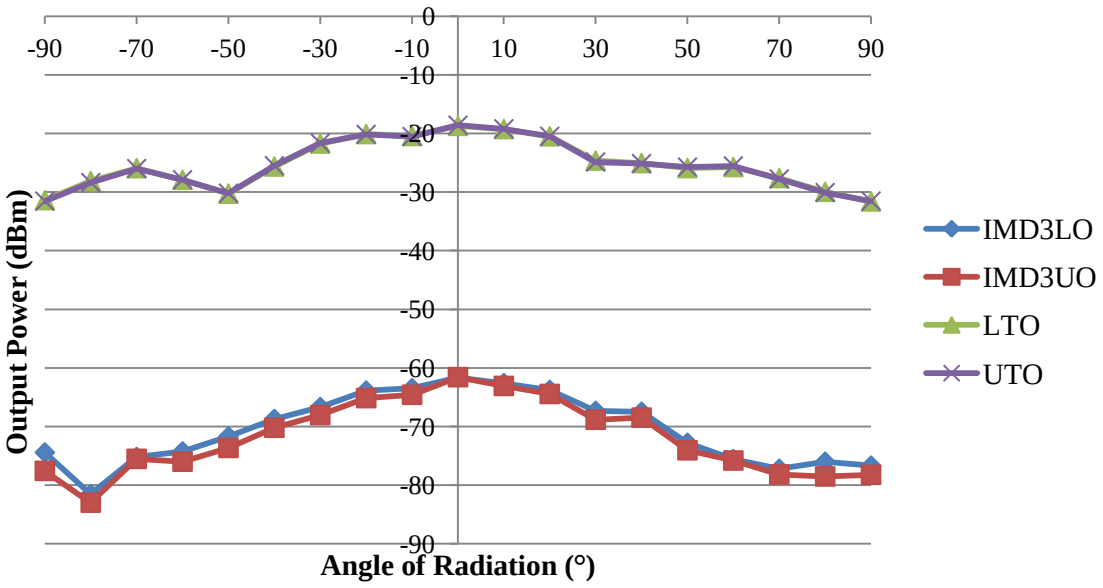

(b)

Figure 6.27: Transmitted IMD products of reconfigurable PIFA with PIN diode (Gap, G_1 = 5 mm) in OFF state at; (a) 1.35 GHz (b) 1.85 GHz

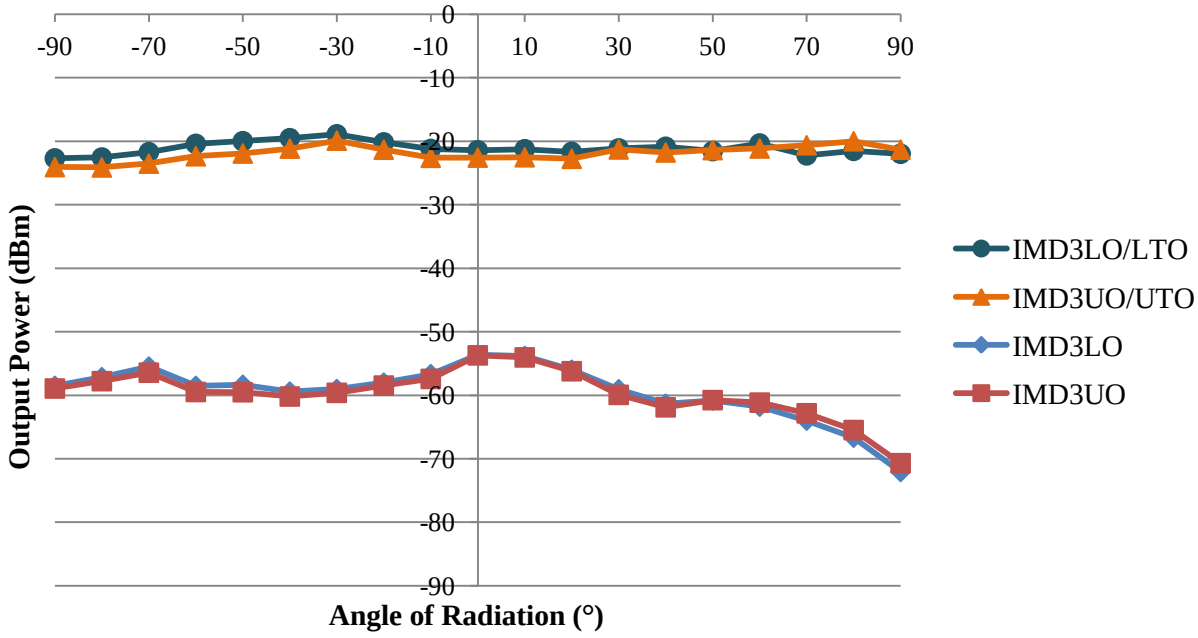

(a)

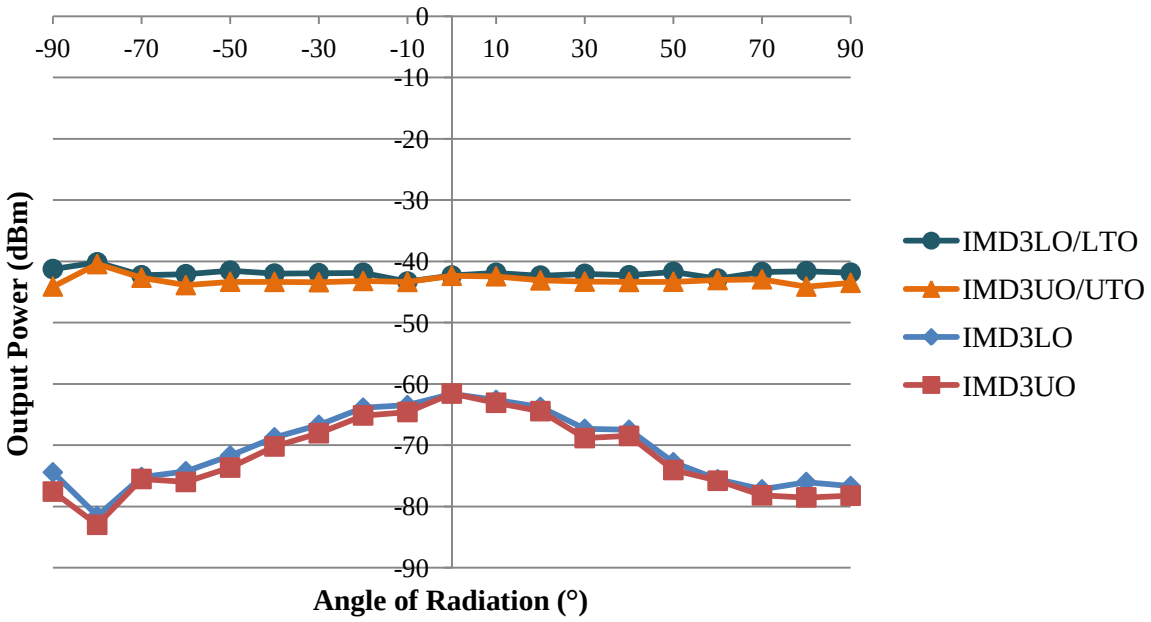

(b)

Figure 6.28: Ratio of IMD products to fundamental tones of reconfigurable with PIN diode (Gap, G_1 = 5 mm) in OFF state at; (a) 1.35 GHz (b) 1.85 GHz

6.3.2.2.2 Measurement of IMD3 Products Asymmetry

The measured IMD3 products asymmetry of the reconfigurable PIFA at 1.35 and 1.85 GHz are shown in Figure 6.29. From the figure, the IMD3 products asymmetries at both frequencies are relatively small with respect to 0 dB. This implies that the antenna is almost memoryless in the OFF state of the PIN diode.

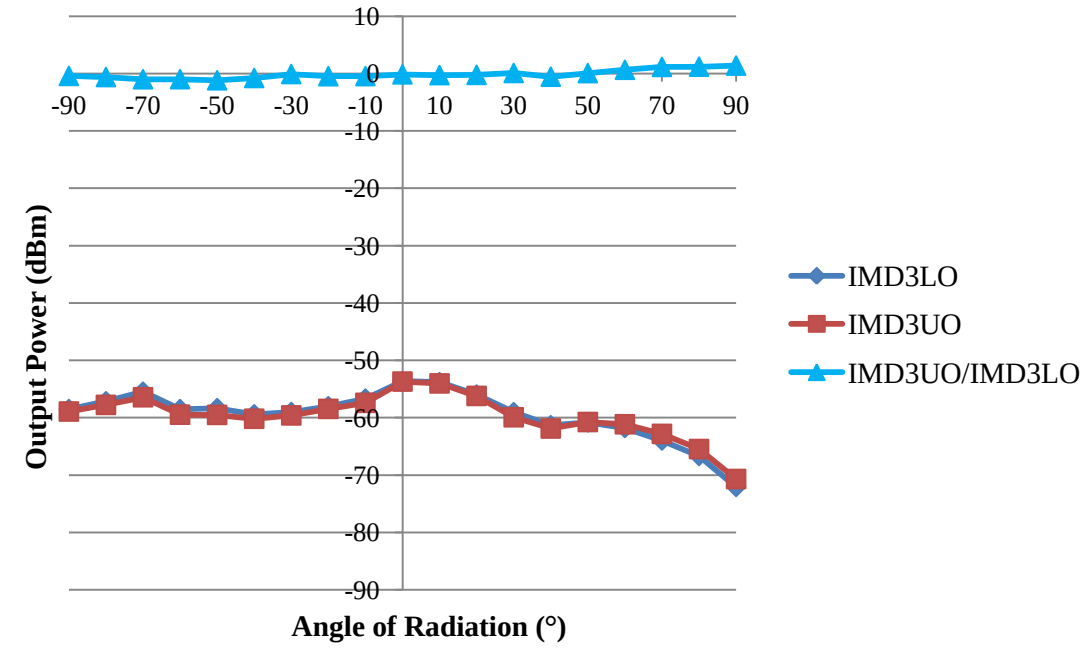

(a)

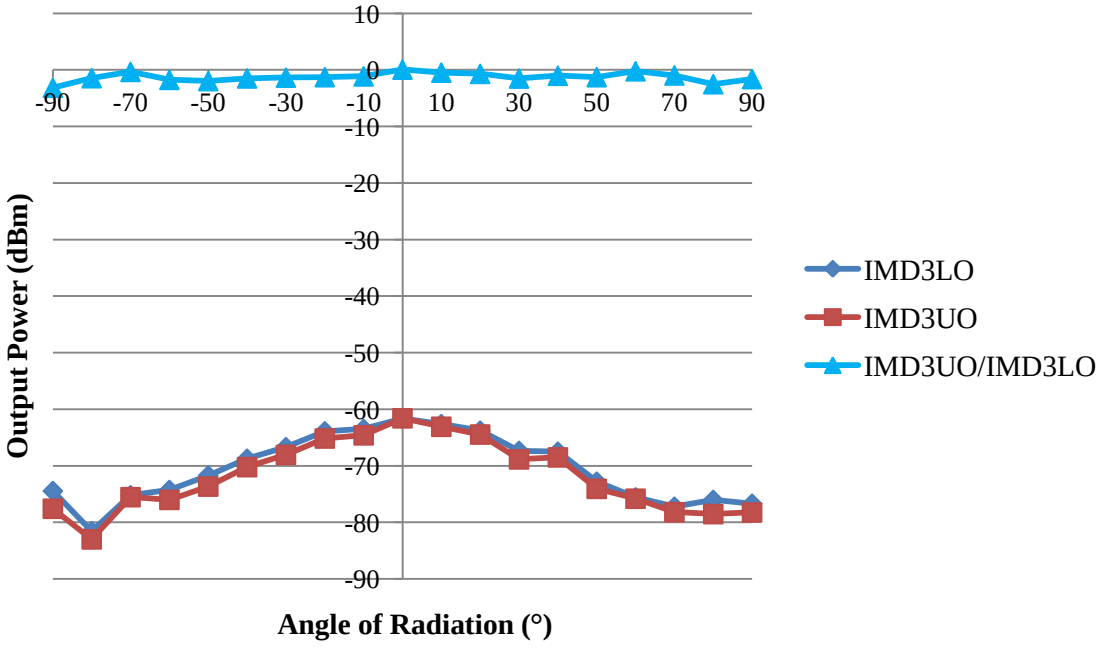

(b)

Figure 6.29: IMD3 products asymmetry of the reconfigurable PIFA with PIN diode (Gap, G_1 = 5 mm) in OFF state at; (a) 1.35 GHz (b) 1.85 GHz

6.3.2.2.3 Measurement of IIP3

The location of IIP3 from the intersection of the linear regression lines of the IMD3 products and fundamental tones can be viewed in Figure 6.30 and Figure 6.31. The intersection point of IIP3 at 1.35 GHz is at 26 dBm with respect to the input power. On the other hand, the IIP3 at 1.85 GHz is at 42 dBm.

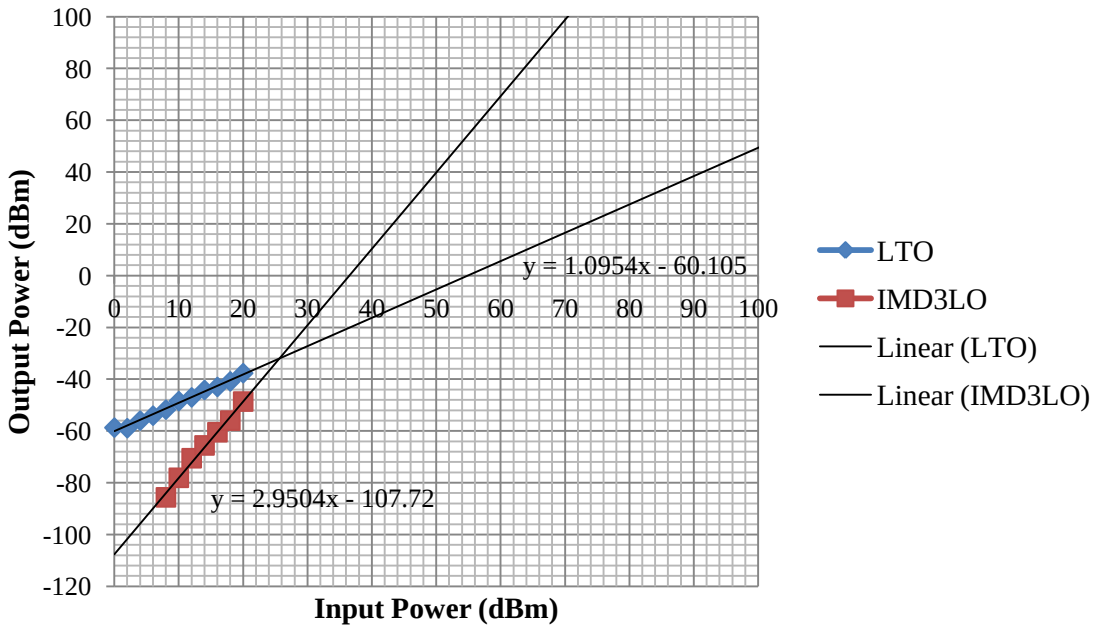

(a)

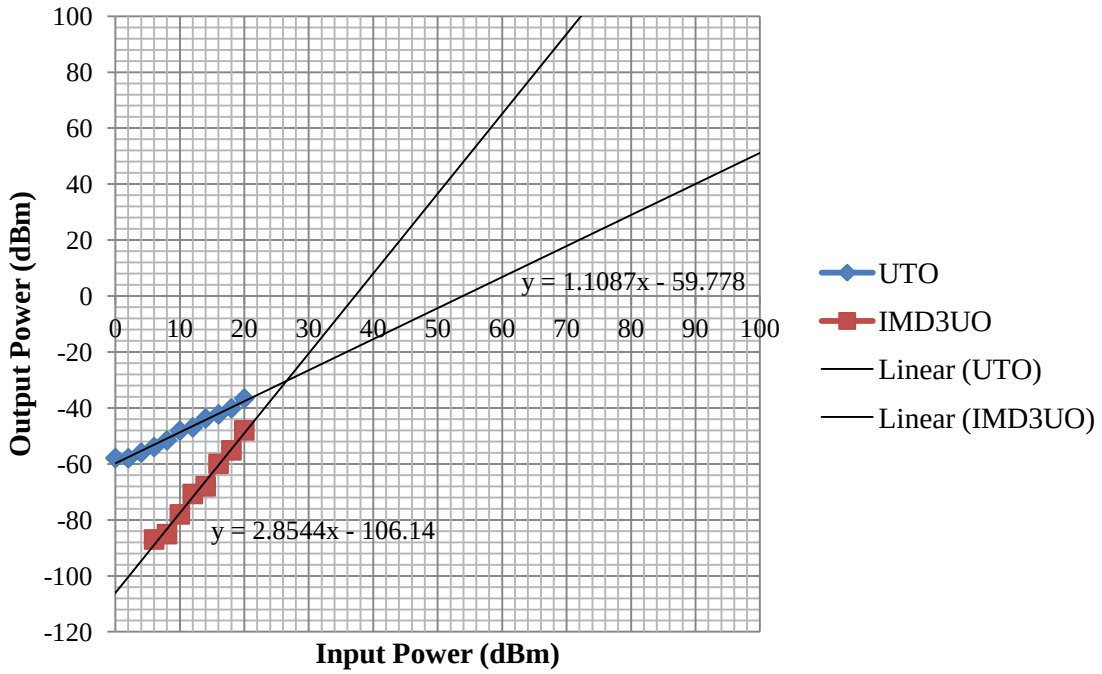

(b)

Figure 6.30: IIP3 of reconfiigurable PIFA with PIN diode (Gap, G_1 = 5 mm) in OFF state at 1.35 GHz for; (a) Fundamental and lower tones (b) Fundamental and upper tones

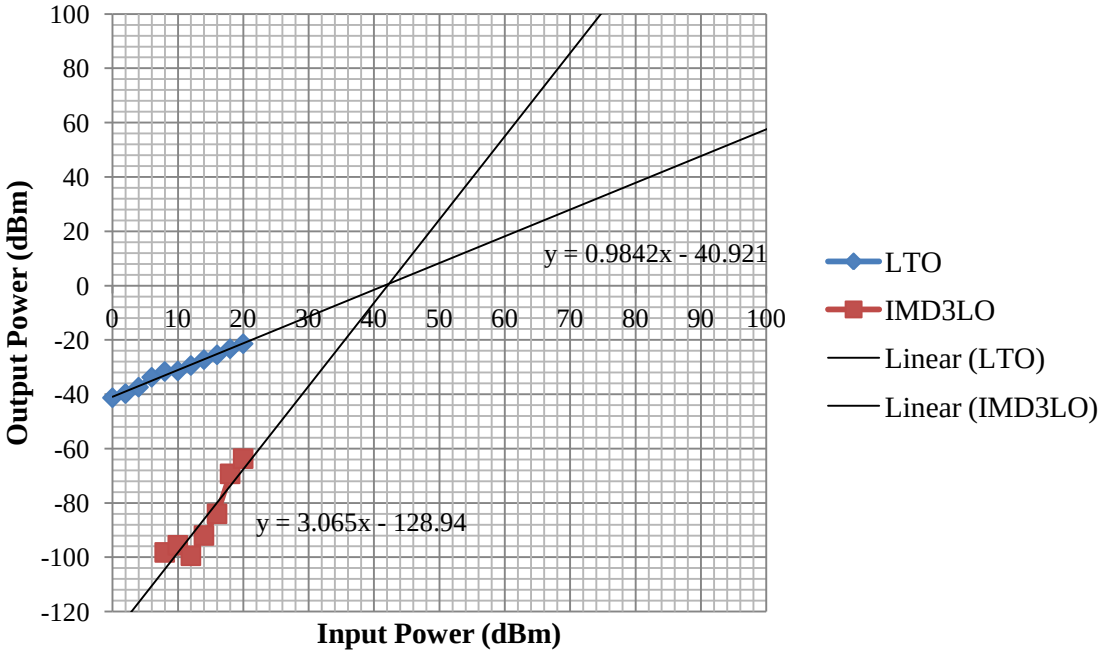

(a)

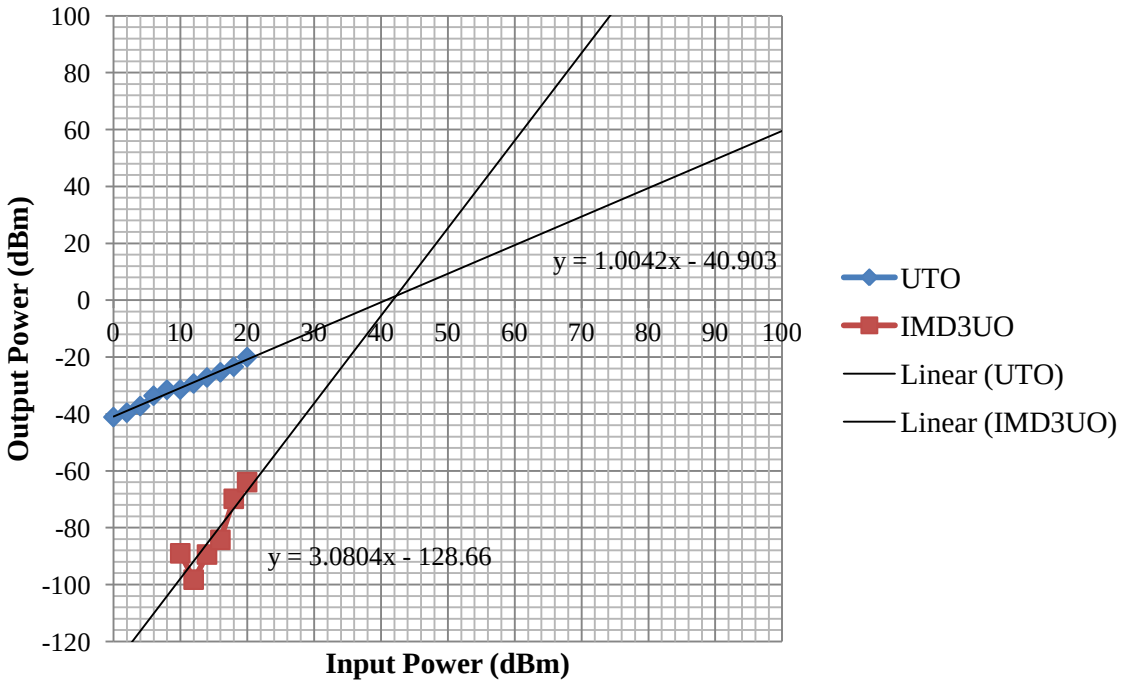

(b)

Figure 6.31: IIP3 of reconfiigurable PIFA with PIN diode (Gap, G_1 = 5 mm) in OFF state at 1.85 GHz for; (a) Fundamental and lower tones (b) Fundamental and upper tones

6.3.2.2.4 Measurement of $P_{1\text{-}dB}$

Similarly, the $P_{1\text{-}dB}$ was measured at 1.35 and 1.85 GHz for this antenna. The plots are shown in Figure 6.32. From both figures, the $P_{1\text{-}dB}$ could not be located at 1.85 GHz. On the contrary, the gain compression was able to be measured at 1.35 GHz which implies that the point is located within the range of input power. From Figure 6.32(a), the $P_{1\text{-}dB}$ is 17.3 dBm from the reading on ZVA67 VNA. In addition, the IIP3 value of 26 dBm at this frequency implies that the gain compression is predicted to be at 16 dBm which is almost similar to the measured $P_{1\text{-}dB}$.

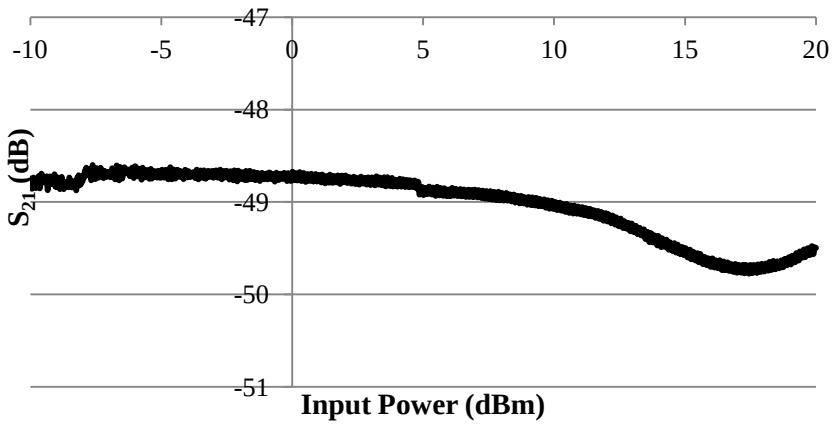

(a)

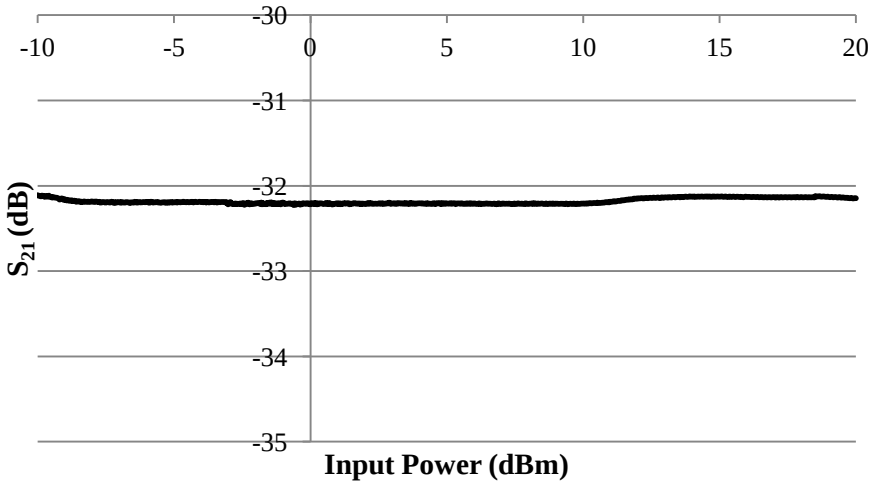

(b)

Figure 6.32: Transmission loss compression plot of reconfigurable PIFA with PIN diode (Gap, G_1 = 5 mm) in OFF state at; (a) 1.35 GHz (b) 1.85 GHz

6.3.3 Reconfigurable PIFA with ATF 54143 E-PHEMT Switch

The nonlinearity measurements conducted on the reconfigurable PIFA with ATF 54143 E-PHEMT switch are discussed in this section. It has been mentioned previously that the gap between the radiation planes of the antenna has to be increased to 5 mm to accommodate the bigger size of the transistor and biasing components.

6.3.3.1 E-PHEMT Switch in ON State

In the ON state of the E-PHEMT switch, the IMD3 products can be observed significantly at 1.85 GHz. Hence, all the measurements were performed at this particular frequency in the ON state.

6.3.3.1.1 Measurement of IMD3 Products

The measured IMD3 products of the reconfigurable PIFA with fundamental tones at 1.85 GHz across the radiation angles from -90° to 90° are displayed in Figure 6.33. From the figure, the IMD suppression is approximately 26 dBc in the direction of maximum radiation as compared to 43 dBc suppression of the previous reconfigurable PIFA with PIN diode (Gap, G_1 = 5 mm). In addition, the IMD3 products are larger across the angles of radiation. These indicate that the antenna behaves in a more nonlinear manner. The ratio of the IMD3 products to carrier can be seen in Figure 6.34. From the figure, the ratios are stable from -50° to 60° radiation angles.

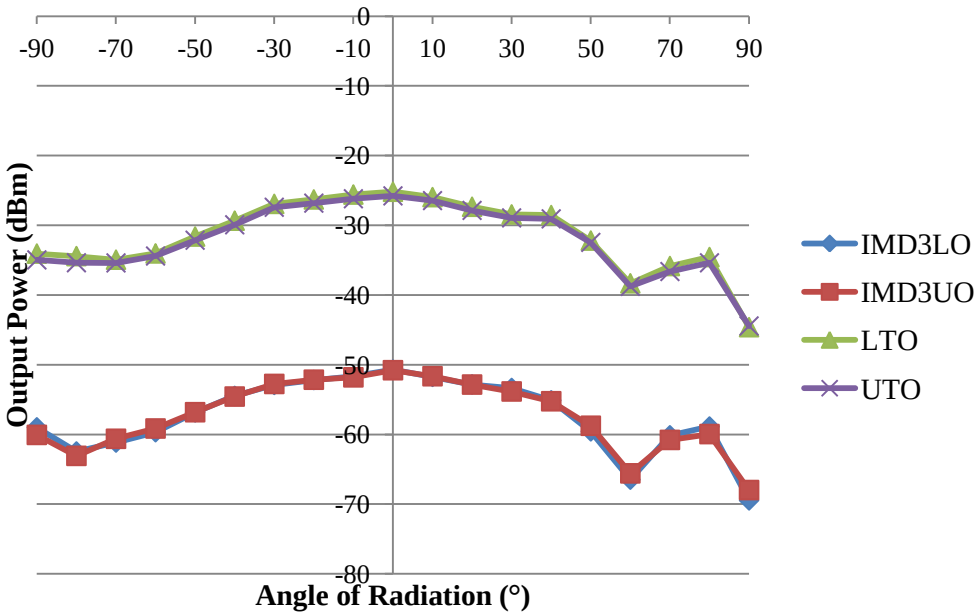

Figure 6.33: Transmitted IMD3 products of reconfigurable PIFA with E-PHEMT switch in ON state at 1.85 GHz

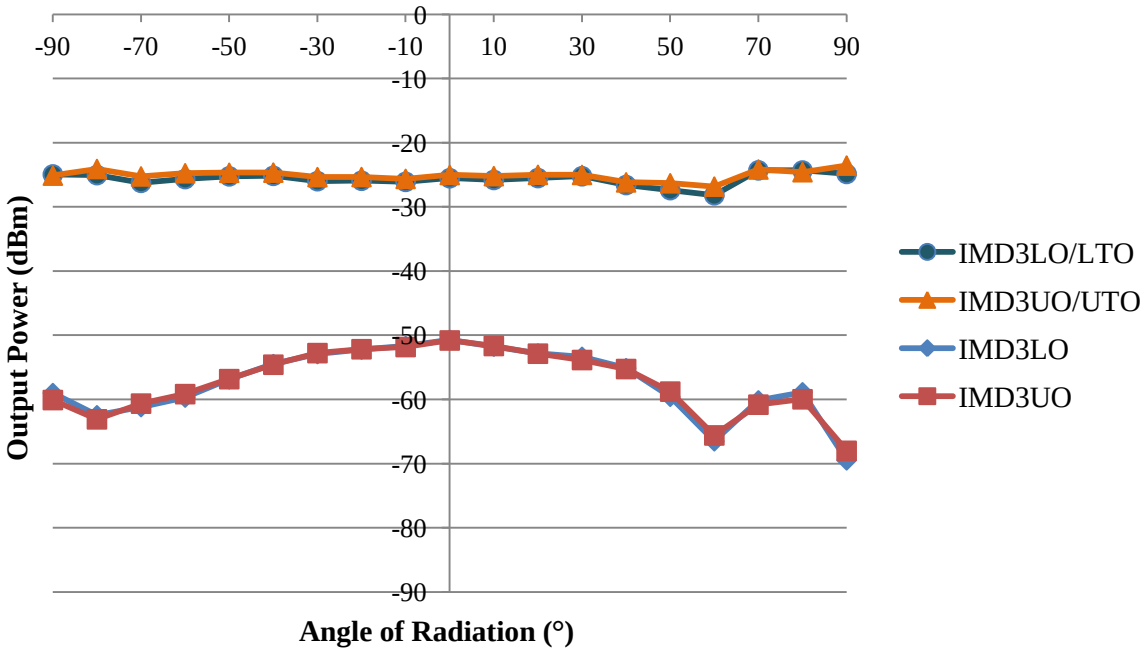

Figure 6.34: Ratio of IMD3 products to carrier of reconfigurable PIFA with E-PHEMT switch in ON state at 1.85 GHz

6.3.3.1.2 Measurement of IMD3 Products Asymmetry

The IMD3 products asymmetry of the antenna is shown Figure 6.35. From the figure, the variations across the angles of radiation are fairly small. Thus, the reconfigurable PIFA with E-PHEMT switch is almost memoryless, similar to the reconfigurable PIFA with PIN diode.

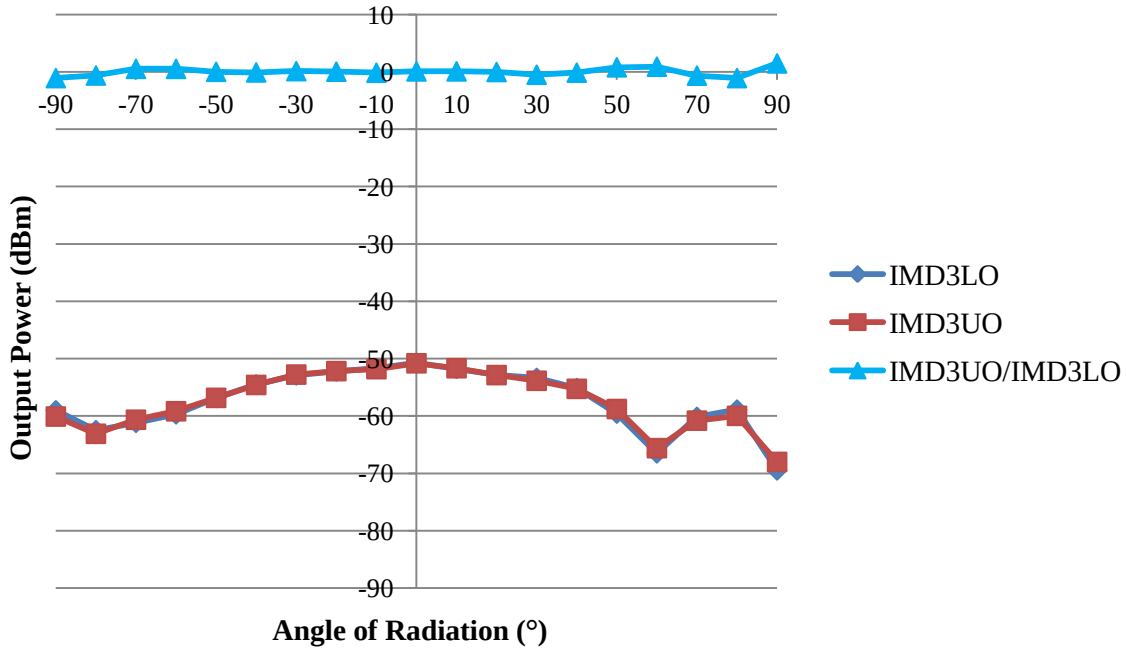

Figure 6.35: IMD3 products asymmetry of reconfigurable PIFA with E-PHEMT switch in ON state at 1.85 GHz

6.3.3.1.3 Measurement of IIP3

The IIP3 of the antenna in the ON state of the E-PHEMT switch can be viewed in Figure 6.36. From the figure, the IIP3 in the lower and upper tones is approximately 32 dBm which is lower than the IIP3 of the reconfigurable PIFA with PIN diode at 42 dBm. This further confirms that the antenna with E-PHEMT switch is more nonlinear.

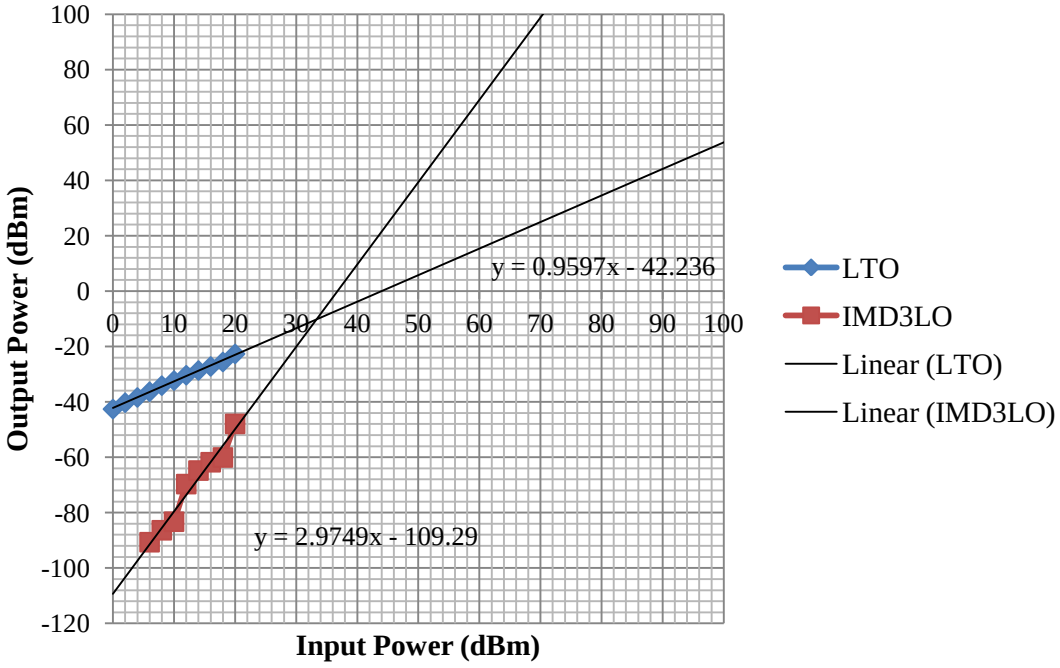

(a)

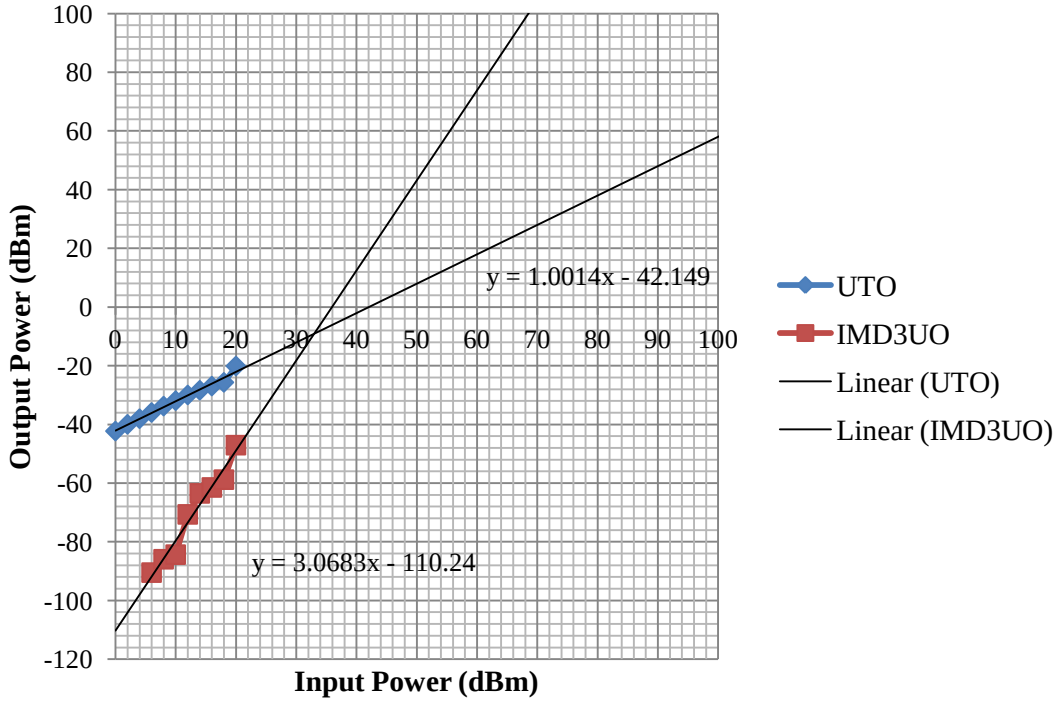

(b)

Figure 6.36: IIP3 of reconfigurable PIFA with E-PHEMT switch in ON state at 1.85 GHz for; (a) Fundamental and lower tones (b) Fundamental and upper tones

6.3.3.1.4 Measurement of $P_{1\text{-}dB}$

The IMD3 products suppression and IIP3 of the antenna shows that it is more nonlinear than the antenna with PIN diode. $P_{1\text{-}dB}$ is another measure of nonlinearity that will further clarify to the statement. The plot to locate the gain compression is shown in Figure 6.37. From the figure, the $P_{1\text{-}dB}$ is approximately 19 dBm. On the contrary, the $P_{1\text{-}dB}$ of the reconfigurable PIFA with PIN diode in the ON state could not be measured since it is located outside the range of input power. From the measured IIP3 value of 32 dBm, the gain compression is predicted to occur at 22 dBm which is at close approximation to the measured 19 dBm gain compression.

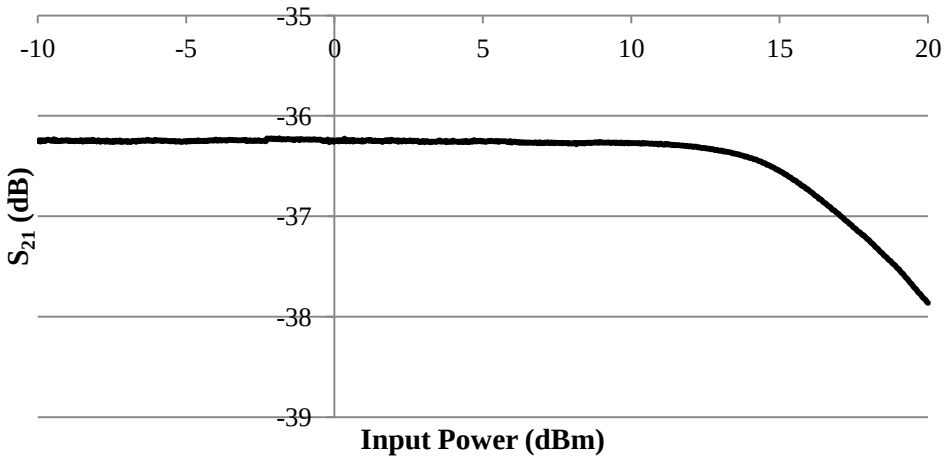

Figure 6.37: Transmission loss compression plot of reconfigurable PIFA with E-PHEMT switch in ON state at 1.85 GHz

6.3.3.2 E-PHEMT Switch in OFF State

The nonlinearity measurements in the OFF state were also conducted at 1.85 GHz since there is no new resonance resurfaced before the first resonant frequency unlike the reconfigurable PIFAs with PIN diodes.

6.3.3.2.1 Measurement of IMD3 Products

The IMD3 products of the antenna can be viewed in Figure 6.38. From the figure, the IMD3 products suppression in the direction of maximum radiation is approximately 26 dBc which is similar to the suppression in the ON state. However, the higher IMD3 products imply that the antenna is more nonlinear in the OFF state of the switch. The ratio of the IMD3 products to carrier is plotted in Figure 6.39. The ratios are fairly stable from -50° to 50° angles of radiation.

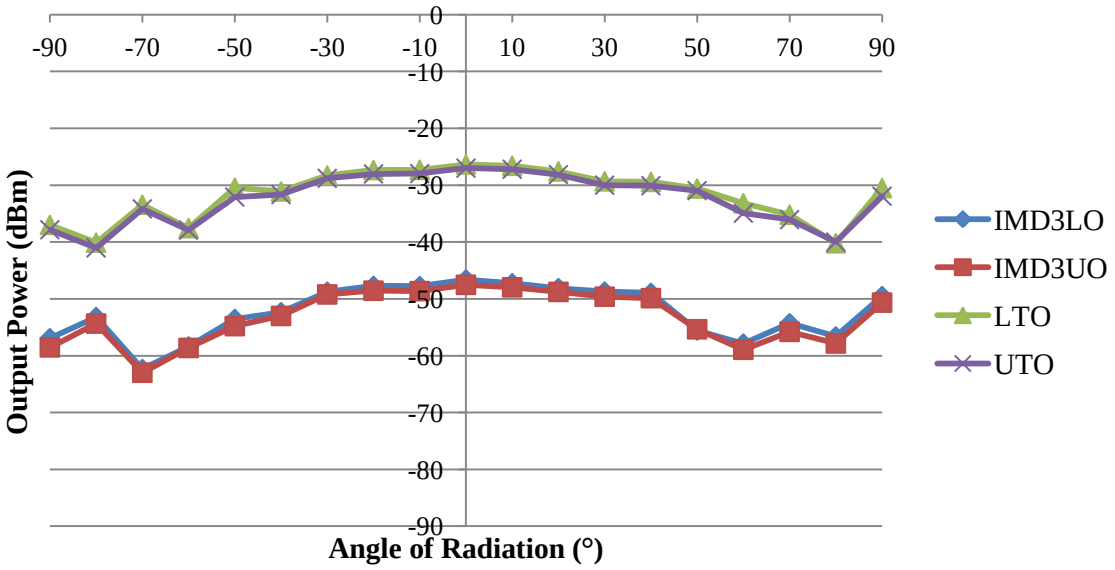

Figure 6.38: Transmitted IMD3 products of reconfigurable PIFA with E-PHEMT switch in OFF state at 1.85 GHz

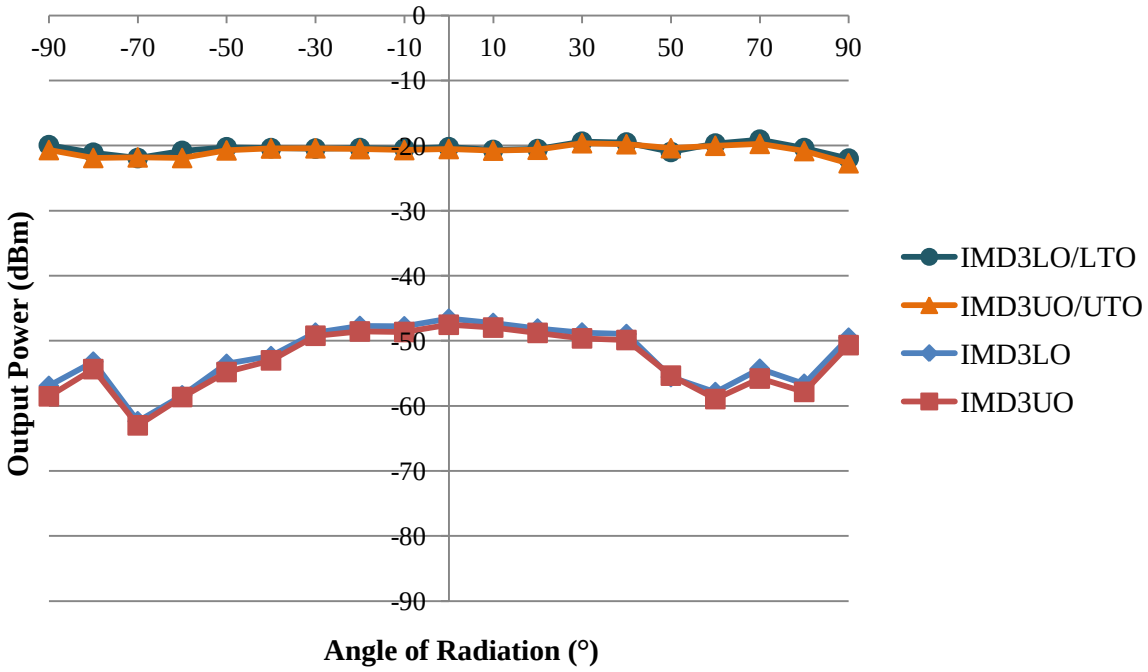

Figure 6.39: Ratio of IMD3 products to carrier of reconfigurable PIFA with E-PHEMT switch in OFF state at 1.85 GHz

6.3.3.2.2 Measurement of IMD3 Products Asymmetry

The IMD3 products asymmetry of the antenna shown in Figure 6.40 confirms that it is almost memoryless. Thus, the antenna may not require more complicated and expensive devices to linearize the output signals.

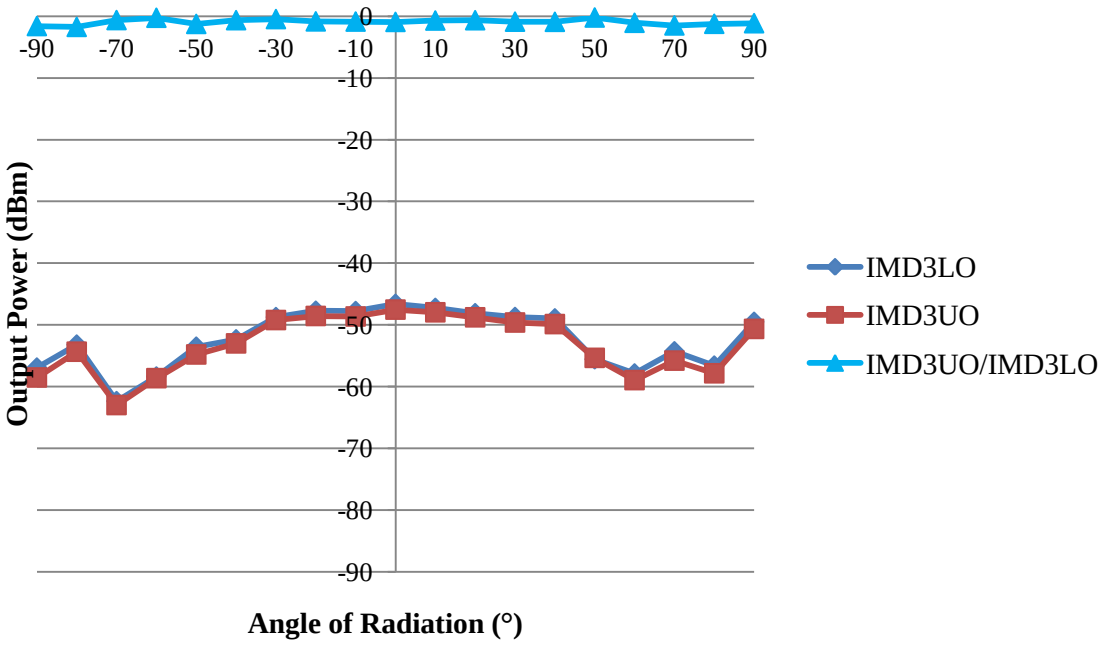

Figure 6.40: IMD3 products asymmetry of reconfigurable PIFA with E-PHEMT switch in OFF state at 1.85 GHz

6.3.3.2.3 Measurement of IIP3

The location of the IIP3 for the antenna in the OFF state can be viewed in Figure 6.41. From the figures, the IIP3 is located at 31 dBm in both lower and upper tones which is slightly lower than the IIP3 in the ON state.

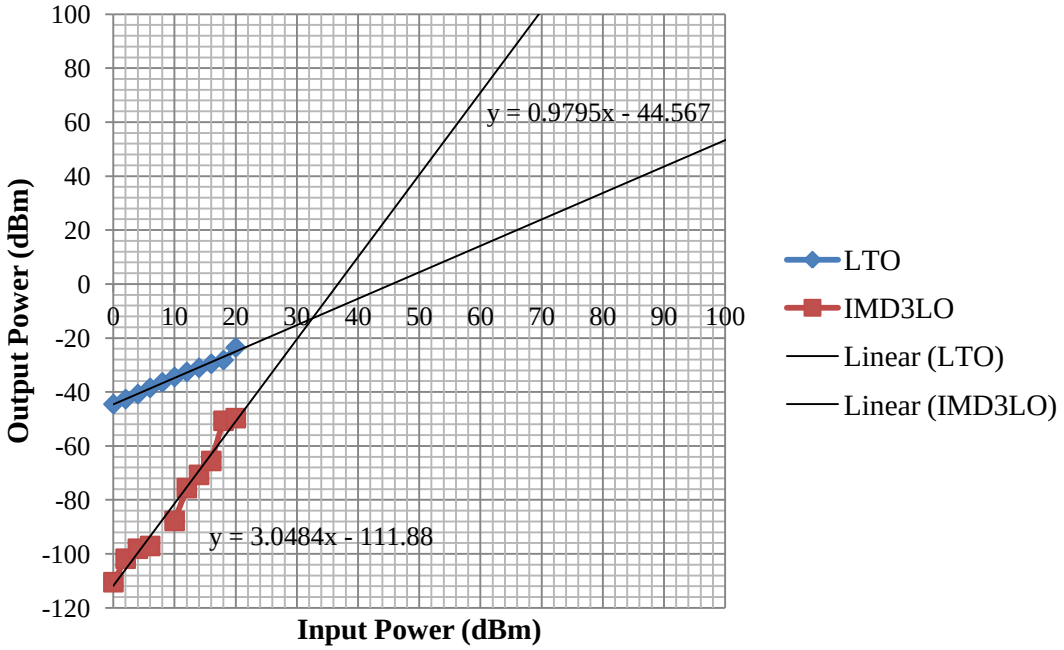

(a)

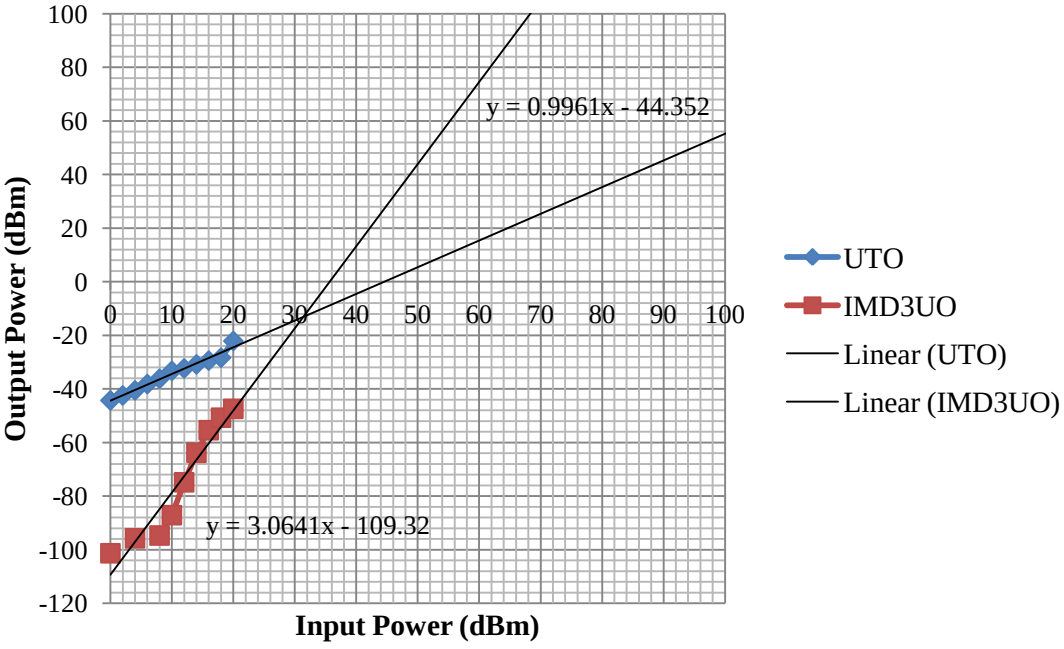

(b)

Figure 6.41: IIP3 of reconfigurable PIFA with E-PHEMT switch in OFF state at 1.85 GHz for; (a) Fundamental and lower tones (b) Fundamental and upper tones

6.3.3.2.4 Measurement of $P_{1\text{-}dB}$

The measured $P_{1\text{-}dB}$ of the reconfigurable PIFA when the E-PHEMT switch is in the OFF state can be seen in Figure 6.42. From the figure, the gain compression is located at 17 dBm which is lower than the gain compression in the ON state at 19 dBm. Again, this suggests that the antenna is more nonlinear in the OFF state of the E-PHEMT switch.

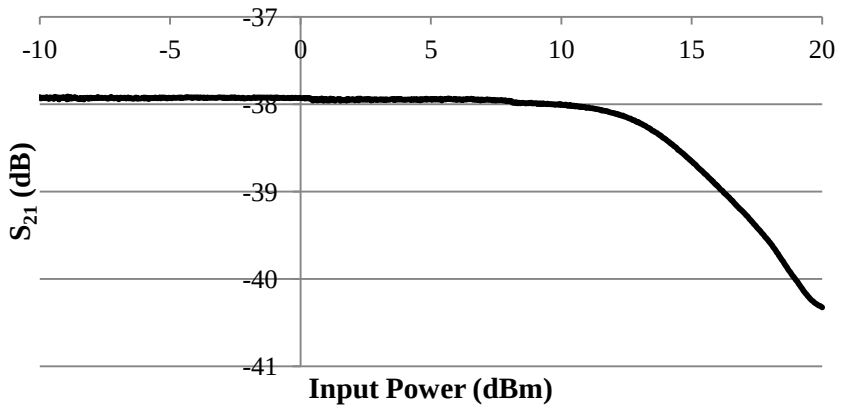

Figure 6.42: Transmission loss compression plot of reconfigurable PIFA with E-PHEMT switch in OFF state 1.85 GHz

6.4 Nonlinearity Measurements of PIFAs with Copper Bridges

The section discusses the nonlinearity measurements performed on the PIFAs with copper bridges. The copper bridge provides a linear interconnection and thus, it was chosen to replace the active switches for a highly linear substitute.

6.4.1 PIFA with a 2 × 1 mm^2 Copper Bridge

6.4.1.1 Measurement of IMD3 Products

The IMD3 products of the PIFA were measured using the similar manner as the previous antenna. Since a copper bridge was used to connect the radiating planes, it represents the ON state of the switch. Thus, the measurements were taken at 2 GHz based on the previous measurements performed on the reconfigurable PIFA with PIN diode (Gap, G_1 = 2 mm). Figure **6.43** shows the measured IMD3 products of the antenna at 2 GHz across the angles of radiation from -90° to 90°. From the figure, the IMD3 products fall below the noise floor of -80 dBm which shows that the antenna does not produce any IMD3 products. The IMD3 products suppression is also very high at approximately 65 dBc in the direction of maximum radiation. This suggests that the antenna is highly linear at the matched frequency of 2 GHz. Figure 6.44 shows the ratio of the transmitted IMD3 products to carrier. From the figure, the ratios are unreliable since almost all of the IMD3 products fall below the noise floor level.

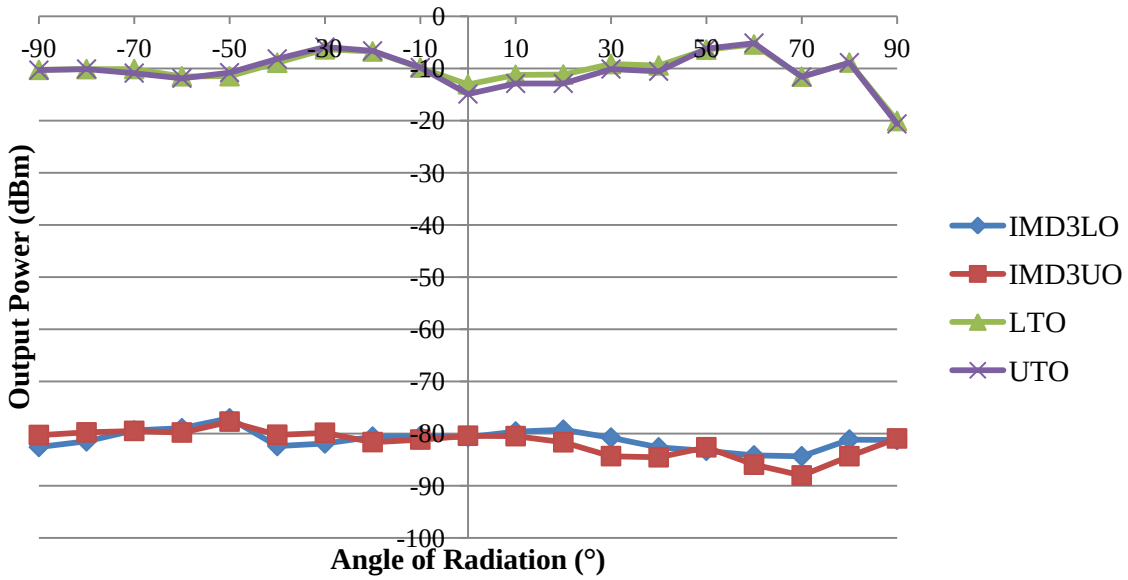

Figure 6.43: Transmitted IMD3 products of PIFA with 2 × 1 mm^2 copper bridge

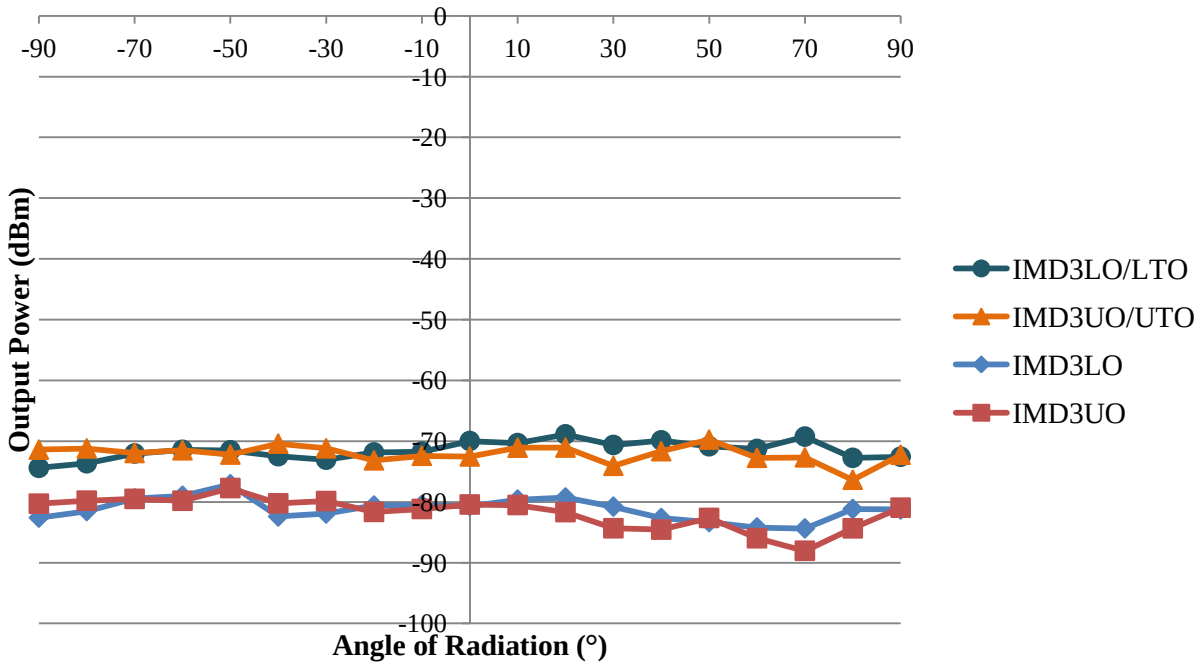

Figure 6.44: Ratio of IMD3 products to carrier of PIFA with 2 × 1 mm^2 copper bridge

6.4.1.2 *Measurement of IMD3 Products Asymmetry*

The IMD3 products asymmetry of the PIFA is shown in Figure 6.45. From the figure, the asymmetry of the antenna is fairly small with respect to 0 dB. Thus, the PIFA is almost memoryless at 2 GHz.

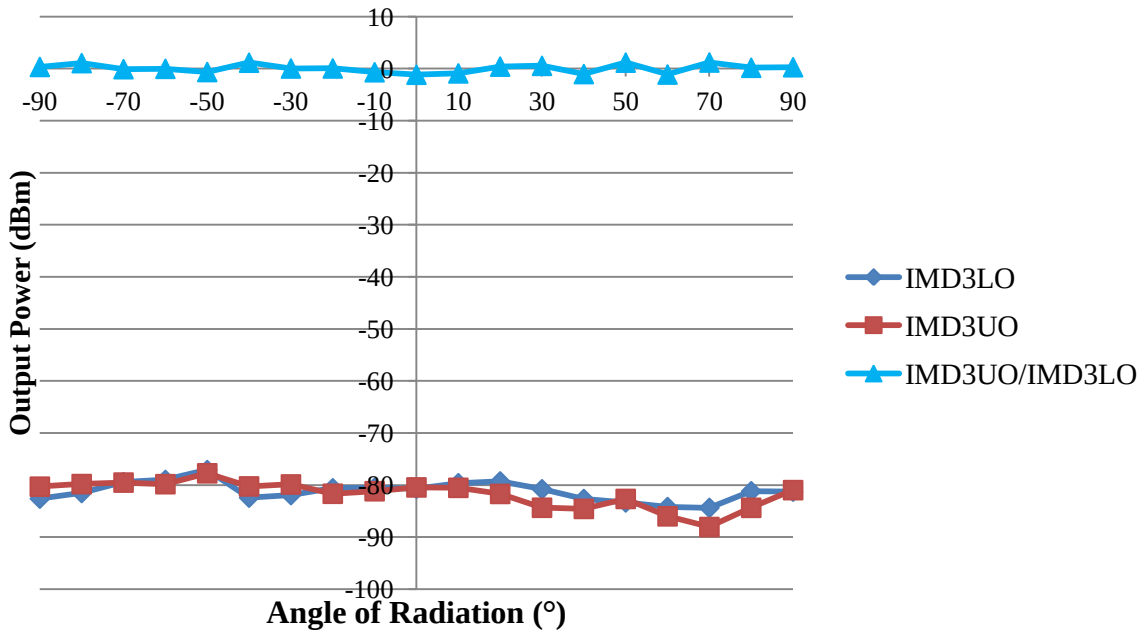

Figure 6.45: IMD3 products asymmetry of PIFA with 2 × 1 mm^2 copper bridge

6.4.1.3 *Measurement of IIP3*

The graph to locate the IIP3 of the PIFA at 2 GHz is plotted and can be viewed in Figure 6.46 for the lower and upper tones. From the figures, the IIP3 cannot be located since there is no point of saturation in the IMD3 products in the lower and upper tones. In addition, the linear regression line of the IMD3 products is not reliable to be constructed since the data are very noisy. This conveys an information that the antenna is highly linear at 2 GHz.

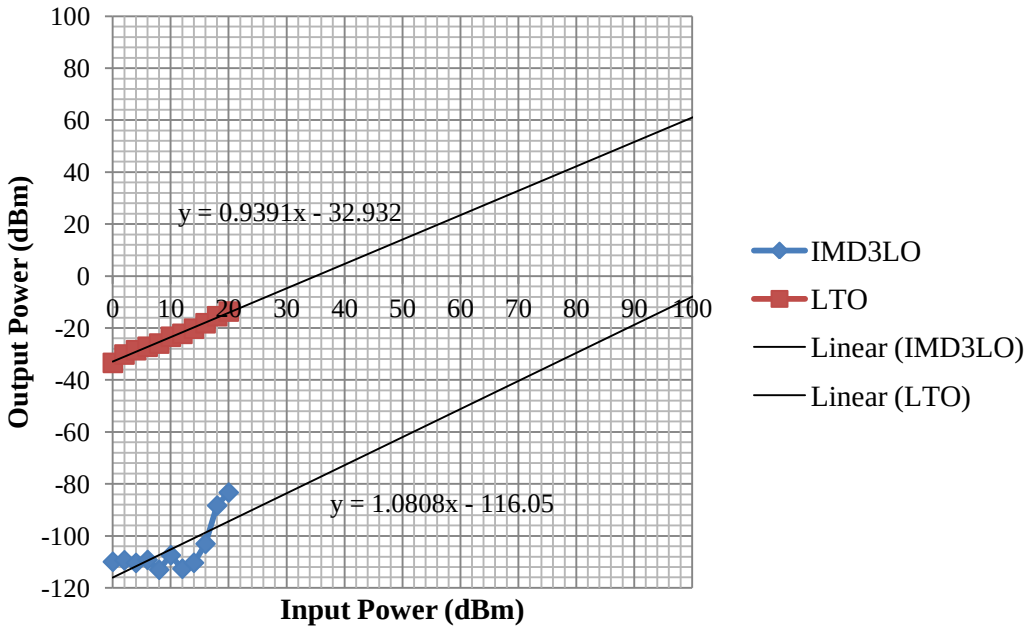

(a)

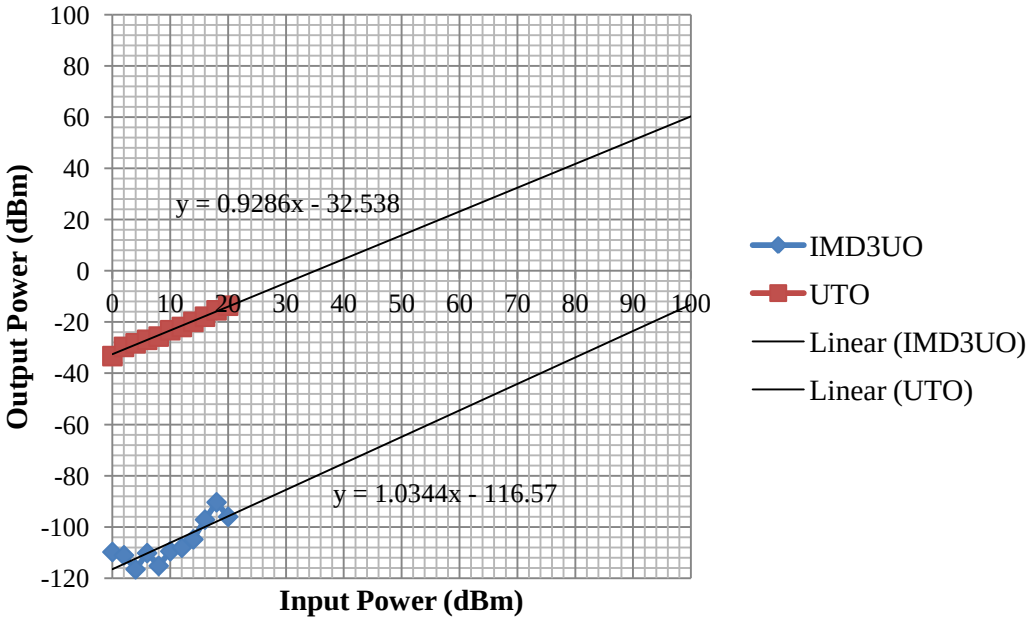

(b)

Figure 6.46: IIP3 of PIFA with 2 x 1 mm^2 copper bridge at 2 GHz for;
(a) Fundamental and lower tones (b) Fundamental and upper tones

6.4.1.4 Measurement of $P_{1\text{-}dB}$

The $P_{1\text{-}dB}$ measurement performed on the PIFA with copper bridge reveals that the point lies outside the range of the input power from -10 to 20 dBm and could not be measured as can be viewed in Figure 6.47. This demonstrates that the PIFA is highly linear.

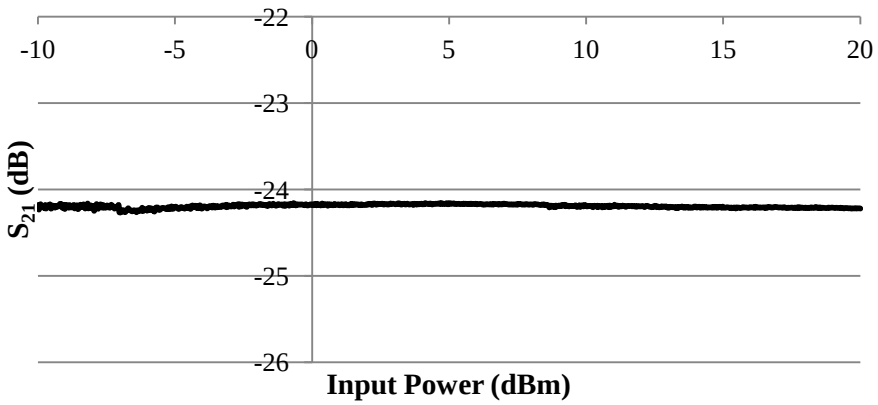

Figure 6.47: Transmission loss compression plot of PIFA with 2 x 1 mm^2 copper bridge at 2 GHz

6.4.2 PIFA with a 5 × 1 mm^2 Copper Bridge

6.4.2.1 Measurement of IMD3 Products

The IMD3 product measurements on the PIFA with 5 × 1 mm^2 copper bridge were taken at 1.85 GHz as previously mentioned. The measured transmitted IMD3 products of the antenna are displayed in Figure 6.48. The figure verifies that the IMD3 products of the lower and upper tones are well below the noise floor. In this case, the IMD3 products are located at approximately 69 dB below the fundamental tones. The high suppression implies that the antenna is highly

linear at 1.85 GHz. The ratio of the IMD3 products to carrier is plotted in Figure 6.49. However, the ratios are not reliable since all the IMD3 products are below the noise floor level.

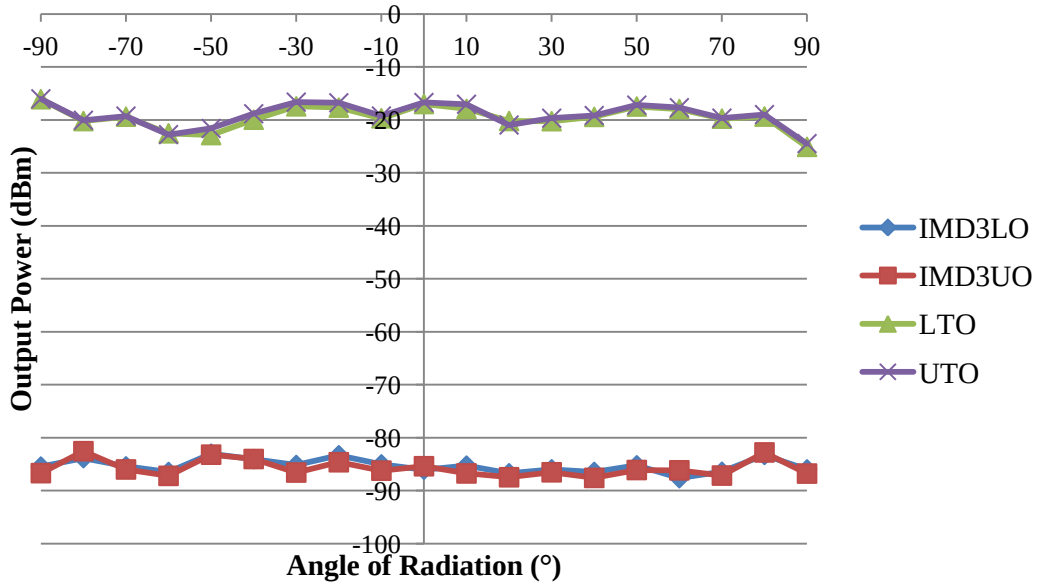

Figure 6.48: Transmitted IMD3 products of PIFA with 5 × 1 mm^2 copper bridge

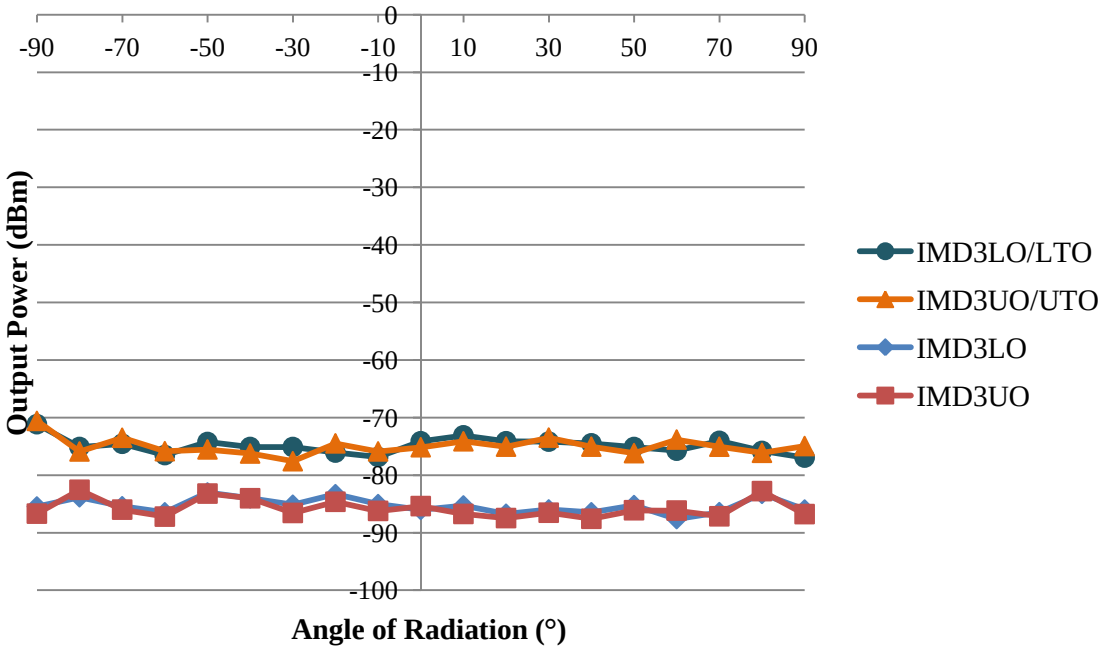

Figure 6.49: Ratio of IMD3 products to carrier of PIFA with 5 × 1 mm^2 copper bridge

6.4.2.2 Measurement of IMD3 Products Asymmetry

Figure 6.50 shows the IMD3 products asymmetry of the antenna. It can be clearly seen from the figure that the variations between the IMD3 products in the upper and lower tones are small which suggests that the antenna is almost memoryless at 1.85 GHz and may only require a simple predistortion technique to linearize the signals.

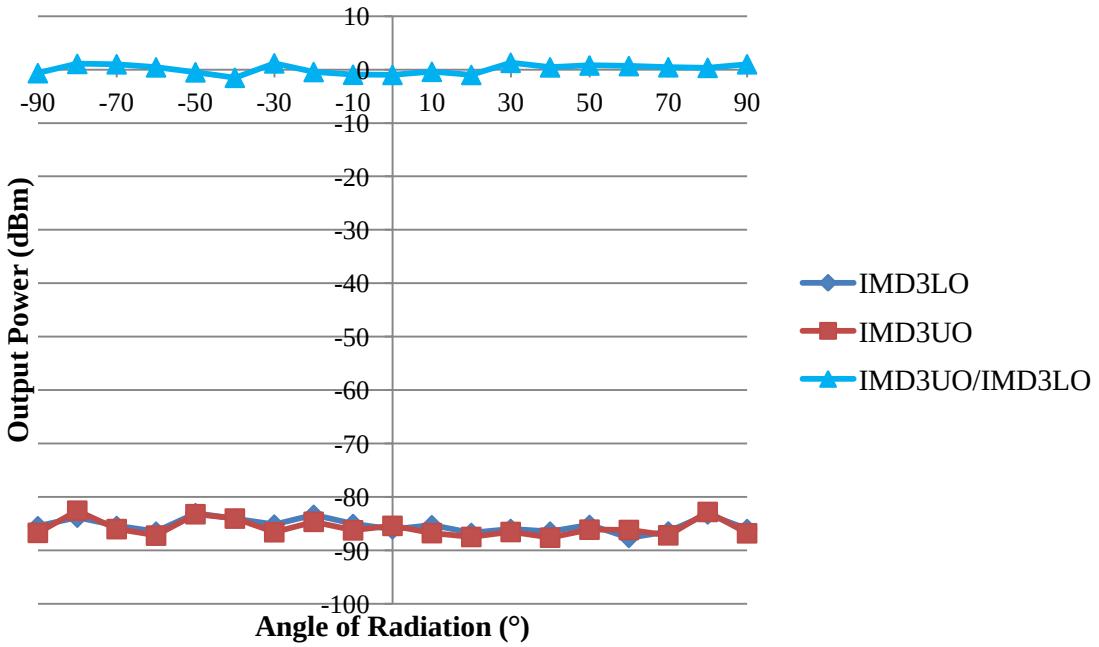

Figure 6.50: Intermodulation asymmetry of PIFA with 5 × 1 mm^2 copper bridge

6.4.2.3 Measurement of IIP3

The IIP3 measurement performed on the antenna revealed that the intercept point could not be located. Figure 6.51 shows the unreliable linear regression line of the IMD3 products that does not intersect with the regression line of the fundamentals in the lower and upper tones. Again, this reveals that the antenna is a highly linear substitute.

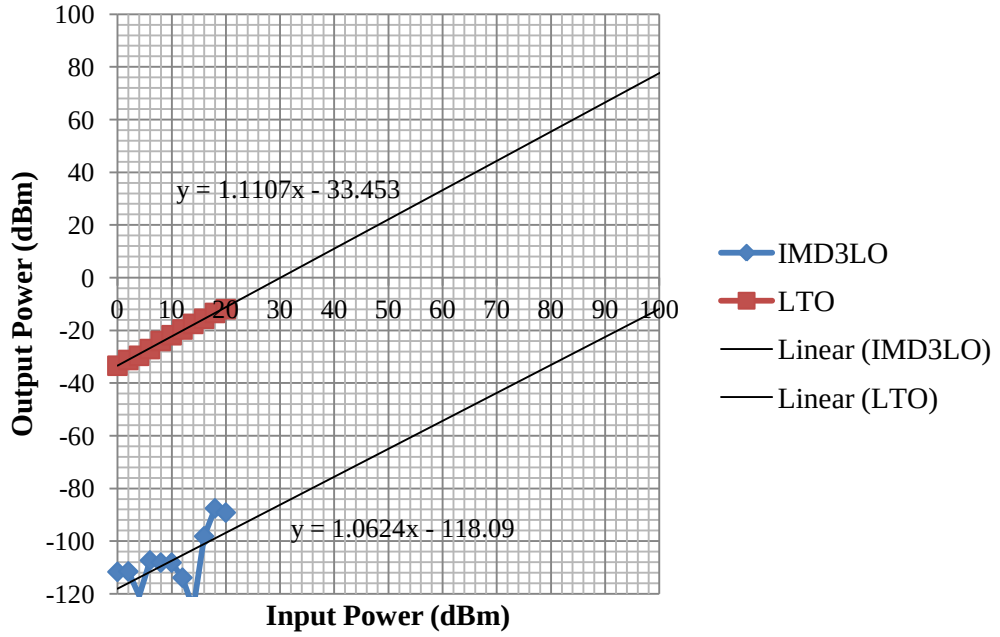

(a)

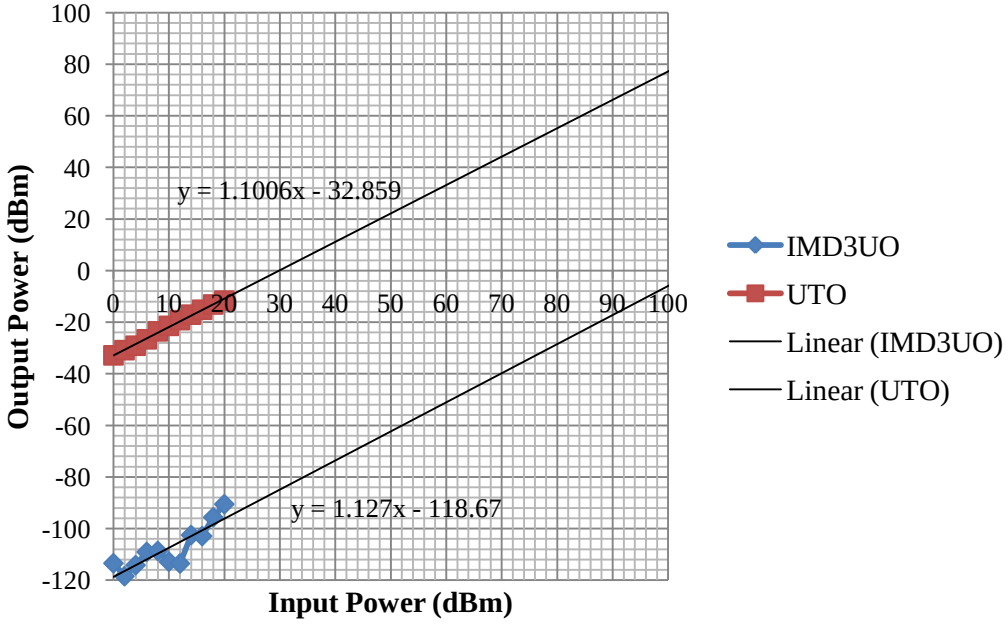

(b)

Figure 6.51: IIP3 of PIFA with 5 x 1 mm^2 copper bridge at 1.85 GHz for;
(a) Fundamental and lower tones (b) Fundamental and upper tones

6.4.2.4 Measurement of $P_{1\text{-}dB}$

The plot to measure the $P_{1\text{-}dB}$ of the antenna is shown in Figure 6.52. From the figure, the gain compression could not be located with similar behaviour observed in the previous PIFA. This implies that the antenna is highly linear as the gain compression lies outside the range of input power.

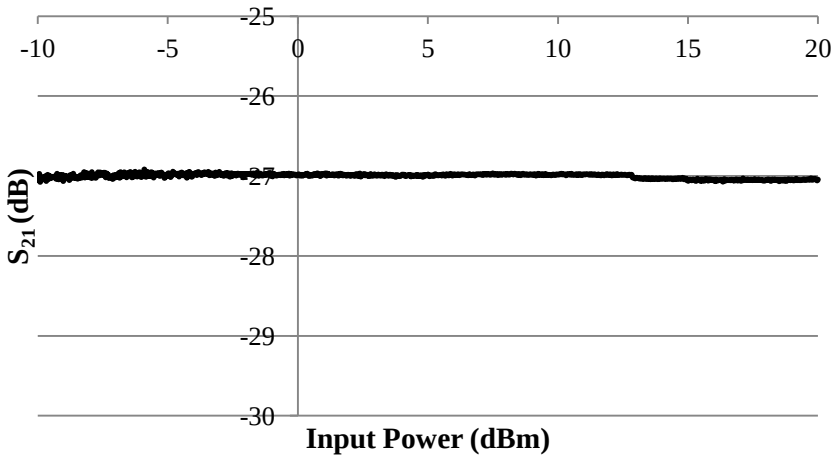

Figure 6.52: Transmission loss compression plot of PIFA with 5×1 mm^2 copper bridge at 1.85 GHz

6.5 Summary of Nonlinearity Measurement Results

Table 6.2 compares the results from the nonlinearity measurement performed on the antennas

Table 6.2: Comparison of nonlinearity measurement results

Antenna	**IIP3 (dBm)**	**$P_{1\text{-}dB}$ (dBm)**	Worst Case **IMD3UO / IMD3LO**	Largest **IMD3LO LTO** Variation with Angle of Radiation	Largest **IMD3UO UTO** Variation with Angle of Radiation
PIFA with 2×1 mm^2 Copper Bridge	-	> 20	Unreliable	Unreliable	Unreliable
PIFA with 5×1 mm^2 Copper Bridge	-	> 20	Unreliable	Unreliable	Unreliable
PIFA with PIN Diode (Gap = 2 mm) **ON State at 2 GHz**	44	> 20	1.89	2.38	2.17
PIFA with PIN Diode (Gap = 2 mm) **OFF State at 1.4 GHz**	27	17.7	1.39	2.8	2.78
PIFA with PIN Diode (Gap = 2 mm) **OFF State at 2 GHz**	44	> 20	1.95	1.92	2.68
PIFA with PIN Diode (Gap = 5 mm) **ON State at 1.85 GHz**	42	> 20	1.83	2.4	1.7
PIFA with PIN Diode (Gap = 5 mm) **OFF State at 1.35 GHz**	26	17.3	1.09	2.77	2.86

PIFA with PIN Diode (Gap = 5 mm) **OFF State at 1.85 GHz**	42	> 20	1.88	1.77	1.52
PIFA with E-PHEMT switch **ON State at 1.85 GHz**	33	19	1.07	2.23	2.18
PIFA with E-PHEMT switch **OFF State at 1.85 GHz**	32	17	1.03	1.89	2.27

6.6 Conclusion

The nonlinearity measurements on the reconfigurable PIFAs with active switches and the PIFAs with copper bridges for highly linear comparison were successfully conducted and discussed. A thorough understanding on the nonlinearity behaviour of the antennas has been developed and the analysis and discussion are presented. A few conclusions can be made from the findings which are listed below:

i. The presence of active switches in the reconfigurable antennas has introduced some degree of nonlinearity in the first resonant frequency regardless of the state of the switch. An interesting finding was discovered in the OFF state of the PIN diode in both antennas (Gap, G_1 = 2 and 5 mm) where the source of IMD3 products was the strongest at the new resonance (attributed to the bias inductor) at 1.34 and 1.4 GHz. From the analysis, the nonlinearity is badly compromised at these particular frequencies.

However, at the first resonant frequency (1.85 and 2 GHz), the antennas behave in a highly linear manner which is evident from the high values of IIP3 and the gain compression.

ii. The reconfigurable PIFA with E-PHEMT switch is more nonlinear than its PIN diode counterpart. This is evident from the larger IMD3 products generated in the ON and OFF states of the antenna. Furthermore, when comparing the nonlinearity between both states, the OFF state of the switch generates greater nonlinearity behaviour than the ON state. This can be explained from the fact that in a typical microwave FET/HEMT, the effect of nonlinearity associated with the voltage-dependent Gate and Drain capacitance values is considerably larger than that associated with the reverse Schottky leakage current in the ON state [104]. Due to the fact that the IMD3 products are only 26 dB down as compared to the carriers, it is unlikely that the E-PHEMT-based switching antenna will be usable in the CR communication systems.

iii. In configurations for which $P_{1\text{-dB}}$ and IIP3 can be measured with reasonable accuracy, the expectation of a 10.6 dB difference between these measures is approximately met. This is valuable information, because it provides a practical way of putting an upper bound on active antenna IMD3 products level without complex measurements.

iv. IMD3 suppression was found to be almost independent of angle, within the measurement accuracy limits, for the reconfigurable antennas tested in this work.

v. The fabricated antennas in this work can be considered almost memoryless since only small variations were detected between the upper and lower IMD3 products from the

plots. Therefore, the antennas may not require more complicated and expensive devices for linearization [105].

vi. The PIFAs with copper bridges as highly linear substitutes have served as a good reference. From the analysis, these antennas have several characteristics which demonstrate their high linearity performance:

(a) The IMD3 products at the first resonant frequency are below the noise floor at -80 dBm across all radiation angles from -90° to 90°.

(b) The IMD suppression is very high, greater than 65 dBc.

(c) The IIP3 could not be located since the intersection point between the linear regression lines of the fundamental tones (1:1 slope) and IMD3 products (3:1 slope) could not be constructed reliably from very noisy data.

(d) The $P_{1\text{-}dB}$ could not be measured since the compression point lies outside the range of input power from -10 to 20 dBm.

vii. The nonlinear measurements have shown that as expected, the copper bridge-based antenna generates the lowest IMD3 products followed by the PIN diode version. The E-PHEMT switch antenna gives the worst IMD characteristics of the three.

CHAPTER 7

7. CONCLUSION AND FUTURE WORKS

7.1 Conclusion

In this work, the nonlinearity issue faced by the reconfigurable antennas with active switches were comprehensively studied and investigated. In order to do so, three reconfigurable PIFAs with active switches were proposed as the platforms to perform nonlinearity measurements. A PIFA was chosen as the best candidate due to its popularity in the mobile communication handsets. Two active switches, namely BAR50-02V PIN diode and ATF 54143 E-PHEMT were selected for frequency reconfigurations. These switches consume little power, have good isolation and low insertion loss. However, they suffer from poor linearity performances. For comparison purposes, two reference PIFAs with copper bridges as linear interconnections were proposed. Table **7.1** summarizes the proposed antennas for nonlinearity measurements. From the table, the differences in the Gap, G_1 connecting the main and the additional planes are necessary to accommodate the variation in the sizes of the active switch.

Table 7.1: Proposed reconfigurable PIFAs in this work

Reconfigurable PIFA	PIFA (Reference Antenna)
Reconfigurable PIFA with PIN diode (Gap, G_1 = 2 mm)	PIFA with 2 × 1 mm^2 copper bridge
Reconfigurable PIFA with PIN diode (Gap, G_1 = 5 mm)	PIFA with 5 × 1 mm^2 copper bridge
Reconfigurable PIFA with E-PHEMT switch (Gap, G_1 = 5 mm)	-

The reconfigurable PIFA is capable to produce two distinct resonant frequencies in each state of the active switch. The first resonant frequency remains similar in both states of the switch while the second resonant frequency is being switched from the upper to the lower resonant frequency or vice versa, depending on the state of the switch. The switching property of the PIN diode has enabled a considerable switching frequency in the upper and lower resonant frequencies. In the reconfigurable PIFA with PIN diode (Gap, G_1 = 2 mm) for instance, the second resonant frequency is switched to 3.67 GHz in the ON state from 5.16 GHz in the OFF state. On the contrary, the switching capability of the E-PHEMT switch is still within a good range with a difference of only 680 MHz (from 4.06 to 3.38 GHz). A logical explanation can be made from the S_{11} and S_{21} graphs of the switch where the low isolation in the upper frequency range of the OFF state might be a contributing factor.

A set of nonlinearity measurements were conducted on these antennas and the results and analysis are presented. The measurements were performed on the ZVA67 R&S VNA which has the capability to perform the nonlinearity measurements with only a power combiner as an external device. However, alternative experimental setups may be useful if the VNA is not available. From the measurements, the conclusion can be made based on the antennas tested in this work:

i. Reconfigurable PIFAs with PIN diode (Gap, G_1 = 2 mm)

In this antenna, the IMD3 products are significant at 2 GHz in the ON state. In the OFF state, two significant IMD3 products can be located at 1.4 and 2 GHz with the strongest being at 1.4 GHz. From the reflection coefficient graph, the 1.4 GHz was caused by the bias inductor and the 2 GHz

is the first resonant frequency of the antenna in both states of the PIN diode. However, from the measurements of IIP3 and $P_{1\text{-}dB}$, the antenna is very linear at 2 GHz. On the other hand, the nonlinearity is greatly affected at 1.4 GHz.

ii. Reconfigurable PIFAs with PIN diode (Gap, G_1 = 5 mm)

The width of the gap in this antenna is increased to 5 mm for comparison with the reconfigurable PIFA with E-PHEMT switch. From nonlinearity point of view, similar behaviour is observed in this antenna. In the ON state, the IMD3 products are very significant at 1.85 GHz while in the OFF state, strong IMD3 products can be detected at 1.35 and 1.85 GHz. Based on the nonlinearity investigation, the antenna behaves linearly at 1.85 GHz and nonlinearly at 1.35 GHz.

iii. Reconfigurable PIFA with E-PHEMT switch

The use of ATF 54143 E-PHEMT to reconfigure the frequencies of PIFA in this work is the first to be reported in the literature. The bigger size of the transistor and its biasing components has made it necessary for the gap between the radiating planes to be increased to 5 mm. From the reflection coefficient graph, there was no appearance of new resonance within the range of operating frequency from 1 to 6 GHz. Thus, significant IMD3 products can be located at 1.85 GHz in the ON and OFF states of the switch. From the nonlinearity measurements conducted, it reveals that the antenna with E-PHEMT switch is more nonlinear than the antenna with PIN diode. Furthermore, the nonlinearity behaviour is more prominent in the OFF state of the switch as compared to the ON state.

iv. PIFA with 2×1 mm^2 copper bridge

This antenna employs a copper bridge as a highly linear interconnection to replace the active switches. From the nonlinearity measurements, the IMD3 products are below the noise floor at -80 dBm, implying that the antenna is very linear at 2 GHz. The IIP3 and $P_{1\text{-dB}}$ measurements also demonstrate that the antenna behaves linearly.

v. PIFA with 5×1 mm^2 copper bridge

The same conclusion can be made with this antenna as the linear behaviour is very similar to the previous reference antenna.

Furthermore, two significant findings are discovered from the nonlinearity measurements which are listed below:

i. Based on the power-series-based approximation, the 10 dB difference between the measured $P_{1\text{-dB}}$ and IIP3 is shown to be reasonable.

ii. The ratio of the IMD3 products to carrier is shown to be almost independent of radiation angles.

7.2 Future Works

Based on the reflection coefficient graphs of the reconfigurable PIFAs, the comparison with the simulation and measurement results reflects a very good agreement in the ON state. Although the comparison in the OFF state shows a reasonable comparison, the appearance of a new resonance at 1.4 GHz (reconfigurable PIFA with PIN diode) and spurious resonances (reconfigurable PIFA

with E-PHEMT switch) are questionable. Further investigations disclosed that the source of interference came from the bias chip inductor of the biasing circuit. Interestingly, the nonlinearity measurements conducted on the antennas revealed that the IMD3 products were more pronounced at that new resonance. Given that finding in this work, it is recommended that an alternative component should replace the bias inductor for future works where the linearity is a critical requirement.

The nonlinearity measurements were performed on the reconfigurable PIFA as the main platform with only one active switch introduced to the radiating structure. This is due to the small dimensions of the antenna. However, in the real world, an active antenna should be able to support multiple frequency bands to cater for the increasing demand of wireless applications. Thus, instead of using a single switch, more switches should be introduced to investigate their nonlinearity effects on the performance of the antenna. In addition, the measurements could be extended to other types of antenna to study the variations of nonlinearity behaviour among different antenna structures.

The reference antenna used in this work is the PIFA with a copper bridge. The copper bridge in this case serves as a linear interconnection and is highly linear. Alternatively, an active switch of a superior linearity performance could also be employed to reconfigure the antenna and at the same time became the reference antenna. RF MEMS switches are well-known for their excellent linearity performance and therefore, result in very low IMD products in the switching and tuning operations although the high cost and intricate fabrication procedures will become the impeding factors. Furthermore, a typical RF MEMS switch requires a voltage up converter between 30 – 90 V for its electrostatic actuation.

Extensive nonlinearity measurements were performed on the reconfigurable antennas in this work which can be verified from the number of crucial measurements conducted and the amount of data gathered. The laborious process in gathering the required data to present the study in a systematic approach was made possible by the high-end ZVA67 Rohde & Schwarz VNA. Conversely, due to the limitations of the anechoic chamber equipment, the measurements of IMD3 products radiation patterns with respect to the fundamentals could not be executed. Therefore, this type of measurement is suggested for future work.

Approximate radiation patterns were measured in the near-field region and the results suggested no significant variation of the IMD3 products to carrier ratio with angle. In future work, a more sensitive receiver should be developed to allow true far-field IMD3 product measurements.

Furthermore, the nonlinearity measurements were conducted when the antenna is transmitting signals (transmit mode). However, other than being radiated, the IMD3 products generated in the reconfigurable antennas may be reflected back through the feed network. Unlike radiated IMD products, the reflected IMD3 products do not experience free space losses. Thus, they could be larger in magnitudes which will degrade the overall antenna system performance and could not be neglected. Further work might reveal an interesting finding on the reflected IMD3 products in the reconfigurable antennas.

APPENDICES

Appendix A:

Datasheet of BAR50-02V PIN diode from Infineon Technologies

Appendix B:

Datasheet of ATF 54143 E-PHEMT from Avago Technologies

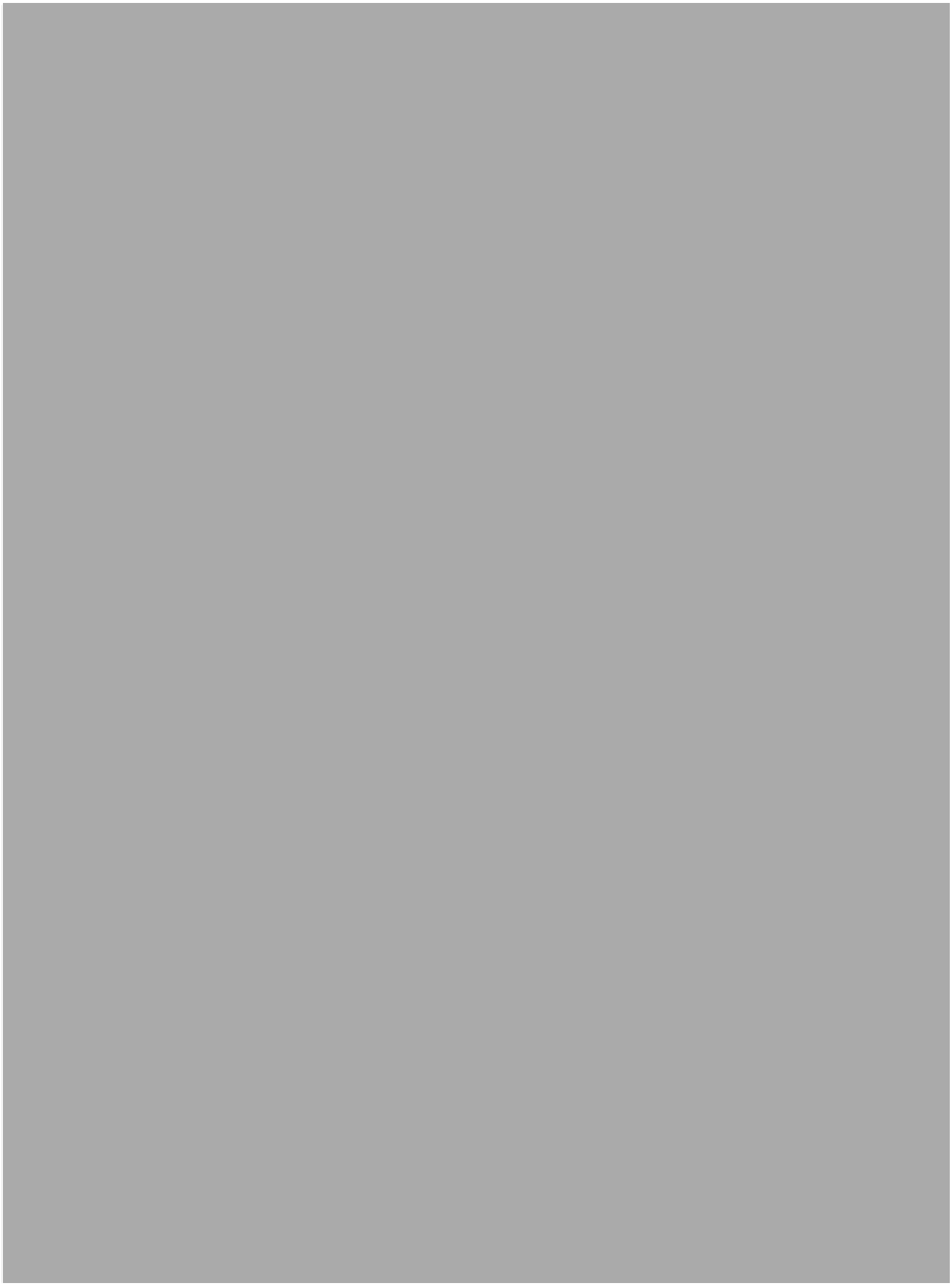

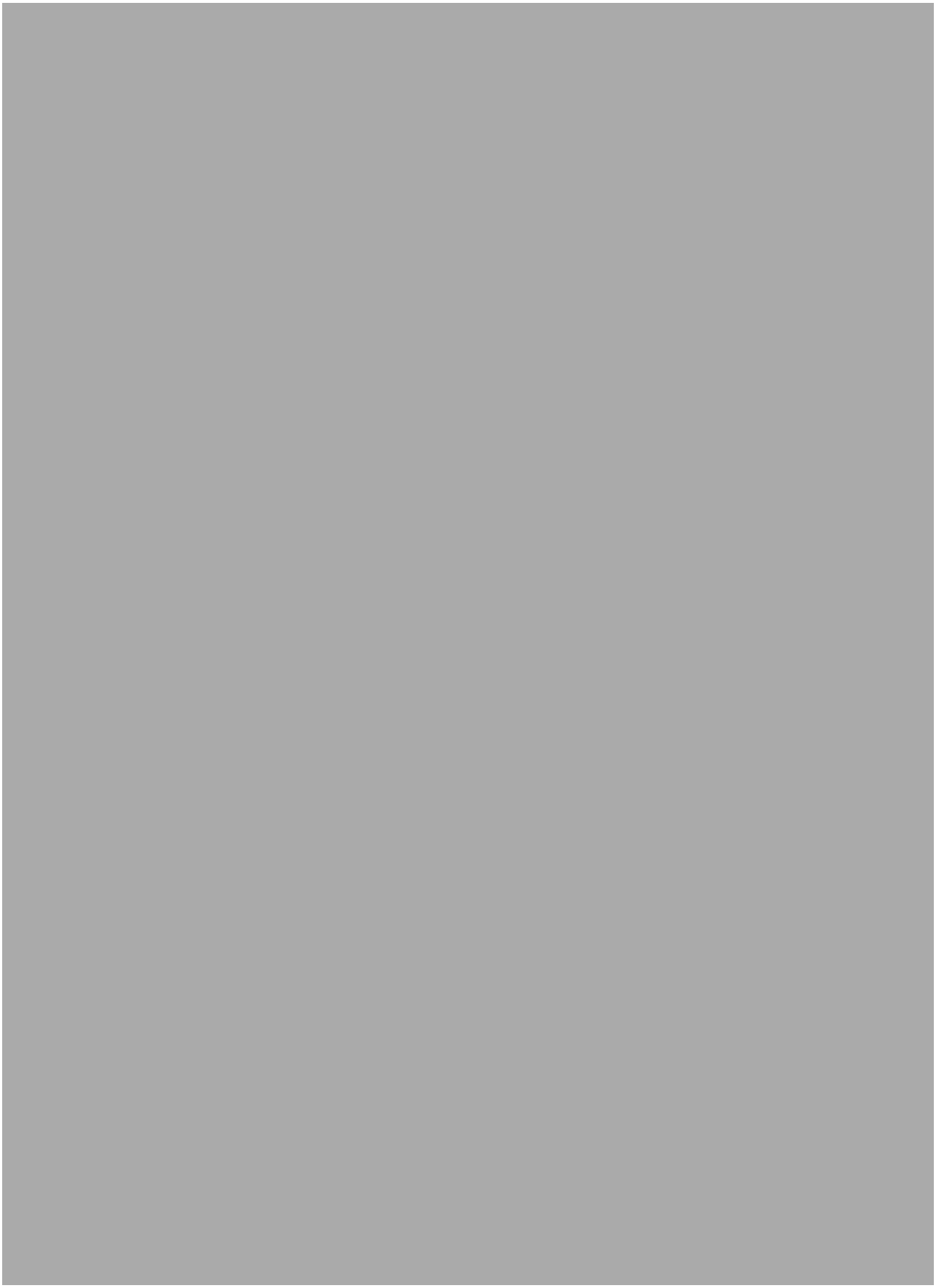

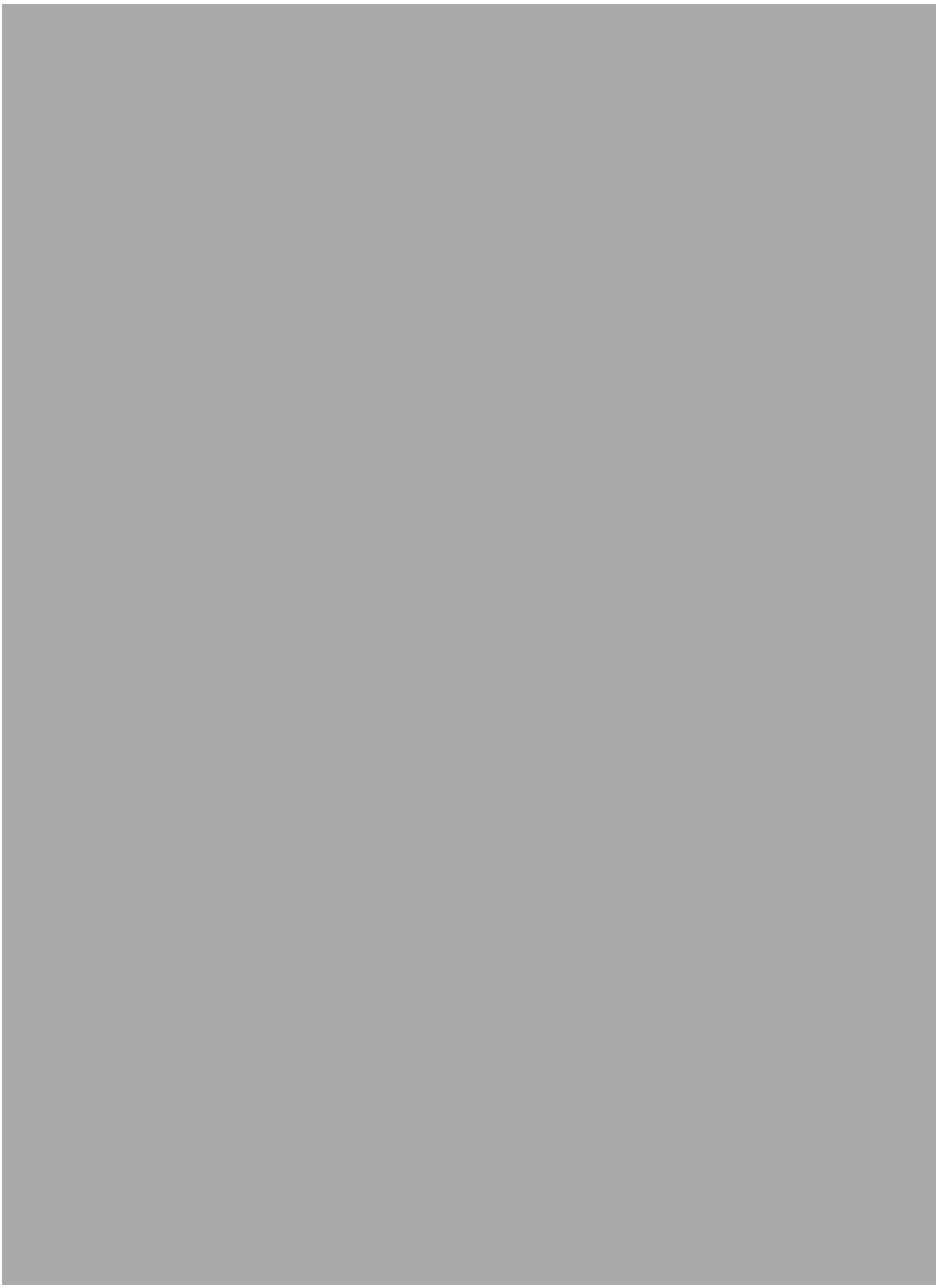

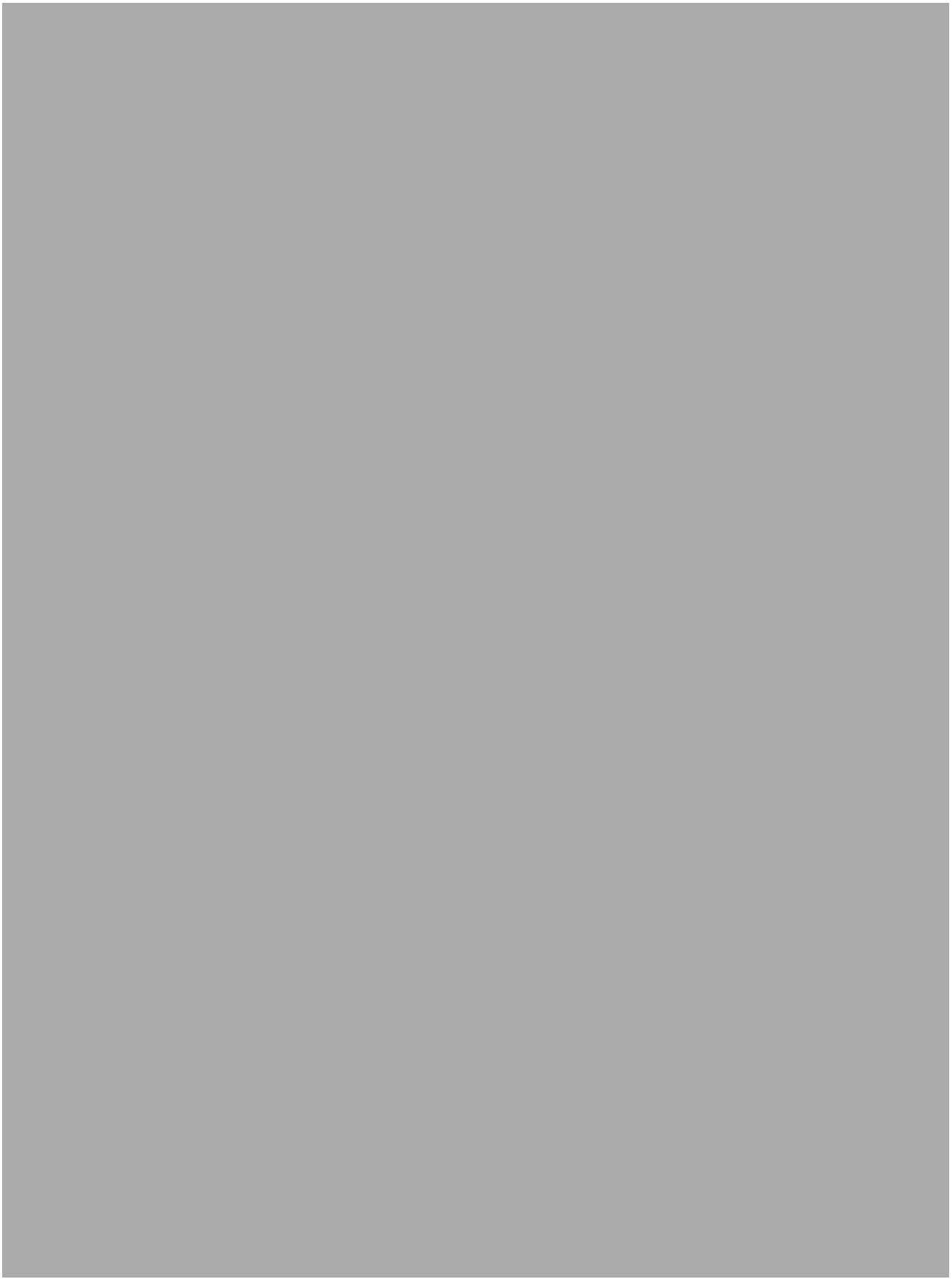

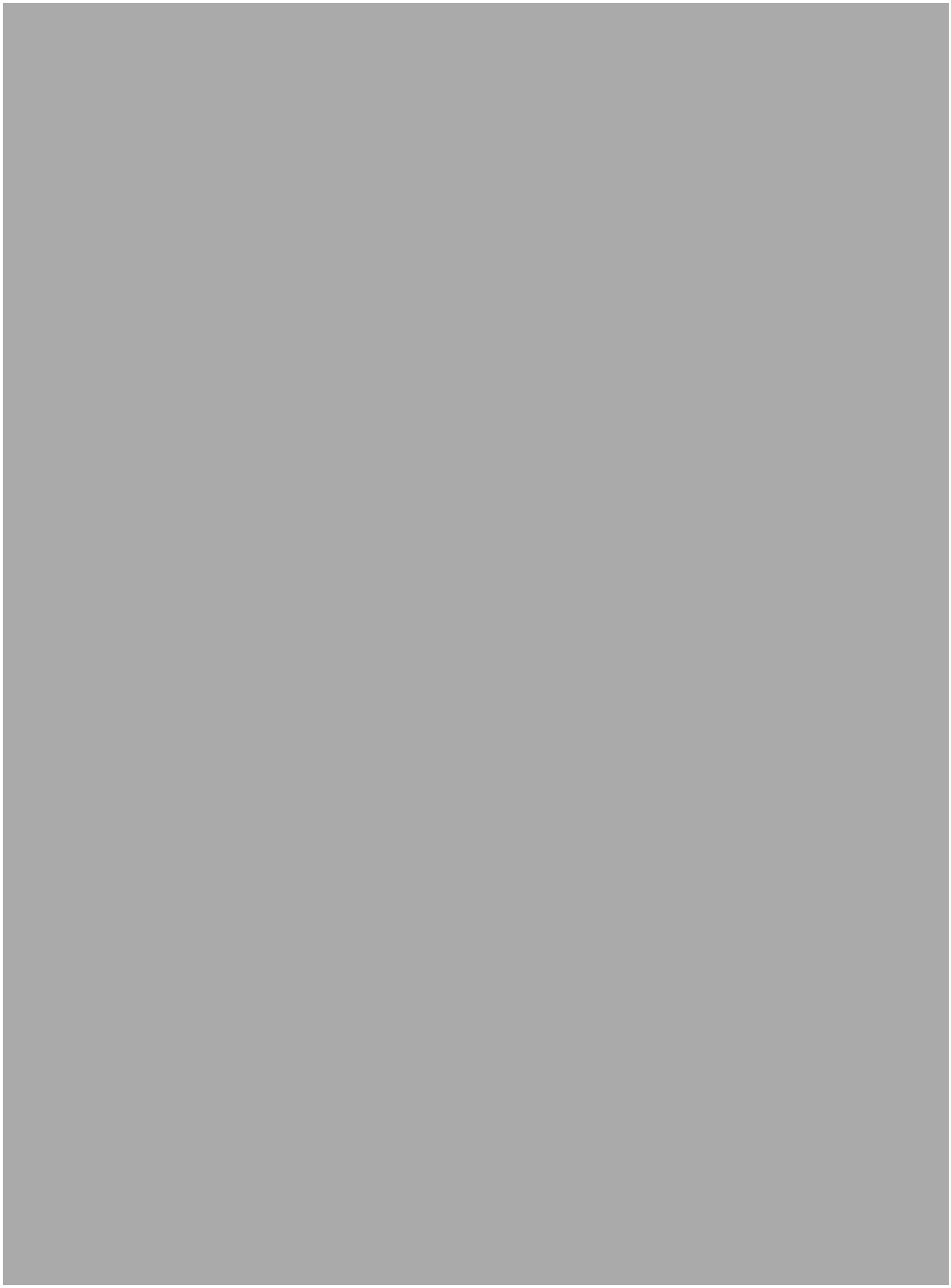

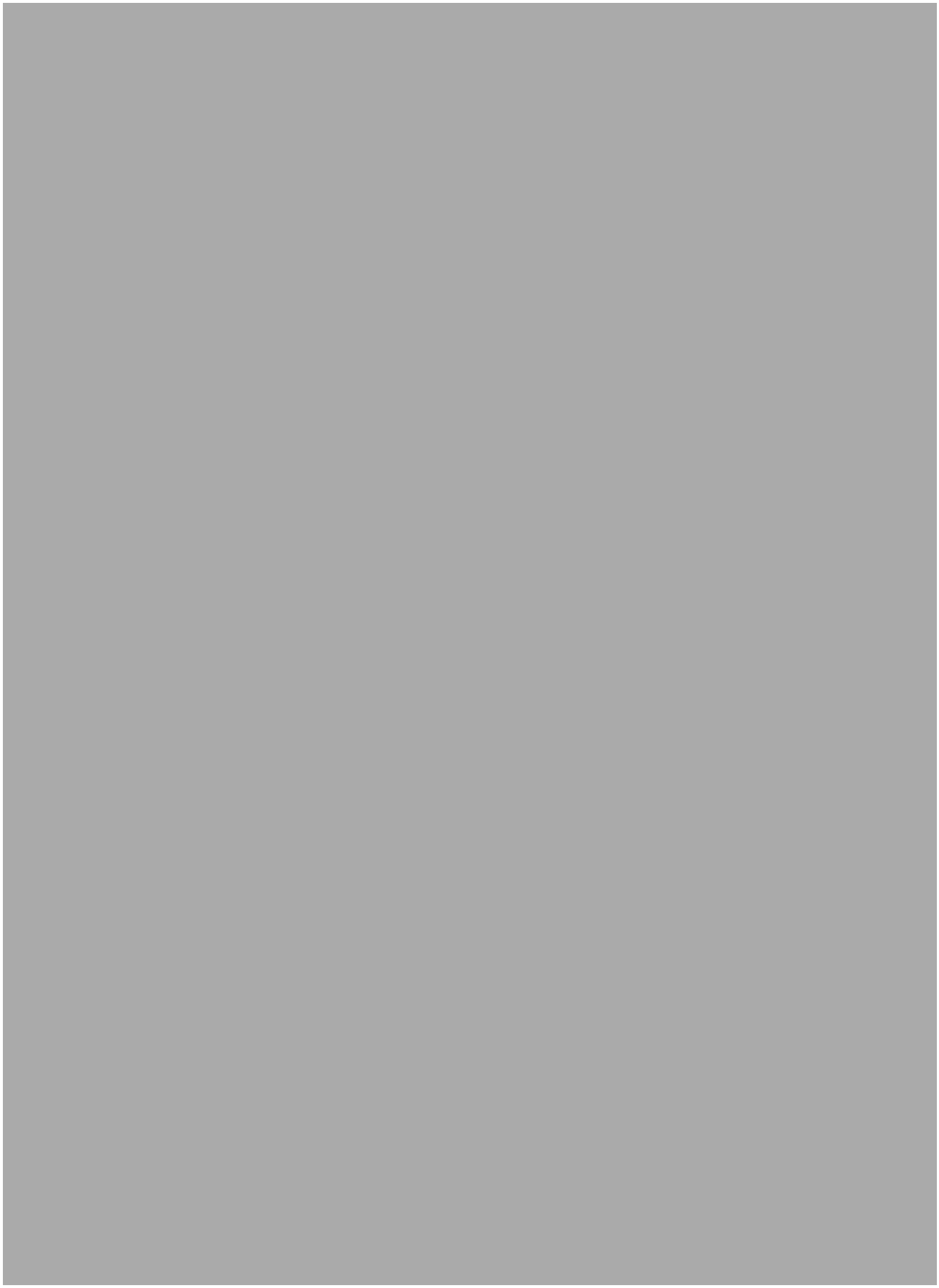

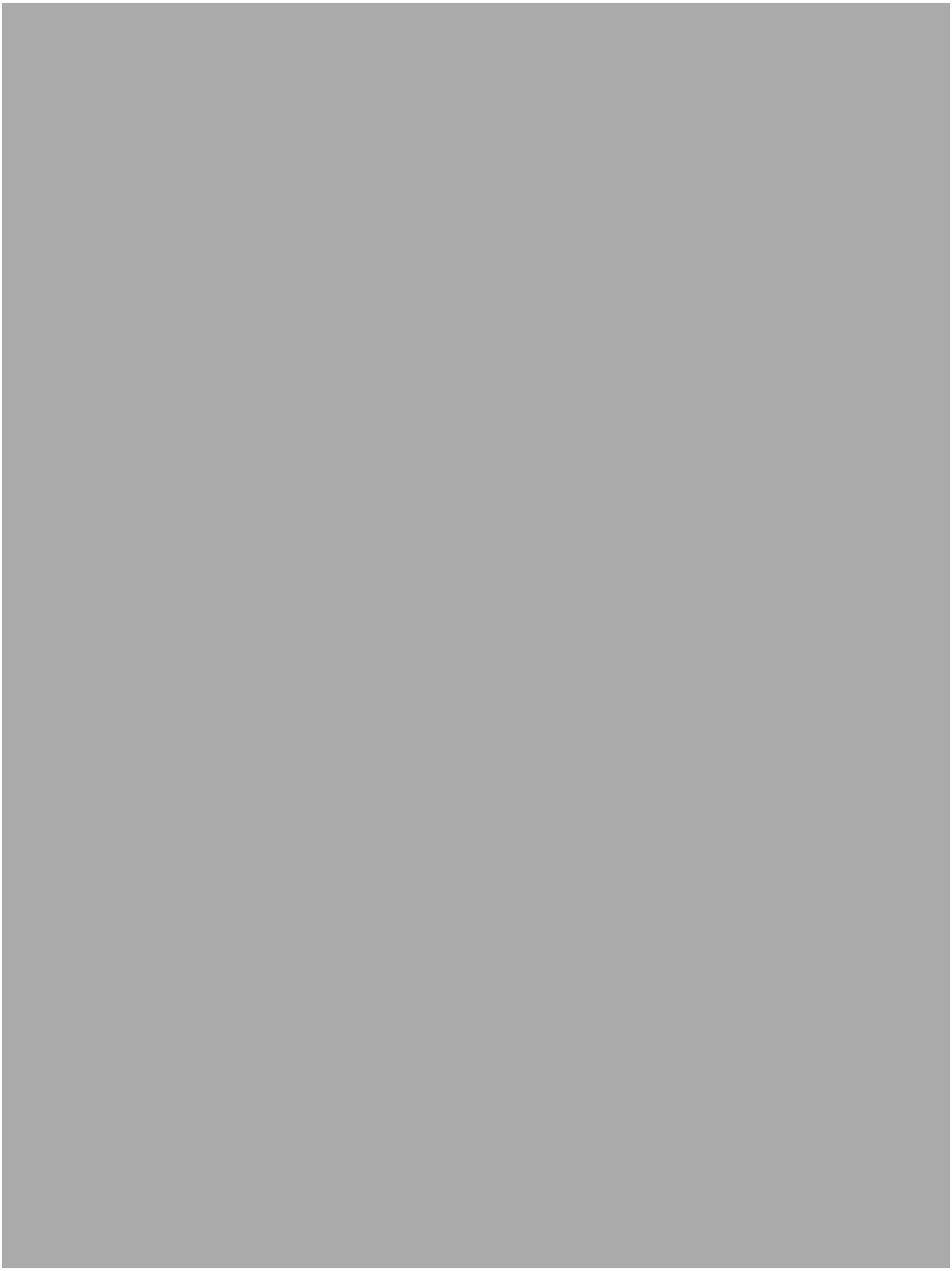

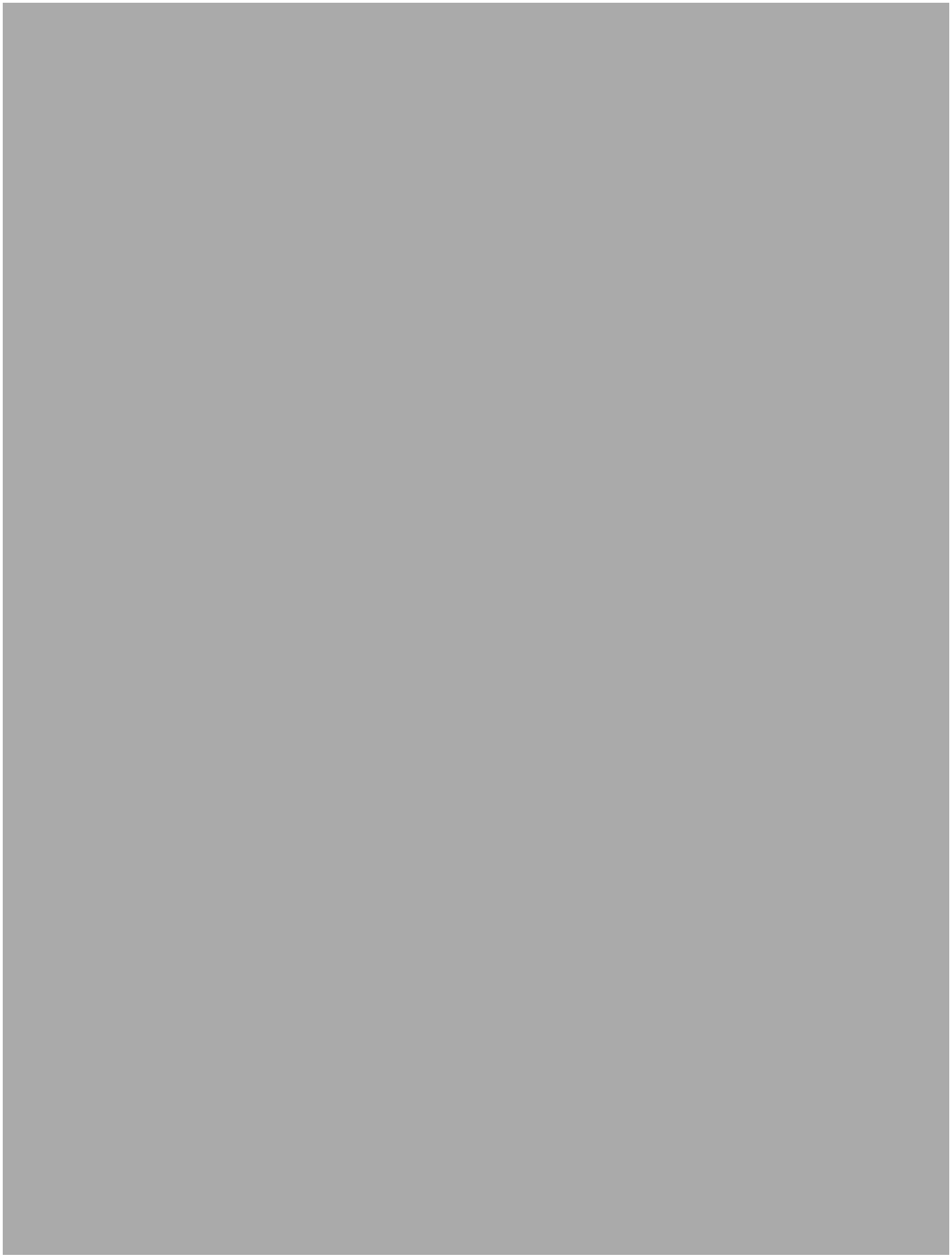

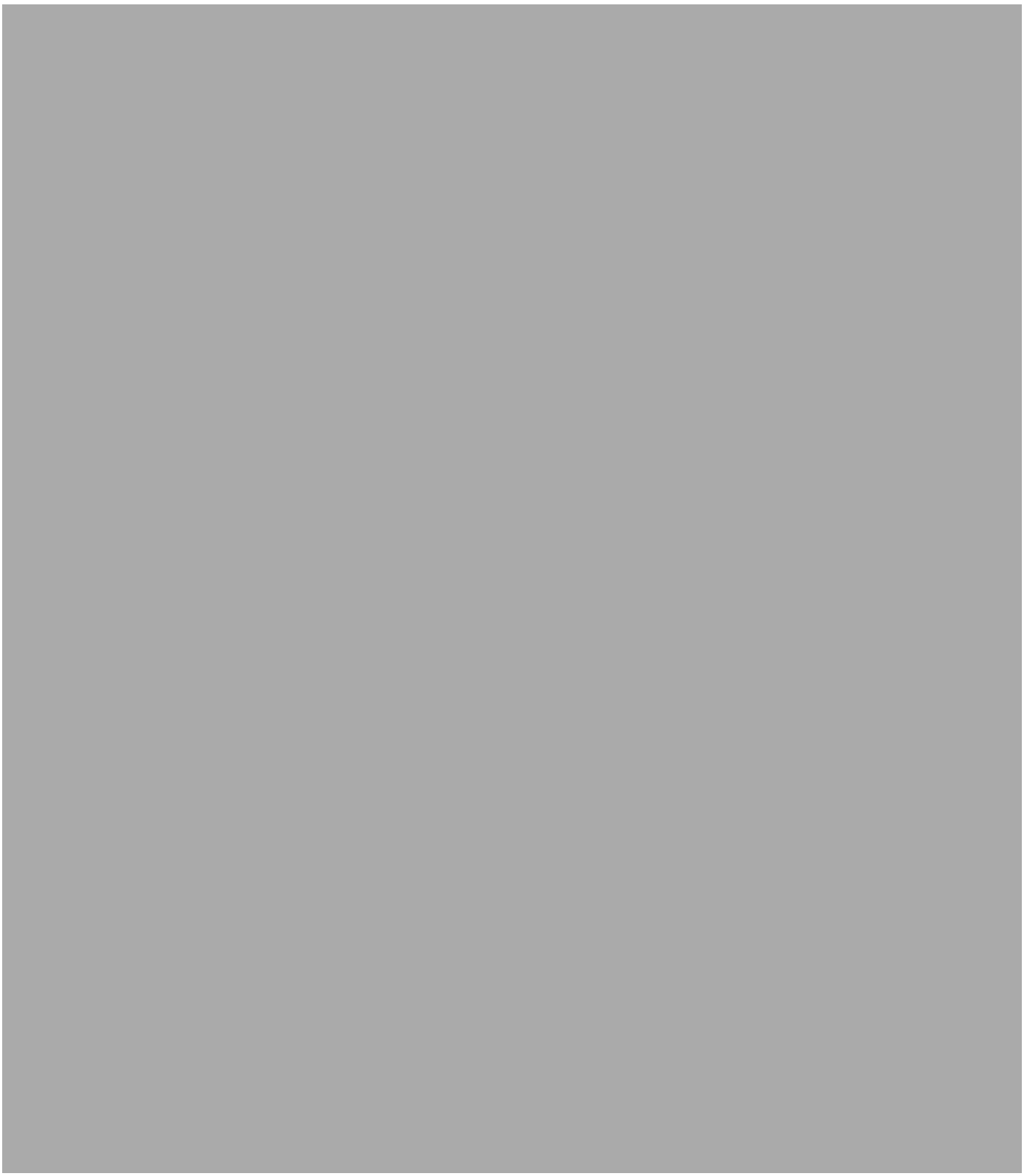

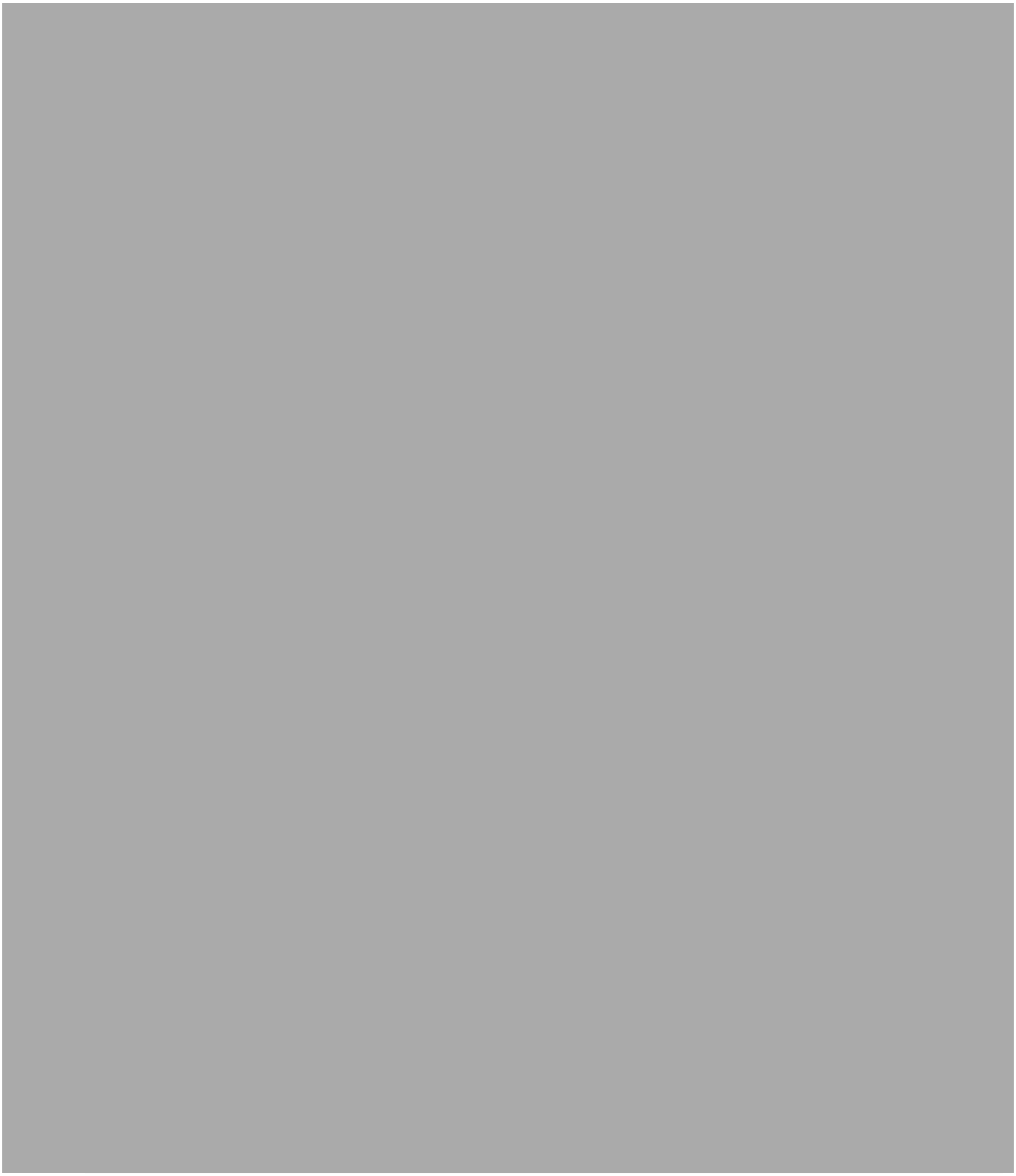

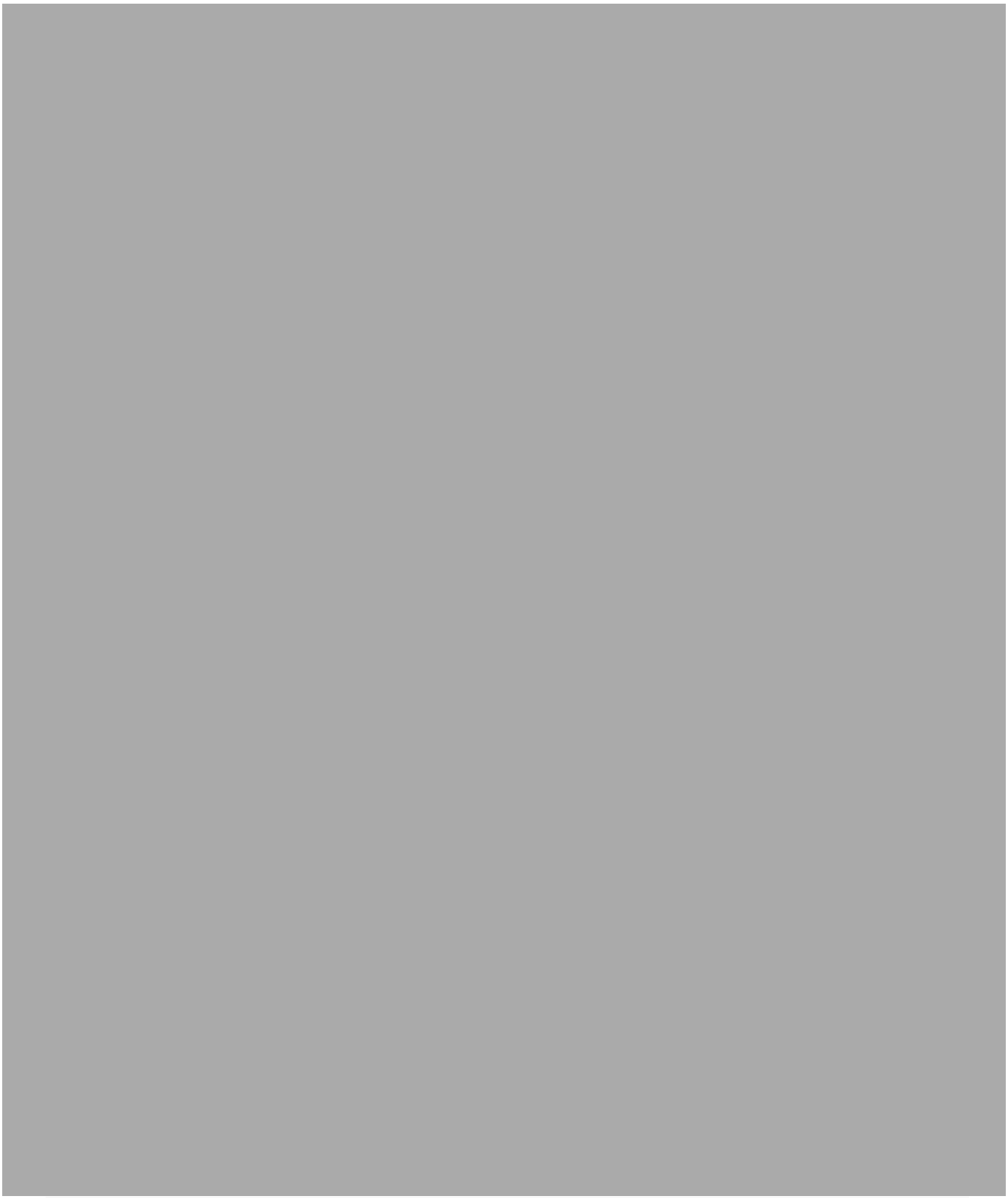

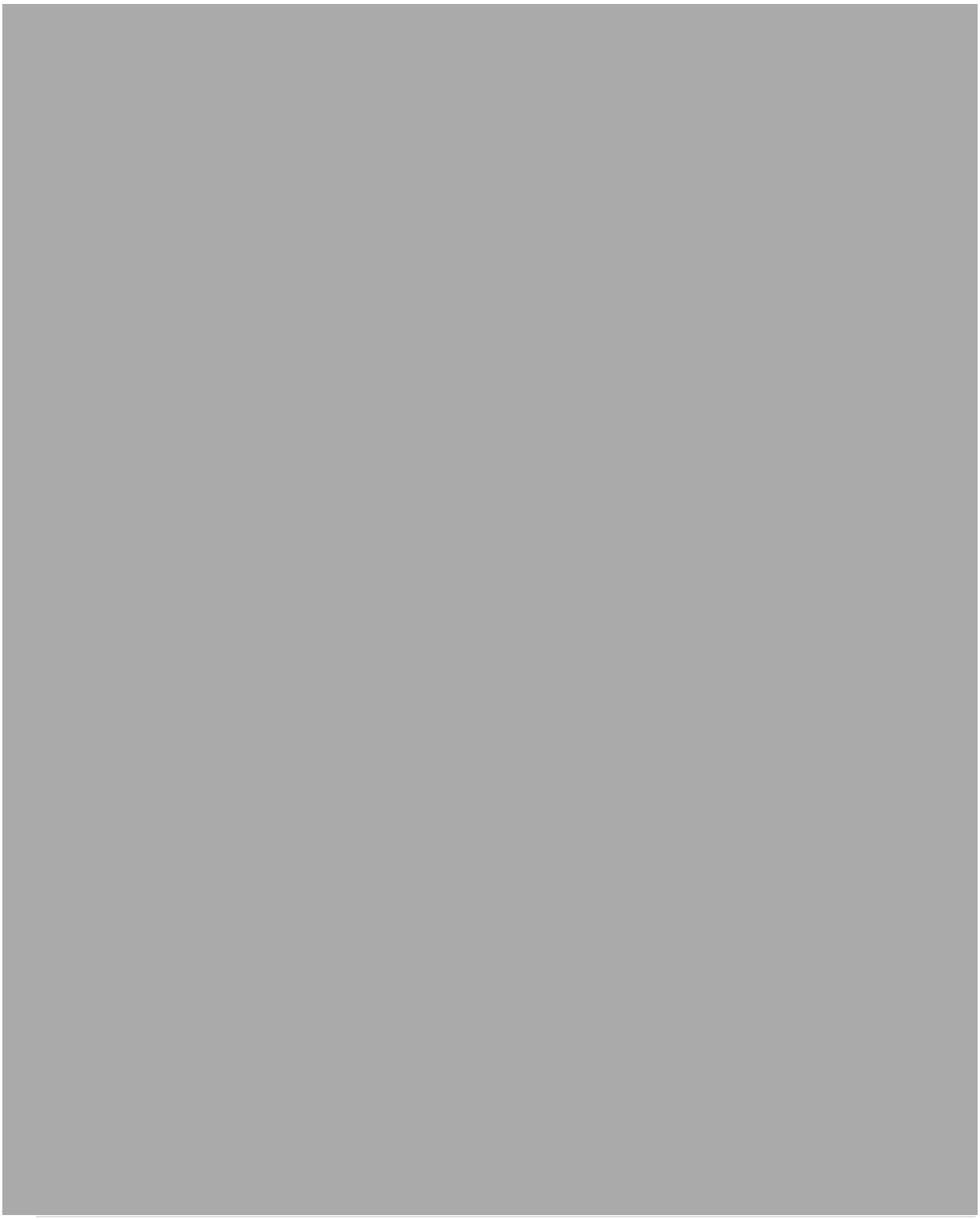

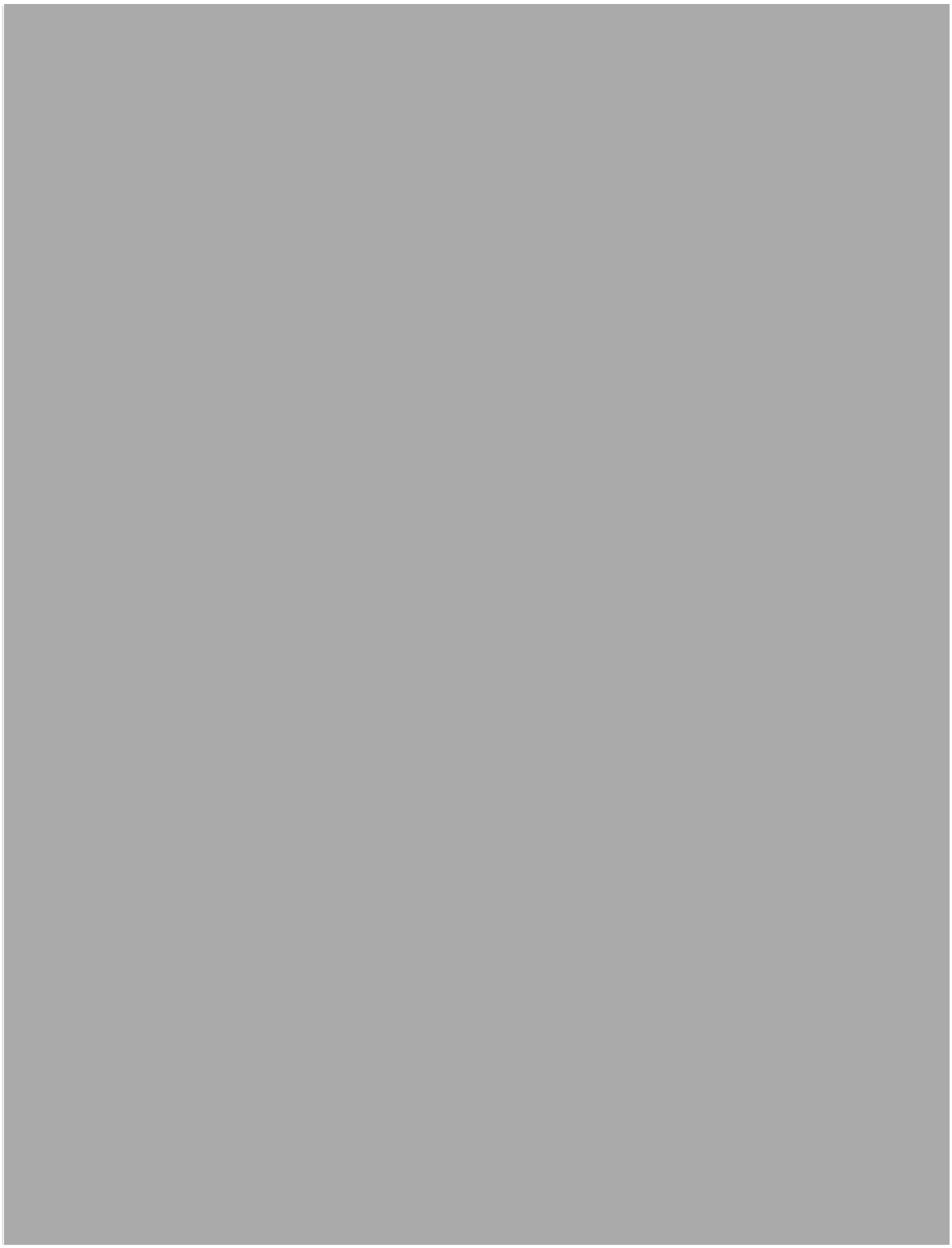

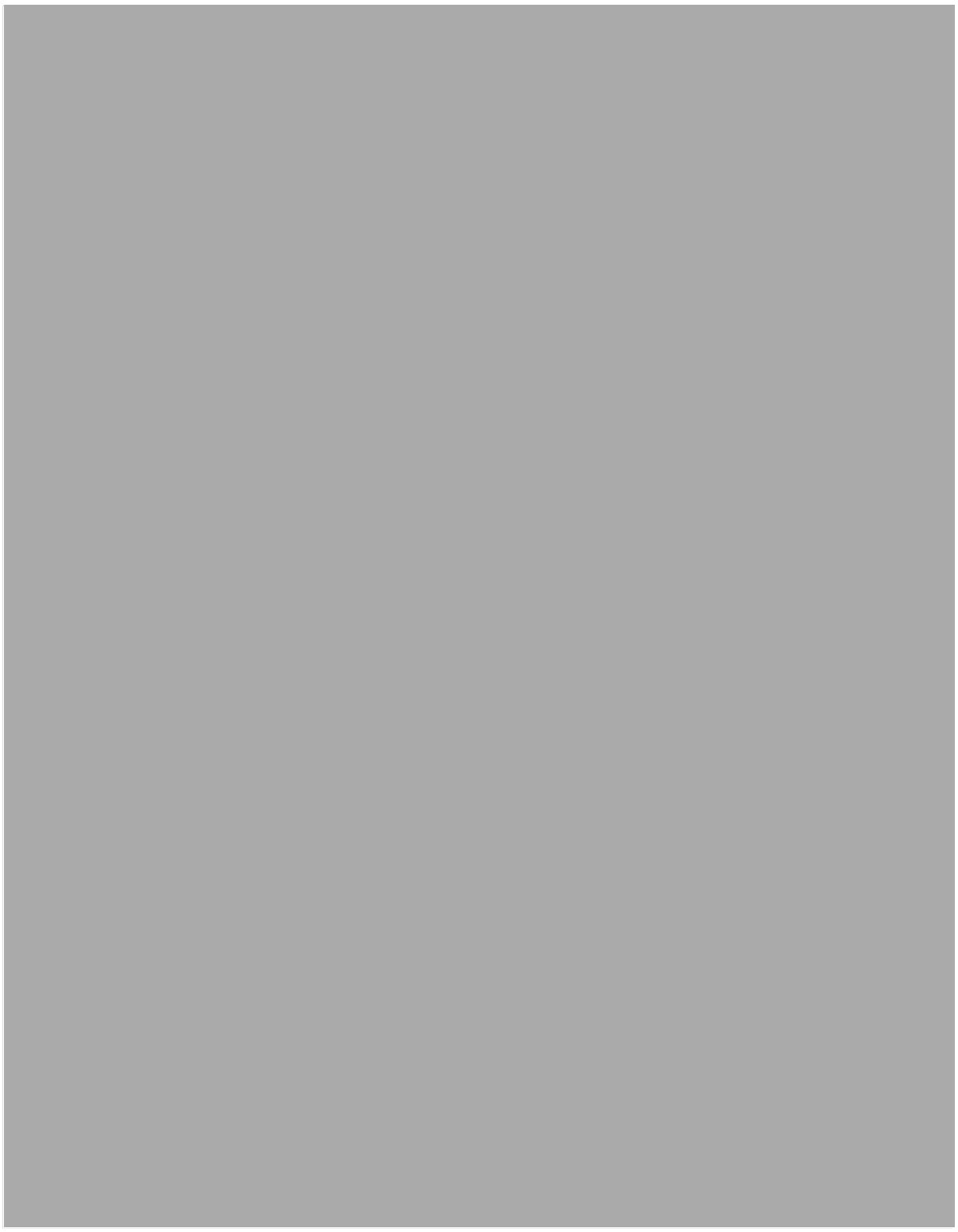

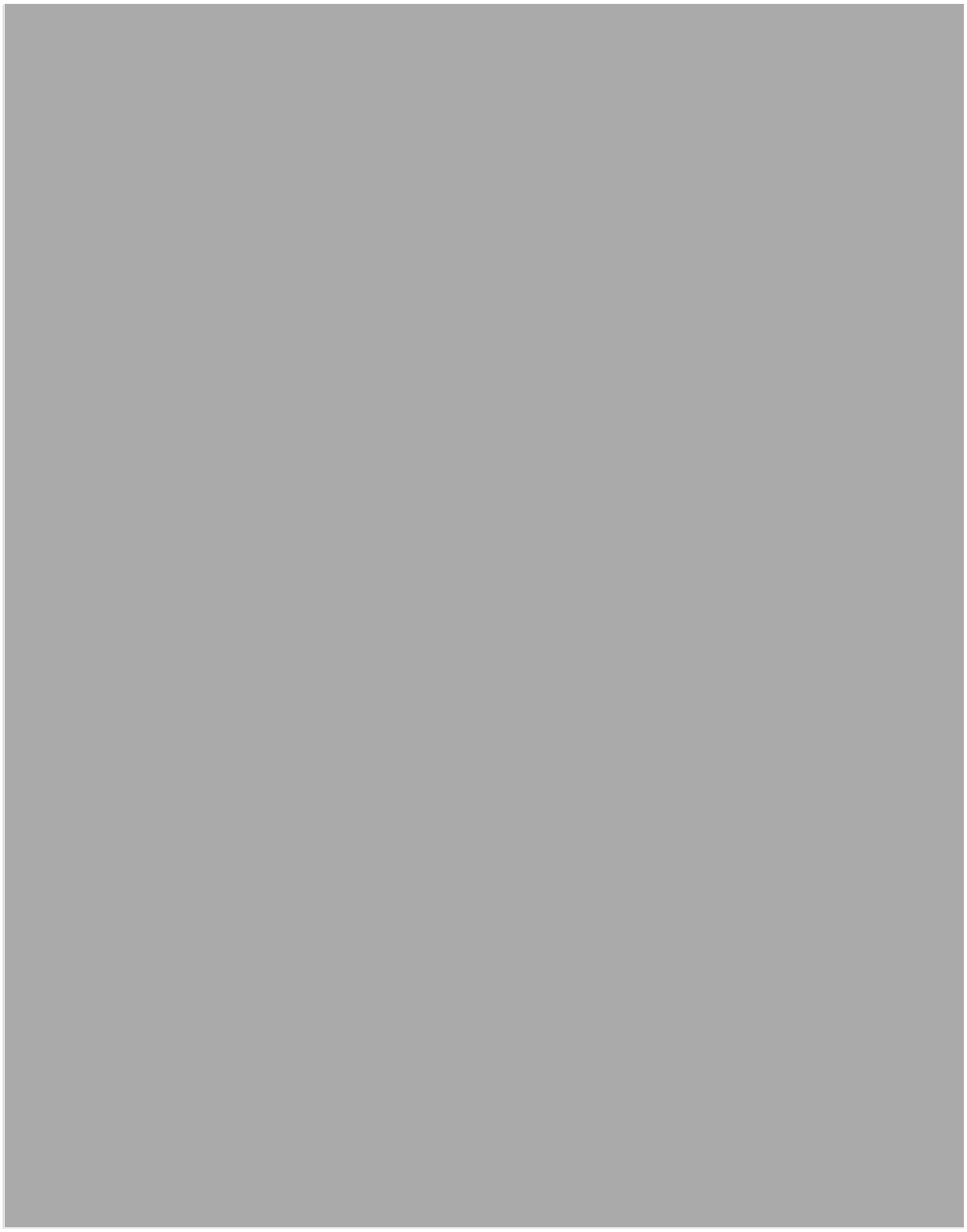

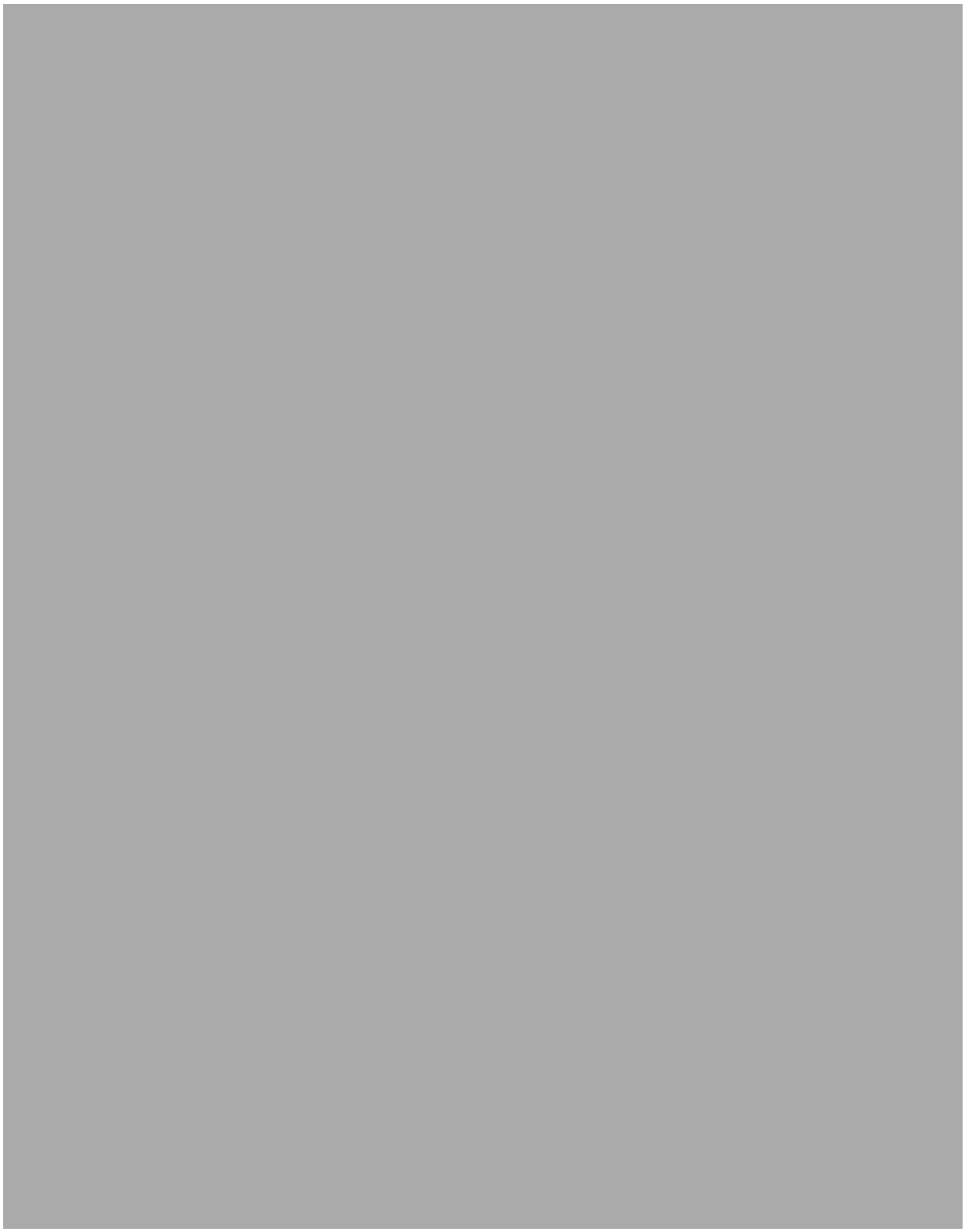

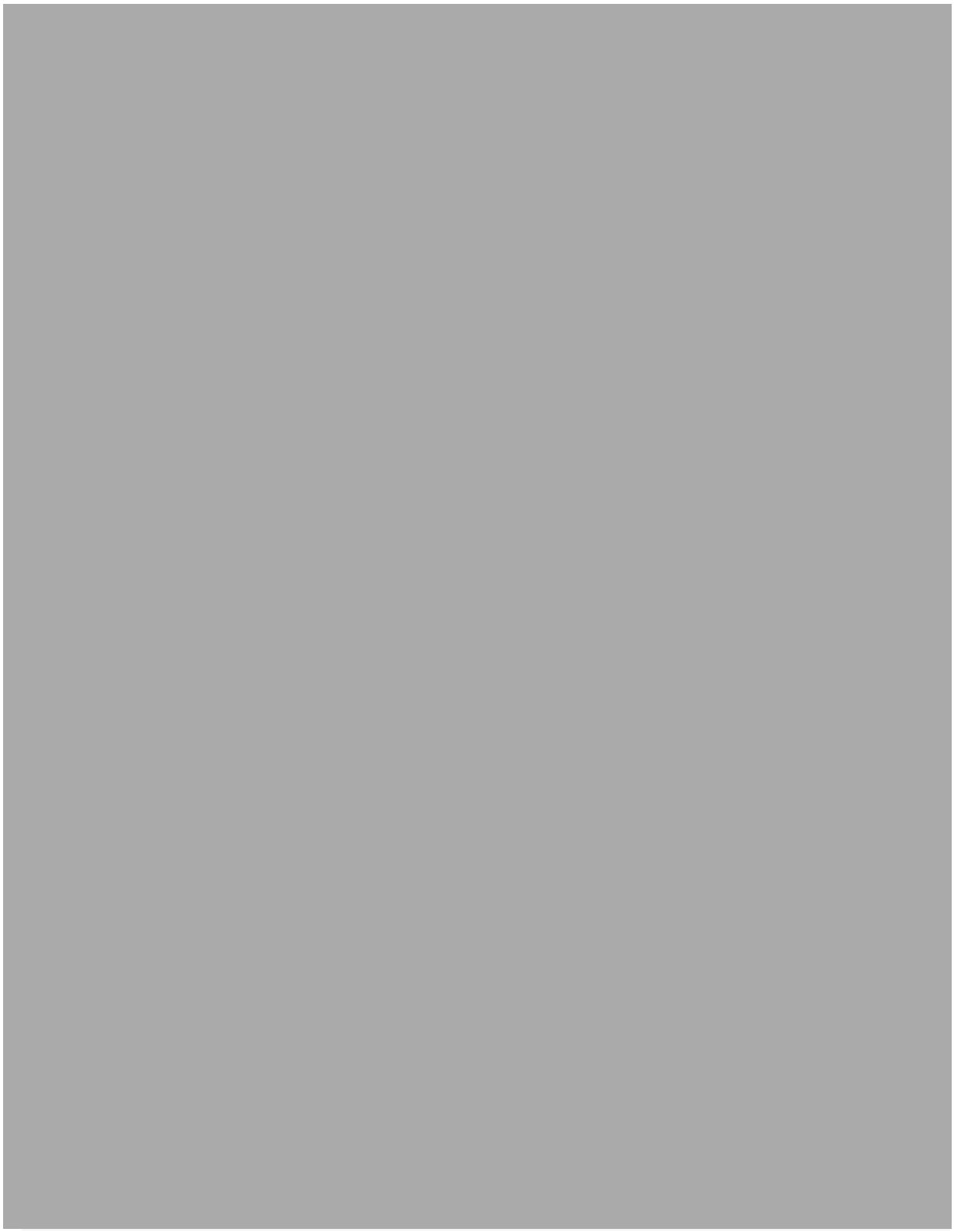

REFERENCES

[1] B. A. Cetiner, *et al.*, "Multifunctional reconfigurable MEMS integrated antennas for adaptive MIMO systems," *Communications Magazine, IEEE,* vol. 42, pp. 62-70, 2004.

[2] R. L. Haupt and M. Lanagan, "Reconfigurable Antennas," *Antennas and Propagation Magazine, IEEE,* vol. 55, pp. 49-61, 2013.

[3] DelfMEMS, "RF MEMS Advantages Over SOI," in *Application Note*, ed, 2010, p. 6.

[4] G. M. Rebeiz, "RF MEMS switches: status of the technology," in *TRANSDUCERS, Solid-State Sensors, Actuators and Microsystems, 12th International Conference on, 2003*, 2003, pp. 1726-1729 vol.2.

[5] F. B. Gross, *Frontiers in antennas: next generation design & engineering*: McGraw-Hill New York, NY, 2011.

[6] P. S. Hall, *et al.*, "Reconfigurable antenna challenges for future radio systems," in *Antennas and Propagation, 2009. EuCAP 2009. 3rd European Conference on*, 2009, pp. 949-955.

[7] E. Ebrahimi, *et al.*, "Integrated wide-narrowband antenna for multi-standard radio," *Antennas and Propagation, IEEE Transactions on,* vol. 59, pp. 2628-2635, 2011.

[8] E. Biglieri, *et al.*, *Principles of Cognitive Radio*: Cambridge University Press, 2012.

[9] P. Gardner, *et al.*, "Reconfigurable antennas for cognitive radio: Requirements and potential design approaches," in *2008 Institution of Engineering and Technology Seminar on Wideband, Multiband Antennas and Arrays for Defence or Civil Applications*, 2008.

[10] P. S. Hall, *et al.*, "Antenna Requirements for Software Defined and Cognitive Radios," *Proceedings of the IEEE,* vol. 100, pp. 2262-2270, 2012.

[11] M. Stuchly, "Spectrum Congestion," 2009.

[12] B. S. Collins, *Handset antennas* vol. 2: chapter, 2007.

[13] D. Peroulis, *et al.*, "Design of reconfigurable slot antennas," *Antennas and Propagation, IEEE Transactions on,* vol. 53, pp. 645-654, 2005.

[14] S.-L. S. Yang, *et al.*, "Frequency reconfigurable U-slot microstrip patch antenna," *Antennas and Wireless Propagation Letters, IEEE,* vol. 7, pp. 127-129, 2008.

[15] H. Jiang, *et al.*, "Miniaturized and reconfigurable CPW square-ring slot antenna using thin film varactor technology," in *Microwave Symposium Digest (MTT), 2011 IEEE MTT-S International*, 2011, pp. 1-4.

[16] H. Jiang, *et al.*, "Miniaturized and reconfigurable CPW square-ring slot antenna loaded with ferroelectric BST thin film varactors," *Antennas and Propagation, IEEE Transactions on,* vol. 60, pp. 3111-3119, 2012.

[17] K. R. Boyle and P. G. Steeneken, "A five-band reconfigurable PIFA for mobile phones," *IEEE Transactions on Antennas and Propagation,* vol. 55, p. 3300, 2007.

[18] A. P. Saghati, *et al.*, "A novel switchable single-and multifrequency triple-slot antenna for 2.4-GHz bluetooth, 3.5-GHz WiMax, and 5.8-GHz WLAN," *Antennas and Wireless Propagation Letters, IEEE,* vol. 9, pp. 534-537, 2010.

[19] C. Sai-Xiong, *et al.*, "A reconfigurable microstrip antenna with agile polarization using diode switches," in *Antennas and Propagation (APSURSI), 2011 IEEE International Symposium on*, 2011, pp. 1566-1569.

[20] H. F. Abutarboush, *et al.*, "A reconfigurable wideband and multiband antenna using dual-patch elements for compact wireless devices," *Antennas and Propagation, IEEE Transactions on*, vol. 60, pp. 36-43, 2012.

[21] A. Khidre, *et al.*, "Circular polarization reconfigurable wideband E-shaped patch antenna for wireless applications," *Antennas and Propagation, IEEE Transactions on*, vol. 61, pp. 960-964, 2013.

[22] G. D. Sworo, *et al.*, "Design and analysis of reconfigurable antennas for WiMAX applications," in *Wireless and Microwave Technology Conference (WAMICON), 2013 IEEE 14th Annual*, 2013, pp. 1-3.

[23] S. Yang, *et al.*, "Frequency-reconfigurable antennas for multiradio wireless platforms," *Microwave magazine, IEEE*, vol. 10, pp. 66-83, 2009.

[24] T. J. Jung, *et al.*, "Circular/linear polarization reconfigurable antenna on simplified RF-MEMS packaging platform in K-band," *Antennas and Propagation, IEEE Transactions on*, vol. 60, pp. 5039-5045, 2012.

[25] X. Cai, *et al.*, "Novel radiation pattern reconfigurable antenna using shorting probe," in *Electronics, Communications and Control (ICECC), 2011 International Conference on*, 2011, pp. 2727-2730.

[26] U. S. Modani and A. Kanwaria, "A Survey on Polarization Reconfigurable Patch Antennas," *International Journal of Recent Technology and Engineering (IJRTE)*, vol. 1, pp. 126-129.

[27] G. Monti, *et al.*, "Patch antenna with reconfigurable polarization," *Progress In Electromagnetics Research C*, vol. 9, pp. 13-23, 2009.

[28] G. M. Rebeiz, *RF MEMS: theory, design, and technology*: John Wiley & Sons, 2004.

[29] U. Shah, *et al.*, "Analysis of Linearity Deterioration in Multidevice RF MEMS Circuits," *Electron Devices, IEEE Transactions on,* vol. 61, pp. 1529-1535, 2014.

[30] E. R. Brown, "RF-MEMS switches for reconfigurable integrated circuits," *Microwave Theory and Techniques, IEEE Transactions on,* vol. 46, pp. 1868-1880, 1998.

[31] S. Lucyszyn, "Review of radio frequency microelectromechanical systems technology," in *Science, Measurement and Technology, IEE Proceedings-*, 2004, pp. 93-103.

[32] RadantMEMS, "RMSW101 SPST RF-MEMS Switch DC to 12 GHz," in *Application Note*, ed, 2010.

[33] L. Dussopt and G. M. Rebeiz, "Intermodulation distortion and power handling in RF MEMS switches, varactors, and tunable filters," *Microwave Theory and Techniques, IEEE Transactions on,* vol. 51, pp. 1247-1256, 2003.

[34] G. M. Rebeiz and J. B. Muldavin, "RF MEMS switches and switch circuits," *Microwave magazine, IEEE,* vol. 2, pp. 59-71, 2001.

[35] G. H. Huff and J. T. Bernhard, "Integration of packaged RF MEMS switches with radiation pattern reconfigurable square spiral microstrip antennas," *Antennas and Propagation, IEEE Transactions on,* vol. 54, pp. 464-469, 2006.

[36] H. Rajagopalan, *et al.*, "RF MEMS actuated reconfigurable reflectarray patch-slot element," *Antennas and Propagation, IEEE Transactions on,* vol. 56, pp. 3689-3699, 2008.

[37] B. Cetiner, *et al.*, "RF MEMS integrated frequency reconfigurable annular slot antenna," *Antennas and Propagation, IEEE Transactions on,* vol. 58, pp. 626-632, 2010.

[38] N. Kingsley, *et al.*, "RF MEMS sequentially reconfigurable sierpinski antenna on a flexible organic substrate with novel DC-biasing technique," *Microelectromechanical Systems, Journal of*, vol. 16, pp. 1185-1192, 2007.

[39] S. Penmetsa, *et al.*, "Design and modeling of a tunable optical antenna enabled by a micromachined actuator," in *Nano/Micro Engineered and Molecular Systems, 2009. NEMS 2009. 4th IEEE International Conference on*, 2009, pp. 176-180.

[40] J.-C. Chiao, *et al.*, "MEMS reconfigurable Vee antenna," in *Microwave Symposium Digest, 1999 IEEE MTT-S International*, 1999, pp. 1515-1518.

[41] A. Mahanfar, *et al.*, "Smart antennas using electro-active polymers for deformable parasitic elements," *Electronics Letters*, vol. 44, pp. 1113-1114, 2008.

[42] K. Daheshpour, *et al.*, "Pattern reconfigurable antenna based on moving V-shaped parasitic elements actuated by dielectric elastomer," *Electronics Letters*, vol. 46, pp. 886-888, 2010.

[43] S. J. Mazlouman, *et al.*, "Reconfigurable axial-mode helix antennas using shape memory alloys," *Antennas and Propagation, IEEE Transactions on*, vol. 59, pp. 1070-1077, 2011.

[44] C. G. Christodoulou, *et al.*, "Reconfigurable antennas for wireless and space applications," *Proceedings of the IEEE*, vol. 100, pp. 2250-2261, 2012.

[45] K. Pan, *et al.*, "A Reconfigurable Coplanar Waveguide Bowtie Antenna Using an Integrated Ferroelectric Thin-Film Varactor," *International Journal of Antennas and Propagation*, vol. 2012, 2012.

[46] L. V. Chen, *et al.*, "Analog tunable matching network using integrated thin-film BST capacitors," in *Microwave Symposium Digest, 2004 IEEE MTT-S International*, 2004, pp. 261-264.

[47] Y. Li, *et al.*, "A compact hepta-band loop-inverted F reconfigurable antenna for mobile phone," *Antennas and Propagation, IEEE Transactions on*, vol. 60, pp. 389-392, 2012.

[48] W. Kang and K. Kim, "A radiation pattern-reconfigurable antenna for wireless communications," in *Antennas and Propagation (APSURSI), 2011 IEEE International Symposium on*, 2011, pp. 1545-1548.

[49] M. Ismail, *et al.*, "Log-Periodic patch antenna with tunable frequency," in *Antennas and Propagation (EUCAP), Proceedings of the 5th European Conference on*, 2011, pp. 2165-2169.

[50] A. S. Nagra, *et al.*, "Bias free optical control of microwave circuits and antennas using improved optically variable capacitors," in *Microwave Symposium Digest. 2000 IEEE MTT-S International*, 2000, pp. 687-690 vol.2.

[51] A. S. Daryoush, *et al.*, "Optically tuned patch antenna for phased array applications," in *Antennas and Propagation Society International Symposium, 1986*, 1986, pp. 361-364.

[52] C. J. Panagamuwa, *et al.*, "Frequency and beam reconfigurable antenna using photoconducting switches," *Antennas and Propagation, IEEE Transactions on*, vol. 54, pp. 449-454, 2006.

[53] C.-H. Chen and D. Peroulis, "Liquid RF MEMS wideband reflective and absorptive switches," *Microwave Theory and Techniques, IEEE Transactions on*, vol. 55, pp. 2919-2929, 2007.

[54] G. M. Rebeiz, *et al.*, "Tuning in to RF MEMS," *Microwave magazine, IEEE,* vol. 10, pp. 55-72, 2009.

[55] A. Berezniak and A. Korotkov, "Solid-state microwave switches: Circuitry, manufacturing technologies and development trends. Review (part 1)," *Radioelectronics and communications systems,* vol. 56, pp. 159-177, 2013.

[56] Y. Fan and Y. Rahmat-Samii, "A reconfigurable patch antenna using switchable slots for circular polarization diversity," *Microwave and Wireless Components Letters, IEEE,* vol. 12, pp. 96-98, 2002.

[57] C. Martin-Pascual, *et al.*, "Invited tutorial:'Patches: The most versatile radiator?'," in *IASTED Int. Conf. Advanced in Communications*, 2001, pp. 3-6.

[58] L. Hui, *et al.*, "A Simple Compact Reconfigurable Slot Antenna With a Very Wide Tuning Range," *Antennas and Propagation, IEEE Transactions on,* vol. 58, pp. 3725-3728, 2010.

[59] C.-Y. Chiu and R. D. Murch, "Reconfigurable multi-slot multi-port antennas using RF-MEMS switches for handheld devices," in *Microwave Conference Proceedings (APMC), 2010 Asia-Pacific,* 2010, pp. 999-1002.

[60] F. Yang and Y. Rahmat-Samii, "Patch antennas with switchable slots (PASS) in wireless communications: Concepts, designs, and applications," *Antennas and Propagation Magazine, IEEE,* vol. 47, pp. 13-29, 2005.

[61] W. Y. Li and K. L. Wong, "Internal printed loop-type mobile phone antenna for penta-band operation," *Microwave and Optical Technology Letters,* vol. 49, pp. 2595-2599, 2007.

[62] K.-L. Wong and C.-H. Huang, "Printed loop antenna with a perpendicular feed for penta-band mobile phone application," *Antennas and Propagation, IEEE Transactions on,* vol. 56, pp. 2138-2141, 2008.

[63] H. Hsuan-Wei, *et al.*, "Design of a Multiband Antenna for Mobile Handset Operations," *Antennas and Wireless Propagation Letters, IEEE,* vol. 8, pp. 200-203, 2009.

[64] at&t, "Antenna Fundamentals," in *Application Note*, ed, 2009, p. 35.

[65] H. F. AbuTarboush, *et al.*, "Design of planar inverted-F antennas (PIFA) for multiband wireless applications," in *Electromagnetics in Advanced Applications, 2009. ICEAA'09. International Conference on*, 2009, pp. 78-81.

[66] J. R. De Luis, *et al.*, "Tunable antenna systems for wireless transceivers," in *Antennas and Propagation (APSURSI), 2011 IEEE International Symposium on*, 2011, pp. 730-733.

[67] C. Chih-Hua and W. Kin-Lu, "Printed PIFA for Penta-Band WWAN Operation in the Mobile Phone," *Antennas and Propagation, IEEE Transactions on,* vol. 57, pp. 1373-1381, 2009.

[68] Y. K. Park and Y. Sung, "A Reconfigurable Antenna for Quad-Band Mobile Handset Applications," *Antennas and Propagation, IEEE Transactions on,* vol. 60, pp. 3003-3006, 2012.

[69] H. F. AbuTarboush, *et al.*, "Multiband Inverted-F Antenna With Independent Bands for Small and Slim Cellular Mobile Handsets," *Antennas and Propagation, IEEE Transactions on,* vol. 59, pp. 2636-2645, 2011.

[70] P. Panaïa, *et al.*, "MEMS-based reconfigurable antennas," in *Industrial Electronics, 2004 IEEE International Symposium on*, 2004, pp. 175-179.

[71] O. O. Tade, *et al.*, "Negative impedance converters for broadband antenna matching," in *Microwave Conference (EuMC), 2012 42nd European*, 2012, pp. 613-616.

[72] J.-H. Lim, *et al.*, "A reconfigurable PIFA using a switchable PIN-diode and a fine-tuning varactor for USPCS/WCDMA/m-WiMAX/WLAN," *Antennas and Propagation, IEEE Transactions on*, vol. 58, pp. 2404-2411, 2010.

[73] J.-H. Lim, *et al.*, "Frequency reconfigurable planar inverted-F antenna using switchable radiator and capacitive load," *Microwaves, Antennas & Propagation, IET*, vol. 7, pp. 430-435, 2013.

[74] E. K. Kowalczuk, *et al.*, "Characterising the linearity of an optically controlled photoconductive microwave switch," in *Antennas and Propagation Conference (LAPC), 2010 Loughborough*, 2010, pp. 597-600.

[75] R. Caverley and G. Hiller, "Distortion properties of MESFET and PIN diode microwave switches," in *Microwave Symposium Digest, 1992., IEEE MTT-S International*, 1992, pp. 533-536.

[76] J. C. Pedro and N. B. Carvalho, *Intermodulation distortion in microwave and wireless circuits*: Artech House, 2002.

[77] Anritsu, "Intermodulation Distortion (IMD) Measurements," in *Application Note*, ed, 2000.

[78] U. L. Rohde and M. Rudolph, *RF/microwave circuit design for wireless applications*: John Wiley & Sons, 2013.

[79] TestEdge, "IP3 (3rd Order Intercept)," in *Application Note*, ed, 2010.

[80] M. Hiebel, *Fundamentals of vector network analysis*: Rohde & Schwarz, 2008.

[81] D. M. Pozar, *Microwave engineering*: John Wiley & Sons, 2009.

[82] J. Karki. (2003, Calculating Noise Figure and Third-Order Intercept in ADCs. *Analog Application Journal,* 11 - 15.

[83] ZVA67. (2015). Available: http://www.rohde-schwarz.co.uk/en/product/zva-productstartpage_63493-9660.html

[84] M. Sonkki, *et al.*, "Varactor tunable helical antenna," in *Antennas and Propagation, 2007. EuCAP 2007. The Second European Conference on*, 2007, pp. 1-6.

[85] P. Hall, *et al.*, "Microstrip patch antenna with integrated adaptive tuning," in *Antennas and Propagation, Tenth International Conference on (Conf. Publ. No. 436)*, 1997, pp. 506-509.

[86] S. Lim, *et al.*, "Metamaterial-based electronically controlled transmission-line structure as a novel leaky-wave antenna with tunable radiation angle and beamwidth," *Microwave Theory and Techniques, IEEE Transactions on*, vol. 53, pp. 161-173, 2005.

[87] C. Kalialakis and P. Hall, "Analysis and experiment on harmonic radiation and frequency tuning of varactor-loaded microstrip antennas," *IET Microwaves, Antennas & Propagation*, vol. 1, pp. 527-535, 2007.

[88] C. R. White and G. M. Rebeiz, "Single-and dual-polarized tunable slot-ring antennas," *Antennas and Propagation, IEEE Transactions on*, vol. 57, pp. 19-26, 2009.

[89] S. Yong, "Design and analysis of pattern null reconfigurable antennas," University of Illinois at Urbana-Champaign, 2012.

[90] Y. Cai, *et al.*, "A frequency reconfigurable printed Yagi-Uda dipole antenna for cognitive radio applications," *Antennas and Propagation, IEEE Transactions on,* vol. 60, pp. 2905-2912, 2012.

[91] D. Patron, *et al.*, "Design and harmonic balance analysis of a wideband planar antenna having reconfigurable omnidirectional and directional patterns," in *Wireless and Microwave Technology Conference (WAMICON), 2013 IEEE 14th Annual*, 2013, pp. 1-5.

[92] I. Reines, *et al.*, "Compact low-loss tunable-band bandstop filter with miniature RF-MEMS switches," *Microwave Theory and Techniques, IEEE Transactions on,* vol. 58, pp. 1887-1895, 2010.

[93] K. Entesari, *et al.*, "A 25–75-MHz RF MEMS Tunable Filter," *Microwave Theory and Techniques, IEEE Transactions on,* vol. 55, pp. 2399-2405, 2007.

[94] M. El-Tanani and G. M. Rebeiz, "High-performance 1.5–2.5-GHz RF-MEMS tunable filters for wireless applications," *Microwave Theory and Techniques, IEEE Transactions on,* vol. 58, pp. 1629-1637, 2010.

[95] K. V. Caekenberghe and T. Vaha-Heikkila, "An analog RF MEMS slotline true-time-delay phase shifter," *Microwave Theory and Techniques, IEEE Transactions on,* vol. 56, pp. 2151-2159, 2008.

[96] T. Vähä-Heikkilä and G. M. Rebeiz, "A 4–18-GHz reconfigurable RF MEMS matching network for power amplifier applications," *International Journal of RF and Microwave Computer‐Aided Engineering,* vol. 14, pp. 356-372, 2004.

[97] T. Aboufoul, *et al.*, "Reconfiguring UWB monopole antenna for cognitive radio applications using GaAs FET switches," *Antennas and Wireless Propagation Letters, IEEE*, vol. 11, pp. 392-394, 2012.

[98] Microsemi, "PIN Diode Fundamentals," in *MicroNote Series 701*, ed, 2010.

[99] Digi-Key. (2010, RF Switches Add Flexibility. *Article Library*.

[100] D. E. Anagnostou, *et al.*, "Design, fabrication, and measurements of an RF-MEMS-based self-similar reconfigurable antenna," *Antennas and Propagation, IEEE Transactions on*, vol. 54, pp. 422-432, 2006.

[101] Infineon. (2009). *BAR50-02V Silicon PIN Diodes*. Available: http://www.infineon.com/

[102] M. R. Hamid, "Wideband reconfigurable antennas," University of Birmingham, 2011.

[103] N. Viet-Anh, *et al.*, "A Simple PIFA-Based Tunable Internal Antenna for Personal Communication Handsets," *Antennas and Wireless Propagation Letters, IEEE,* vol. 7, pp. 130-133, 2008.

[104] S. Takatani and C. Cheng-Duan, "Nonlinear Steady-State III-V FET Model for Microwave Antenna Switch Applications," *Electron Devices, IEEE Transactions on*, vol. 58, pp. 4301-4308, 2011.

[105] J. H. K. Vuolevi, *et al.*, "Measurement technique for characterizing memory effects in RF power amplifiers," *IEEE Transactions on Microwave Theory and Techniques*, vol. 49, pp. 1383-1389, 2001.